

AUTONOMIC MODULATION IN A RABBIT MODEL OF HEART FAILURE

by

SHUI HAO CHIN
MBBChir (Cantab), MA (Cantab)

**A thesis submitted to the
University of Leicester
for the degree of
DOCTOR OF PHILOSOPHY**

Department of Cardiovascular Sciences
College of Medicine, Biological Sciences and Psychology
University of Leicester

January, 2017

Abstract of Thesis

AUTONOMIC MODULATION IN A RABBIT MODEL OF HEART FAILURE

Shui Hao Chin

In this thesis, autonomic modulation of atrial and ventricular electrophysiology was studied in both normal and diseased models of rabbit hearts using isolated, dual-innervated, Langendorff-perfused heart preparation. In normal hearts, *accentuated antagonism* was present in heart rate changes during sympatho-vagal interaction, with a dominant vagal effect of heart rate reduction observed. At the ventricular level, sympathetic effect prevailed with the resultant lowering of ventricular fibrillation threshold (VFT) and steepening of action potential duration restitution (APD-RT) despite concurrent vagal stimulation, suggesting a different pre-synaptic neuro-cardiac interaction at the ventricular level. No sympatho-vagal interaction was demonstrated for ventricular refractoriness (ERP). Beta-blockade during sympatho-vagal interaction abolished the prevailing sympathetic effect in ventricular electrophysiology in addition to raising overall VFT. An infarct-driven heart failure model was created by surgical ligation of circumflex artery whilst sham model underwent open-chest surgeries with no coronary ligation. A learning curve was encountered with post-operative mortality improved by various refinements. Six weeks following coronary ligation, transthoracic echocardiography revealed cardiac remodelling evident as left atrial and ventricular dilatation correlating with impaired systolic function. Ex-vivo cardiac magnetic resonance imaging confirmed apical myocardial scarring in heart failure rabbits. Systemic remodelling manifested as increased weights of heart, lungs and liver, all correlating with impaired systolic function. At baseline, heart failure rabbits exhibited longer atrio-ventricular delay, lower VFT, steeper APD-RT, greater apico-basal restitution dispersion and shorter ERP when compared to the shams. There was exaggerated sympathetic response in heart failure animals with significantly greater heart rate increment and atrio-ventricular delay shortening, VFT lowering, ERP shortening, APD-RT steepening, and greater apico-basal restitution dispersion. Simultaneously, the opposing effects of vagal stimulation were attenuated. Infarct-driven heart failure in rabbits following coronary ligation resulted in adverse structural and electrical remodelling which promotes ventricular fibrillation in response to autonomic dysfunction characterised by sympathetic overdrive and vagal attenuation.

Acknowledgement

The journey through this doctoral research has been enlightening and refreshing. The completion of this thesis would be improbable without the guidance, encouragement, experience, inspiration and support from the generous and helpful staff at the University of Leicester.

First and foremost, I would like to express my utmost gratitude to my supervisors, Prof. G. André Ng and Dr. Kieran Brack. To Prof. Ng, you are the guiding torch in my research endeavour, not only giving me the opportunity to write this research grant, but also inspiring me with the relentless drive required to complete the project. Your intellectual tenacity is highly aspiring and made me realise that possession of an analytical mind is not a talent but a mandatory research skill that is attainable by mere mortals. To Kieran, thank you for being there since the inception of this research idea. Throughout my research fellowship, you have been providing the much needed guidance at different stages of my experimental works. Without you, I would not have appreciated the importance of cultivating a high level of mental focus and adopting a deep work philosophy to complete my written works.

I would like to express my heartfelt thanks to my collaborators at the Institute of Cardiovascular and Medical Sciences, University of Glasgow. I am especially indebted to Prof. Smith who has been very supportive in this fellowship, contributing his expertise in the development of the rabbit heart failure model. The realisation of this heart failure model at the University of Leicester would have been impossible without

his palpable involvement. To Mike, I am fortunate to have you as my mentor in the surgical theatre. Your surgical skills in rabbit surgeries are nothing short of amazing. Your practical knowledge in the surgical set-ups is truly cherished. More importantly, I appreciate your time in visiting our department to provide the necessary guidance in refining our surgical skills during the initial stage of creating this heart failure model.

I am thankful for the tremendous help from my research colleagues: Emily, Gabi and James. You are truly my comrade-in-arms throughout my research fellowship, assisting me in all the surgical procedures in rabbits. Your technical reliability and consistent work ethics in the laboratory and the surgical theatre play a vital role in ensuring successful extraction of meaningful experimental data. Your presence at the office till the late hours of the day had always served as an emotional anchor throughout my three years at the Department of Cardiovascular Sciences.

This research would not have come to fruition without the help I received from all the wonderful animal technicians, research and administrative staff in the Central Research Facility. To Lucy, Pauline and Debbie, I am extremely grateful for your help in looking after all the rabbits before and after their surgical procedures. You have showed me your skills, kindness, patience and tenderness in animal husbandry. You have been by my side during the emotionally draining period when we were faced with post-operative mortality in rabbits. Your dedication in looking after the rabbits and your calmness when faced with ill rabbits are the reasons for me to emotionally matured as a scientist and a clinician.

To Justyna and Mike, thank you for providing the support for various imaging protocols required for the rabbits. I am particularly grateful for you in going the extra mile to accommodate my rabbits for transthoracic echocardiography during your busy schedule. I am especially thankful for having Mike to perform *ex-vivo* cardiac magnetic resonance imaging on the rabbit hearts towards the second half of my research fellowship. Your support and skills in processing magnetic resonance images are much appreciated. To Christine and Alex, your tremendous administrative help in organizing rabbit deliveries and in booking surgical theatres ensure the smooth-running of this research fellowship. Your prompt responses and admirable organizational skills are the keystone for the successful execution of many surgical and experimental procedures.

Importantly, I would like to acknowledge the generosity of British Heart Foundation for granting a clinical research fellowship in full support of my pursuit of this PhD research project. Your financial support not only enabled a clinician in training to fully immerse in a basic science research, but also gave me the opportunity to hone my presentation skills by disseminating my research findings both nationwide and internationally. I would always be grateful for this research fellowship for it plants the seeds for my passion in both basic science and clinical research.

Last but not least, I would like to thank my family for their unfailing support and love in my research endeavour. To mum and dad, thank you for believing in me and for providing all the support necessary in overcoming all obstacles in life. You are my source of spiritual strength and irrespective how far I have ventured in life, you will always be close to my heart.

To my beloved wife, Winnie, you shower me with boundless affection and unflagging support in my life. Words are inadequate to express my deepest gratitude for your infallible dedication in helping me to achieve the dream of pursuing this research. You are the embodiment of a perpetually youthful dreamer, a cautious master advisor, a keen learner, a resilient fighter, and a graceful companion in my life. Your unwavering encouragement is the sole driving force for the completion of my thesis.

Worship the spirit of criticism.

*If reduced to itself, it is not an awakener of ideas or a stimulant to great things;
but without it everything is fallible; it always has the last word.*

- Louis Pasteur, 1888

Table of Contents

List of Tables	i
List of Figures	ii – ix
List of Abbreviations	x – xvii
Conference Presentations by the Candidate	xviii – xix
Other Oral and Poster Presentations during Candidacy	xx – xxiii
External Academic Engagement during Candidacy	xxiv

Chapter 1: Heart Failure and Dysautonomia 1 – 52

1.1 Background	2
1.2 Heart Failure	2
1.2.1 Definition of Heart Failure	2
1.2.2 Epidemiology of Heart Failure	3
1.2.3 Aetiology of Heart Failure	4
1.2.4 Prognosis of Heart Failure	7
1.3 Measurement of Sympathetic and Parasympathetic Nervous Systems	
Activity	8
1.3.1 Plasma Norepinephrine	8
1.3.2 Neural Tracer Imaging	10
1.3.3 Microneurography	11
1.3.4 Baroreflex Sensitivity	12
1.3.5 Heart Rate Variability	13
1.4 Mechanisms of Dysautonomia in Heart Failure	14
1.4.1 Sympathetic Hyperactivity	14
1.4.2 Parasympathetic Attenuation	24
1.5 Heart Failure and Nitric Oxide (NO)	27
1.6 Autonomic Nerve Innervation and the Effect of Myocardial Infarction ..	28
1.7 Autonomic Nerve Stimulation, Electrical Restitution and SCD	30
1.8 Conclusion	32
1.9 References	33

Chapter 2: Thesis Aims and Layout 53 – 56

2.1	Aims of Study	54
2.2	Thesis Layout	55
2.3	References	56

Chapter 3: General Methods 57 – 102

3.1	Coronary Artery Ligation in the Rabbit.....	58
3.1.1	Background	58
3.1.2	Method	59
3.2	Challenges of Building a Leporine Heart Failure Model by Coronary Ligation	69
3.2.1	Background	69
3.2.2	Pre-operative Animal Weight	70
3.2.3	Type of Surgeries: Coronary Ligation or Sham Procedures ...	70
3.2.4	Premature Mortality	72
3.2.5	Refinements and Learning Curve	73
3.3	Transthoracic Echocardiography	80
3.3.1	Background	80
3.3.2	Method	81
3.4	Measurements of Ventricular Fibrillation Threshold and Ventricular Refractoriness in Langendorff-perfused Rabbit Hearts	84
3.4.1	Background	84
3.4.2	Method	85
3.4.2.1	Isolation of Heart with Intact Dual Autonomic Innervation	85
3.4.2.2	Langendorff Preparation Protocol and Cardiac Electrical Signal Recording	86
3.4.2.3	Autonomic Nerve Stimulation	87
3.4.2.4	Measurement of Heart Rate, Atrio-ventricular	

	Delay and Ventricular Electrophysiology	88
3.4.2.4.1	Measurement of Heart Rate and Atrio-ventricular Delay	88
3.4.2.4.2	Measurement of Ventricular Electrophysiology ...	88
3.5	Cardiac Remodelling and Organ Congestion	92
3.5.1	Background	92
3.5.2	Method	92
3.5.2.1	Measurement of Wet and Dry Organ Weights ...	92
3.5.2.2	Ex-vivo Cardiac Magnetic Resonance Imaging ..	93
3.6	Data Presentation and Statistical Analysis	95
3.7	References	96

Chapter 4: Sympatho-vagal Interaction in Isolated Dual-innervated, Langendorff-perfused Rabbit's Heart 103 – 139

4.1	Introduction	104
4.2	Aim	105
4.3	Method	105
4.3.1	Isolated Rabbit Heart Preparation with Intact Dual Autonomic Nerve Innervation	105
4.3.2	Langendorff Perfusion	106
4.3.3	Autonomic Nerve Stimulation	106
4.3.4	Cardiac Electrical Recording and Pacing	107
4.3.5	Measurement of Ventricular Electrophysiology: VFT, ERP and RT	107
4.4	Results	107
4.4.1	Effects of Sympatho-vagal Interaction on Heart Rate	107
4.4.1.1	Effects of Background High-frequency Vagus Nerve Stimulation on Heart Rate Response during Low and High-frequency Sympathetic Nerve Stimulations	107
4.4.1.2	Effects of Background High-frequency Sympathetic Nerve Stimulation on Heart Rate Response during Low and High-frequency Vagus Nerve Stimulations ...	110

4.4.1.3	Algebraic Sum of Heart Rate Changes with Sympathetic and Vagus Nerve Stimulations	112
4.4.2	Effects of Sympatho-vagal Interaction on Ventricular Fibrillation Threshold	113
4.4.2.1	Effects of Background High-frequency Vagus Nerve Stimulation on Ventricular Fibrillation Threshold during Low and High-frequency Sympathetic Nerve Stimulations	113
4.4.2.2	Effects of Background High-frequency Sympathetic Nerve Stimulation on Ventricular Fibrillation Threshold during Low and High-frequency Vagus Nerve Stimulations	115
4.4.2.3	Algebraic Sum of Ventricular Fibrillation Threshold Changes with Sympathetic and Vagus Nerve Stimulations	116
4.4.3	Effects of Sympatho-vagal Interaction on Action Potential Duration Restitution	117
4.4.3.1	Effects of Background High-frequency Vagus Nerve Stimulation on Cardiac Restitution during Low and High-frequency Sympathetic Nerve Stimulations	117
4.4.3.2	Effects of Background High-frequency Sympathetic Nerve Stimulation on Cardiac Restitution during Low and High-frequency Vagus Nerve Stimulations	120
4.4.4	Effects of Sympatho-vagal Interaction on Ventricular Effective Refractory Period	123
4.4.4.1	Effects of Background High-frequency Vagus Nerve Stimulation on Ventricular Effective Refractory Period during Low and High-frequency Sympathetic Nerve Stimulations	123
4.4.4.2	Effects of Background High-frequency Sympathetic Nerve Stimulation on Ventricular Effective Refractory Period during Low and High-frequency Vagus Nerve Stimulations	125

4.4.4.3	Algebraic Sum of Ventricular Effective Refractory Period Changes with Sympathetic and Vagus Nerve Stimulations	126
4.5	Discussion	127
4.5.1	Effect of Sympatho-vagal Interaction on Intrinsic Heart Rate ...	128
4.5.1.1	Frequency-dependent Heart Rate Response during Autonomic Nerve Stimulation	128
4.5.1.2	Accentuated Antagonism	129
4.5.2	Effect of Sympatho-vagal Interaction on Ventricular Fibrillation Thresholds	131
4.5.3	Effect of Sympatho-vagal Interaction on Action Potential Duration Restitution Slopes	132
4.5.4	Effect of Sympatho-vagal Interaction on Ventricular Refractoriness	134
4.5.5	Absence of Accentuated Antagonism in Ventricular Electrophysiology during Sympatho-vagal Interaction	135
4.6	Conclusion	136
4.7	References	136

Chapter 5:	Beta-blocker Modulation of Heart Rate and Ventricular Electrophysiology in Sympatho-vagal Interaction – Potential Mechanisms	140 – 169
-------------------	---	------------------

5.1	Introduction	141
5.2	Aim	142
5.3	Method	142
5.3.1	Isolated Rabbit Heart Preparation with Intact Dual Autonomic Innervation	142
5.3.2	Langendorff Perfusion with Acetate-free and Acetate-containing Tyrode solutions	143
5.3.3	Autonomic Nerve Stimulation	143
5.3.4	Cardiac Electrical Recording and Pacing	144
5.3.5	Measurement of Ventricular Electrophysiology: VFT, ERP and	

RT	144
5.4 Results	144
5.4.1 Effect of Metoprolol on Sympatho-vagal Interaction of Heart Rate	144
5.4.2 Effect of Metoprolol on Sympatho-vagal Interaction of Ventricular Fibrillation Inducibility	147
5.4.3 Effect of Metoprolol on Sympatho-vagal Interaction of Ventricular Restitution	149
5.4.4 Effect of Metoprolol on Sympatho-vagal Interaction of Ventricular Refractoriness	151
5.4.5 Effect of Sodium Acetate on Metoprolol-induced Heart Rate Changes and Metoprolol-conferred Protective Effect of Ventricular Fibrillation Inducibility	153
5.5 Discussion	159
5.5.1 Effect of Metoprolol on VFT during Sympatho-vagal Interaction	159
5.5.2 Effect of Metoprolol on APD Restitution Slopes during Sympatho-vagal Interaction	161
5.5.3 Effect of Metoprolol on Ventricular Refractoriness during Sympatho-vagal Interaction	162
5.5.4 Is Sodium Acetate Responsible for Additional Antiarrhythmic Properties of Metoprolol beyond Adrenergic Blockade?	163
5.6 Conclusion	165
5.7 References	165

Chapter 6: Myocardial Remodelling and Organ Congestion in Infarct-driven Heart Failure Model in Rabbits 170 – 187

6.1 Introduction	171
6.2 Aim.....	172
6.3 Method	172
6.3.1 Transthoracic Echocardiography	172
6.3.2 Measurement of Organ Weights	173

6.3.3	Ex-vivo Cardiac Magnetic Resonance Imaging	173
6.4	Results	175
6.4.1	Cardiac Remodelling	175
6.4.2	Organ Congestion	178
6.4.3	Ex-vivo Left Ventricular Scar Quantification	181
6.5	Discussion	181
6.6	Conclusion	184
6.7	References	184

**Chapter 7: Characterisation of Autonomic Electrocardiology in
Isolated Rabbit Heart Failure Model 188 – 223**

7.1	Introduction	189
7.2	Aim	191
7.3	Method	191
7.3.1	Rabbit Myocardial Infarction Heart Failure Model	191
7.3.2	Isolated Langendorff-perfused Rabbit Heart Preparation with Intact Dual Autonomic Nerve Innervation	192
7.3.3	Autonomic Nerve Stimulation	192
7.3.4	Cardiac Electrical Recording and Pacing	193
7.3.5	Measurement of Atrio-ventricular and Ventricular Electrophysiology	193
7.4	Results	194
7.4.1	Effect of Autonomic Stimulation on Stimulus-Heart Rate Response	194
7.4.1.1	Effect of Varying Stimulus Strength	194
7.4.1.2	Effect of Varying Stimulus Frequency	195
7.4.2	Effect of Low- and High-frequency Autonomic Nerve Stimulation on Atrio-ventricular Delay	197
7.4.3	Effect of Autonomic Stimulation on Left Ventricular Pressure at Different Stimulation Frequencies	200
7.4.4	Effect of Autonomic Stimulation on Ventricular Electrophysiology	201

7.4.4.1	Effect of Autonomic Stimulation on Ventricular Fibrillation Thresholds	201
7.4.4.2	Effect of Autonomic Stimulation on Action Potential Duration-Restitution and Restitution Dispersion	203
7.4.4.2.1	Effect of Sympathetic and Vagus Nerve Stimulation on Action Potential Duration Restitution	203
7.4.4.2.2	Effect of Sympathetic and Vagus Nerve Stimulation on Apico-basal Restitution Dispersion	205
7.4.4.3	Effect of Autonomic Stimulation on Ventricular Refractoriness	206
7.5	Discussion	207
7.5.1	Effect of Autonomic Nerve Stimulation on Intrinsic Heart Rate	207
7.5.2	Effect of Autonomic Nerve Stimulation on Atrio- ventricular Delay	209
7.5.3	Effect of Autonomic Nerve Stimulation on Left Ventricular Contractility	211
7.5.4	Effect of Autonomic Nerve Stimulation on Ventricular Electrophysiology	211
7.5.4.1	Electrical Restitution, Spatial Restitution Dispersion and Ventricular Fibrillation Inducibility in Normal Hearts and Heart Failure ..	212
7.5.4.2	Autonomic Modulation of Electrical Restitution and Ventricular Refractoriness in Normal Hearts and Heart Failure	213
7.5.4.3	Mechanisms of Neuro-cardiac Remodelling in the Failing Ventricles	215
7.6	Conclusion	217
7.7	References	217

Chapter 8: Synopsis 224 – 235

8.1	Introduction	225
8.2	Sympatho-vagal Interaction in Isolated Dual-innervated Langendorff-perfused Rabbit Hearts	225
8.3	Effect of Beta-Blockade on Heart Rate and Ventricular Electrophysiology during Sympatho-vagal Interaction	226
8.4	Development of a Surgical Heart Failure Model in Rabbits by Coronary Ligation	228
8.5	Structural Remodelling in Heart Failure	229
8.6	Characterisation of Electrophysiologic Response under Autonomic Stimulation in Heart Failure	230
8.7	Future Direction	233
8.8	References	233

List of Tables

CHAPTER 1

Table 1.1	Aetiology of Heart Failure	6
Table 1.2	Experimental mouse models on β-AR signalling and myocardial pathology.....	18

CHAPTER 3

Table 3.1	Common animal models of heart failure	62
Table 3.2	Refinements developed during the course of building a surgical heart failure model in rabbits	75

CHAPTER 6

Table 6.1	Echocardiographic data of rabbits in heart failure (HF) and sham (SHM) group	176
Table 6.2	Body weights as well as wet/dry weights of hearts, livers and lungs for rabbits in heart failure (HF) and sham (SHM) groups	179
Table 6.3	Scar volume measured by ex-vivo cardiac magnetic resonance imaging.....	181

CHAPTER 7

Table 7.1	Summary of baseline pre-stimulation values	196
-----------	--	-----

List of Figures

CHAPTER 3

Figure 3.1	Apical infarct following ligation of circumflex artery in rabbit heart	68
Figure 3.2	Overall survival in rabbits undergoing coronary ligation and sham procedures	69
Figure 3.3	Premature mortality by pre-operative rabbit weight	70
Figure 3.4	Overall survival of rabbits by procedure type	71
Figure 3.5	Survival rate of rabbits undergoing coronary ligation (HF) vs. sham (SHM) procedures	71
Figure 3.6	Timing of premature mortality in rabbits	72
Figure 3.7	Histopathological findings in rabbits undergoing post-mortem examination following premature death	73
Figure 3.8	Timing of post-operative premature mortality in rabbits	73
Figure 3.9	Temporal association of refinements with premature post-operative mortality in rabbits	78
Figure 3.10	Time trend of percentage premature mortality in rabbits	79
Figure 3.11	Parasternal echocardiographic windows in rabbits illustrating long-axis view of mitral valve in M-mode (Figure 3.11a) and short axis view of basal left ventricle (Figure 3.11b).....	83
Figure 3.12	Langendorff-perfused rabbit heart preparation with intact dual-autonomic innervation	87
Figure 3.13	An example of MAP Recording with VF induction by burst pacing following a drive train at 240 ms cycle length.....	90
Figure 3.14	Figure 3.14 MAP recordings during an S1-S2 protocol at 240 ms S1 cycle length, with S2 capturing the ventricle in one drive train (Figure 3.14a) but failing to capture the ventricle in the next drive train (Figure 3.14b).....	91
Figure 3.15	Sagittal representation of rabbit heart taken from 3D T1-weighted MP-RAGE scan (a) with superimposed scar region	

(b) (highlighted red) generated by semi-automated region growing analysis in 3D Slicer	94
--	----

CHAPTER 4

Figure 4.1 An example of intrinsic heart rate changes following low- or high-frequency sympathetic nerve stimulation at baseline (Figure 4.1A) and with concurrent high-frequency vagus nerve stimulation (Figure 4.1B)	109
Figure 4.2 Absolute heart rate (Figure 4.2A) and relative heart rate changes (Figure 4.2B) following low- (LS) and high-frequency (HS) sympathetic stimulation at baseline (BL), as well as following low- (HV-LS) and high-frequency (HV-HS) sympathetic stimulation with concurrent high-frequency vagal stimulation (HV)	110
Figure 4.3 An example of intrinsic heart rate changes following low- or high-frequency vagus nerve stimulation at baseline (Figure 4.3A) and with concurrent high-frequency sympathetic nerve stimulation (Figure 4.3B)	111
Figure 4.4 Absolute heart rate (Figure 4.4A) and relative heart rate changes (Figure 4.4B) following low- (LV) and high-frequency (HV) vagal stimulation at baseline (BL), as well as following low- (HS-LV) and high-frequency (HS-HV) vagal stimulation with concurrent high-frequency sympathetic stimulation (HS) ..	112
Figure 4.5 Comparison of expected (algebraic summed) and observed heart rate changes during sympatho-vagal interaction.....	113
Figure 4.6 Absolute ventricular fibrillation threshold (VFT) (Figure 4.6A) and relative VFT changes (Figure 4.6B) at baseline (BL), following low- (LS) and high-frequency (HS) sympathetic stimulation, high-frequency vagal stimulation (HV) and during vago-sympathetic interaction (HV-LS, HV-HS)	114
Figure 4.7 Absolute ventricular fibrillation threshold (VFT) (Figure 4.7A) and relative VFT changes (Figure 4.7B) at baseline (BL),	

following low- (LV) and high-frequency (HV) vagal stimulation, high-frequency sympathetic stimulation (HV) and during sympatho-vagal interaction (HS-LV, HS-HV)	116
Figure 4.8 Comparison of expected (algebraic summed) and observed ventricular fibrillation threshold (VFT) changes during vago-sympathetic (Figure 4.8A) and sympatho-vagal interactions (Figure 4.8B)	117
Figure 4.9 An example of action potential duration (APD)-restitution (RT) curves with steepest slope gradients (r) measured at baseline (BL), following low- (LS) and high-frequency (HS) sympathetic stimulation (Figure 4.9A) as well as during vago-sympathetic interaction (Figure 4.9B) with concurrent high-frequency vagal stimulation (HV)	119
Figure 4.10 Absolute restitution slope gradients (Figure 4.10A) and relative changes (Figure 4.10B) at baseline (BL), following low- (LS) and high-frequency (HS) sympathetic stimulation, high-frequency (HV) vagal stimulation and during vago-sympathetic interactions (HV-LS, HV-HS)	120
Figure 4.11 An example of action potential duration (APD)-restitution (RT) curves with steepest slope gradients (r) measured at baseline (BL), following low- (LV) and high-frequency (HV) vagal stimulation (Figure 4.11A) as well as during sympatho-vagal interaction (Figure 4.11B) with concurrent high-frequency sympathetic stimulation (HS)	122
Figure 4.12 Absolute restitution slope gradients (Figure 4.12A) and relative changes (Figure 4.12B) at baseline (BL), following low- (LV) and high-frequency (HV) vagal stimulation, high-frequency (HS) sympathetic stimulation and during sympatho-vagal interactions (HS-LV, HS-HV)	123
Figure 4.13 Absolute ventricular effective refractory period (ERP) (Figure 4.13A) and ERP changes (Figure 4.13B) at baseline (BL), following low- (LS) and high-frequency (HS) sympathetic stimulation, high-frequency vagal stimulation (HV) and during	

vago-sympathetic interaction (HV-LS, HV-HS).....	124
Figure 4.14 Absolute ventricular effective refractory period (ERP) (Figure 4.14A) and ERP changes (Figure 4.14B) at baseline (BL), following low- (LV) and high-frequency (HV) vagal stimulation, high-frequency sympathetic stimulation (HS) and during sympatho-vagal interaction (HS-LV, HS-HV)	126
Figure 4.15 Comparison of expected (algebraic summed) and observed ventricular effective refractory period (VFT) changes during vago-sympathetic (Figure 4.15A) and sympatho-vagal interactions (Figure 4.15B)	127

CHAPTER 5

Figure 5.1 Intrinsic heart rate at baseline (BL), during low- (LV) and high-frequency (HV) vagal stimulation, high-frequency sympathetic stimulation (HS) and sympatho-vagal interaction (HS-LV, HS-HV) prior to commencing burst pacing (Figure 5.1A) or S1-S2 pacing protocol (Figure 5.1B) in control condition, during metoprolol infusion and following washout	145
Figure 5.2 Intrinsic heart rate at baseline, during high-frequency vagal stimulation (VNS) (Figure 5.2A) and sympatho-vagal interaction (Figure 5.2B) with and without metoprolol in a typical experiment.....	146
Figure 5.3 Ventricular fibrillation threshold (VFT) at baseline (BL), during low- (LV) and high-frequency (HV) vagal stimulation, high-frequency sympathetic stimulation (HS) and sympatho-vagal interaction (HS-LV, HS-HV) in control condition, during metoprolol infusion and following washout	149
Figure 5.4 Maximum action-potential duration restitution (RT) slope gradients at baseline (BL), during low- (LV) and high-frequency (HV) vagal stimulation, high-frequency sympathetic stimulation (HS) and sympatho-vagal interaction (HS-LV, HS-HV) in control condition and during metoprolol infusion.....	150

Figure 5.5	Relative changes in maximum restitution (RT) slope gradients from baseline values during vagal stimulation and sympatho-vagal interactions in control condition and following metoprolol infusion	151
Figure 5.6	Ventricular effective refractory period (V-ERP) at baseline (BL), during low- (LV) and high-frequency (HV) vagal stimulation, high-frequency sympathetic stimulation (HS) and sympatho-vagal interaction (HS-LV, HS-HV) in control condition, during metoprolol infusion and following washout	152
Figure 5.7	Intrinsic heart rate at baseline (BL), during low- (LV) and high-frequency (HV) vagal stimulation, high-frequency sympathetic stimulation (HS) and sympatho-vagal interaction (HS-LV, HS-HV) in control condition, during metoprolol infusion and following washout in Langendorff rabbit's heart preparation perfused with acetate-containing Tyrode solution.....	154
Figure 5.8	Absolute heart rate changes during low- (LV) and high-frequency (HV) vagal stimulation at baseline (BL) and with concurrent high-frequency sympathetic stimulation (HS) in control condition (Figure 5.7A) as well as during metoprolol infusion (Figure 5.7B) in Langendorff rabbit's heart preparation perfused with acetate-containing Tyrode solution.....	155
Figure 5.9	Ventricular fibrillation thresholds (VFT) at baseline (BL), during low- (LV) and high-frequency (HV) vagal stimulation, high-frequency sympathetic stimulation (HS) and sympatho-vagal interaction (HS-LV, HS-HV) in control condition, during metoprolol infusion and following washout in Langendorff rabbit's heart preparation perfused with acetate-containing Tyrode solution	156
Figure 5.10	Absolute changes in ventricular fibrillation threshold (VFT) during low- (LV) and high-frequency (HV) vagal stimulation at baseline (BL) and with concurrent high-frequency sympathetic stimulation (HS) in control condition (Figure 5.7A) as well as during metoprolol infusion (Figure 5.7B) in Langendorff rabbit's	

heart preparation perfused with acetate-containing Tyrode solution	157
Figure 5.11 Comparison of heart rate and ventricular fibrillation threshold between acetate-containing and acetate-free Tyrode solutions at control condition, during metoprolol infusion and following washout	158

CHAPTER 6

Figure 6.1 Ex-vivo T2-weighted 2D slice montage representations of rabbit hearts eight weeks following coronary ligation (Figure 6.1A) or sham procedures (Figure 6.1B)	174
Figure 6.2 Gross appearance of rabbit heart eight weeks after coronary ligation	175
Figure 6.3 Correlation between left ventricular end-diastolic diameter (LVEDD) and left ventricular ejection fraction (EF)	177
Figure 6.4 Correlation between left atrial systolic diameter (LAD) and left ventricular ejection fraction (EF).....	177
Figure 6.5 Correlation between left ventricular ejection fraction (EF) with various organ weights corrected by body weight: heart dry weight (Figure 6.5A), liver wet weight (Figure 6.5B) and lung wet weight (Figure 6.5C)	180

CHAPTER 7

Figure 7.1 Comparison of heart rate changes with increasing stimulus strength between heart failure (HF) and sham (SHM) groups during vagus nerve stimulation (VNS) and sympathetic stimulation (SNS)	195
Figure 7.2 Comparison of heart rate changes with increasing stimulus frequency between heart failure (HF) and sham (SHM) groups during vagus nerve stimulation (VNS) and sympathetic	

stimulation (SNS)	197
Figure 7.3 Atrio-ventricular delay (AVD) measured under constant atrial pacing at 300 ms cycle length with MAP recordings from an unstimulated Langendorff's heart preparation in heart failure (HF) and sham (SHM) groups. Action potential duration was noted to be longer in HF group (data not shown).....	198
Figure 7.4 Comparison of atrio-ventricular (AV) delay (Figure 7.4A, 7.4C) and changes in AV delay (Figure 7.4B, 7.4D) between heart failure (HF) and sham (SHM) groups at baseline as well as during right and left vagal stimulation	199
Figure 7.5 Comparison of atrio-ventricular (AV) delay (Figure 7.5A) and changes in AV delay (Figure 7.5B) between heart failure (HF) and sham (SHM) groups at baseline and during sympathetic stimulation	200
Figure 7.6 Comparison of changes in left ventricular peak pressure with increasing stimulus frequency between heart failure (HF) and sham (SHM) groups during vagus nerve stimulation (VNS) (Figure 7.6A and 7.6B) and sympathetic stimulation (SNS) (Figure 7.6C)	201
Figure 7.7 Comparison of ventricular fibrillation threshold (Figure 7.7A) and relative changes from baseline (Figure 7.7B) between heart failure (HF) and sham (SHM) groups at baseline (BL), during sympathetic (SNS) and vagal (VNS) stimulations	202
Figure 7.8 Comparison of basal (Figure 7.8A) and apical (Figure 7.8B) action potential duration-restitution (APD-RT) between heart failure (HF) and sham (SHM) groups at baseline (BL), during sympathetic (SNS) and vagal (VNS) stimulations	204
Figure 7.9 Comparison of relative changes from baseline values in basal (Figure 7.9A) and apical (Figure 7.9B) action potential duration- restitution (APD-RT) between heart failure (HF) and sham (SHM) groups during sympathetic (SNS) and vagal (VNS) stimulations	204
Figure 7.10 Comparison of relative apico-basal restitution (RT) dispersion	

between heart failure (HF) and sham (SHM) groups.....	205
Figure 7.11 Comparison of ventricular effective refractory period (Figure 7.10A) and relative changes from baseline (Figure 7.10B) between heart failure (HF) and sham (SHM) groups at baseline (BL), during sympathetic (SNS) and vagal (VNS) stimulations ...	206

List of Abbreviations

CHAPTER 1

AC	Adenyl cyclase
Ach	Acetylcholine
AHA	American Heart Association
AKAP	A-kinase anchoring proteins
APD	Action potential duration
AR	Adrenoreceptor
ARI	Activation recovery interval
ATRAMI	Autonomic Tone and Reflexes After Myocardial Infarction
AV	Atrio-ventricular
BRS	Baroreflex sensitivity
Ca ²⁺	Calcium ion
cAMP	Cyclic adenosine monophosphate
CIBIS-II	Cardiac Insufficiency Bisoprolol Study-II
[¹¹ C]-mHED	[¹¹ C]-Meta-Hydroxyephedrine
DHPG	Dihydroxyphenylglycol
DI	Diastolic interval
ERP	Effective refractory period
Extr	Extraction
[¹⁸ F]-LMI1195.....	1-(3-bromo-4-(3-(18)F-fluoro-propoxy)benzyl)guanidine
G _i	Inhibitory G protein
G _s	Stimulatory G protein
GRK5	G protein-coupled receptor kinase 5
HF	Heart failure
HR	Heart rate
HRV	Heart rate variability
I-1	Inhibitor -1
I _{Ks}	Slow delayed rectifier potassium current
([¹²³ I]-MIBG	[¹²³ Iodine]-Metaiodobenzylguanidine

INOVATE-HF.....	Increase of Vagal Tone in Heart Failure
IR	Ischaemia-reperfusion
KCNQ1	Potassium voltage-gated channel subfamily Q member 1
KO	Knockout
LAD	Left anterior descending artery
LCSD	Left cardiac sympathetic denervation
LTCC	L-type calcium channel
LV	Left ventricle
mAChRs	Muscarinic acetylcholine receptors
MERIT-HF	Metoprolol Randomized Intervention Trial in Congestive Heart Failure
MI	Myocardial infarction
mRNA	Messenger ribonucleic acid
MSNA	Skeletal muscle sympathetic nerve activity
NE	Norepinephrine
NEa	Arterial concentration of norepinephrine
NEv	Venous concentration of norepinephrine
NECTAR-HF.....	Neural Cardiac Therapy for Heart Failure
NES	Norepinephrine spillover
NGF	Nerve growth factor
NHANES-1	National Health and Nutrition Examination Survey
NO	Nitric oxide
NOS	Nitric oxide synthase
NYHA	New York Heart Association
PF	Plasma flow
PKA	Protein kinase A
PLB	Phospholamban
REACH	Resource Utilization Among Congestive Heart Failure
RyR2	Ryanodine receptor 2
SCD	Sudden cardiac death
SR	Sarcoplasmic reticulum
TAC	Transaortic constriction
TG	Transgenic

UK-HEART	United Kingdom Heart Failure Evaluation and Assessment of Risk Trial
VF	Ventricular fibrillation
VNS	Vagus nerve stimulation

CHAPTER 3

ANOVA	Analysis of variance
CaCl ₂	Calcium chloride
CRF	Central research facility
DC	Direct current
DI	Diastolic interval
ECG	Electrocardiograph
ET	Endotracheal
ERP	Effective refractory period
FSE	Fast spin echo
HF	Heart failure
IVS.....	Interventricular septal thickness
LAD	Left atrial systolic diameter
LVEDD	Left ventricular end-diastolic diameter
LVPW.....	Left ventricular posterior wall thickness
MAPs	Monophasic action potentials
MAPD	Monophasic action potential duration
KCl	Potassium chloride
LVNS	Left vagus nerve stimulation
LVP	Left ventricular pressure
MgCl ₂	Magnesium chloride
MP-RAGE	Magnetization prepared rapid gradient-echo
MRI	Magnetic resonance imaging
Na ⁺ /Ca ⁺	Sodium/calcium
NaCl	Sodium chloride
NaHCO ₃	Sodium hydrogen carbonate
NaH ₂ PO ₄	Sodium dihydrogen phosphate

PP	Perfusion pressure
PRESS	Point resolved spectroscopy
RA _{EG}	Right atrial electrogram
RF	Radiofrequency
RV	Right ventricular
RVNS	Right vagus nerve stimulation
SHM	Sham
SNS	Sympathetic nerve stimulation
VF	Ventricular fibrillation
VFT	Ventricular fibrillation threshold

CHAPTER 4

APD	Action potential duration
APD ₉₀	Action potential duration at 90% repolarization
BL	Baseline
DI	Diastolic interval
ERP	Effective refractory period
Gi	Inhibitory G protein
HR	Heart rate
HS	High-frequency sympathetic nerve stimulation
HV	High-frequency vagus nerve stimulation
I _{CaL}	L-type calcium current
I _f	“Pacemaker” current
I _{K(Ach)}	Acetylcholine-activated potassium current
I _{Kr}	Rapid delayed-rectifier potassium current
LS	Low-frequency sympathetic nerve stimulation
LV	Low-frequency vagus nerve stimulation
MAP	Monophasic action potential
r	Maximum restitution slope gradient
RT	Restitution
SNS	Sympathetic nerve stimulation
VF	Ventricular fibrillation

VFT	Ventricular fibrillation threshold
VNS	Vagus nerve stimulation

CHAPTER 5

ANOVA	Analysis of normal variance
APD	Action potential duration
BL	Baseline
Ca ²⁺	Calcium
CaCl ₂	Calcium chloride
cAMP	Cyclic adenosine monophosphate
CAST	Cardiac Arrhythmia Suppression Trial
CIBIS-II	Cardiac Insufficiency Bisoprolol Study-II
ERP	Effective refractory period
G _s	Stimulatory G protein
HR	Heart rate
HS	High-frequency sympathetic nerve stimulation
HV	High-frequency vagus nerve stimulation
I _{K1}	Inward rectifier potassium current
I _{Kr}	Rapid delayed-rectifier potassium current
I _{ks}	Slow delayed-rectifier potassium current
I _{Na}	Inward sodium current
I _{to}	Transient outward current
KCl	Potassium chloride
LV	Low-frequency vagus nerve stimulation
MAP	Monophasic action potential
MgCl ₂	Magnesium chloride
MI	Myocardial infarction
NaCl	Sodium chloride
NaHCO ₃	Sodium hydrogen carbonate
NaH ₂ PO ₄	Sodium dihydrogen phosphate
PKA	Protein kinase A
ROS	Reactive oxygen species

RT	Restitution
SNS	Sympathetic nerve stimulation
V-ERP	Ventricular effective refractory period
VFT	Ventricular fibrillation threshold
VNS	Vagus nerve stimulation

CHAPTER 6

EF.....	Ejection fraction
FAC	Fractional area change
IVS	Interventricular septum
HF	Heart failure
LAD	Left atrial systolic diameter
LVEDD	Left ventricular end-diastolic diameter
LVPW	Left ventricular posterior wall
MP-RAGE	Magnetization prepared rapid gradient-echo
MRI	Magnetic resonance imaging
PRESS	Point resolved spectroscopy
RF	Radiofrequency
ROI	Region of interest
SHM	Sham

CHAPTER 7

APD	Action potential duration
AN	Atrio-nodal
AV	Atrio-ventricular
AVD	Atrio-ventricular delay
BL	Baseline
BRS	Baroreflex sensitivity
CaCl ₂	Calcium chloride
cAMP	Cyclic adenosine monophosphate

ERP	Effective refractory period
HCN	Hyperpolarization-activated, cyclic-nucleotide gated
hERG	Human ether-a-go-go-related gene
HF	Heart failure
HR	Heart rate
HRV	Heart rate variability
ICD	Implantable cardioverter-defibrillator
I_{Ca}	Inward calcium current
I_{CaL}	L-type calcium current
I_f	“Pacemaker” current
I_{K1}	Inward rectifier potassium current
I_{Kr}	Rapid delayed-rectifier potassium current
I_{Ks}	Slow delayed-rectifier potassium current
KCl	Potassium chloride
LVP	Left ventricular pressure
MAP	Monophasic action potential
MgCl ₂	Magnesium chloride
N	Nodal
NaCl	Sodium chloride
NaHCO ₃	Sodium hydrogen carbonate
NaH ₂ PO ₄	Sodium dihydrogen phosphate
NH	Nodal-His
PKA	Protein kinase A
RT	Restitution
SA	Sino-atrial
SHM	Sham
SNS	Sympathetic nerve stimulation
VF	Ventricular fibrillation
VFT	Ventricular fibrillation threshold
VNS	Vagus nerve stimulation

CHAPTER 8

APD	Action potential duration
APD-RT	Action potential duration-restitution
AV	Atrio-ventricular
ECG	Electrocardiogram
ERP	Effective refractory period
HF	Heart failure
MRI	Magnetic resonance imaging
SHM	Sham
VFT	Ventricular fibrillation threshold

Conference Presentations by the Candidate

Oral Presentation with Published Abstract:

Chin SH, Winter J, Brack KE & Ng GA. Vago-sympathetic Interaction of Ventricular Fibrillation Inducibility in Isolated Rabbit Hearts, Winter J, Brack KE & Ng GA (2013). Vago-sympathetic Interaction of Ventricular Fibrillation Inducibility in Isolated Rabbit Hearts. Heart Rhythm Congress, Birmingham, UK.

Published Abstract: Chin SH, Winter J, Brack KE & Ng GA. Vago-sympathetic Interaction of Ventricular Fibrillation Inducibility in Isolated Rabbit Hearts: *Europace* 2013; 15(11) suppl 4: iv9

Late Breaking Poster Presentation:

Chin SH, Winter J, Brack KE, Ng GA (2013) *Vago-sympathetic Interaction on Heart Rate and Ventricular Fibrillation Inducibility in Isolated Rabbit Hearts*, 37th Congress of The International Union of Physiological Sciences, Birmingham, UK.

Poster Presentation with Published Abstract:

Chin SH, Brack KE, Ng GA (2014) *Sympathovagal Interaction on Heart Rate and Ventricular Fibrillation Inducibility*, World Congress in Cardiac Electrophysiology and Cardiac Techniques 2014, Nice, France.

Published Abstract: Chin SH, Brack KE, Ng GA. Sympatho-vagal Interaction on Heart Rate and Ventricular Fibrillation Inducibility. *Europace*. 2014; 16(6) suppl 2: ii8

Poster Presentation with Published Abstract:

Chin SH, Wake E, Brack KE, Ng GA (2014) *Modulation of Ventricular Fibrillation Inducibility and Electrical Restitution during Sympatho-vagal Interaction by Beta-blocker in Isolated Rabbit Hearts*. Heart Rhythm 2015, 36th Annual Scientific Session, Boston, Massachusetts, USA.

Published Abstract: Chin SH, Wake E, Brack KE, Ng GA. Modulation of Ventricular Fibrillation Inducibility and Electrical Restitution during Sympatho-vagal Interaction by Beta-blocker in Isolated Rabbit Hearts. *Heart Rhythm*. 2015; 12(5): S409

Poster Presentation with Published Abstract:

Chin SH, Wake E, Brack KE, Ng GA (2015) *The Effect of Sympatho-vagal Interaction and Beta-blocker on Heart Rate and Ventricular Refractoriness in Isolated Rabbit Hearts*, European Heart Rhythm Association Europace-Cardiostim 2015, Milan, Italy.

Published Abstract: Chin SH, Wake E, Brack KE, Ng GA. The Effect of Sympatho-vagal Interaction and Beta-blocker on Heart Rate and Ventricular Refractoriness in Isolated Rabbit Hearts. *Europace*. 2015; 17(suppl3): iii30 – iii55

Poster Presentation with Published Abstract:

Chin SH, Wake E, Brack KE, Ng GA (2015) *The Effect of Beta-blocker in Modulating Ventricular Fibrillation Inducibility and Electrical Restitution during Sympatho-vagal Interaction in Isolated Rabbit Hearts*, European Heart Rhythm Association Europace-Cardiostim 2015, Milan, Italy.

Published Abstract: Chin SH, Wake E, Brack KE, Ng GA. The Effect of Beta-blocker in Modulating Ventricular Fibrillation Inducibility and Electrical Restitution during Sympatho-vagal Interaction in Isolated Rabbit Hearts. *Europace*. 2015; 17(suppl3): iii3237 – iii259

Poster Presentation with Published Abstract:

Chin SH, Wake E, Kocsis-Fodor G, Brack KE, Ng GA (2016) *Autonomic Characterisation of Electro-Mechanical Remodelling in an In-vitro Leporine Model of Heart Failure*, Frontiers in CardioVascular Biology 2016, Florence, Italy.

Published Abstract: Chin SH, Wake E, Kocsis-Fodor G, Brack KE, Ng GA. Autonomic Characterisation of Electro-Mechanical Remodelling in an In-vitro Leporine Model of Heart Failure. *Cardiovasc Res*. 2016; 111(suppl1): S16– S42

Poster Presentation with Published Abstract:

Chin SH, Wake E, Kocsis-Fodor G, Brack KE, Ng GA (2016) *Autonomic Nerve Stimulation in an In-vitro Model of Heart Failure*, World Congress in Cardiac Electrophysiology and Cardiac Techniques 2016, Nice, France

Published Abstract: Chin SH, Wake E, Kocsis-Fodor G, Brack KE, Ng GA. Autonomic Nerve Stimulation in an In-vitro Model of Heart Failure. *Europace*. 2016; 18(suppl1): i1– i188

Other Oral and Poster Presentations during Candidacy

Oral Presentation with Published Abstract:

Chin SH, Varanasi S, Chu GS, Siddiqui S, Sandilands AJ, Stafford PJ & Ng GA (2014). *Is Multipolar Irrigated Catheter better than Conventional Focal Catheters in First-time Atrial Fibrillation Ablation?* Heart Rhythm Congress, Birmingham, UK.

Published Abstract: Chin SH, Varanasi S, Chu GS, Siddiqui S, Sandilands AJ, Stafford PJ & Ng GA. Is Multipolar Irrigated Catheter better than Conventional Focal Catheters in First-time Atrial Fibrillation Ablation? *Europace* 2014; 16(6) suppl 3: iii11

Moderated Poster Presentation with Published Abstract:

Chin SH, Varanasi S, Chu GS, Siddiqui S, Sandilands AJ, Stafford PJ & Ng GA (2013). *First Experience of the new nMARQ Multi-electrode Catheter for Mapping and Ablation of Paroxysmal and Persistent Atrial Fibrillation.* Finalist for chaired poster Ablation category, 6th Asia Pacific Heart Rhythm Society and CardioRhythm 2013, Hong Kong.

Published Abstract: Chin SH, Varanasi S, Chu GS, Siddiqui S, Sandilands AJ, Stafford PJ & Ng GA. First Experience of the new nMARQ Multi-electrode Catheter for Mapping and Ablation of Paroxysmal and Persistent Atrial Fibrillation. *Journal of Arrhythmia* 2013; 29(5): i226

Moderated Poster Presentation with Published Abstract:

Chin SH, Varanasi S, Chu GS, Siddiqui S, Man S, Somani R, Sandilands AJ, Stafford PJ & Ng GA (2015). *Superiority of Irrigated Multipolar Catheter over Conventional Catheters in Atrial Fibrillation Ablation.* European Heart Rhythm Association Europace-Cardiotim 2015, Milan, Italy.

Published Abstract: Chin SH, Varanasi S, Chu GS, Siddiqui S, Man S, Somani R, Sandilands AJ, Stafford PJ & Ng GA. Superiority of Irrigated Multipolar Catheter over Conventional Catheters in Atrial Fibrillation Ablation. *Europace* 2015; 17(6) suppl3: iii11

Poster Presentation with Published Abstract:

Chin SH, Varanasi S, Chu GS, Siddiqui S, Sandilands AJ, Stafford PJ & Ng GA (2014) *First Experience of the new nMARQ Multi-electrode Catheter for Mapping and Ablation of Paroxysmal and Persistent Atrial Fibrillation.* AF Symposium 2014, Orlando, Florida, USA

Published Abstract: Chin SH, Varanasi S, Chu GS, Siddiqui S, Sandilands AJ, Stafford PJ & Ng GA. First Experience of the new nMARQ Multi-electrode Catheter for Mapping and Ablation of Paroxysmal and Persistent Atrial Fibrillation. *J Cardiovasc Electrophysiol.* 2014; 25(5): 559

Poster Presentation with Published Abstract:

Chin SH, Winter J, Brack KE & Ng GA (2014) *Sympathetic Nerve Stimulation Increases Spatial Heterogeneity of Electrical Restitution in Isolated Rabbit Hearts.* Heart Rhythm 2014, 35th Annual Scientific Session, San Francisco, California, USA

Published Abstract: Chin SH, Winter J, Brack KE & Ng GA. Sympathetic Nerve Stimulation Increases Spatial Heterogeneity of Electrical Restitution in Isolated Rabbit Hearts. *Heart Rhythm.* 2014; 11(5): S420

Poster Presentation with Published Abstract:

Chin SH, Varanasi S, Chu GS, Siddiqui S, Sandilands AJ, Stafford PJ & Ng GA (2014) *Comparison of the new nMARQ Catheter for Atrial Fibrillation Ablation with Conventional Technique: Short-term Clinical Effectiveness and Safety.* Heart Rhythm 2014, 35th Annual Scientific Session, San Francisco, California, USA

Published Abstract: Chin SH, Varanasi S, Chu GS, Siddiqui S, Sandilands AJ, Stafford PJ & Ng GA. Comparison of the new nMARQ Catheter for Atrial Fibrillation Ablation with Conventional Technique: Short-term Clinical Effectiveness and Safety. *Heart Rhythm.* 2014; 11(5): S523

Poster Presentation with Published Abstract:

Chin SH, Winter J, Brack KE & Ng GA (2014) *Spatial Heterogeneity of Electrical Restitution by Sympathetic Nerve Stimulation in Isolated Rabbit Hearts*. World Congress in Cardiac Electrophysiology and Cardiac Techniques 2014, Nice, France

Published Abstract: Chin SH, Winter J, Brack KE & Ng GA. Spatial Heterogeneity of Electrical Restitution by Sympathetic Nerve Stimulation in Isolated Rabbit Hearts.

Europace. 2014; 16(6) suppl2: ii67

Poster Presentation with Published Abstract:/

Chin SH, Varanasi S, Chu GS, Siddiqui S, Sandilands AJ, Stafford PJ & Ng GA (2014) *Comparison of the new nMARQ Catheter for Atrial Fibrillation Ablation with Conventional Technique: Short-term Clinical Effectiveness and Safety*. World Congress in Cardiac Electrophysiology and Cardiac Techniques 2014, Nice, France

Published Abstract: Chin SH, Varanasi S, Chu GS, Siddiqui S, Sandilands AJ, Stafford PJ & Ng GA. Comparison of the new nMARQ Catheter for Atrial Fibrillation Ablation with Conventional Technique: Short-term Clinical Effectiveness and Safety. *Europace*. 2014; 16(6) suppl2: ii130 (doi: <http://dx.doi.org/10.1093/europace/euu115>)

Poster Presentation with Published Abstract:

Chin SH, Varanasi S, Chu GS, Siddiqui S, Sandilands AJ, Stafford PJ & Ng GA (2014) *Short-term Ablation Outcome and Safety Profile of nMARQ Catheter in Atrial Fibrillation Ablation in Comparison to Conventional Catheters*. European Society of Cardiology Congress, Barcelona, Spain

Published Abstract: Chin SH, Varanasi S, Chu GS, Siddiqui S, Sandilands AJ, Stafford PJ & Ng GA. Short-term Ablation Outcome and Safety Profile of nMARQ Catheter in Atrial Fibrillation Ablation in Comparison to Conventional Catheters. *Eur Heart J*. 2014; 35(suppl 1): 513 – 850 (doi: <http://dx.doi.org/10.1093/eurheartj/ehu324>)

Poster Presentation with Published Abstract:

Chin SH, Varanasi S, Chu GS, Siddiqui S, Sandilands AJ, Stafford PJ & Ng GA (2014)

Novel Use of Irrigated Multipolar Catheter beyond Pulmonary Vein Isolation in Atrial Fibrillation Ablation. Heart Rhythm 2015, 36th Annual Scientific Session, Boston, Massachusetts, USA.

Published Abstract: Chin SH, Varanasi S, Chu GS, Siddiqui S, Man S, Somani R, Sandilands AJ, Stafford PJ & Ng GA. Novel Use of Irrigated Multipolar Catheter beyond Pulmonary Vein Isolation in Atrial Fibrillation Ablation. *Heart Rhythm.* 2015; 12(5) S183 (doi: <http://dx.doi.org/10.1016/j.hrthm.2015.03.052>)

Poster Presentation with Published Abstract:

Chin SH, Varanasi S, Chu GS, Siddiqui S, Man S, Somani R, Sandilands AJ, Stafford PJ & Ng GA (2015). *Novel Experience of Irrigated Multipolar Catheter in Stepwise Approach for Atrial Fibrillation Ablation.* European Heart Rhythm Association Europace-Cardiotim 2015, Milan, Italy.

Published Abstract: Chin SH, Varanasi S, Chu GS, Siddiqui S, Man S, Somani R, Sandilands AJ, Stafford PJ & Ng GA. Novel Experience of Irrigated Multipolar Catheter in Stepwise Approach for Atrial Fibrillation Ablation. *Europace* 2015; 17(6) suppl3: iii30 – iii55 (doi: <http://dx.doi.org/10.1093/europace/euv156>)

External Academic Engagement during Candidacy

2013 – 2016

Co-ordinator of clinical trial INOVATE-HF as chief-investigator site in the UK

2013 – 2016

Financial co-ordinator for all clinical trials under the Neuro-Cardiology group,
Department of Cardiovascular Sciences, University of Leicester

2013 – 2015

Laboratory supervision of iBSc students assigned to the Neuro-Cardiology group,
Department of Cardiovascular Sciences, University of Leicester

Chapter 1

Heart Failure and Dysautonomia

Autonomic Modulation in a Rabbit Model of Heart Failure

Chapter 1: Heart Failure and Dysautonomia

1.1 Background

Abnormal autonomic tone, otherwise known as dysautonomia, is the hallmark of certain cardiac conditions including myocardial ischaemia and infarction, heart failure (HF) and sudden cardiac death (SCD). Indeed, clinical measurement of autonomic disturbance provides a robust prognostic marker for mortality, in particular SCD (Gunther et al., 2010, Mazzeo et al., 2011, Ponikowski et al., 1997, Vinik et al., 2011). The autonomic nervous system has historically played a paramount role in the development, maintenance and interruption of ventricular arrhythmias (Tomaselli and Zipes, 2004), especially in the context of ventricular fibrillation (VF), a major cause of SCD. Sympathetic nerve stimulation precipitates VF, and conversely vagal stimulation exerts direct protective anti-VF effects in the normal heart (Brack et al., 2011, Ng et al., 2007). Understanding the mechanisms of autonomic modulation of VF will provide us an insight to development of novel strategies for prophylaxis against these ventricular arrhythmias with high fatality. This is particularly relevant in the HF population where mortality due to arrhythmic death is proportionally higher in the lower NYHA classes (Hjalmarson and Fagerberg, 2000).

This chapter summarizes experimental evidence encompassing our understanding of autonomic neural regulation that characterises the brain-heart axis, outlines different methods of assessing sympathetic and parasympathetic activities, and discusses potential therapeutic implications of autonomic modulation in heart failure patients.

1.2 Heart Failure

1.2.1 Definition of Heart Failure

Heart Failure is a clinical syndrome characterised by poor tissue perfusion and fatigue of all dimensions due to underlying cardiac pump dysfunction. Conventionally cardiac pump dysfunction has been described in the form of impaired ventricular contraction (namely *systolic* dysfunction) or less commonly impaired ventricular filling (namely

diastolic dysfunction). Although the arbitrary subdivision of heart failure into two distinctive pathologies may aid in clinical management, it is increasingly recognised that these two entities could arguably, though inconclusively, be physiologically linked (De Keulenaer and Brutsaert, 2011, Borlaug and Redfield, 2011). This is further corroborated by the linear relationship between different cardiac indexes indicative of diastolic and systolic impairments over a wide spectrum of ventricular ejection fractions (Yip et al., 2002, Komamura, 2013, Januzzi et al., 2006, De Keulenaer and Brutsaert, 2009, Chatterjee and Massie, 2007). Therefore, the artificial subdivision of the heart failure into two entities may appear pragmatic but ultimately flawed conceptually, indirectly demonstrating the heterogeneity of clinical spectrum in heart failure.

1.2.2 Epidemiology of Heart Failure

The clinical and financial burden imposed by heart failure is well recognised. Symptomatic heart failure afflicts up to 15 million people worldwide as reported by the American Heart Association (AHA) 2004 update on Heart Disease and Stroke. Specifically, in the United States, 5 million people are estimated to have heart failure, with 55,000 new diagnoses annually (Thom et al., 2006). In the Framingham Study, the screening rate for heart failure is 3/1000 cases, with all identified subjects no older than 63 years old (McKee et al., 1971). At the end of a 34-year follow-up, there is an age-dependent increase in the estimated prevalence of heart failure: the prevalence for the groups aged below 60 years of age was 8/1000 cases vs. 91/1000 cases in groups aged beyond 80 years of age (Ho et al., 1993).

Other studies attempted to refine the epidemiology of heart failure with objective assessment of cardiac dysfunction. By defining heart failure as left ventricular ejection fraction <30% on echocardiography, a study from Scotland conducted in a cohort of 2000 subjects aged 25-74 years living in Glasgow reported an overall heart failure prevalence of 2.9% (McDonagh et al., 1997). Symptomatic heart failure was found in 1.5% of the cohort. Heart failure was also shown to have predilection in male and older age: 6.4% prevalence in men aged 65-74 years compared to 4.9% in women of identical age group. A study in Minnesota investigated the prevalence of systolic and diastolic dysfunctions, reporting an overall prevalence of 6% for systolic dysfunction and up to 21% for diastolic

dysfunction (Redfield et al., 2003). This prevalence reduced with the severity of the systolic and/or diastolic dysfunction. The prevalence for moderate or severe systolic dysfunction was 2% whereas that for moderate or severe diastolic dysfunction was 6.7%. Interestingly in this study, there was a prevalence of 5.6% in moderate or severe diastolic dysfunction with normal ejection fraction. Less than 50% of those with moderate or severe diastolic or systolic dysfunction had clinically recognised heart failure despite prognostic implications in all-cause mortality.

With increasing life expectancy, both the prevalence and the incidence of heart failure are projected to increase rapidly. In the general population, the unadjusted prevalence ranges 3 - 20/100 with the crude incidence being 1 – 5 cases/1000 (McMurray and Stewart, 2000). In one study, age- and gender-adjusted prevalence was found to almost tripled over the decade of the 1990's (McCullough et al., 2002). A study in the United Kingdom demonstrated an annual referral rate of 6.5/1000 to a heart failure clinic in a cohort of 150,000 people, 29% of whom with subsequent clear diagnoses, giving rise to an annual heart failure incidence of 1.85/1000 (Cowie et al., 1999). A Canadian study has projected at least doubling of the incidence of heart failure hospital admission by the year 2025 (Johansen et al., 2003).

1.2.3 Aetiology of Heart Failure

Heart failure represents the end stage of various forms of cardiovascular disease, accounting for its heterogeneity in clinical spectrum. The aetiology can broadly be divided into several types: cardiomyopathies, overloading conditions on the myocardium, pericardial abnormalities, or arrhythmias (Table 1.1). Although the culprit cardiac conditions have been identified, the mechanistic nature of the initial cardiac injury leading to ventricular impairment in heart failure remains unclear. The link between structural and functional changes is complex and multi-modal, involving neuro-humoral, vascular and other extra-cardiac pathologies, all contributing to debilitating symptoms and premature deaths.

Data from Framingham study has provided invaluable insights into the natural history of relative attribution of various cardiovascular diseases to heart failure since the 1950's

(Kannel and Belanger, 1991). Hypertension was initially accountable for 39% of heart failure in males and 59% in females. Previous myocardial infarction was the second commonest aetiology for heart failure in males (34%) and females (13%), followed by valvular heart disease accounting for 7-8% of heart failure. Over the next two decades, the relative contribution of hypertension and valvular heart disease dwindled as ischaemic heart disease become more prevalent as the etiologic contribution to heart failure, increasing from 22% to about 70%. In contrast, diabetes mellitus maintain as a strong risk factor for heart failure, with diabetic women having an annual heart failure incidence of 3.0% compared to 0.4% in non-diabetic women (Bibbins-Domingo et al., 2004). Additional risk factors, including elevated body mass index, depressed creatinine clearance, raised fasting glucose level appears to further increase the annual heart failure incidence rate of the diabetics.

Table 1.1 Aetiology of heart failure

Aetiology	Cardiac insults	Pathologies
Cardiomyopathies	Ischaemic heart disease	Myocardial infarction/stunning/hibernation
	Genetic	Dilated cardiomyopathy Hypertrophic cardiomyopathy
	Infectious/inflammatory	Chagas disease
	Metabolic	Diabetes mellitus Obesity
	Toxic	Alcohol Anti-cancer drugs e.g. anthracyclines, doxorubicin
	Infiltrative	Amyloidosis Hemochromatosis
Myocardial Overload	Pressure overload	Hypertension Aortic stenosis
	Volume overload	Mitral regurgitation Aortic regurgitation
Conduction abnormalities	Dyssynchrony	Atrio-ventricular dyssynchrony Inter-ventricular dyssynchrony Intra-ventricular dyssynchrony
	Bradycardias	Sick sinus syndrome Heart block
	Tachycardias	Atrial fibrillation Pacing-induced cardiomyopathy
Pericardial diseases	Pericarditis	Constrictive pericarditis
	Pericardial effusions	Cardiac tamponade

1.2.4 Prognosis of Heart Failure

Heart failure imposes grave outcome in terms of morbidity and mortality (Arnold et al., 2007, Johansen et al., 2003, McDonagh et al., 1997, Thom et al., 2006). The Framingham Heart Study follow-up study reported that in the cohort of patients under 65 years of age, 80% of males and 70% of females diagnosed with heart failure died within 8 years. In particular, the 1-year mortality rate was reported to be as high as 20% whilst the 5-year mortality was 62% in male, and 42% in female. Indeed, sudden cardiac death occurs at 6 – 9 times the rate it occurs in the general population. Interestingly the mortality rate observed in the Metoprolol Randomized Intervention Trial in Congestive Heart Failure (MERIT-HF) over a 20-month period demonstrated sudden cardiac death to be of higher proportional attribution to the total mortality among those with mild-moderate heart failure compared to those with severe heart failure. Similarly, the Rochester epidemiology project that investigated 107 patients admitted with new onset heart failure in 1981 and 141 patients in 1991 reported a 1-year and 5-year mortality rate of 28% and 66% respectively in the 1981 cohort, and 23% and 67% in the 1991 cohort (Senni et al., 1999, Senni et al., 1998). In short, there is a lack of temporal evolution in the short and long-term prognosis of heart failure between these studies. In contrast, the National Health and Nutrition Examination Survey (NHANES-1) conducted between 1971 and 1975 concluded a lower 10-year mortality of 42.8% (49.8% in male and 36% in female) for subjects aged 25-74 years, and 65.4% (71.8% in male and 59.5% in female) for subjects aged 65-74 years correspondingly (Schocken et al., 1992). However, the findings from NHANES-1 were confounded by several points: 1) the patients were not institutionalised, 2) heart failure was self-reported and 3) follow-up was incomplete. In addition, there is a gender bias in heart failure survival with male having poorer prognosis. In the Resource Utilization Among Congestive Heart Failure (REACH) study, the overall median survival in female was 4.5 years compared to 3.7 years for male. These compared favourably with the previous data from the combined Framingham Heart and Offspring study cohorts reporting a median survival of 3.2 years for female and 1.7 years for male. It is noteworthy that both studies shared similar mean ages at diagnosis (REACH 69.5 ± 14.5 years vs. Framingham 70.0 ± 10.8 years) (Kannel et al., 1994, McCullough et al., 2002).

Hospital admission for heart failure has served as a useful and objective index of measurement for morbidity. Over the last 3 decades, heart failure has become the commonest cause for hospital admission (Haldeman et al., 1999). In the United Kingdom, this accounted for 0.2% hospital admission rate annually, constituting 4% of the combined adult and geriatric hospital admissions (McMurray et al., 1993). These hospital admissions were long with high readmission rate. The mean hospital stay for heart failure ranged from 11 days in the acute medical ward to 29 days in the geriatric wards. One third of these patients were readmitted with further symptoms of heart failure within 12 months. These trends were echoed in a Canadian study evaluating over 82000 heart failure patients in 1996-1997. The mean hospital stay was 26.9 days with a 50% hospital readmission rate within the first year of the study (Johansen et al., 2003).

1.3 Measurement of Sympathetic and Parasympathetic Nervous Systems Activity

Distinctive methods have been developed over the years for assessment of specific aspects of sympathetic and parasympathetic nervous systems. These non-invasive and invasive methods can complement one another, contributing to a global picture of autonomic status. Whilst these methods provided key insights into the abnormal autonomic characteristics in heart failure, they remain rooted in the realm of research, each with their unique strength and limitations.

1.3.1 Plasma Norepinephrine

Central catecholaminergic neurons synthesize norepinephrine (NE), epinephrine and dopamine, all of which are identified by immunoreactivity for tyrosine hydroxylase (Saper et al., 1991, Benarroch et al., 1998). Catecholamines have been implicated in modulation of sympathetic preganglionic neurons (Guyenet, 1991), facilitation of the baroreflex at the level of the nucleus of the solitary tract, presynaptic inhibition of C1 neurons, and stimulation of vasopressin and corticotrophin-releasing hormone from the hypothalamus (Chen et al., 2004).

Venous plasma NE represents a crude method of assessing sympathetic neural activity as it relies on the immediate rate of NE reuptake and clearance from circulation (Esler et al., 1990). As such, sympathetic hyperactivity are represented by increased plasma NE levels, central sympathetic outflow, and NE plasma spillover (Pepper and Lee, 1999). In normal healthy subjects, only a finite amount of NE released from sympathetic vesicles acts on postganglionic adrenoreceptors or spills over into plasma. However, in the presence of low cardiac output in heart failure, there is an increase in NE plasma spillover as a result of reduction of neuronal and extraneuronal clearances. Indeed, measurement of cardiac NE spillover was demonstrated by isotope dilution method to increase up to 50-fold, similar to levels observed in healthy hearts during maximal exercise (Morris et al., 1997).

The isotope dilution method was developed to increase the accuracy of plasma NE spillover measurement, taking into account of local neuronal and extraneuronal clearance mechanisms (Esler, 2010). In principle, total body plasma NE spillover is determined from dilution of tritium-labelled NE during its steady-state infusion in tracer concentrations through an organ. If arterial affluent and venous effluent are both collected simultaneously during the infusion of tritium-labelled NE, the local NE extraction (Extr) by neuronal and extraneuronal clearance systems can be calculated. As such, organ-specific NE spillover (NES) can be deduced from this equation: -

$$\text{NES} = [(NE_v - NE_a) + (NE_a \times \text{Extr})] \times PF$$

Where NE_a and NE_v represent arterial and venous concentrations of unlabelled NE respectively, and PF represents plasma flow.

Additionally, measurement of NE metabolites, i.e. tritium-labelled dihydroxyphenylglycol (DHPG), enhances understanding of the neuronal and extraneuronal clearance during abnormal NE spillover (Eisenhofer et al., 1992, Brunner-La Rocca et al., 2001). Whilst these mathematical models improve discrimination between central and regional NE spillover, other novel techniques including nuclear tracer imaging and microneurography have been developed to provide independent and

complementary topographical and functional information of sympathetic nervous activity.

1.3.2 Neural Tracer Imaging

Over the last few decades, neural imaging techniques have been developed and employed using several different tracers that allow for direct visualisation of sympathetic nervous innervation in the heart. These tracers target molecular landmarks at the presynaptic and postsynaptic side as well as second messenger systems of the sympathetic nervous system, and are thereby capable of portraying the overall picture of sympathetic signal transduction. The majority of these radiotracers mimic the structure of NE and other catecholamines to enable them to target the endogenous reuptake pathway of sympathetic neurons. These tracers are exemplified by labelled neurotransmitters ($[^{18}\text{F}]\text{-dopamine}$, $[^{11}\text{C}]\text{-epinephrine}$), “false neurotransmitters” serving as substrate analogues ($[^{123}\text{I}]\text{-MIBG}$, $[^{11}\text{C}]\text{-mHED}$, $[^{18}\text{F}]\text{-LMI1195}$, $[^{11}\text{C}]\text{-phenylephrine}$, $[^{11}\text{C}]\text{-phenethylguanidines}$), and uptake-1 inhibitors ($[^{11}\text{C}]\text{=methylreboxetine}$, $[^{11}\text{C}]\text{-desipramine}$). Each tracer possesses unique uptake and retention characteristics, contributing information on various aspects of neuronal reuptake, uptake-1 density, vesicular packaging, vesicular release, and NE metabolism. In heart failure, a chronic state of sympathetic overdrive fuels a decrease in neuronal reuptake, downregulation of uptake-1 and increased synaptic NE content and regional spillover.

The two most commonly utilised tracers in clinical practice are $[^{123}\text{Iodine}]\text{-Metaiodobenzylguanidine}$ ($[^{123}\text{I}]\text{-MIBG}$) and $[^{11}\text{C}]\text{-Meta-Hydroxyephedrine}$ ($[^{11}\text{C}]\text{-mHED}$). The former was first developed to image neuroendocrine tumours with early studies identified $[^{123}\text{I}]\text{-MIBG}$ uptake in myocardium in inverse correlation with plasma and urinary catecholamines (Nakajo et al., 1983) due to its high affinity to neuronal uptake-1 and extraneuronal uptake-2 (Degrado et al., 1995, Dae et al., 1995). Using semi-quantitative analyses in single-photon emission computed tomography (SPECT), an estimation of sympathetic tone can be inferred from the rate of $[^{123}\text{I}]\text{-MIBG}$ washout, as well as early and late heart-to-mediastinum ratios (Narula and Sarkar, 2003). Reduced late heart-to-mediastinum or raised $[^{123}\text{I}]\text{-MIBG}$ washout in semiquantitative myocardial $[^{123}\text{I}]\text{-MIBG}$ measurements has been shown to be a poor prognostic marker in a

systematic meta-analysis (Verberne et al., 2008). Conversely beta-blockade and renin-angiotensin–aldosterone inhibition are characterised by an increase in [¹²³I]-MIBG uptake and a reduced myocardial washout. Pertinently large-scale clinical trials have recognised [¹²³I]-MIBG imaging as an independent prognostic tool in identification of heart failure patients at the greatest risk of disease progression (Kasama et al., 2011, Boogers et al., 2010, Bax et al., 2008) and sudden cardiac death independent of left ventricular ejection fraction and B-type natriuretic peptide (Verberne et al., 2008, Tamaki et al., 2009, Kuramoto et al., 2011, Kioka et al., 2007, Jacobson et al., 2009).

In positron emission tomography (PET), [¹¹C]-mHED is the most widely used radiotracer for sympathetic neuronal imaging. As it is devoid of postsynaptic activity, the retention of [¹¹C]-mHED reflects solely presynaptic function of sympathetic neurons due to its selectivity for uptake-1 over other reuptake transporters (Foley et al., 2002). [¹¹C]-mHED has a predilection for tissue retention in organs with complex adrenergic networks including the heart, adrenal glands and spleen, with gradual accumulation in the liver. This is supported by the findings of selective competitive inhibitors of uptake-1, including true or false neurotransmitters, attenuating myocardial accumulation of [¹¹C]-mHED, with consequent increase in hepatic activity due to accumulation of metabolites (Tipre et al., 2008, Thackeray et al., 2013, Thackeray et al., 2007, Rosenspire et al., 1990, Law et al., 2010, Law et al., 1997, Degrado et al., 1995). High-speed liquid chromatography further confirmed plasma accumulation of [¹¹C]-mHED metabolites in guinea pigs and rats within 30 minutes after injection (Thackeray et al., 2007, Rosenspire et al., 1990, Law et al., 1997), and in human subjects within 10-20 minutes (Link et al., 1997).

1.3.3 Microneurography

Whilst neural tracer imaging provides a means of direct visualisation of sympathetic innervation, microneurography allows direct multi-fibre or single-fibre microelectrode measurements of post-ganglionic sympathetic nerve activity, thereby serving as a real-time recording of the dynamic sympathetic nerve and reflex controls (Wallin and Fagius, 1988, Elam and Macefield, 2001). Skin and muscle sympathetic nerves exhibit distinctive discharge patterns: the former preferentially responding to external acoustic, tactile or temperature stimuli independent of cardiac cycles whilst the latter being heavily

entrained by input from cardiopulmonary and arterial mechanoreceptors. As such, skeletal muscle sympathetic nerve activity (MSNA) possesses unique pulse-synchronicity, firing discharges 1.1 to 1.3 seconds after the preceding R wave of the electrocardiogram. At rest, MSNA is found to correlate with both cardiac and renal NE spillover whereas during isometric exercises, there is a concordant increase of sympathetic nerve activity between MSNA and cardiac NE spillover (Wallin et al., 1996, Wallin et al., 1992). This phenomenon is absent in heart failure (Rundqvist et al., 1997). Indeed, in heart failure, evidence of sympathetic hyperactivity manifested as increased firing probability and frequency with possible recruitment of otherwise silent sympathetic nerve fibres (Elam and Macefield, 2001).

1.3.4 Baroreflex Sensitivity

Baroreflex sensitivity (BRS) describes the acuity of arterial baroreceptor control of the heart rate in response to blood pressure changes. The heart rate changes in response to acute perturbation in blood pressure is thought to be an indication of reflex vagal response due to the preferential influence of cardiac cycles to the release of acetylcholine as opposed to NE. The strength of this reflex vagal response can be assessed by three techniques: 1) analysis of bradycardic response following the increase of blood pressure with vasoconstrictors such as phenylephrine; 2) assessment of reflex sympathetic-induced tachycardic response following the reduction of blood pressure by vasodilators such as nitroprusside or nitroglycerin; and 3) direct stimulation of carotid baroreceptors with neck suction or unloading by neck pressure, allowing these neck manoeuvres to elicit counter-regulatory responses from aortic arch baroreceptors. These techniques are not without their limitations. Prolonged infusion of vasoactive agents can simulate a steady state, leading to competing sympathetic responses. Additionally, these vasoactive agents may exert a confounding effect on sino-atrial node discharges, baroreceptor nerve endings as well as atrial and pulmonary mechanoreceptors (Musialek and Casadei, 2000, Casadei and Paterson, 2000). To circumvent these limitations, algorithms have been developed with the ability of identifying spontaneous concordant fluctuations in blood pressure and heart rate within the brief time window from continuous non-invasive or invasive recordings (Parati et al., 2000).

Central to all these three techniques is the utilization of a regression equation correlating changes in pulse interval to changes in systolic blood pressure during the immediate preceding cardiac cycles. The gradient of the resulting graph describes the gain of the arterial baroreflex regulation on heart rate. The final results therefore inform the sensitivity of vagal response towards stress response in blood pressure changes but lacks the ability to identify the root of autoimmune impairment. Nonetheless, low BRS has been shown to correlate with poor prognostic outcome. A reduced BRS after myocardial infarction (MI) predisposed to VF in canine MI models (Schwartz et al., 1988a). These findings were extrapolated to post-MI human studies demonstrating that a depressed BRS of < 3ms/mmHg was associated with high arrhythmic deaths (Taggart et al., 2003, Schwartz et al., 1988b, La Rovere et al., 1998).

1.3.5 Heart Rate Variability

Beat-to-beat heart rate variation is under the influence of tonic vagal control of the sinus node. This is therefore a non-invasive surrogate marker of autonomic control of the heart, with its analysis being performed in time (e.g. the standard deviation of all non-ectopic pulse intervals within a specified period) or frequency (frequency domain method of estimating non-neural and neural contributions to short- and long-term oscillations in heart rate) domains. High frequencies (0.15 – 0.5 Hz) are thought to be a representation of parasympathetic component of the autonomic nervous system with vagal blockade abolishing oscillations in heart rate within this frequency band. Low frequencies (0.05 – 0.15 Hz) are mediated by both sympathetic and parasympathetic nervous system and are affected by BRS. This is supported by observations that the low-frequency spectral power was increased by manoeuvres that stimulate central sympathetic output such as standing up, tilting and exercising. Conversely the spectral power in this frequency band of 0.05 – 0.15 Hz were decreased by beta-blockade, clonidine and during sleep. Very-low frequencies (< 0.05 Hz) are under the influence of many in vivo factors including renin-angiotensin system and thermoregulation. In heart failure, the spectral power appears to be markedly reduced and concentrated within the very-low- and low-frequency ranges (Butler et al., 1997). Similar to BRV, heart rate variability (HRV) provides insight into sympathetic and parasympathetic contributions to heart rate modulation and contributes to estimation of prognostic outlook despite the lack of specificity to the degree of regional

sympathetic output. Historically, a depressed HRV demonstrated a high sensitivity and specificity in predicting susceptibility to VF in MI canine models (Hull et al., 1990). This is further corroborated by the finding of HRV recovery in low-risk post-MI dogs compared to high-risk dogs with persistent depressed HRV parameters independent of beta-blockade (Adamson et al., 1994). These preclinical findings were echoed by subsequent human studies involving post-MI patients. In these trials, HRV was a significant predictor of SCD after adjusting for clinical and demographic factors including ejection fraction (Farrell et al., 1991, Kleiger et al., 1987, La Rovere et al., 1998). Furthermore HRV improvement over time following MI coincided with decreasing risk of arrhythmic death (Odemuyiwa et al., 1994). In one study, a HRV of < 5 ms conferred a hazard relative risk of 5.3 in SCD, compared with low-risk patients with a HRV of > 10 ms during a follow-up period of 31 months (Kleiger et al., 1987). Notably a depressed HRV have also been observed in patients with idiopathic dilated cardiomyopathy with a history of SCD compared to those without fatal ventricular arrhythmias (Lanza et al., 2000, Hoffmann et al., 1996).

1.4 Mechanisms of Dysautonomia in Heart Failure

HF resulting from systolic and/or diastolic dysfunction is followed by secondary damage to most body organs, including the vasculature, kidneys and the immune system (Braunwald and Bristow, 2000, Mann and Bristow, 2005). Dysautonomia is a well-known feature in HF, being present in all aspects of cardiovascular regulation including alterations to afferent activity, central processing of neuronal control, ganglionic and cardiac efferent innervation. Vagal tone, which normally restrains sympathetic drive, is diminished in HF whilst the excitatory influences of arterial chemoreceptors (Sun et al., 1999) and cardiac sympathetic afferent fibres (Rundqvist et al., 1997) are enhanced, thereby raising the sympathetic drive.

1.4.1 Sympathetic Hyperactivity

Heart failure is fundamentally a clinical syndrome that represents the common final pathway of a variety of diseases characterised by compromised cardiac contractility. This leads to neurohumoral activation in an attempt to stabilise blood pressure and cardiac

output. Acutely, there is hyperactivity of sympathetic nerves with resultant increase in its transmitters of norepinephrine and epinephrine. This stimulates the heart to utilise its remaining chronotropic and inotropic reserve. Chronically, however, the concomitant increase in afterload, raised energy consumption as well as hypertrophic and apoptotic actions on the cardiac myocyte further deteriorate cardiac function, constituting a vicious circle.

A major hallmark of heart failure is β -adrenergic desensitisation, resulting in blunted adrenergic agonist effects on contractile performance (Vatner et al., 2000, Mudd and Kass, 2008, Movsesian and Bristow, 2005, Mann and Bristow, 2005, Lohse et al., 2003, Eschenhagen, 2008, El-Armouche et al., 2003b, Dorn and Molkentin, 2004). In patients with heart failure as well as in isolated ventricular preparations from failing human hearts, the positive inotropic response to catecholamines is diminished (Feldman et al., 1987, Colucci et al., 1988, Bohm et al., 1988). Conversely, force development under unstimulated, basal conditions (low pacing rates, low Ca^{2+} , no catecholamines) is normal (Houser and Margulies, 2003, Hasenfuss and Pieske, 2002, Hasenfuss, 1998). Collectively, these findings point to a specific defect in the β -adrenoreceptor (AR)/cAMP system in heart failure.

Over the years, a characteristic set of molecular alterations in components of the β -AR signalling pathway has been identified, including a decrease in β -AR density and mRNA (Engelhardt et al., 1996, Bristow et al., 1982), uncoupling of β -AR from G_s as a result of increased β -AR-kinase activity (Ungerer et al., 1993), as well as increased G_i protein and mRNA (Neumann et al., 1988, Feldman et al., 1988, Eschenhagen et al., 1992, Bohm et al., 1990). In addition, the small amplifier I-1 is downregulated and dephosphorylated (El-Armouche et al., 2003a, El-Armouche et al., 2004), contributing to the possible increase in sarcoplasmic reticulum (SR)-related protein phosphatase-1 activity (Neumann et al., 1997), the major phosphatase dephosphorylating phospholamban (PLB) (MacDougall et al., 1991). β -AR signalling abnormalities in heart failure also include defects in AKAP-based supramolecular complexes with impaired compartmentalisation of cAMP/Protein kinase A signalling (Zakhary et al., 2000, Dodge-Kafka et al., 2006, Diviani, 2008).

Indeed, hypophosphorylation of PKA substrates have been reported in the failing human hearts, including PLB, Troponin I, and cardiac myosin-binding protein C (Messer et al., 2007, El-Armouche et al., 2007, Bodor et al., 1997, Bartel et al., 1996), contributing partly to the relaxation deficit. However, noteworthy exceptions have been observed, in particular the increase in sarcolemmal Ca^{2+} channel (LTCC) activity (thereby suggesting hyperphosphorylation) (Schroder et al., 1998) and hyperphosphorylation of ryanodine receptors (RyR2) (Marx et al., 2000). Both these phenomena point to cellular subcompartments in which the balance of phosphorylation-dephosphorylation is tilted towards the former. Hyperphosphorylation at the LTCC-RyR2 interface may cause an increase in systolic transsarcolemmal Ca^{2+} influx together with an increased propensity for diastolic SR Ca^{2+} release (“ Ca^{2+} leak”), a dangerous precondition for ectopic cardiac automaticity and arrhythmias (Marx et al., 2000).

The phenomenon of β -AR desensitisation in heart failure appears to be one of protective adaptation. The protective nature of this process can be illustrated by several observations. A mouse strain which downregulates its β -AR density in response to chronic infusion of catecholamines was protected against cardiac toxicity compared to one that did not (Faulx et al., 2005). Furthermore, a genetic variant resulting in gain of function of GRK5, an enzyme providing uncoupling and hence desensitisation of β -AR, was associated with improved survival in heart failure population among the African-Americans (Liggett et al., 2008). Conversely, numerous transgenic mouse models have shown that over-activity of the β -AR pathway induces a heart failure phenotype (Table 1.2). Pragmatically, therapeutic interventions to suppress β -AR desensitisation such as catecholamines and phosphodiesterase inhibitors lead to increased mortality (Stevenson, 2003, O'Connor et al., 1999, Feldman et al., 1993) whilst beta-blockers are established in the mantra of heart failure therapy, resulting in reversed LV remodelling, improved long-term systolic function, ultimately translating to decrease mortality in patients with chronic heart failure (Satwani et al., 2004, Packer, 2001, Bristow, 2000).

β -AR desensitisation appears to be a dynamic process following the increase in norepinephrine plasma levels in heart failure. However, the downstream molecular pathway following downregulation of β -AR and upregulation of G_i remains to be elucidated although cAMP and PKA involvements have been implicated (Hadcock et al.,

1991, Eschenhagen et al., 1996). It appears to be in the form of a closed-loop feedback system keeping intracellular cAMP concentration constant. Indeed, despite increased norepinephrine plasma levels, the concentration of cAMP was normal in myocardial biopsies from patients with heart failure (Regitz-Zagrosek et al., 1994).

The differences in phosphorylation levels between the 2 arrays of proteins, i.e. PLB, Troponin I and cardiac myosin-binding protein-C on one hand, and RyR2 and LTCC on the other, points towards compartmentalisation. The mouse data (Table 1.2) is highly rewarding but creates some uncertainty. Whilst one study supports the inhibition of I-1 to delay the development of heart failure (El-Armouche et al., 2008), another study argues for I-1 overexpression as a protection against isoprenaline-induced cardiac apoptosis (Chen et al., 2010). Similarly, there is a search for AC5 inhibitors (Yan et al., 2007) whilst paradoxically, AC6 overexpression demonstrates potential therapeutic effect (Phan et al., 2007). Integrating all these opposing concepts poses a challenging task in searching new targets beyond beta-blockers in curbing the deleterious effects of sympathetic overdrive in heart failure.

Chapter 1

Table 1.2 Experimental mouse models on β -AR signalling and myocardial pathology

Investigator	Genetic model	β -AR signalling components	Myocardial contractility	Cardiac pathology	Results of experimental HF models or after cross-breeding
Engelhardt et al (Engelhardt et al., 1999, Engelhardt et al., 2004)	TG	β_1	↑ at baseline in young ↓ in older animals (EF~20%)	Hypertrophy, dilation and fibrosis	Functional and morphological rescue by cross-breeding with PLB-KO
Cross et al (Cross et al., 1999) Milano et al (Milano et al., 1994) Dorn et al (Dorn et al., 1999)	TG, low	β_2	↑ at baseline and throughout life	No overt pathology	↑ myocardial injury after IR-injury functional and morphological improvement of G _{qa} -TGs
Liggett et al (Liggett et al., 2000) Du et al (Du et al., 2000b, Du et al., 2000a)	TG, high	β_2	↑ in young ↓ in older animals	Hypertrophy and progressive HF	Preserved contractility after MI Exacerbation of HF after TAC

Chapter 1

Table 1.2 (Continued)

Investigator	Genetic model	β -AR signalling components	Myocardial contractility	Cardiac pathology	Results of experimental HF models or after cross-breeding
Kohout <i>et al</i> (Kohout et al., 2001)	TG	β_3	↓ systolic pressure under anaesthesia, but normal in conscious mice; cAMP and positive inotropic response to β_3 agonist	Smaller heart	Not determined
Gaudin <i>et al</i> (Gaudin et al., 1995) Iwase <i>et al</i> (Iwase et al., 1997) Asai <i>et al</i> (Asai et al., 1999)	TG	G_{as}	↑ response to β -AR stimulation in young ↓ reduced EF in older animals	Sudden death, arrhythmias, dilation and fibrosis	Functional and morphological rescue by chronic propranolol therapy
DeGeorge <i>et al</i> (DeGeorge and Koch, 2008)	TG (cond. with tetracycline)	$G_{\alpha i-2}$ inhibitor	Normal at baseline	No overt pathology	↑ myocardial injury after IR

Chapter 1

Table 1.2 (Continued)

Investigator	Genetic model	β-AR signalling components	Myocardial contractility	Cardiac pathology	Results of experimental HF models or after cross-breeding
Koch <i>et al</i> (Koch et al., 1995)	TG	βARK ₁	Normal at baseline ↓ response to β-AR stimulation	No overt pathology	Not determined
Dorn <i>et al</i> (Dorn et al., 1999) Koch <i>et al</i> (Koch et al., 1995) Harding <i>et al</i> (Harding et al., 2001) Rockman <i>et al</i> (Rockman et al., 1998)	TG	βARKct	↑ at baseline and in response to β-AR stimulation throughout life	No overt pathology	Functional improvement of MLP-KO and CSQ-TGs synergistic beneficial effects with metoprolol no rescue of G _{qa} -TGs
Matkovich <i>et al</i> (Matkovich et al., 2006)	KO (early cardiac-specific)	βARK (GRK2)	Normal at baseline	Normal heart development	↑ force response ↓ tachyphylaxis to isoprenaline accelerated catecholamine toxicity

Chapter 1

Table 1.2 (Continued)

Investigator	Genetic model	β-AR signalling components	Myocardial contractility	Cardiac pathology	Results of experimental HF models or after cross-breeding
Raake <i>et al</i> (Raake et al., 2008)	KO (cond. Cardiac-specific, with tamoxifen α-MHC- MCM)	βARK (GRK2)	Normal at baseline	No overt pathology	↑ function and survival up to 4 months after MI
Okumura <i>et al</i> (Okumura et al., 2003b, Okumura et al., 2003a) Yan <i>et al</i> (Yan et al., 2007)	KO	AC5	Normal at baseline	No overt pathology; protected from aging cardiomyopathy	Prevention of heart failure after TAC and after long-term β-AR stimulation
Lai <i>et al</i> (Lai et al., 2008) Roth <i>et al</i> (Roth et al., 2002) Gao <i>et al</i> (Gao et al., 1999)	TG	AC6	↑ response to β-AR stimulation but normal basal cAMP or contractility	No overt pathology	Functional/morphology improvement of G _{qα} -TGs; rescue after MI (Tet-regulated TG)

Chapter 1

Table 1.2 (Continued)

Investigator	Genetic model	β-AR signalling components	Myocardial contractility	Cardiac pathology	Results of experimental HF models or after cross-breeding
Antos <i>et al</i> (Antos <i>et al.</i>, 2001)	TG	PKAc	↓↓ at baseline	Sudden death, arrhythmias, dilation and fibrosis	Functional/morphology improvement of G _{qα} -TGs; rescue after MI (Tet-regulated TG)
Pathak <i>et al</i> (Pathak <i>et al.</i>, 2005)	TG	I-1	↑ at baseline throughout life	No overt pathology	Preserved contractility after TAC
Carr <i>et al</i> (Carr <i>et al.</i>, 2002) El-Armouche <i>et al</i> (El-Armouche et al., 2008)	KO	I-1	Normal at baseline with mildly decreased sensitivity to β-AR stimulation	No overt pathology	Partial prevention of cardiac hypertrophy and arrhythmias after pathological β-AR stimulation
Lehnart <i>et al</i> (Lehnart <i>et al.</i>, 2005)	KO	PDE-4D	Normal in young ↓ in older animals	Sudden death, arrhythmias, dilation and fibrosis (in older animals)	Functional and morphological rescue through RyR2-KO mice (i.e. no PKA-phosphorylation of RyR2)

Chapter 1

Table 1.2 (Continued)

Investigator	Genetic model	β-AR signalling components	Myocardial contractility	Cardiac pathology	Results of experimental HF models or after cross-breeding
Crackower <i>et al</i> (Crackower et al., 2002)	KO	PI3 K γ	↑ at baseline ↑ basal cAMP	No overt pathology	↑↑ in fibrosis and dilation after TAC
Patrucco <i>et al</i> (Patrucco et al., 2004)					
Gilsbach <i>et al</i> (Gilsbach et al., 2007)	KO	α_{2C} -AR (± and -/-)	Normal in ± mice	No overt pathology	↑↑ in mortality, hypertrophy and fibrosis after TAC

TG transgenic overexpression, in general cardiac-specific; *KO* knockout (genetic ablation); *TAC* transaortic constriction inducing acute pressure overload; *MI* myocardial infarction by coronary artery (LAD) ligation; *IR* ischaemia-reperfusion

1.4.2 Parasympathetic Attenuation

Autonomic imbalance occurs early in the natural history of HF, often preceding other key derangements including clinical manifestations. In a tachycardia-induced HF canine model, vagal tone was found to be decrease on the 3rd day after cardiac dysfunction, preceding sympathetic activation (Ishise et al., 1998). Interestingly in patients with symptomatic HF from mild left ventricular (LV) impairment, reduced parasympathetic drive was evident early on whilst in patients with asymptomatic LV dysfunction, sympathetic activation preceded symptoms (Grassi et al., 2001). In all cases, autonomic imbalance is strongly associated with raised mortality due to lethal ventricular arrhythmias, irrespective of aetiology (Grassi et al., 2001). The clinical and prognostic implications of raised sympathetic drive are well established (Floras, 2003), underpinning the undeniably important role of beta-blockers in standard HF therapy (CIBIS-II Investigators and Committees, 1999, Eichhorn and Bristow, 2001, Hjalmarson et al., 2000). On the other hand, the reduced parasympathetic tone in HF has received less limelight although some studies have surfaced to highlight its importance in cardiac pathologies. Indirect markers of parasympathetic tone include HRV and BRS. Animal studies have inferred a correlation between reduced BRS and the occurrence of sudden cardiac death (De Ferrari et al., 1991, Billman et al., 1982). In larger studies, a depressed BRS is associated with higher risk of sudden death both before and after MI (Schwartz et al., 1988a). An early clinical trial reported a strong association between low BRS and all-cause mortality (La Rovere et al., 1988) with subsequent follow-up trial demonstrating a strong association between BRS and malignant arrhythmias but not all-cause mortality (Farrell et al., 1992). Several time domain measures of HRV, in particular those of low-frequency (typically <0.04Hz), have been implicated as powerful predictor of all-cause mortality following MI (Tuininga et al., 1994, Nolan et al., 1992, Kleiger et al., 1987, Farrell et al., 1991, Bigger et al., 1992). The prognostic value of BRS and HRV has been affirmed in large-scale randomised clinical trials, namely ATRAMI and UK-HEART, involving post-MI patients (La Rovere et al., 1998) as well as patients with chronic heart failure respectively (Nolan et al., 1998).

In terms of direct measurement of vagal activity, vagal blockade in canine models with atropine increased the occurrence of SCD (De Ferrari et al., 1991), whereas direct stimulation of the cervical vagus nerve prevented VF during acute MI (Vanoli et al., 1991), translating into decreased mortality from 50% to 14% in over 140 days in rats in a separate study (Li et al., 2004a). Whilst a large proportion of SCDs is attributable to ventricular arrhythmias, and may be prevented by vagal stimulation, the effect of vagal stimulation appears to extend beyond prevention of these arrhythmias. It is thought that ectopic beats or runs of non-sustained ventricular tachycardia occur in up to 80% of all HF patients (Maskin et al., 1984, Podrid and Myerburg, 2005). In rat model of post-MI HF, chronic right cervical vagus nerve stimulation for 3-5 months following MI for a period of 7 days prevented the characteristic occurrence of premature supraventricular and ventricular contractions (Zheng et al., 2005). Sabbah conducted chronic vagus nerve stimulation in canine model of microembolism-induced HF for a 3-month period to characterise the effect on ventricular remodelling and haemodynamics. By using a negative-feedback loop to maintain heart rate at a level 10% below baseline, vagal nerve stimulation reverses the reduction in connexin-43 mRNA and protein expression associated with HF (Sabbah, 2011). Reduced expression of connexin-43 in HF results in a disruption in cell-to-cell coupling, slowing ventricular conduction and increasing the dispersion of transmural action potential duration (APD) which is linked to increased incidence of ventricular arrhythmogenesis and SCD (Ai and Pogwizd, 2005, Wang and Gerdes, 1999). This provides indirect evidence of anti-arrhythmic properties of vagal nerve stimulation in HF. Further indirect biochemical evidence is seen in the improved survival rate in pacing-induced HF in dogs, characterised by lower plasma norepinephrine and angiotensin levels (Zucker et al., 2007). The use of clonidine, a centrally acting α_2 adrenoreceptor agonist in HF to suppress sympathetic activity hints at the potential antagonising role vagal nerve stimulation against the pro-arrhythmic effect of the sympathetic nervous system (Zhang et al., 1998).

The cardiovascular physiological changes of negative chronotropy, dromotropy and *atrial* inotropy induced by vagal postganglionic nerves are mediated by acetylcholine (ACh) acting on muscarinic receptors (mAChRs). Conventional thinking historically advocates the lack of negative *ventricular* inotropic effect by vagus nerve stimulation.

However, the advent of modern techniques reveals the presence of a dense and intricate network of Ach-containing nerves in both ventricles of all species studied (Taggart et al., 2011, Saburkina et al., 2010, Rysevaite et al., 2011, Pauza et al., 2000, Johnson et al., 2004, Batulevicius et al., 2005). Studies have demonstrated the connection between the anti-fibrillatory effect of the vagus nerve and activation of mAChRs. There are five subtypes of mAChRs (M_1 - M_5). ACh binds to mAChRs, on the pre-synaptic sympathetic nerve terminals (M_3) and M_2 receptors on cardiomyocytes to inhibit epinephrine release and/or accumulation of intracellular cAMP (Vincent and Ellis, 1963, Stiles et al., 1984, Muscholl, 1980, Murad et al., 1962, Levy and Blattberg, 1976). In particular, works on the M_3 receptor has shed light on vagal control of cardiovascular physiology. The G_q -protein coupled to M_3 mAChR is shown to modulate heart rate and cardiac repolarisation, regulate cell-to-cell communication, protects against ischaemic and oxidative injury, and promote or suppress the triggering of arrhythmias depending on the location and phenotype of arrhythmias (atrial – increased vs. ventricular – decreased) (Wang et al., 2007). Pharmacological activation of M_3 receptors lead to reduced occurrence of ventricular arrhythmias induced by ischaemic, aconitine and ouabain (Wang et al., 2007). Furthermore, overexpression of the M_3 receptor gene diminishes the occurrence of spontaneous arrhythmias in a ischaemia-reperfusion mouse model (Wang et al., 2007). Relevantly, M_3 receptor activation can stimulate I_{KM3} (Liu Y, 2005), thereby regulating cardiac repolarisation (Wang et al., 2012). Additionally, calcium overload has been reduced in ventricular myocytes, possibly mediating the protective effect of M_3 receptor activation in ischaemia-induced arrhythmias (Wang et al., 2012). M_3 receptor activation in response to efferent vagus nerve stimulation also appears to regulate the expression of connexin-43, another plausible explanation for its protective effect in ischaemia-induced arrhythmias (Ando et al., 2005). Importantly although mechanistically unclear, there appears to be an increased M_3 receptor expression in patients with heart failure (Wang et al., 2007).

The beneficial effects of chronic vagus nerve stimulation appear to be multi-modality in nature. Apart from anti-arrhythmic properties, it has been shown to reverse the contractile dysfunction and adverse remodelling in experimental HF models (Li et al., 2004a, Sabbah, 2011, Sabbah et al., 2005, Zhang et al., 2009), even when applied at subthreshold intensities insufficient to cause chronotropic effect (De Ferrari and

Schwartz, 2011). Pioneered by Schwartz *et al*, vagus nerve stimulation was first studied in eight HF patients with improvements in NYHA class, quality of life scores, 6-minute walk test, and LV end-systolic volume after a 6-month treatment period (Schwartz et al., 2008). This success is further echoed by De Ferrari *et al* demonstrating an increase in the 6-minute walk test following vagus nerve stimulation in a 32 patient cohort, providing convincing evidence of improvement in exercise capacity coupled to an improvement in LV ejection fraction (De Ferrari et al., 2011). In spite of the lack of detailed understanding of cellular mechanisms of vagus nerve stimulation in HF, multi-centre international trials, namely INOVATE-HF and NECTAR-HF, have been designed and conducted to assess clinical application of chronic vagus nerve stimulation in HF.

1.5 Heart Failure and Nitric Oxide

Nitric oxide (NO) is produced by three isoforms of NO synthase (NOS): NOS 1 (neuronal), NOS 2 (inducible) and NOS 3 (endothelial). NOS expression is found in endothelial cells, myocytes and neuronal cells, regulating a wide variety of biological functions in a site-specific manner (Guix et al., 2005, Lundberg et al., 2008, Massion et al., 2003, Moncada et al., 1991). NOS positive autonomic neurons express mainly NOS 1 but NOS 3 and NOS 2 immunostaining have been found in neurons and astrocytes in the brainstem (Lin et al., 2007, Chan et al., 2003). NOS 1 and NOS 3 are under tight transcriptional control and their protein levels can be markedly altered in a variety of conditions including heart failure. In autonomic nerves and most vascular beds, NOS 1 and NOS 3 are downregulated in heart failure(Patel et al., 1996, Bauersachs and Widder, 2008) but there are exceptions such as in cardiac tissue (Danson et al., 2005). In the heart, NO appears to modulate the actions of the parasympathetic nervous system, regulating the change in heart rate (HR) in response to parasympathetic stimulation (Conlon and Kidd, 1999). Although there is a suggestion that NO acts presynaptically to reduce the bradycardic response to vagus nerve stimulation (VNS) (Herring et al., 2000), other investigators have noted that NO modulates changes in AV conduction in response to VNS in a similar manner, suggesting that NO has a role in the ventricular effects of VNS (Conlon and Kidd, 1999). Subsequently a direct evidence of vagus-mediated NO release was obtained in

a study using NO-sensitive dye (DAF-2 DA) (Brack et al., 2009). Indeed, these vagus-mediated NO releases occur independently of muscarinic receptors as perfusion with atropine at a concentration sufficient to block changes in HR and effective refractory period (ERP) did not influence the vagal effect on DAF-2 fluorescence (Brack et al., 2011).

In heart failure, the cellular signalling pathways and transcription factors responsible for altered NOS expression are not well defined. The influences of NO on cardiac function are complex, probably reflecting site-specific modes of NO-signalling that are spatially located in different subcellular compartments (Champion et al., 2003). Genetic studies have shown that autonomic imbalance in HF could be linked to an endothelial NOS promoter polymorphism. Patients homozygous for this polymorphism had HRV parameters indicating increased sympathetic drive and reduced parasympathetic tone (Binkley et al., 2005). Furthermore, dysregulation of the NO pathway can have a deleterious effect on contractile function. Pertinently chronic vagus nerve stimulation normalises both mRNA and gene expression of NOS in canine models of microembolism-induced HF (Sabbah, 2011). Currently there is a paucity of information on how alterations of NOS expression may alter ventricular arrhythmia susceptibility, particularly in HF. In addition, the role on the NO-dependent anti-fibrillatory effects of vagus nerve stimulation remain to be crystalised in experimental HF studies.

1.6 Autonomic Nerve Innervation and the Effect of Myocardial Infarction

Ventricular myocardium is richly innervated by sympathetic nerve fibres and to a lesser degree by vagal nerve fibres, rendering both attractive targets to be modulated following MI. Both nerve fibres exhibited a heterogeneous, location-sensitive density gradient, i.e. from basal/high to apical/low regions. Detailed neuroanatomical information is lacking on rabbit heart, the latter a preferred experimental model to investigate arrhythmogenesis, remodelling and HF in the setting of MI relevant to the human counterpart of these conditions. Apart from the death of actual ventricular myocardium, transmural MI results in the death of sympathetic nerves within the infarct areas (i.e. denervation) (Stanton et al., 1989, Zipes, 1990), rendering these areas

refractory to sympathetic nerve stimulation or norepinephrine infusion (Li et al., 2004b). It has been demonstrated that peri-infarct sites show effective refractory period (ERP) shortening with stellate ganglia stimulation and norepinephrine infusion, whereas remote non-infarcted sites showed heterogeneous effects on ERP (Zipes et al., 1983). Yet, most of these remote non-infarcted sites showed ERP shortening with norepinephrine infusion, and a few showed ERP shortening with stimulation of either the left or the right stellate ganglion, but not both. In addition, these non-infarcted sites were hypersensitive to adrenergic transmitters with no detectable differences in β -adrenergic receptor density, $G_s \alpha$ -subunit density, or affinity in the apical vs. basal areas (Inoue and Zipes, 1988, Kammerling et al., 1987, Warner et al., 1993). Transmural MI in dogs resulted in a loss of efferent sympathetic nerves in non-infarcted apical sites as early as 5-20 minutes following occlusion of the diagonal branch of the left anterior descending artery, with more significant loss occurring within 3 hours (Inoue and Zipes, 1988). Henceforth, disruption of sympathetic fibres terminating within and axons passing through these areas has the potential to greatly exacerbate the natural electrophysiological response from autonomic activation, even in areas of viable remote non-infarcted myocardium. In rabbits with epicardially applied phenol to achieve regional denervation, activation recovery interval (ARI), a surrogate of APD, was shortened in 98% of denervated regions by norepinephrine with an augmented shortening and dispersion of ARI in more severely denervated regions, implying supersensitivity in the adjacent regions (Yoshioka et al., 2000). However, left stellate stimulation shortened ARI in only 30% of denervated areas with ARI prolongation in the remaining 70%. In summary, transmural MI not only creates a substrate for scar-related ventricular arrhythmias, but also disrupts innervation to myocardial sites distant to the infarct, contributing to heterogeneous electrophysiological responses key in promoting further ventricular arrhythmias.

With time, sympathetic denervation occurring in the acute setting of MI and HF, is followed by an adaptive process characterised by nerves regrowing, otherwise known as “nerve sprouting”. This phenomenon can lead to heterogeneous hyper-innervation (Cao et al., 2000b, Chen et al., 2001). Nerve sprouting has been demonstrated in the right atrial free wall, right atrial isthmus, and right ventricle in dogs after radiofrequency catheter ablation (Okuyama et al., 2004). Histologically, hyper-

innervation has been illustrated as co-localization of Schwann cells, sympathetic nerves and axons (Chen et al., 2001). Further observation of regional hyper-innervation was obtained in explanted native hearts of transplant recipients suffering from ischaemic or idiopathic cardiomyopathy, with the most abundant sprouting found in the peri-infarct and peri-vascular myocardial regions (Cao et al., 2000b). Infusion of nerve growth factor (NGF) into thoracic sympathetic nerves promotes cardiac nerve sprouting coupled with increased SCD in dogs with an MI (Cao et al., 2000a). Conversely infusion of NGF into the left stellate ganglion of normal dogs resulted in nerve sprouting with no consequence on occurrence of ventricular arrhythmias and sudden cardiac death. NGF infusion into left or right sympathetic chains was also shown to produce differential effects on QT interval and hence susceptibility to ventricular arrhythmias. NGF infusion into the left stellate ganglion caused LV nerve sprouting with resultant QT prolongation and SCD occurring in 50% of dogs, whereas right stellate ganglionic infusion of NGF caused right ventricular nerve sprouting, shortened QT interval with no evidence of SCD (Zhou et al., 2001). These findings provide the additional evidence of pathological lateral control from sympathetic nerves in MI-induced HF.

In HF, there is reduced vagal ganglionic transmission, altered mAChR density and composition, as well as attenuated acetylcholinesterase activity. Muscarinic blockade exerted a more modest effect on HR in experimental HF models compared to normal hearts (Bibebski and Dunlap, 1999, Dunlap et al., 2003). In the absence of HF, muscarinic blockade increases cardiac norepinephrine spillover but in HF, there exists a blunting of parasympathetic response over sympathetic activity (Azevedo and Parker, 1999). In spite of these physiological observations, there is no data to date on parasympathetic innervation in the peri-infarct setting.

1.7 Autonomic Nerve Stimulation, Electrical Restitution and SCD

The onset of ventricular tachycardia and more relevantly lethal VF is believed to be associated with breakup of spiral waves or rotors into multiple wavelets and oscillations (Weiss et al., 2000). This belief led to the understanding of APD restitution (Chialvo et al., 1990, Taggart et al., 1990) – a myocardial property which describes the

relationship between APD and its preceding diastolic intervals (DI) (Boyett and Jewell, 1980). Conventionally the restitution hypothesis adopts the steepness of restitution curve as a surrogate marker of arrhythmia vulnerability, and has been validated as an additional risk stratification tool in susceptible patients (Selvaraj et al., 2007). Restitution curves with a steep gradient of >1 provides large changes in APD for small changes in DI, thereby promoting complex unstable ventricular arrhythmias. This is in contrast with a shallow slope where small changes in DI only lead to small changes of APD, encouraging conduction blocks and wave breaks (Cao et al., 1999, Gilmour and Chialvo, 1999, Karma, 1994, Qu et al., 1999). Under sympathetic nerve stimulation, an apex-base difference in restitution kinetics has been demonstrated in normal rabbit hearts, with a basal predilection of APD shortening (Mantravadi et al., 2007). This spatial heterogeneity of restitution kinetics was attributed to regional differences in the expression of tyrosine hydroxylase and KCNQ1 protein, suggesting a greater density of sympathetic nerves and I_{Ks} respectively at the base of the heart (Cheng et al., 1999, Kawano et al., 2003). In porcine models and humans, restitution slope was increased by sympathetic activation with epinephrine, adrenaline or isoproterenol (Taggart et al., 2003, Taggart et al., 1990). In rabbits, similar phenomenon was seen with physiological stimulation of sympathetic nerves in the isolated innervated rabbit heart, leading to an increased susceptibility to VF and alternans level (Ng et al., 2007). In canine models of SCD, VT was demonstrated by 2 distinct types of left sympathetic nerve stimulation: low amplitude bursts and high amplitude spike discharges, with the latter being more arrhythmic in nature (Zhou et al., 2008). High level of left stellate ganglionic activity was found to precede premature ventricular contracts and VT (Ogawa et al., 2007). In a canine HF model, the heightened left stellate ganglionic activity was associated with an increased QT interval and QT variability index (Piccirillo et al., 2009), as well as vulnerability to ventricular arrhythmias. The link between adrenergic activity and arrhythmic susceptibility is further supported by evidence that in humans, left cardiac sympathetic denervation (LCSD) yields a favourable outcome in several cardiac conditions characterized by adrenergically driven life-threatening arrhythmias.

Historically the concept of LCSD was first suggested by Francois-Franck (Francois-Franck, 1899) in 1899 as a therapeutic option for angina and subsequently implemented by Jonnesco (Jonnesco, 1921), who, in 1916, performed the first unilateral section of

the left stellate ganglion in a patient incapacitated by angina and arrhythmias. As a therapeutic option, LCSD is partially effective in patients susceptible to ventricular arrhythmias (Estes and Izlar, 1961, Zipes et al., 1968). In particular, some patients with long QT syndrome were protected (Moss and McDonald, 1971), with one patient remaining symptom-free for 36 years (Schwartz et al., 1975). This protection against ventricular arrhythmia in long QT patients were postulated to be due to a reduction in T-wave alternans (Schwartz and Malliani, 1975) and absence of post-denervation supersensitivity (Schwartz and Stone, 1982), thereby raising the VF threshold (Schwartz et al., 1976). The therapeutic scope of LCSD broadens into post-MI patient population, resulting in a reduction in SCD incidence from 22% to 3% (Schwartz et al., 1992). Recently, similar therapeutic benefit of LCSD has also been demonstrated in other potentially lethal cardiac conditions such as catecholaminergic polymorphic ventricular tachycardia (Wilde et al., 2008) and VT storm (Bourke et al., 2010). In spite of the encouraging results of LCSD on curbing ventricular arrhythmias, not all patients are responsive to this type of treatment, highlighting the need to develop additional approaches of autonomic modulation. One such alternative intervention is VNS where early evidence suggests protection against VF (Brack et al., 2011) utilising an NO-dependent pathway in healthy rabbit heart (Brack et al., 2007).

1.8 Conclusion

The study of the intricate interplay between the neurological system and the cardiovascular system has led to the emergence of a new field known as Neurocardiology. As our understanding of the biochemical and physiological interactions of the brain-heart axis expands via preclinical and clinical studies, realisation of the significant link between pathophysiology and clinical outcome in terms of heart failure progression and arrhythmic death is forged. Over the last few decades, there has been great stride in dissecting the molecular, histological and anatomical characteristics of the sympathetic nervous system. The disparate research in the other arm of the autonomic system, namely the parasympathetic nervous system, has afforded an opportunity to further our knowledge in the global contribution of the autonomic nervous system in heart failure. Functional studies of vagus nerve stimulation in preclinical studies of normal heart and MI models lead naturally to

translation into human clinical trials. A better understanding of the global and regional innervations, as well as the complex interaction between the sympathetic and parasympathetic nervous system, is of paramount importance in crystallising the idea of manipulating the autonomic nervous system for therapeutic purposes in heart failure.

1.9 References

- ADAMSON, P. B., HUANG, M. H., VANOLI, E., FOREMAN, R. D., SCHWARTZ, P. J. & HULL, S. S., JR. 1994. Unexpected interaction between beta-adrenergic blockade and heart rate variability before and after myocardial infarction. A longitudinal study in dogs at high and low risk for sudden death. *Circulation*, 90, 976-82.
- AI, X. & POGWIZD, S. M. 2005. Connexin 43 downregulation and dephosphorylation in nonischemic heart failure is associated with enhanced colocalized protein phosphatase type 2A. *Circ Res*, 96, 54-63.
- ANDO, M., KATARE, R. G., KAKINUMA, Y., ZHANG, D., YAMASAKI, F., MURAMOTO, K. & SATO, T. 2005. Efferent vagal nerve stimulation protects heart against ischemia-induced arrhythmias by preserving connexin43 protein. *Circulation*, 112, 164-70.
- ANTOS, C. L., FREY, N., MARX, S. O., REIKEN, S., GABURJAKOVA, M., RICHARDSON, J. A., MARKS, A. R. & OLSON, E. N. 2001. Dilated cardiomyopathy and sudden death resulting from constitutive activation of protein kinase a. *Circ Res*, 89, 997-1004.
- ARNOLD, J. M., HOWLETT, J. G., DORIAN, P., DUCHARME, A., GIANNETTI, N., HADDAD, H., HECKMAN, G. A., IGNASZEWSKI, A., ISAAC, D., JONG, P., LIU, P., MANN, E., MCKELVIE, R. S., MOE, G. W., PARKER, J. D., SVENDSEN, A. M., TSUYUKI, R. T., O'HALLORAN, K., ROSS, H. J., RAO, V., SEQUEIRA, E. J. & WHITE, M. 2007. Canadian Cardiovascular Society Consensus Conference recommendations on heart failure update 2007: Prevention, management during intercurrent illness or acute decompensation, and use of biomarkers. *Can J Cardiol*, 23, 21-45.
- ASAI, K., YANG, G. P., GENG, Y. J., TAKAGI, G., BISHOP, S., ISHIKAWA, Y., SHANNON, R. P., WAGNER, T. E., VATNER, D. E., HOMCY, C. J. & VATNER, S. F. 1999. Beta-adrenergic receptor blockade arrests myocyte damage and preserves cardiac function in the transgenic G(salpha) mouse. *J Clin Invest*, 104, 551-8.
- AZEVEDO, E. R. & PARKER, J. D. 1999. Parasympathetic control of cardiac sympathetic activity: normal ventricular function versus congestive heart failure. *Circulation*, 100, 274-9.
- BARTEL, S., STEIN, B., ESCHENHAGEN, T., MENDE, U., NEUMANN, J., SCHMITZ, W., KRAUSE, E. G., KARCZEWSKI, P. & SCHOLZ, H. 1996. Protein phosphorylation in isolated trabeculae from nonfailing and failing human hearts. *Mol Cell Biochem*, 157, 171-9.

- BATULEVICIUS, D., PAUZIENE, N. & PAUZA, D. H. 2005. Architecture and age-related analysis of the neuronal number of the guinea pig intrinsic cardiac nerve plexus. *Ann Anat*, 187, 225-43.
- BAUERSACHS, J. & WIDDER, J. D. 2008. Endothelial dysfunction in heart failure. *Pharmacol Rep*, 60, 119-26.
- BAX, J. J., KRAFT, O., BUXTON, A. E., FJELD, J. G., PARIZEK, P., AGOSTINI, D., KNUUTI, J., FLOTATS, A., ARRIGHI, J., MUXI, A., ALIBELLI, M. J., BANERJEE, G. & JACOBSON, A. F. 2008. 123 I-mIBG scintigraphy to predict inducibility of ventricular arrhythmias on cardiac electrophysiology testing: a prospective multicenter pilot study. *Circ Cardiovasc Imaging*, 1, 131-40.
- BENARROCH, E. E., SMITHSON, I. L., LOW, P. A. & PARISI, J. E. 1998. Depletion of catecholaminergic neurons of the rostral ventrolateral medulla in multiple systems atrophy with autonomic failure. *Ann Neurol*, 43, 156-63.
- BIBBINS-DOMINGO, K., LIN, F., VITTINGHOFF, E., BARRETT-CONNOR, E., HULLEY, S. B., GRADY, D. & SHLIPAK, M. G. 2004. Predictors of heart failure among women with coronary disease. *Circulation*, 110, 1424-30.
- BIBEVSKI, S. & DUNLAP, M. E. 1999. Ganglionic mechanisms contribute to diminished vagal control in heart failure. *Circulation*, 99, 2958-63.
- BIGGER, J. T., JR., FLEISS, J. L., STEINMAN, R. C., ROLNITZKY, L. M., KLEIGER, R. E. & ROTTMAN, J. N. 1992. Frequency domain measures of heart period variability and mortality after myocardial infarction. *Circulation*, 85, 164-71.
- BILLMAN, G. E., SCHWARTZ, P. J. & STONE, H. L. 1982. Baroreceptor reflex control of heart rate: a predictor of sudden cardiac death. *Circulation*, 66, 874-80.
- BINKLEY, P. F., NUNZIATTA, E., LIU-STRATTON, Y. & COOKE, G. 2005. A polymorphism of the endothelial nitric oxide synthase promoter is associated with an increase in autonomic imbalance in patients with congestive heart failure. *Am Heart J*, 149, 342-8.
- BODOR, G. S., OAKELEY, A. E., ALLEN, P. D., CRIMMINS, D. L., LADENSON, J. H. & ANDERSON, P. A. 1997. Troponin I phosphorylation in the normal and failing adult human heart. *Circulation*, 96, 1495-500.
- BOHM, M., BEUCKELMANN, D., BROWN, L., FEILER, G., LORENZ, B., NABAUER, M., KEMKES, B. & ERDMANN, E. 1988. Reduction of beta-adrenoceptor density and evaluation of positive inotropic responses in isolated, diseased human myocardium. *Eur Heart J*, 9, 844-52.
- BOHM, M., GIERSCHIK, P., JAKOBS, K. H., PIESKE, B., SCHNABEL, P., UNGERER, M. & ERDMANN, E. 1990. Increase of Gi alpha in human hearts with dilated but not ischemic cardiomyopathy. *Circulation*, 82, 1249-65.
- BOOGERS, M. J., BORLEFFS, C. J., HENNEMAN, M. M., VAN BOMMEL, R. J., VAN RAMSHORST, J., BOERSMA, E., DIBBETS-SCHNEIDER, P., STOKKEL, M. P., VAN DER WALL, E. E., SCHALIJ, M. J. & BAX, J. J. 2010. Cardiac sympathetic denervation assessed with 123-iodine metaiodobenzylguanidine imaging predicts ventricular arrhythmias in implantable cardioverter-defibrillator patients. *J Am Coll Cardiol*, 55, 2769-77.
- BORLAUG, B. A. & REDFIELD, M. M. 2011. Diastolic and systolic heart failure are distinct phenotypes within the heart failure spectrum. *Circulation*, 123, 2006-13; discussion 2014.

- BOURKE, T., VASEGHI, M., MICHOWITZ, Y., SANKHLA, V., SHAH, M., SWAPNA, N., BOYLE, N. G., MAHAJAN, A., NARASIMHAN, C., LOKHANDWALA, Y. & SHIVKUMAR, K. 2010. Neuraxial modulation for refractory ventricular arrhythmias: value of thoracic epidural anesthesia and surgical left cardiac sympathetic denervation. *Circulation*, 121, 2255-62.
- BOYETT, M. R. & JEWELL, B. R. 1980. Analysis of the effects of changes in rate and rhythm upon electrical activity in the heart. *Prog Biophys Mol Biol*, 36, 1-52.
- BRACK, K. E., COOTE, J. H. & NG, G. A. 2011. Vagus nerve stimulation protects against ventricular fibrillation independent of muscarinic receptor activation. *Cardiovasc Res*, 91, 437-46.
- BRACK, K. E., PATEL, V. H., COOTE, J. H. & NG, G. A. 2007. Nitric oxide mediates the vagal protective effect on ventricular fibrillation via effects on action potential duration restitution in the rabbit heart. *J Physiol*, 583, 695-704.
- BRACK, K. E., PATEL, V. H., MANTRAVARDI, R., COOTE, J. H. & NG, G. A. 2009. Direct evidence of nitric oxide release from neuronal nitric oxide synthase activation in the left ventricle as a result of cervical vagus nerve stimulation. *J Physiol*, 587, 3045-54.
- BRAUNWALD, E. & BRISTOW, M. R. 2000. Congestive heart failure: fifty years of progress. *Circulation*, 102, IV14-23.
- BRISTOW, M. R. 2000. beta-adrenergic receptor blockade in chronic heart failure. *Circulation*, 101, 558-69.
- BRISTOW, M. R., GINSBURG, R., MINOBE, W., CUBICCIOTTI, R. S., SAGEMAN, W. S., LURIE, K., BILLINGHAM, M. E., HARRISON, D. C. & STINSON, E. B. 1982. Decreased catecholamine sensitivity and beta-adrenergic-receptor density in failing human hearts. *N Engl J Med*, 307, 205-11.
- BRUNNER-LA ROCCA, H. P., ESLER, M. D., JENNINGS, G. L. & KAYE, D. M. 2001. Effect of cardiac sympathetic nervous activity on mode of death in congestive heart failure. *Eur Heart J*, 22, 1136-43.
- BUTLER, G. C., ANDO, S. & FLORAS, J. S. 1997. Fractal component of variability of heart rate and systolic blood pressure in congestive heart failure. *Clin Sci (Lond)*, 92, 543-50.
- CAO, J. M., CHEN, L. S., KENKNIGHT, B. H., OHARA, T., LEE, M. H., TSAI, J., LAI, W. W., KARAGUEUZIAN, H. S., WOLF, P. L., FISHBEIN, M. C. & CHEN, P. S. 2000a. Nerve sprouting and sudden cardiac death. *Circ Res*, 86, 816-21.
- CAO, J. M., FISHBEIN, M. C., HAN, J. B., LAI, W. W., LAI, A. C., WU, T. J., CZER, L., WOLF, P. L., DENTON, T. A., SHINTAKU, I. P., CHEN, P. S. & CHEN, L. S. 2000b. Relationship between regional cardiac hyperinnervation and ventricular arrhythmia. *Circulation*, 101, 1960-9.
- CAO, J. M., QU, Z., KIM, Y. H., WU, T. J., GARFINKEL, A., WEISS, J. N., KARAGUEUZIAN, H. S. & CHEN, P. S. 1999. Spatiotemporal heterogeneity in the induction of ventricular fibrillation by rapid pacing: importance of cardiac restitution properties. *Circ Res*, 84, 1318-31.
- CARR, A. N., SCHMIDT, A. G., SUZUKI, Y., DEL MONTE, F., SATO, Y., LANNER, C., BREEDEN, K., JING, S. L., ALLEN, P. B., GREENGARD, P., YATANI, A., HOIT, B. D., GRUPP, I. L., HAJJAR, R. J., DEPAOLI-ROACH, A. A. & KRANIAS, E. G. 2002. Type 1 phosphatase, a negative regulator of cardiac function. *Mol Cell Biol*, 22, 4124-35.

- CASADEI, B. & PATERSON, D. J. 2000. Should we still use nitrovasodilators to test baroreflex sensitivity? *J Hypertens*, 18, 3-6.
- CHAMPION, H. C., SKAF, M. W. & HARE, J. M. 2003. Role of nitric oxide in the pathophysiology of heart failure. *Heart Fail Rev*, 8, 35-46.
- CHAN, S. H., WANG, L. L. & CHAN, J. Y. 2003. Differential engagements of glutamate and GABA receptors in cardiovascular actions of endogenous nNOS or iNOS at rostral ventrolateral medulla of rats. *Br J Pharmacol*, 138, 584-93.
- CHATTERJEE, K. & MASSIE, B. 2007. Systolic and diastolic heart failure: differences and similarities. *J Card Fail*, 13, 569-76.
- CHEN, G., ZHOU, X., FLOREA, S., QIAN, J., CAI, W., ZHANG, Z., FAN, G. C., LORENZ, J., HAJJAR, R. J. & KRANIAS, E. G. 2010. Expression of active protein phosphatase 1 inhibitor-1 attenuates chronic beta-agonist-induced cardiac apoptosis. *Basic Res Cardiol*, 105, 573-81.
- CHEN, P. S., CHEN, L. S., CAO, J. M., SHARIFI, B., KARAGUEUZIAN, H. S. & FISHBEIN, M. C. 2001. Sympathetic nerve sprouting, electrical remodeling and the mechanisms of sudden cardiac death. *Cardiovasc Res*, 50, 409-16.
- CHEN, X. Q., DU, J. Z. & WANG, Y. S. 2004. Regulation of hypoxia-induced release of corticotropin-releasing factor in the rat hypothalamus by norepinephrine. *Regul Pept*, 119, 221-8.
- CHENG, J., KAMIYA, K., LIU, W., TSUJI, Y., TOYAMA, J. & KODAMA, I. 1999. Heterogeneous distribution of the two components of delayed rectifier K⁺ current: a potential mechanism of the proarrhythmic effects of methanesulfonanilideclass III agents. *Cardiovasc Res*, 43, 135-47.
- CHIALVO, D. R., GILMOUR, R. F., JR. & JALIFE, J. 1990. Low dimensional chaos in cardiac tissue. *Nature*, 343, 653-7.
- CIBIS-II INVESTIGATORS AND COMMITTEES 1999. The Cardiac Insufficiency Bisoprolol Study II (CIBIS-II): a randomised trial. *Lancet*, 353, 9-13.
- COLUCCI, W. S., DENNISS, A. R., LEATHERMAN, G. F., QUIGG, R. J., LUDMER, P. L., MARSH, J. D. & GAUTHIER, D. F. 1988. Intracoronary infusion of dobutamine to patients with and without severe congestive heart failure. Dose-response relationships, correlation with circulating catecholamines, and effect of phosphodiesterase inhibition. *J Clin Invest*, 81, 1103-10.
- CONLON, K. & KIDD, C. 1999. Neuronal nitric oxide facilitates vagal chronotropic and dromotropic actions on the heart. *J Auton Nerv Syst*, 75, 136-46.
- COWIE, M. R., WOOD, D. A., COATS, A. J., THOMPSON, S. G., POOLE-WILSON, P. A., SURESH, V. & SUTTON, G. C. 1999. Incidence and aetiology of heart failure: a population-based study. *Eur Heart J*, 20, 421-8.
- CRACKOWER, M. A., OUDIT, G. Y., KOZIERADZKI, I., SARAO, R., SUN, H., SASAKI, T., HIRSCH, E., SUZUKI, A., SHIOI, T., IRIE-SASAKI, J., SAH, R., CHENG, H. Y., RYBIN, V. O., LEMBO, G., FRATTA, L., OLIVEIRA-DOS-SANTOS, A. J., BENOVIC, J. L., KAHN, C. R., IZUMO, S., STEINBERG, S. F., WYMAN, M. P., BACKX, P. H. & PENNINGER, J. M. 2002. Regulation of myocardial contractility and cell size by distinct PI3K-PTEN signaling pathways. *Cell*, 110, 737-49.
- CROSS, H. R., STEENBERGEN, C., LEFKOWITZ, R. J., KOCH, W. J. & MURPHY, E. 1999. Overexpression of the cardiac beta(2)-adrenergic receptor and expression of a beta-adrenergic receptor kinase-1 (betaARK1) inhibitor

- both increase myocardial contractility but have differential effects on susceptibility to ischemic injury. *Circ Res*, 85, 1077-84.
- DAE, M. W., O'CONNELL, J. W., BOTVINICK, E. H. & CHIN, M. C. 1995. Acute and chronic effects of transient myocardial ischemia on sympathetic nerve activity, density, and norepinephrine content. *Cardiovasc Res*, 30, 270-80.
- DANSON, E. J., CHOATE, J. K. & PATERSON, D. J. 2005. Cardiac nitric oxide: emerging role for nNOS in regulating physiological function. *Pharmacol Ther*, 106, 57-74.
- DE FERRARI, G. M., CRIJNS, H. J., BORGGREFE, M., MILASINOVIC, G., SMID, J., ZABEL, M., GAVAZZI, A., SANZO, A., DENNERT, R., KUSCHYK, J., RASPOPOVIC, S., KLEIN, H., SWEDBERG, K., SCHWARTZ, P. J. & CARDIOFIT MULTICENTER TRIAL, I. 2011. Chronic vagus nerve stimulation: a new and promising therapeutic approach for chronic heart failure. *Eur Heart J*, 32, 847-55.
- DE FERRARI, G. M. & SCHWARTZ, P. J. 2011. Vagus nerve stimulation: from pre-clinical to clinical application: challenges and future directions. *Heart Fail Rev*, 16, 195-203.
- DE FERRARI, G. M., VANOLI, E., STRAMBA-BADIALE, M., HULL, S. S., JR., FOREMAN, R. D. & SCHWARTZ, P. J. 1991. Vagal reflexes and survival during acute myocardial ischemia in conscious dogs with healed myocardial infarction. *Am J Physiol*, 261, H63-9.
- DE KEULENAER, G. W. & BRUTSAERT, D. L. 2009. The heart failure spectrum: time for a phenotype-oriented approach. *Circulation*, 119, 3044-6.
- DE KEULENAER, G. W. & BRUTSAERT, D. L. 2011. Systolic and diastolic heart failure are overlapping phenotypes within the heart failure spectrum. *Circulation*, 123, 1996-2004; discussion 2005.
- DEGEORGE, B. R. & KOCH, W. J. 2008. Gi/o signaling and its potential role in cardioprotection. *Expert Rev Cardiovasc Ther*, 6, 785-7.
- DEGRADO, T. R., ZALUTSKY, M. R. & VAIDYANATHAN, G. 1995. Uptake mechanisms of meta-[123I]iodobenzylguanidine in isolated rat heart. *Nucl Med Biol*, 22, 1-12.
- DIVIANI, D. 2008. Modulation of cardiac function by A-kinase anchoring proteins. *Curr Opin Pharmacol*, 8, 166-73.
- DODGE-KAFKA, K. L., LANGEBERG, L. & SCOTT, J. D. 2006. Compartmentation of cyclic nucleotide signaling in the heart: the role of A-kinase anchoring proteins. *Circ Res*, 98, 993-1001.
- DORN, G. W., 2ND & MOLKENTIN, J. D. 2004. Manipulating cardiac contractility in heart failure: data from mice and men. *Circulation*, 109, 150-8.
- DORN, G. W., 2ND, TEPE, N. M., LORENZ, J. N., KOCH, W. J. & LIGGETT, S. B. 1999. Low- and high-level transgenic expression of beta2-adrenergic receptors differentially affect cardiac hypertrophy and function in Galphaq-overexpressing mice. *Proc Natl Acad Sci U S A*, 96, 6400-5.
- DU, X. J., AUTELITANO, D. J., DILLEY, R. J., WANG, B., DART, A. M. & WOODCOCK, E. A. 2000a. beta(2)-adrenergic receptor overexpression exacerbates development of heart failure after aortic stenosis. *Circulation*, 101, 71-7.
- DU, X. J., GAO, X. M., JENNINGS, G. L., DART, A. M. & WOODCOCK, E. A. 2000b. Preserved ventricular contractility in infarcted mouse heart overexpressing beta(2)-adrenergic receptors. *Am J Physiol Heart Circ Physiol*, 279, H2456-63.

- DUNLAP, M. E., BIBEVSKI, S., ROSENBERRY, T. L. & ERNSBERGER, P. 2003. Mechanisms of altered vagal control in heart failure: influence of muscarinic receptors and acetylcholinesterase activity. *Am J Physiol Heart Circ Physiol*, 285, H1632-40.
- EICHHORN, E. J. & BRISTOW, M. R. 2001. The Carvedilol Prospective Randomized Cumulative Survival (COPERNICUS) trial. *Curr Control Trials Cardiovasc Med*, 2, 20-23.
- EISENHOFER, G., ESLER, M. D., MEREDITH, I. T., DART, A., CANNON, R. O., 3RD, QUYYUMI, A. A., LAMBERT, G., CHIN, J., JENNINGS, G. L. & GOLDSTEIN, D. S. 1992. Sympathetic nervous function in human heart as assessed by cardiac spillovers of dihydroxyphenylglycol and norepinephrine. *Circulation*, 85, 1775-85.
- EL-ARMOUCHE, A., PAMMINGER, T., DITZ, D., ZOLK, O. & ESCHENHAGEN, T. 2004. Decreased protein and phosphorylation level of the protein phosphatase inhibitor-1 in failing human hearts. *Cardiovasc Res*, 61, 87-93.
- EL-ARMOUCHE, A., POHLMANN, L., SCHLOSSAREK, S., STARBATTEY, J., YEH, Y. H., NATTEL, S., DOBREV, D., ESCHENHAGEN, T. & CARRIER, L. 2007. Decreased phosphorylation levels of cardiac myosin-binding protein-C in human and experimental heart failure. *J Mol Cell Cardiol*, 43, 223-9.
- EL-ARMOUCHE, A., RAU, T., ZOLK, O., DITZ, D., PAMMINGER, T., ZIMMERMANN, W. H., JACKEL, E., HARDING, S. E., BOKNIK, P., NEUMANN, J. & ESCHENHAGEN, T. 2003a. Evidence for protein phosphatase inhibitor-1 playing an amplifier role in beta-adrenergic signaling in cardiac myocytes. *FASEB J*, 17, 437-9.
- EL-ARMOUCHE, A., WITTKOPPER, K., DEGENHARDT, F., WEINBERGER, F., DIDIE, M., MELNYCHENKO, I., GRIMM, M., PEECK, M., ZIMMERMANN, W. H., UNSOLD, B., HASENFUSS, G., DOBREV, D. & ESCHENHAGEN, T. 2008. Phosphatase inhibitor-1-deficient mice are protected from catecholamine-induced arrhythmias and myocardial hypertrophy. *Cardiovasc Res*, 80, 396-406.
- EL-ARMOUCHE, A., ZOLK, O., RAU, T. & ESCHENHAGEN, T. 2003b. Inhibitory G-proteins and their role in desensitization of the adenylyl cyclase pathway in heart failure. *Cardiovasc Res*, 60, 478-87.
- ELAM, M. & MACEFIELD, V. 2001. Multiple firing of single muscle vasoconstrictor neurons during cardiac dysrhythmias in human heart failure. *J Appl Physiol (1985)*, 91, 717-24.
- ENGELHARDT, S., BOHM, M., ERDMANN, E. & LOHSE, M. J. 1996. Analysis of beta-adrenergic receptor mRNA levels in human ventricular biopsy specimens by quantitative polymerase chain reactions: progressive reduction of beta 1-adrenergic receptor mRNA in heart failure. *J Am Coll Cardiol*, 27, 146-54.
- ENGELHARDT, S., HEIN, L., DYACHENKOW, V., KRANIAS, E. G., ISENBERG, G. & LOHSE, M. J. 2004. Altered calcium handling is critically involved in the cardiotoxic effects of chronic beta-adrenergic stimulation. *Circulation*, 109, 1154-60.
- ENGELHARDT, S., HEIN, L., WIESMANN, F. & LOHSE, M. J. 1999. Progressive hypertrophy and heart failure in beta1-adrenergic receptor transgenic mice. *Proc Natl Acad Sci U S A*, 96, 7059-64.

- ESCHENHAGEN, T. 2008. Beta-adrenergic signaling in heart failure-adapt or die. *Nat Med*, 14, 485-7.
- ESCHENHAGEN, T., FRIEDRICHSEN, M., GSELL, S., HOLLMANN, A., MITTMANN, C., SCHMITZ, W., SCHOLZ, H., WEIL, J. & WEINSTEIN, L. S. 1996. Regulation of the human Gi alpha-2 gene promotor activity in embryonic chicken cardiomyocytes. *Basic Res Cardiol*, 91 Suppl 2, 41-6.
- ESCHENHAGEN, T., MENDE, U., NOSE, M., SCHMITZ, W., SCHOLZ, H., HAVERICH, A., HIRT, S., DORING, V., KALMAR, P., HOPPNER, W. & ET AL. 1992. Increased messenger RNA level of the inhibitory G protein alpha subunit Gi alpha-2 in human end-stage heart failure. *Circ Res*, 70, 688-96.
- ESLER, M. 2010. The 2009 Carl Ludwig Lecture: Pathophysiology of the human sympathetic nervous system in cardiovascular diseases: the transition from mechanisms to medical management. *J Appl Physiol (1985)*, 108, 227-37.
- ESLER, M., JENNINGS, G., LAMBERT, G., MEREDITH, I., HORNE, M. & EISENHOFER, G. 1990. Overflow of catecholamine neurotransmitters to the circulation: source, fate, and functions. *Physiol Rev*, 70, 963-85.
- ESTES, E. H., JR. & IZLAR, H. L., JR. 1961. Recurrent ventricular tachycardia. A case successfully treated by bilateral cardiac sympathectomy. *Am J Med*, 31, 493-7.
- FARRELL, T. G., BASHIR, Y., CRIPPS, T., MALIK, M., POLONIECKI, J., BENNETT, E. D., WARD, D. E. & CAMM, A. J. 1991. Risk stratification for arrhythmic events in postinfarction patients based on heart rate variability, ambulatory electrocardiographic variables and the signal-averaged electrocardiogram. *J Am Coll Cardiol*, 18, 687-97.
- FARRELL, T. G., ODEMUYIWA, O., BASHIR, Y., CRIPPS, T. R., MALIK, M., WARD, D. E. & CAMM, A. J. 1992. Prognostic value of baroreflex sensitivity testing after acute myocardial infarction. *Br Heart J*, 67, 129-37.
- FAULX, M. D., ERNSBERGER, P., VATNER, D., HOFFMAN, R. D., LEWIS, W., STRACHAN, R. & HOIT, B. D. 2005. Strain-dependent beta-adrenergic receptor function influences myocardial responses to isoproterenol stimulation in mice. *Am J Physiol Heart Circ Physiol*, 289, H30-6.
- FELDMAN, A. M., BRISTOW, M. R., PARMLEY, W. W., CARSON, P. E., PEPINE, C. J., GILBERT, E. M., STROBECK, J. E., HENDRIX, G. H., POWERS, E. R., BAIN, R. P. & ET AL. 1993. Effects of vesnarinone on morbidity and mortality in patients with heart failure. Vesnarinone Study Group. *N Engl J Med*, 329, 149-55.
- FELDMAN, A. M., CATES, A. E., VEAZEY, W. B., HERSHBERGER, R. E., BRISTOW, M. R., BAUGHMAN, K. L., BAUMGARTNER, W. A. & VAN DOP, C. 1988. Increase of the 40,000-mol wt pertussis toxin substrate (G protein) in the failing human heart. *J Clin Invest*, 82, 189-97.
- FELDMAN, M. D., COPELAS, L., GWATHMEY, J. K., PHILLIPS, P., WARREN, S. E., SCHOEN, F. J., GROSSMAN, W. & MORGAN, J. P. 1987. Deficient production of cyclic AMP: pharmacologic evidence of an important cause of contractile dysfunction in patients with end-stage heart failure. *Circulation*, 75, 331-9.
- FLORAS, J. S. 2003. Sympathetic activation in human heart failure: diverse mechanisms, therapeutic opportunities. *Acta Physiol Scand*, 177, 391-8.

- FOLEY, K. F., VAN DORT, M. E., SIEVERT, M. K., RUOHO, A. E. & COZZI, N. V. 2002. Stereospecific inhibition of monoamine uptake transporters by meta-hydroxyephedrine isomers. *J Neural Transm*, 109, 1229-40.
- FRANCOIS-FRANCK, C. 1899. Signification physiologique e la resection du sympathetique dans la maladie de Basedow, l'epilepsie, l'idiotie et de glaucoma. *Bull ACAD MED*, 41, 565.
- GAO, M. H., LAI, N. C., ROTH, D. M., ZHOU, J., ZHU, J., ANZAI, T., DALTON, N. & HAMMOND, H. K. 1999. Adenylylcyclase increases responsiveness to catecholamine stimulation in transgenic mice. *Circulation*, 99, 1618-22.
- GAUDIN, C., ISHIKAWA, Y., WIGHT, D. C., MAHDAVI, V., NADAL-GINARD, B., WAGNER, T. E., VATNER, D. E. & HOMCY, C. J. 1995. Overexpression of Gs alpha protein in the hearts of transgenic mice. *J Clin Invest*, 95, 1676-83.
- GILMOUR, R. F., JR. & CHIALVO, D. R. 1999. Electrical restitution, critical mass, and the riddle of fibrillation. *J Cardiovasc Electrophysiol*, 10, 1087-9.
- GILSBACH, R., BREDE, M., BEETZ, N., MOURA, E., MUTHIG, V., GERSTNER, C., BARRETO, F., NEUBAUER, S., VIEIRA-COELHO, M. A. & HEIN, L. 2007. Heterozygous alpha 2C-adrenoceptor-deficient mice develop heart failure after transverse aortic constriction. *Cardiovasc Res*, 75, 728-37.
- GRASSI, G., SERAVALLE, G., BERTINIERI, G., TURRI, C., STELLA, M. L., SCOPELLITI, F. & MANCIA, G. 2001. Sympathetic and reflex abnormalities in heart failure secondary to ischaemic or idiopathic dilated cardiomyopathy. *Clin Sci (Lond)*, 101, 141-6.
- GUIX, F. X., URIBESALGO, I., COMA, M. & MUÑOZ, F. J. 2005. The physiology and pathophysiology of nitric oxide in the brain. *Prog Neurobiol*, 76, 126-52.
- GUNTHER, A., WITTE, O. W. & HOYER, D. 2010. Autonomic dysfunction and risk stratification assessed from heart rate pattern. *Open Neurol J*, 4, 39-49.
- GUYENET, P. G. 1991. Central noradrenergic neurons: the autonomic connection. *Prog Brain Res*, 88, 365-80.
- HADCOCK, J. R., PORT, J. D. & MALBON, C. C. 1991. Cross-regulation between G-protein-mediated pathways. Activation of the inhibitory pathway of adenylylcyclase increases the expression of beta 2-adrenergic receptors. *J Biol Chem*, 266, 11915-22.
- HALDEMAN, G. A., CROFT, J. B., GILES, W. H. & RASHIDEE, A. 1999. Hospitalization of patients with heart failure: National Hospital Discharge Survey, 1985 to 1995. *Am Heart J*, 137, 352-60.
- HARDING, V. B., JONES, L. R., LEFKOWITZ, R. J., KOCH, W. J. & ROCKMAN, H. A. 2001. Cardiac beta ARK1 inhibition prolongs survival and augments beta blocker therapy in a mouse model of severe heart failure. *Proc Natl Acad Sci U S A*, 98, 5809-14.
- HASENFUSS, G. 1998. Alterations of calcium-regulatory proteins in heart failure. *Cardiovasc Res*, 37, 279-89.
- HASENFUSS, G. & PIESKE, B. 2002. Calcium cycling in congestive heart failure. *J Mol Cell Cardiol*, 34, 951-69.
- HERRING, N., GOLDING, S. & PATERSON, D. J. 2000. Pre-synaptic NO-cGMP pathway modulates vagal control of heart rate in isolated adult guinea pig atria. *J Mol Cell Cardiol*, 32, 1795-804.
- HJALMARSON, A. & FAGERBERG, B. 2000. MERIT-HF mortality and morbidity data. *Basic Res Cardiol*, 95 Suppl 1, I98-103.

- HJALMARSON, A., GOLDSTEIN, S., FAGERBERG, B., WEDEL, H., WAAGSTEIN, F., KJEKSHUS, J., WIKSTRAND, J., EL ALLAF, D., VITOVEC, J., ALDERSHVILE, J., HALINEN, M., DIETZ, R., NEUHAUS, K. L., JANOSI, A., THORGEIRSSON, G., DUNSELMAN, P. H., GULLESTAD, L., KUCH, J., HERLITZ, J., RICKENBACHER, P., BALL, S., GOTTLIEB, S. & DEEDWANIA, P. 2000. Effects of controlled-release metoprolol on total mortality, hospitalizations, and well-being in patients with heart failure: the Metoprolol CR/XL Randomized Intervention Trial in congestive heart failure (MERIT-HF). MERIT-HF Study Group. *JAMA*, 283, 1295-302.
- HO, K. K., PINSKY, J. L., KANNEL, W. B. & LEVY, D. 1993. The epidemiology of heart failure: the Framingham Study. *J Am Coll Cardiol*, 22, 6A-13A.
- HOFFMANN, J., GRIMM, W., MENZ, V., KNOP, U. & MAISCH, B. 1996. Heart rate variability and major arrhythmic events in patients with idiopathic dilated cardiomyopathy. *Pacing Clin Electrophysiol*, 19, 1841-4.
- HOUSER, S. R. & MARGULIES, K. B. 2003. Is depressed myocyte contractility centrally involved in heart failure? *Circ Res*, 92, 350-8.
- HULL, S. S., JR., EVANS, A. R., VANOLI, E., ADAMSON, P. B., STRAMBA-BADIALE, M., ALBERT, D. E., FOREMAN, R. D. & SCHWARTZ, P. J. 1990. Heart rate variability before and after myocardial infarction in conscious dogs at high and low risk of sudden death. *J Am Coll Cardiol*, 16, 978-85.
- INOUE, H. & ZIPES, D. P. 1988. Time course of denervation of efferent sympathetic and vagal nerves after occlusion of the coronary artery in the canine heart. *Circ Res*, 62, 1111-20.
- ISHISE, H., ASANOI, H., ISHIZAKA, S., JOHO, S., KAMEYAMA, T., UMENO, K. & INOUE, H. 1998. Time course of sympathovagal imbalance and left ventricular dysfunction in conscious dogs with heart failure. *J Appl Physiol* (1985), 84, 1234-41.
- IWASE, M., UECHI, M., VATNER, D. E., ASAII, K., SHANNON, R. P., KUDEJ, R. K., WAGNER, T. E., WIGHT, D. C., PATRICK, T. A., ISHIKAWA, Y., HOMCY, C. J. & VATNER, S. F. 1997. Cardiomyopathy induced by cardiac Gs alpha overexpression. *Am J Physiol*, 272, H585-9.
- JACOBSON, A. F., LOMBARD, J., BANERJEE, G. & CAMICI, P. G. 2009. ¹²³I-mIBG scintigraphy to predict risk for adverse cardiac outcomes in heart failure patients: design of two prospective multicenter international trials. *J Nucl Cardiol*, 16, 113-21.
- JANUZZI, J. L., VAN KIMMENADE, R., LAINCHBURY, J., BAYES-GENIS, A., ORDONEZ-LLANOS, J., SANTALO-BEL, M., PINTO, Y. M. & RICHARDS, M. 2006. NT-proBNP testing for diagnosis and short-term prognosis in acute destabilized heart failure: an international pooled analysis of 1256 patients: the International Collaborative of NT-proBNP Study. *Eur Heart J*, 27, 330-7.
- JOHANSEN, H., STRAUSS, B., ARNOLD, J. M., MOE, G. & LIU, P. 2003. On the rise: The current and projected future burden of congestive heart failure hospitalization in Canada. *Can J Cardiol*, 19, 430-5.
- JOHNSON, T. A., GRAY, A. L., LAUENSTEIN, J. M., NEWTON, S. S. & MASSARI, V. J. 2004. Parasympathetic control of the heart. I. An interventriculo-septal ganglion is the major source of the vagal intracardiac innervation of the ventricles. *J Appl Physiol* (1985), 96, 2265-72.

- JONNESCO, T. 1921. Traitement chirurgical de l'angine de poitrine par la resection du sympathique cervico-thoracique. *Press Med*, 20, 221-230.
- KAMMERLING, J. J., GREEN, F. J., WATANABE, A. M., INOUE, H., BARBER, M. J., HENRY, D. P. & ZIPES, D. P. 1987. Denervation supersensitivity of refractoriness in noninfarcted areas apical to transmural myocardial infarction. *Circulation*, 76, 383-93.
- KANNEL, W. B. & BELANGER, A. J. 1991. Epidemiology of heart failure. *Am Heart J*, 121, 951-7.
- KANNEL, W. B., HO, K. & THOM, T. 1994. Changing epidemiological features of cardiac failure. *Br Heart J*, 72, S3-9.
- KARMA, A. 1994. Electrical alternans and spiral wave breakup in cardiac tissue. *Chaos*, 4, 461-472.
- KASAMA, S., TOYAMA, T., SUMINO, H., KUMAKURA, H., TAKAYAMA, Y., MINAMI, K., ICHIKAWA, S., MATSUMOTO, N., SATO, Y. & KURABAYASHI, M. 2011. Prognostic value of cardiac sympathetic nerve activity evaluated by [123I]m-iodobenzylguanidine imaging in patients with ST-segment elevation myocardial infarction. *Heart*, 97, 20-6.
- KAWANO, H., OKADA, R. & YANO, K. 2003. Histological study on the distribution of autonomic nerves in the human heart. *Heart Vessels*, 18, 32-9.
- KIOKA, H., YAMADA, T., MINE, T., MORITA, T., TSUKAMOTO, Y., TAMAKI, S., MASUDA, M., OKUDA, K., HORI, M. & FUKUNAMI, M. 2007. Prediction of sudden death in patients with mild-to-moderate chronic heart failure by using cardiac iodine-123 metaiodobenzylguanidine imaging. *Heart*, 93, 1213-8.
- KLEIGER, R. E., MILLER, J. P., BIGGER, J. T., JR. & MOSS, A. J. 1987. Decreased heart rate variability and its association with increased mortality after acute myocardial infarction. *Am J Cardiol*, 59, 256-62.
- KOCH, W. J., ROCKMAN, H. A., SAMAMA, P., HAMILTON, R. A., BOND, R. A., MILANO, C. A. & LEFKOWITZ, R. J. 1995. Cardiac function in mice overexpressing the beta-adrenergic receptor kinase or a beta ARK inhibitor. *Science*, 268, 1350-3.
- KOHOUT, T. A., TAKAOKA, H., MCDONALD, P. H., PERRY, S. J., MAO, L., LEFKOWITZ, R. J. & ROCKMAN, H. A. 2001. Augmentation of cardiac contractility mediated by the human beta(3)-adrenergic receptor overexpressed in the hearts of transgenic mice. *Circulation*, 104, 2485-91.
- KOMAMURA, K. 2013. Similarities and Differences between the Pathogenesis and Pathophysiology of Diastolic and Systolic Heart Failure. *Cardiol Res Pract*, 2013, 824135.
- KURAMOTO, Y., YAMADA, T., TAMAKI, S., OKUYAMA, Y., MORITA, T., FURUKAWA, Y., TANAKA, K., IWASAKI, Y., YASUI, T., UEDA, H., OKADA, T., KAWASAKI, M., LEVY, W. C., KOMURO, I. & FUKUNAMI, M. 2011. Usefulness of cardiac iodine-123 meta-iodobenzylguanidine imaging to improve prognostic power of Seattle heart failure model in patients with chronic heart failure. *Am J Cardiol*, 107, 1185-90.
- LA ROVERE, M. T., BIGGER, J. T., JR., MARCUS, F. I., MORTARA, A. & SCHWARTZ, P. J. 1998. Baroreflex sensitivity and heart-rate variability in prediction of total cardiac mortality after myocardial infarction. ATRAMI (Autonomic Tone and Reflexes After Myocardial Infarction) Investigators. *Lancet*, 351, 478-84.

- LA ROVERE, M. T., SPECCHIA, G., MORTARA, A. & SCHWARTZ, P. J. 1988. Baroreflex sensitivity, clinical correlates, and cardiovascular mortality among patients with a first myocardial infarction. A prospective study. *Circulation*, 78, 816-24.
- LAI, N. C., TANG, T., GAO, M. H., SAITO, M., TAKAHASHI, T., ROTH, D. M. & HAMMOND, H. K. 2008. Activation of cardiac adenylyl cyclase expression increases function of the failing ischemic heart in mice. *J Am Coll Cardiol*, 51, 1490-7.
- LANZA, G. A., BENDINI, M. G., INTINI, A., DE MARTINO, G., GALEAZZI, M., GUIDO, V. & SESTITO, A. 2000. Prognostic role of heart rate variability in patients with idiopathic dilated cardiomyopathy. *Ital Heart J*, 1, 56-63.
- LAW, M. P., OSMAN, S., DAVENPORT, R. J., CUNNINGHAM, V. J., PIKE, V. W. & CAMICI, P. G. 1997. Biodistribution and metabolism of [N-methyl-11C]m-hydroxyephedrine in the rat. *Nucl Med Biol*, 24, 417-24.
- LAW, M. P., SCHAFERS, K., KOPKA, K., WAGNER, S., SCHOBER, O. & SCHAFERS, M. 2010. Molecular imaging of cardiac sympathetic innervation by 11C-mHED and PET: from man to mouse? *J Nucl Med*, 51, 1269-76.
- LEHNART, S. E., WEHRENS, X. H., REIKEN, S., WARRIER, S., BELEVYCH, A. E., HARVEY, R. D., RICHTER, W., JIN, S. L., CONTI, M. & MARKS, A. R. 2005. Phosphodiesterase 4D deficiency in the ryanodine-receptor complex promotes heart failure and arrhythmias. *Cell*, 123, 25-35.
- LEVY, M. N. & BLATTBERG, B. 1976. Effect of vagal stimulation on the overflow of norepinephrine into the coronary sinus during cardiac sympathetic nerve stimulation in the dog. *Circ Res*, 38, 81-4.
- LI, M., ZHENG, C., SATO, T., KAWADA, T., SUGIMACHI, M. & SUNAGAWA, K. 2004a. Vagal nerve stimulation markedly improves long-term survival after chronic heart failure in rats. *Circulation*, 109, 120-4.
- LI, W., KNOWLTON, D., VAN WINKLE, D. M. & HABEKER, B. A. 2004b. Infarction alters both the distribution and noradrenergic properties of cardiac sympathetic neurons. *Am J Physiol Heart Circ Physiol*, 286, H2229-36.
- LIGGETT, S. B., CRESCI, S., KELLY, R. J., SYED, F. M., MATKOVICH, S. J., HAHN, H. S., DIWAN, A., MARTINI, J. S., SPARKS, L., PAREKH, R. R., SPERTUS, J. A., KOCH, W. J., KARDIA, S. L. & DORN, G. W., 2ND 2008. A GRK5 polymorphism that inhibits beta-adrenergic receptor signaling is protective in heart failure. *Nat Med*, 14, 510-7.
- LIGGETT, S. B., TEPE, N. M., LORENZ, J. N., CANNING, A. M., JANTZ, T. D., MITARAI, S., YATANI, A. & DORN, G. W., 2ND 2000. Early and delayed consequences of beta(2)-adrenergic receptor overexpression in mouse hearts: critical role for expression level. *Circulation*, 101, 1707-14.
- LIN, L. H., TAKTAKISHVILI, O. & TALMAN, W. T. 2007. Identification and localization of cell types that express endothelial and neuronal nitric oxide synthase in the rat nucleus tractus solitarius. *Brain Res*, 1171, 42-51.
- LINK, J. M., SYNOVEC, R. E., KROHN, K. A. & CALDWELL, J. H. 1997. High speed liquid chromatography of phenylethanolamines for the kinetic analysis of [11C]-meta-hydroxyephedrine and metabolites in plasma. *J Chromatogr B Biomed Sci Appl*, 693, 31-41.
- LIU Y, X. C., JIAO J, WANG H, DONG D, YANG B 2005. M3-R/IKM3 - a new target of antiarrhythmic agents. *Acta Pharmace Sinica*, 50, 8-12.

- LOHSE, M. J., ENGELHARDT, S. & ESCHENHAGEN, T. 2003. What is the role of beta-adrenergic signaling in heart failure? *Circ Res*, 93, 896-906.
- LUNDBERG, J. O., WEITZBERG, E. & GLADWIN, M. T. 2008. The nitrate-nitrite-nitric oxide pathway in physiology and therapeutics. *Nat Rev Drug Discov*, 7, 156-67.
- MACDOUGALL, L. K., JONES, L. R. & COHEN, P. 1991. Identification of the major protein phosphatases in mammalian cardiac muscle which dephosphorylate phospholamban. *Eur J Biochem*, 196, 725-34.
- MANN, D. L. & BRISTOW, M. R. 2005. Mechanisms and models in heart failure: the biomechanical model and beyond. *Circulation*, 111, 2837-49.
- MANTRAVADI, R., GABRIS, B., LIU, T., CHOI, B. R., DE GROAT, W. C., NG, G. A. & SALAMA, G. 2007. Autonomic nerve stimulation reverses ventricular repolarization sequence in rabbit hearts. *Circ Res*, 100, e72-80.
- MARX, S. O., REIKEN, S., HISAMATSU, Y., JAYARAMAN, T., BURKHOFF, D., ROSEMLIT, N. & MARKS, A. R. 2000. PKA phosphorylation dissociates FKBP12.6 from the calcium release channel (ryanodine receptor): defective regulation in failing hearts. *Cell*, 101, 365-76.
- MASKIN, C. S., SISKIND, S. J. & LEJEMTEL, T. H. 1984. High prevalence of nonsustained ventricular tachycardia in severe congestive heart failure. *Am Heart J*, 107, 896-901.
- MASSION, P. B., FERON, O., DESSY, C. & BALLIGAND, J. L. 2003. Nitric oxide and cardiac function: ten years after, and continuing. *Circ Res*, 93, 388-98.
- MATKOVICH, S. J., DIWAN, A., KLANKE, J. L., HAMMER, D. J., MARREEZ, Y., ODLEY, A. M., BRUNSKILL, E. W., KOCH, W. J., SCHWARTZ, R. J. & DORN, G. W., 2ND 2006. Cardiac-specific ablation of G-protein receptor kinase 2 redefines its roles in heart development and beta-adrenergic signaling. *Circ Res*, 99, 996-1003.
- MAZZEO, A. T., LA MONACA, E., DI LEO, R., VITA, G. & SANTAMARIA, L. B. 2011. Heart rate variability: a diagnostic and prognostic tool in anesthesia and intensive care. *Acta Anaesthesiol Scand*, 55, 797-811.
- MCCULLOUGH, P. A., PHILBIN, E. F., SPERTUS, J. A., KAATZ, S., SANDBERG, K. R., WEAVER, W. D. & RESOURCE UTILIZATION AMONG CONGESTIVE HEART FAILURE, S. 2002. Confirmation of a heart failure epidemic: findings from the Resource Utilization Among Congestive Heart Failure (REACH) study. *J Am Coll Cardiol*, 39, 60-9.
- MCDONAGH, T. A., MORRISON, C. E., LAWRENCE, A., FORD, I., TUNSTALL-PEDOE, H., MCMURRAY, J. J. & DARGIE, H. J. 1997. Symptomatic and asymptomatic left-ventricular systolic dysfunction in an urban population. *Lancet*, 350, 829-33.
- MCKEE, P. A., CASTELLI, W. P., MCNAMARA, P. M. & KANNEL, W. B. 1971. The natural history of congestive heart failure: the Framingham study. *N Engl J Med*, 285, 1441-6.
- MCMURRAY, J., MCDONAGH, T., MORRISON, C. E. & DARGIE, H. J. 1993. Trends in hospitalization for heart failure in Scotland 1980-1990. *Eur Heart J*, 14, 1158-62.
- MCMURRAY, J. J. & STEWART, S. 2000. Epidemiology, aetiology, and prognosis of heart failure. *Heart*, 83, 596-602.
- MESSER, A. E., JACQUES, A. M. & MARSTON, S. B. 2007. Troponin phosphorylation and regulatory function in human heart muscle: dephosphorylation of

- Ser23/24 on troponin I could account for the contractile defect in end-stage heart failure. *J Mol Cell Cardiol*, 42, 247-59.
- MILANO, C. A., ALLEN, L. F., ROCKMAN, H. A., DOLBER, P. C., MCMINN, T. R., CHIEN, K. R., JOHNSON, T. D., BOND, R. A. & LEFKOWITZ, R. J. 1994. Enhanced myocardial function in transgenic mice overexpressing the beta 2-adrenergic receptor. *Science*, 264, 582-6.
- MONCADA, S., PALMER, R. M. & HIGGS, E. A. 1991. Nitric oxide: physiology, pathophysiology, and pharmacology. *Pharmacol Rev*, 43, 109-42.
- MORRIS, M. J., COX, H. S., LAMBERT, G. W., KAYE, D. M., JENNINGS, G. L., MEREDITH, I. T. & ESLER, M. D. 1997. Region-specific neuropeptide Y overflows at rest and during sympathetic activation in humans. *Hypertension*, 29, 137-43.
- MOSS, A. J. & MCDONALD, J. 1971. Unilateral cervicothoracic sympathetic ganglionectomy for the treatment of long QT interval syndrome. *N Engl J Med*, 285, 903-4.
- MOVSESIAN, M. A. & BRISTOW, M. R. 2005. Alterations in cAMP-mediated signaling and their role in the pathophysiology of dilated cardiomyopathy. *Curr Top Dev Biol*, 68, 25-48.
- MUDD, J. O. & KASS, D. A. 2008. Tackling heart failure in the twenty-first century. *Nature*, 451, 919-28.
- MURAD, F., CHI, Y. M., RALL, T. W. & SUTHERLAND, E. W. 1962. Adenyl cyclase. III. The effect of catecholamines and choline esters on the formation of adenosine 3',5'-phosphate by preparations from cardiac muscle and liver. *J Biol Chem*, 237, 1233-8.
- MUSCHOLL, E. 1980. Peripheral muscarinic control of norepinephrine release in the cardiovascular system. *Am J Physiol*, 239, H713-20.
- MUSIALEK, P. & CASADEI, B. 2000. Nitrovasodilators and heart rate: more than the arterial baroreflex. *Cardiovasc Res*, 47, 404-5.
- NAKAJO, M., SHAPIRO, B., GLOWNIAK, J., SISSON, J. C. & BEIERWALTES, W. H. 1983. Inverse relationship between cardiac accumulation of meta-[131I]iodobenzylguanidine (I-131 MIBG) and circulating catecholamines in suspected pheochromocytoma. *J Nucl Med*, 24, 1127-34.
- NARULA, J. & SARKAR, K. 2003. A conceptual paradox of MIBG uptake in heart failure: retention with incontinence! *J Nucl Cardiol*, 10, 700-4.
- NEUMANN, J., ESCHENHAGEN, T., JONES, L. R., LINCK, B., SCHMITZ, W., SCHOLZ, H. & ZIMMERMANN, N. 1997. Increased expression of cardiac phosphatases in patients with end-stage heart failure. *J Mol Cell Cardiol*, 29, 265-72.
- NEUMANN, J., SCHMITZ, W., SCHOLZ, H., VON MEYERINCK, L., DORING, V. & KALMAR, P. 1988. Increase in myocardial Gi-proteins in heart failure. *Lancet*, 2, 936-7.
- NG, G. A., BRACK, K. E., PATEL, V. H. & COOTE, J. H. 2007. Autonomic modulation of electrical restitution, alternans and ventricular fibrillation initiation in the isolated heart. *Cardiovasc Res*, 73, 750-60.
- NOLAN, J., BATIN, P. D., ANDREWS, R., LINDSAY, S. J., BROOKSBY, P., MULLEN, M., BAIG, W., FLAPAN, A. D., COWLEY, A., PRESCOTT, R. J., NEILSON, J. M. & FOX, K. A. 1998. Prospective study of heart rate variability and mortality in chronic heart failure: results of the United Kingdom heart failure

- evaluation and assessment of risk trial (UK-heart). *Circulation*, 98, 1510-6.
- NOLAN, J., FLAPAN, A. D., CAPEWELL, S., MACDONALD, T. M., NEILSON, J. M. & EWING, D. J. 1992. Decreased cardiac parasympathetic activity in chronic heart failure and its relation to left ventricular function. *Br Heart J*, 67, 482-5.
- O'CONNOR, C. M., GATTIS, W. A., URETSKY, B. F., ADAMS, K. F., JR., MCNULTY, S. E., GROSSMAN, S. H., MCKENNA, W. J., ZANNAD, F., SWEDBERG, K., GHEORGHIADE, M. & CALIFF, R. M. 1999. Continuous intravenous dobutamine is associated with an increased risk of death in patients with advanced heart failure: insights from the Flolan International Randomized Survival Trial (FIRST). *Am Heart J*, 138, 78-86.
- ODEMUYIWA, O., POLONIECKI, J., MALIK, M., FARRELL, T., XIA, R., STAUNTON, A., KULAKOWSKI, P., WARD, D. & CAMM, J. 1994. Temporal influences on the prediction of postinfarction mortality by heart rate variability: a comparison with the left ventricular ejection fraction. *Br Heart J*, 71, 521-7.
- OGAWA, M., ZHOU, S., TAN, A. Y., SONG, J., GHOLMIEH, G., FISHBEIN, M. C., LUO, H., SIEGEL, R. J., KARAGUEUZIAN, H. S., CHEN, L. S., LIN, S. F. & CHEN, P. S. 2007. Left stellate ganglion and vagal nerve activity and cardiac arrhythmias in ambulatory dogs with pacing-induced congestive heart failure. *J Am Coll Cardiol*, 50, 335-43.
- OKUMURA, S., KAWABE, J., YATANI, A., TAKAGI, G., LEE, M. C., HONG, C., LIU, J., TAKAGI, I., SADOSHIMA, J., VATNER, D. E., VATNER, S. F. & ISHIKAWA, Y. 2003a. Type 5 adenylyl cyclase disruption alters not only sympathetic but also parasympathetic and calcium-mediated cardiac regulation. *Circ Res*, 93, 364-71.
- OKUMURA, S., TAKAGI, G., KAWABE, J., YANG, G., LEE, M. C., HONG, C., LIU, J., VATNER, D. E., SADOSHIMA, J., VATNER, S. F. & ISHIKAWA, Y. 2003b. Disruption of type 5 adenylyl cyclase gene preserves cardiac function against pressure overload. *Proc Natl Acad Sci U S A*, 100, 9986-90.
- OKUYAMA, Y., PAK, H. N., MIYAUCHI, Y., LIU, Y. B., CHOU, C. C., HAYASHI, H., FU, K. J., KERWIN, W. F., KAR, S., HATA, C., KARAGUEUZIAN, H. S., FISHBEIN, M. C., CHEN, P. S. & CHEN, L. S. 2004. Nerve sprouting induced by radiofrequency catheter ablation in dogs. *Heart Rhythm*, 1, 712-7.
- PACKER, M. 2001. Current role of beta-adrenergic blockers in the management of chronic heart failure. *Am J Med*, 110 Suppl 7A, 81S-94S.
- PARATI, G., DI RIENZO, M. & MANCIA, G. 2000. How to measure baroreflex sensitivity: from the cardiovascular laboratory to daily life. *J Hypertens*, 18, 7-19.
- PATEL, K. P., ZHANG, K., ZUCKER, I. H. & KRUKOFF, T. L. 1996. Decreased gene expression of neuronal nitric oxide synthase in hypothalamus and brainstem of rats in heart failure. *Brain Res*, 734, 109-15.
- PATHAK, A., DEL MONTE, F., ZHAO, W., SCHULTZ, J. E., LORENZ, J. N., BODI, I., WEISER, D., HAHN, H., CARR, A. N., SYED, F., MAVILA, N., JHA, L., QIAN, J., MARREEZ, Y., CHEN, G., MCGRAW, D. W., HEIST, E. K., GUERRERO, J. L., DEPAOLI-ROACH, A. A., HAJJAR, R. J. & KRANIAS, E. G. 2005. Enhancement of cardiac function and suppression of heart failure progression by inhibition of protein phosphatase 1. *Circ Res*, 96, 756-66.

- PATRUCCO, E., NOTTE, A., BARBERIS, L., SELVETELLA, G., MAFFEI, A., BRANCACCIO, M., MARENKO, S., RUSSO, G., AZZOLINO, O., RYBALKIN, S. D., SILENGO, L., ALTRUDA, F., WETZKER, R., WYMAN, M. P., LEMBO, G. & HIRSCH, E. 2004. PI3Kgamma modulates the cardiac response to chronic pressure overload by distinct kinase-dependent and -independent effects. *Cell*, 118, 375-87.
- PAUZA, D. H., SKRIPKA, V., PAUZIENE, N. & STROPUS, R. 2000. Morphology, distribution, and variability of the epicardial neural ganglionated subplexuses in the human heart. *Anat Rec*, 259, 353-82.
- PEPPER, G. S. & LEE, R. W. 1999. Sympathetic activation in heart failure and its treatment with beta-blockade. *Arch Intern Med*, 159, 225-34.
- PHAN, H. M., GAO, M. H., LAI, N. C., TANG, T. & HAMMOND, H. K. 2007. New signaling pathways associated with increased cardiac adenylyl cyclase 6 expression: implications for possible congestive heart failure therapy. *Trends Cardiovasc Med*, 17, 215-21.
- PICCIRILLO, G., MAGRI, D., OGAWA, M., SONG, J., CHONG, V. J., HAN, S., JOUNG, B., CHOI, E. K., HWANG, S., CHEN, L. S., LIN, S. F. & CHEN, P. S. 2009. Autonomic nervous system activity measured directly and QT interval variability in normal and pacing-induced tachycardia heart failure dogs. *J Am Coll Cardiol*, 54, 840-50.
- PODRID, P. J. & MYERBURG, R. J. 2005. Epidemiology and stratification of risk for sudden cardiac death. *Clin Cardiol*, 28, I3-11.
- PONIKOWSKI, P., ANKER, S. D., CHUA, T. P., SZELEMEJ, R., PIEPOLI, M., ADAMOPOULOS, S., WEBB-PEPLOE, K., HARRINGTON, D., BANASIAK, W., WRABEC, K. & COATS, A. J. 1997. Depressed heart rate variability as an independent predictor of death in chronic congestive heart failure secondary to ischemic or idiopathic dilated cardiomyopathy. *Am J Cardiol*, 79, 1645-50.
- QU, Z., WEISS, J. N. & GARFINKEL, A. 1999. Cardiac electrical restitution properties and stability of reentrant spiral waves: a simulation study. *Am J Physiol*, 276, H269-83.
- RAAKE, P. W., VINGE, L. E., GAO, E., BOUCHER, M., RENGO, G., CHEN, X., DEGEORGE, B. R., JR., MATKOVICH, S., HOUSER, S. R., MOST, P., ECKHART, A. D., DORN, G. W., 2ND & KOCH, W. J. 2008. G protein-coupled receptor kinase 2 ablation in cardiac myocytes before or after myocardial infarction prevents heart failure. *Circ Res*, 103, 413-22.
- REDFIELD, M. M., JACOBSEN, S. J., BURNETT, J. C., JR., MAHONEY, D. W., BAILEY, K. R. & RODEHEFFER, R. J. 2003. Burden of systolic and diastolic ventricular dysfunction in the community: appreciating the scope of the heart failure epidemic. *JAMA*, 289, 194-202.
- REGITZ-ZAGROSEK, V., HERTRAMPF, R., STEFFEN, C., HILDEBRANDT, A. & FLECK, E. 1994. Myocardial cyclic AMP and norepinephrine content in human heart failure. *Eur Heart J*, 15 Suppl D, 7-13.
- ROCKMAN, H. A., CHIEN, K. R., CHOI, D. J., IACCARINO, G., HUNTER, J. J., ROSS, J., JR., LEFKOWITZ, R. J. & KOCH, W. J. 1998. Expression of a beta-adrenergic receptor kinase 1 inhibitor prevents the development of myocardial failure in gene-targeted mice. *Proc Natl Acad Sci U S A*, 95, 7000-5.
- ROSENSPIRE, K. C., HAKA, M. S., VAN DORT, M. E., JEWETT, D. M., GILDERSLEEVE, D. L., SCHWAIGER, M. & WIELAND, D. M. 1990. Synthesis

- and preliminary evaluation of carbon-11-met-hydroxyephedrine: a false transmitter agent for heart neuronal imaging. *J Nucl Med*, 31, 1328-34.
- ROTH, D. M., BAYAT, H., DRUMM, J. D., GAO, M. H., SWANEY, J. S., ANDER, A. & HAMMOND, H. K. 2002. Adenylyl cyclase increases survival in cardiomyopathy. *Circulation*, 105, 1989-94.
- RUNDQVIST, B., ELAM, M., BERGMANN-SVERRISDOTTIR, Y., EISENHOFER, G. & FRIBERG, P. 1997. Increased cardiac adrenergic drive precedes generalized sympathetic activation in human heart failure. *Circulation*, 95, 169-75.
- RYSEVAITE, K., SABURKINA, I., PAUZIENE, N., VAITKEVICIUS, R., NOUJAIM, S. F., JALIFE, J. & PAUZA, D. H. 2011. Immunohistochemical characterization of the intrinsic cardiac neural plexus in whole-mount mouse heart preparations. *Heart Rhythm*, 8, 731-8.
- SABBAH, H. N. 2011. Electrical vagus nerve stimulation for the treatment of chronic heart failure. *Cleve Clin J Med*, 78 Suppl 1, S24-9.
- SABBAH, H. N., RASTOGI, S., MISHRA, S., GUPTA, R. C., ILSAR, I., IMAI, M., COHEN, U., BEN-DAVID, T. & BEN-EZRA, O. 2005. 744 Long-term therapy with neuroselective electric Vagus nerve stimulation improves LV function and attenuates global LV remodelling in dogs with chronic heart failure. *European Journal of Heart Failure Supplements*, 4, 166-167.
- SABURKINA, I., RYSEVAITE, K., PAUZIENE, N., MISCHKE, K., SCHAUERTE, P., JALIFE, J. & PAUZA, D. H. 2010. Epicardial neural ganglionated plexus of ovine heart: anatomic basis for experimental cardiac electrophysiology and nerve protective cardiac surgery. *Heart Rhythm*, 7, 942-50.
- SAPER, C. B., SORRENTINO, D. M., GERMAN, D. C. & DE LACALLE, S. 1991. Medullary catecholaminergic neurons in the normal human brain and in Parkinson's disease. *Ann Neurol*, 29, 577-84.
- SATWANI, S., DEC, G. W. & NARULA, J. 2004. Beta-adrenergic blockers in heart failure: review of mechanisms of action and clinical outcomes. *J Cardiovasc Pharmacol Ther*, 9, 243-55.
- SCHOCKEN, D. D., ARRIETA, M. I., LEAVERTON, P. E. & ROSS, E. A. 1992. Prevalence and mortality rate of congestive heart failure in the United States. *J Am Coll Cardiol*, 20, 301-6.
- SCHRODER, F., HANDROCK, R., BEUCKELMANN, D. J., HIRT, S., HULLIN, R., PRIEBE, L., SCHWINGER, R. H., WEIL, J. & HERZIG, S. 1998. Increased availability and open probability of single L-type calcium channels from failing compared with nonfailing human ventricle. *Circulation*, 98, 969-76.
- SCHWARTZ, P. J., DE FERRARI, G. M., SANZO, A., LANDOLINA, M., RORDORF, R., RAINERI, C., CAMPANA, C., REVERA, M., AJMONE-MARSAN, N., TAVAZZI, L. & ODERO, A. 2008. Long term vagal stimulation in patients with advanced heart failure: first experience in man. *Eur J Heart Fail*, 10, 884-91.
- SCHWARTZ, P. J. & MALLIANI, A. 1975. Electrical alternation of the T-wave: clinical and experimental evidence of its relationship with the sympathetic nervous system and with the long Q-T syndrome. *Am Heart J*, 89, 45-50.
- SCHWARTZ, P. J., MOTOLESE, M., POLLAVINI, G., LOTTO, A., RUBERTI, U. G. O., TRAZZI, R., BARTORELLI, C., ZANCHETTI, A. & GROUP, T. I. S. D. P. 1992. Prevention of Sudden Cardiac Death After a First Myocardial Infarction by

- Pharmacologic or Surgical Antiadrenergic Interventions. *Journal of Cardiovascular Electrophysiology*, 3, 2-16.
- SCHWARTZ, P. J., PERITI, M. & MALLIANI, A. 1975. The long Q-T syndrome. *Am Heart J*, 89, 378-90.
- SCHWARTZ, P. J., SNEBOLD, N. G. & BROWN, A. M. 1976. Effects of unilateral cardiac sympathetic denervation on the ventricular fibrillation threshold. *Am J Cardiol*, 37, 1034-40.
- SCHWARTZ, P. J. & STONE, H. L. 1982. Left stellectomy and denervation supersensitivity in conscious dogs. *Am J Cardiol*, 49, 1185-90.
- SCHWARTZ, P. J., VANOLI, E., STRAMBA-BADIALE, M., DE FERRARI, G. M., BILLMAN, G. E. & FOREMAN, R. D. 1988a. Autonomic mechanisms and sudden death. New insights from analysis of baroreceptor reflexes in conscious dogs with and without a myocardial infarction. *Circulation*, 78, 969-79.
- SCHWARTZ, P. J., ZAZA, A., PALA, M., LOCATI, E., BERIA, G. & ZANCHETTI, A. 1988b. Baroreflex sensitivity and its evolution during the first year after myocardial infarction. *J Am Coll Cardiol*, 12, 629-36.
- SELVARAJ, R. J., PICTON, P., NANTHAKUMAR, K. & CHAUHAN, V. S. 2007. Steeper restitution slopes across right ventricular endocardium in patients with cardiomyopathy at high risk of ventricular arrhythmias. *Am J Physiol Heart Circ Physiol*, 292, H1262-8.
- SENNI, M., TRIBOUILLOY, C. M., RODEHEFFER, R. J., JACOBSEN, S. J., EVANS, J. M., BAILEY, K. R. & REDFIELD, M. M. 1998. Congestive heart failure in the community: a study of all incident cases in Olmsted County, Minnesota, in 1991. *Circulation*, 98, 2282-9.
- SENNI, M., TRIBOUILLOY, C. M., RODEHEFFER, R. J., JACOBSEN, S. J., EVANS, J. M., BAILEY, K. R. & REDFIELD, M. M. 1999. Congestive heart failure in the community: trends in incidence and survival in a 10-year period. *Arch Intern Med*, 159, 29-34.
- STANTON, M. S., TULI, M. M., RADTKE, N. L., HEGER, J. J., MILES, W. M., MOCK, B. H., BURT, R. W., WELLMAN, H. N. & ZIPES, D. P. 1989. Regional sympathetic denervation after myocardial infarction in humans detected noninvasively using I-123-metiodobenzylguanidine. *J Am Coll Cardiol*, 14, 1519-26.
- STEVENSON, L. W. 2003. Clinical use of inotropic therapy for heart failure: looking backward or forward? Part II: chronic inotropic therapy. *Circulation*, 108, 492-7.
- STILES, G. L., CARON, M. G. & LEFKOWITZ, R. J. 1984. Beta-adrenergic receptors: biochemical mechanisms of physiological regulation. *Physiol Rev*, 64, 661-743.
- SUN, S. Y., WANG, W., ZUCKER, I. H. & SCHULTZ, H. D. 1999. Enhanced activity of carotid body chemoreceptors in rabbits with heart failure: role of nitric oxide. *J Appl Physiol (1985)*, 86, 1273-82.
- TAGGART, P., CRITCHLEY, H. & LAMBIASE, P. D. 2011. Heart-brain interactions in cardiac arrhythmia. *Heart*, 97, 698-708.
- TAGGART, P., SUTTON, P., CHALABI, Z., BOYETT, M. R., SIMON, R., ELLIOTT, D. & GILL, J. S. 2003. Effect of adrenergic stimulation on action potential duration restitution in humans. *Circulation*, 107, 285-9.

- TAGGART, P., SUTTON, P., LAB, M., DEAN, J. & HARRISON, F. 1990. Interplay between adrenaline and interbeat interval on ventricular repolarisation in intact heart in vivo. *Cardiovasc Res*, 24, 884-95.
- TAMAKI, S., YAMADA, T., OKUYAMA, Y., MORITA, T., SANADA, S., TSUKAMOTO, Y., MASUDA, M., OKUDA, K., IWASAKI, Y., YASUI, T., HORI, M. & FUKUNAMI, M. 2009. Cardiac iodine-123 metaiodobenzylguanidine imaging predicts sudden cardiac death independently of left ventricular ejection fraction in patients with chronic heart failure and left ventricular systolic dysfunction: results from a comparative study with signal-averaged electrocardiogram, heart rate variability, and QT dispersion. *J Am Coll Cardiol*, 53, 426-35.
- THACKERAY, J. T., BEANLANDS, R. S. & DASILVA, J. N. 2007. Presence of specific ¹¹C-meta-Hydroxyephedrine retention in heart, lung, pancreas, and brown adipose tissue. *J Nucl Med*, 48, 1733-40.
- THACKERAY, J. T., RENAUD, J. M., KORDOS, M., KLEIN, R., DEKEMP, R. A., BEANLANDS, R. S. & DASILVA, J. N. 2013. Test-retest repeatability of quantitative cardiac ¹¹C-meta-hydroxyephedrine measurements in rats by small animal positron emission tomography. *Nucl Med Biol*, 40, 676-81.
- THOM, T., HAASE, N., ROSAMOND, W., HOWARD, V. J., RUMSFELD, J., MANOLIO, T., ZHENG, Z. J., FLEGAL, K., O'DONNELL, C., KITTNER, S., LLOYD-JONES, D., GOFF, D. C., JR., HONG, Y., ADAMS, R., FRIDAY, G., FURIE, K., GORELICK, P., KISSELA, B., MARLER, J., MEIGS, J., ROGER, V., SIDNEY, S., SORLIE, P., STEINBERGER, J., WASSERTHIEL-SMOLLER, S., WILSON, M., WOLF, P., AMERICAN HEART ASSOCIATION STATISTICS, C. & STROKE STATISTICS, S. 2006. Heart disease and stroke statistics--2006 update: a report from the American Heart Association Statistics Committee and Stroke Statistics Subcommittee. *Circulation*, 113, e85-151.
- TIPRE, D. N., FOX, J. J., HOLT, D. P., GREEN, G., YU, J., POMPER, M., DANNALS, R. F. & BENGEL, F. M. 2008. In vivo PET imaging of cardiac presynaptic sympathoneuronal mechanisms in the rat. *J Nucl Med*, 49, 1189-95.
- TOMASELLI, G. F. & ZIPES, D. P. 2004. What causes sudden death in heart failure? *Circ Res*, 95, 754-63.
- TUININGA, Y. S., VAN VELDHUISEN, D. J., BROUWER, J., HAAKSMA, J., CRIJNS, H. J., MAN IN'T VELD, A. J. & LIE, K. I. 1994. Heart rate variability in left ventricular dysfunction and heart failure: effects and implications of drug treatment. *Br Heart J*, 72, 509-13.
- UNGERER, M., BOHM, M., ELCE, J. S., ERDMANN, E. & LOHSE, M. J. 1993. Altered expression of beta-adrenergic receptor kinase and beta 1-adrenergic receptors in the failing human heart. *Circulation*, 87, 454-63.
- VANOLI, E., DE FERRARI, G. M., STRAMBA-BADIALE, M., HULL, S. S., JR., FOREMAN, R. D. & SCHWARTZ, P. J. 1991. Vagal stimulation and prevention of sudden death in conscious dogs with a healed myocardial infarction. *Circ Res*, 68, 1471-81.
- VATNER, S. F., VATNER, D. E. & HOMCY, C. J. 2000. beta-adrenergic receptor signaling: an acute compensatory adjustment-inappropriate for the chronic stress of heart failure? Insights from G_salpha overexpression and other genetically engineered animal models. *Circ Res*, 86, 502-6.
- VERBERNE, H. J., BREWSTER, L. M., SOMSEN, G. A. & VAN ECK-SMIT, B. L. 2008. Prognostic value of myocardial ¹²³I-metaiodobenzylguanidine (MIBG)

- parameters in patients with heart failure: a systematic review. *Eur Heart J*, 29, 1147-59.
- VINCENT, N. H. & ELLIS, S. 1963. Inhibitory effect of acetylcholine on glycogenolysis in the isolated guinea-pig heart. *J Pharmacol Exp Ther*, 139, 60-8.
- VINIK, A. I., MASER, R. E. & ZIEGLER, D. 2011. Autonomic imbalance: prophet of doom or scope for hope? *Diabet Med*, 28, 643-51.
- WALLIN, B. G., ESLER, M., DORWARD, P., EISENHOFER, G., FERRIER, C., WESTERMAN, R. & JENNINGS, G. 1992. Simultaneous measurements of cardiac noradrenaline spillover and sympathetic outflow to skeletal muscle in humans. *J Physiol*, 453, 45-58.
- WALLIN, B. G. & FAGIUS, J. 1988. Peripheral sympathetic neural activity in conscious humans. *Annu Rev Physiol*, 50, 565-76.
- WALLIN, B. G., THOMPSON, J. M., JENNINGS, G. L. & ESLER, M. D. 1996. Renal noradrenaline spillover correlates with muscle sympathetic activity in humans. *J Physiol*, 491 (Pt 3), 881-7.
- WANG, H., LU, Y. & WANG, Z. 2007. Function of cardiac M3 receptors. *Auton Autacoid Pharmacol*, 27, 1-11.
- WANG, S., HAN, H. M., JIANG, Y. N., WANG, C., SONG, H. X., PAN, Z. Y., FAN, K., DU, J., FAN, Y. H., DU, Z. M. & LIU, Y. 2012. Activation of cardiac M3 muscarinic acetylcholine receptors has cardioprotective effects against ischaemia-induced arrhythmias. *Clin Exp Pharmacol Physiol*, 39, 343-9.
- WANG, X. & GERDES, A. M. 1999. Chronic pressure overload cardiac hypertrophy and failure in guinea pigs: III. Intercalated disc remodeling. *J Mol Cell Cardiol*, 31, 333-43.
- WARNER, M. R., WISLER, P. L., HODGES, T. D., WATANABE, A. M. & ZIPES, D. P. 1993. Mechanisms of denervation supersensitivity in regionally denervated canine hearts. *Am J Physiol*, 264, H815-20.
- WEISS, J. N., CHEN, P. S., QU, Z., KARAGUEUZIAN, H. S. & GARFINKEL, A. 2000. Ventricular fibrillation: how do we stop the waves from breaking? *Circ Res*, 87, 1103-7.
- WILDE, A. A., BHUIYAN, Z. A., CROTTI, L., FACCHINI, M., DE FERRARI, G. M., PAUL, T., FERRANDI, C., KOOLBERGEN, D. R., ODERO, A. & SCHWARTZ, P. J. 2008. Left cardiac sympathetic denervation for catecholaminergic polymorphic ventricular tachycardia. *N Engl J Med*, 358, 2024-9.
- YAN, L., VATNER, D. E., O'CONNOR, J. P., IVESSA, A., GE, H., CHEN, W., HIROTANI, S., ISHIKAWA, Y., SADOSHIMA, J. & VATNER, S. F. 2007. Type 5 adenylyl cyclase disruption increases longevity and protects against stress. *Cell*, 130, 247-58.
- YIP, G., WANG, M., ZHANG, Y., FUNG, J. W., HO, P. Y. & SANDERSON, J. E. 2002. Left ventricular long axis function in diastolic heart failure is reduced in both diastole and systole: time for a redefinition? *Heart*, 87, 121-5.
- YOSHIOKA, K., GAO, D. W., CHIN, M., STILLSON, C., PENADES, E., LESH, M., O'CONNELL, W. & DAE, M. 2000. Heterogeneous sympathetic innervation influences local myocardial repolarization in normally perfused rabbit hearts. *Circulation*, 101, 1060-6.
- ZAKHARY, D. R., MORAVEC, C. S. & BOND, M. 2000. Regulation of PKA binding to AKAPs in the heart: alterations in human heart failure. *Circulation*, 101, 1459-64.

- ZHANG, Y., POPOVIC, Z. B., BIBEVSKI, S., FAKHRY, I., SICA, D. A., VAN WAGONER, D. R. & MAZGALEV, T. N. 2009. Chronic vagus nerve stimulation improves autonomic control and attenuates systemic inflammation and heart failure progression in a canine high-rate pacing model. *Circ Heart Fail*, 2, 692-9.
- ZHANG, Y. H., ZHU, J. & SONG, Y. C. 1998. Suppressing sympathetic activation with clonidine on ventricular arrhythmias in congestive heart failure. *Int J Cardiol*, 65, 233-8.
- ZHENG, C., LI, M., INAGAKI, M., KAWADA, T., SUNAGAWA, K. & SUGIMACHI, M. 2005. Vagal stimulation markedly suppresses arrhythmias in conscious rats with chronic heart failure after myocardial infarction. *Conf Proc IEEE Eng Med Biol Soc*, 7, 7072-5.
- ZHOU, S., CAO, J. M., TEBB, Z. D., OHARA, T., HUANG, H. L., OMICHI, C., LEE, M. H., KENKNIGHT, B. H., CHEN, L. S., FISHBEIN, M. C., KARAGUEUZIAN, H. S. & CHEN, P. S. 2001. Modulation of QT interval by cardiac sympathetic nerve sprouting and the mechanisms of ventricular arrhythmia in a canine model of sudden cardiac death. *J Cardiovasc Electrophysiol*, 12, 1068-73.
- ZHOU, S., JUNG, B. C., TAN, A. Y., TRANG, V. Q., GHOLMIEH, G., HAN, S. W., LIN, S. F., FISHBEIN, M. C., CHEN, P. S. & CHEN, L. S. 2008. Spontaneous stellate ganglion nerve activity and ventricular arrhythmia in a canine model of sudden death. *Heart Rhythm*, 5, 131-9.
- ZIPES, D. P. 1990. Influence of myocardial ischemia and infarction on autonomic innervation of heart. *Circulation*, 82, 1095-105.
- ZIPES, D. P., BARBER, M. J., TAKAHASHI, N. & GILMOUR, R. F., JR. 1983. Influence of the autonomic nervous system on the genesis of cardiac arrhythmias. *Pacing Clin Electrophysiol*, 6, 1210-20.
- ZIPES, D. P., FESTOFF, B., SCHAAAL, S. F., COX, C., SEALY, W. C. & WALLACE, A. G. 1968. Treatment of ventricular arrhythmia by permanent atrial pacemaker and cardiac sympathectomy. *Ann Intern Med*, 68, 591-7.
- ZUCKER, I. H., HACKLEY, J. F., CORNISH, K. G., HISER, B. A., ANDERSON, N. R., KIEVAL, R., IRWIN, E. D., SERDAR, D. J., PEULER, J. D. & ROSSING, M. A. 2007. Chronic baroreceptor activation enhances survival in dogs with pacing-induced heart failure. *Hypertension*, 50, 904-10.

Chapter 2

Thesis Aims and Layout

Autonomic Modulation in a Rabbit Model of Heart Failure

Chapter 2: Thesis Aims and Layout

2.1 Aims of Study

Dysautonomia, typified by sympathetic overdrive and parasympathetic attenuation, is a prominent feature of heart failure, and has been discussed in detail in Chapter 1. In spite of the epidemiological link between autonomic imbalance and fatal ventricular arrhythmias demonstrable in both experimental and clinical models, our understanding of the mechanistic link between autonomic dysfunction and adverse electrical remodelling in heart failure remains incomplete. Most animal studies involve the use of *in vivo* diseased model which confounded the study of neuro-cardiac interaction in heart failure due to the presence of circulating humoral factors and autonomic reflexes. Throughout this study, an *in vitro* Langendorff-perfused rabbit heart with intact dual-autonomic innervation, first developed by Ng *et al* (Ng et al., 2001) was used to examine various aspects of whole-heart electrophysiology under direct autonomic nerve stimulation, thereby circumventing the confounding issue of circulating humoral factors and autonomic reflexes that occur *in vivo*. The first part of the study aims to extend pre-existing knowledge of the effect of separate autonomic nerve stimulation on atrial and ventricular electrophysiology by examining sympatho-vagal interaction with different stimulation sequences and frequencies in normal rabbit hearts. However, the main aim of this study is to assess potential structural and electrical remodelling in a rabbit heart failure model, in particular assessing the effect of autonomic modulation on various aspects of whole-heart electrophysiology. In the second part of the study, a rabbit surgical heart failure model was developed at the Department of Cardiovascular Sciences, University of Leicester. An infarct model of heart failure was induced followed coronary ligation surgeries in rabbits, a model first developed and characterised by Pye *et al* (Pye and Cobbe, 1996) at the Department of Medical Cardiology, Glasgow Royal Infirmary. This heart failure model provides an ideal vehicle to study the effect of sympathetic and vagal stimulations on atrial, atrio-ventricular and ventricular electrophysiology.

2.2 Thesis Layout

Chapter 3 outlines all the experimental methods involved in the studies described in this thesis. These comprise:-

- a) surgical procedure of coronary artery ligation to produce myocardial infarction and subsequent heart failure in rabbits
- b) transthoracic echocardiography to assess *in vivo* cardiac chamber size and contractile function
- c) cardiac magnetic resonance imaging to assess *ex vivo* myocardial scarring
- d) assessment of cardiac and systemic remodelling by organ weights
- e) the use of Langendorff-perfused, dual-innervated *in vitro* rabbit heart preparation for assessment of various electrophysiologic parameters in response to autonomic stimulation

Furthermore, the challenges of building a surgical heart failure model in rabbits during the study period were discussed and illustrated with mortality data.

Chapter 4 describes the effect of sympatho-vagal interaction on heart rate response and ventricular electrophysiology in normal rabbit hearts. Experiments were designed in two protocols depending of the sequence of sympathetic and vagal stimulations. In addition, frequency response of heart rate and ventricular electrophysiology during autonomic stimulation was also examined.

Chapter 5 extends upon the works of *Chapter 4* by assessing the effect of adrenergic blockade by metoprolol tartrate on heart rate and ventricular electrophysiology during sympatho-vagal interaction. In this study, two compositions (acetate-free vs. acetate-containing) of Tyrode solutions were used to assess for modulation of beta-blockade during sympatho-vagal interaction.

Chapter 6 details cardiac and systemic remodelling in rabbit heart failure model. Transthoracic echocardiography was performed to assess for changes in cardiac chamber sizes and contractile performance. *Ex vivo* cardiac magnetic resonance

imaging were performed on whole heart specimens from both heart failure and sham groups to assess for myocardial scarring. Wet and dry weights of hearts, livers and lungs were measured in both heart failure and sham groups to assess for evidence of systemic remodelling in the form of fluid congestion.

Chapter 7 describes the effect of direct sympathetic and vagal stimulation on atrial, atrio-ventricular and ventricular electrophysiology on hearts procured from rabbits 8 weeks after their corresponding coronary ligation or sham procedure. At the atrial level, heart rate was assessed in response to graded increment in stimulation strength and frequency of sympathetic, right and left vagal stimulation. At the atrio-ventricular level, atrio-ventricular delay was measured during atrial pacing at baseline as well as during low- and high-frequency autonomic nerve stimulations. Finally, at the ventricular level, ventricular fibrillation threshold and effective refractory periods were measured at baseline, and during sympathetic and vagal stimulations. Monophasic action potentials were recorded at the base and apex of the heart, allowing for regional measurements of action-potential-duration restitution. Apico-basal restitution dispersion was subsequently derived. Comparison of all measured electrophysiologic parameters were made between the heart failure and the sham group to assess for evidence of electrical remodelling in response to dysfunctional autonomic tone in heart failure.

Chapter 8 is a synopsis of the thesis, summarising the results of all experimental works with proposals for future studies using the sustainable surgical heart failure model developed in this study.

2.3 References

- NG, G. A., BRACK, K. E. & COOTE, J. H. 2001. Effects of direct sympathetic and vagus nerve stimulation on the physiology of the whole heart--a novel model of isolated Langendorff perfused rabbit heart with intact dual autonomic innervation. *Exp Physiol*, 86, 319-29.
- PYE, M. P. & COBBE, S. M. 1996. Arrhythmogenesis in experimental models of heart failure: the role of increased load. *Cardiovasc Res*, 32, 248-57.

Chapter 3

General Methods

Autonomic Modulation in a Rabbit Model of Heart Failure

Chapter 3: General Methods

3.1 Coronary Artery Ligation in the Rabbit

3.1.1 Background

Experimental models of heart failure contribute significantly to the advancement of our understanding of the pathophysiology and development of effective therapy modalities in heart failure. Animal models are often relied upon to answer questions not easily resolved by clinical observations in patients with heart failure. A variety of animal models of heart failure have been developed over the years to mimic clinical phenotypes of these patients with some success. The use of a particular experimental model of heart failure depends not only on the scientific questions to be addressed, but also on ethical and financial constraints, accessibility to the animal species in question, as well as reproducibility of the relevant heart failure model. Table 3.1 illustrates the various animal models of heart failure discussed in this chapter with the corresponding clinical phenotypes induced.

Rat models have been a popular choice due in part to their low cost and shorter gestation period, thereby allowing for a bigger study sample size. Nonetheless, important differences exist in myocardial structures and functions between rats and humans. In healthy rats, myosin predominates in heavy-chain isoform only with the β -myosin isoform predominating under alterations in haemodynamic or hormonal state (Swynghedauw, 1986). Calcium cycling differs in that calcium removal is achieved predominantly by sarcoplasmic reticulum calcium pump with insignificant role from the Na^+/Ca^+ exchanger (Hasenfuss, 1998). Relevant to the underlying electrophysiologic tone in this thesis, the myocardial action potential duration in rats is short, lacking a plateau phase (Varro et al., 1993). In contrast, larger animal models such as dogs and rabbits, exhibit greater similarity with humans in terms of β -myosin isoform distribution, excitation-contraction coupling process and limited coronary collateral circulation.

In this thesis, heart failure is induced in rabbits by myocardial infarction via complete coronary ligation. This results in variable loss of myocardial function over eight weeks depending on the initial myocardial infarct size. Echoing what has been observed in heart

failure patients, this model of heart failure is characterised by left ventricular dilatation, reduced systolic function, increased filling pressures with neurohumoral activation as demonstrated in rats (van Veldhuisen et al., 1994, Teerlink et al., 1994, Pfeffer et al., 1979), dogs (Sabbah et al., 1991) and rabbits (Pye and Cobbe, 1996, Pye et al., 1996). The poor development of coronary collateral circulation in rabbits, as in humans and pigs, allows for well-defined infarct sizes with corresponding variability in subsequent myocardial impairment (Maxwell et al., 1987). In essence, the rabbit heart failure model employed in this thesis serves as a powerful and clinically relevant model to study the effect of electrophysiologic disturbances by dysautonomia in heart failure.

3.1.2 Method

Adult male New Zealand White rabbits (2.5 – 3.5 kg) were sedated with a subcutaneous injection containing a mixture of Medetomidine Hydrochloride (Sedator, 0.2 mg/kg), Ketamine (Narketan, 10 mg/kg) and Butorphanol (Torbugesic, 0.05 mg/kg). An indwelling cannula was inserted into the marginal ear vein through which a 5 mL warmed normal saline was given. Further subcutaneous injections of meloxicam (Metacam, 0.2 mg/kg) and enrofloxacin (Baytril, 0.2 mL/kg) was given, the former as a pre-emptive analgesia and the latter a pre-operative antibiotic prophylaxis. The rabbit was intubated in prone position with the neck supported in a hyperextended position. An uncuffed size 3 endotracheal tube was inserted with the aid of a disposable straight blade (Miller 1) laryngoscope. The anterior chest wall was shaved and cleaned with Hibidil in isopropyl alcohol.

Upon being transferred into the operating room, the rabbit was placed on a thermostatically-controlled operating table which has been pre-warmed. Throughout the surgery, the body temperature is monitored through a rectal temperature probe. The rabbit was placed on the right lateral position with its left paw extended parallel with the lower jaw and secured. The endotracheal tube was secured by taping to the operating table and was connected to a Harvard small animal ventilator (Harvard Apparatus Ltd, Edenbridge, Kent, UK). The rabbit was ventilated with a 1:1 mixture of nitrous oxide and oxygen containing 1 – 1.5% isofluorane at a tidal volume of 30 mL and a respiratory rate of 55 min⁻¹. The anterior chest wall was further cleaned with Hibidil in isopropyl

alcohol under sterile condition. The first to the fourth ribs were each injected with 0.2 mL bupivacaine (Marcaine). A left thoracotomy was performed with judicious dissection through the 4th intercostal space. The left lung was gently retracted with small gauze. Once the heart was in view, the pericardium was incised. An apical tie was placed with 4 / 0 Ethicon suture through the ventricular apex, allowing the heart to be lifted up for easier manipulation. The left circumflex artery was identified and ligated halfway between the atrio-ventricular groove and the ventricular apex with 4 / 0 Ethicon suture, producing an immediate infarct area covering 30 – 40% of the left ventricle. The rabbits differ from the humans in their coronary circulation in that the left anterior descending artery is short, supplying a small area of the interventricular septum whereas the left circumflex artery with its marginal branch extending to the ventricular apex supplies most of the left ventricular free wall, including the ventricular apex. Similar to humans, rabbits demonstrate very little collateral coronary circulation, allowing a homogenous apical infarct to be formed by ligation of the left circumflex artery (Figure 3.1). Ventricular fibrillation occurred in approximately 30% of coronary ligation cases, usually 15 – 19 minutes following occlusion. Defibrillation was achieved with initially a gentle flick of the heart, and if necessary with a 5 J DC shock using small sterilised paddles applied on the epicardial surface of the heart.

A 20-minute waiting time ensued following the ligation of the left circumflex artery, or in the case of the sham operation, following the apical tie. After 20 minutes had elapsed, an injection of dexamethasone (Duphacort 0.2%, 0.1 mL/kg) was given into the pericardial sac to prevent post-operative pericarditis. The collapsed left lung was then re-inflated by collusion of the ventilator outlet. The chest was closed in layers using 1 / 0 Monocryl interrupted sutures for the 4th and the 5th ribs, 3 / 0 Ethicon interrupted sutures for the muscular and subcutaneous layers, and finally 5 / 0 Vicryl continuous sutures for subcuticular layer. Further analgesia was given as subcutaneous injections with 0.2 mL bupivacaine locally at the incision site, and systemically with buprenorphine (Temgesic, 0.05 mg/kg). The rabbit was given a further 15 mL isotonic saline intravenously to replace any perioperative fluid loss. Atipamezole (Atipam, 1 mg/kg) was given subcutaneously as a sedative-reversal agent. Once the animal regained consciousness, it was transferred to the post-operative room to recover in a closely monitored, warm and clean environment. The animals were only sacrificed 8 weeks post-operatively for the

terminal experimental studies in order to allow for the development of the heart failure following coronary ligation.

Sham-operated rabbits would undergo similar surgeries involving thoracotomy, pericardiotomy and ligation of the ventricular apex for manipulation. Coronary ligation was not performed in this group of rabbits serving as controls. Experimental studies were performed at 8 weeks post-operatively so as the controls would be similar in their maturity as their counterparts which had undergone coronary ligation.

Chapter 3

Table 3.1 Common animal models of heart failure

Species	Model	Investigator	Functional features
Rat	Coronary ligation	Kajstura <i>et al</i> (Kajstura et al., 1994) Teerlink <i>et al</i> (Teerlink et al., 1994) Van Veldhuisen et al (van Veldhuisen et al., 1994) Anversa <i>et al</i> (Anversa et al., 1992, Anversa et al., 1995)	Studies of heart failure progression; survival studies
	Aortic banding	Feldman <i>et al</i> (Feldman et al., 1993) Weinberg <i>et al</i> (Weinberg et al., 1994)	Studies of transition from hypertrophy to failure; survival studies
Toxic cardiomyopathy	Szabo <i>et al</i> (Szabo et al., 1975) Krenek <i>et al</i> (Krenek et al., 2009)		Myocyte loss; decreased myocardial performance

Chapter 3

Table 3.1 Common animal models of heart failure (continued)

Species	Model	Investigator	Functional features
Rat	Spontaneous hypertension	Bing <i>et al</i> (Bing et al., 1991) Boluyt <i>et al</i> (Boluyt et al., 1994) Li <i>et al</i> (Li et al., 1997) Holycross <i>et al</i> (Holycross et al., 1997) Gomez <i>et al</i> (Gomez et al., 1997) Khadour <i>et al</i> (Khadour et al., 1997)	Studies of transition from hypertrophy to failure; apoptosis; extracellular matrix alterations
	Salt-sensitive hypertension	Dahl <i>et al</i> (Dahl et al., 1962) Inoko <i>et al</i> (Inoko et al., 1994)	Studies of transition from hypertrophy to failure
	Aorto-caval fistula	Garcia <i>et al</i> (Garcia and Diebold, 1990) Liu <i>et al</i> (Liu et al., 1991)	Left ventricular hypertrophy; moderate LV dysfunction

Chapter 3

Table 3.1 Common animal models of heart failure (continued)

Species	Model	Investigator	Functional features
Dog	Pacing tachycardia	Whipple <i>et al</i> (Whipple et al., 1961-1962) Moe <i>et al</i> (Moe et al., 1993, Moe and Armstrong, 1999) Huntington <i>et al</i> (Huntington et al., 1998) Grima <i>et al</i> (Grima et al., 1994)	Studies of remodelling, neurohumoral activation and subcellular dysfunction
	Coronary ligation	Sabbah <i>et al</i> (Sabbah et al., 1991) Schwartz <i>et al</i> (Schwartz and Stone, 1980) Vanoli <i>et al</i> (Vanoli et al., 1991)	Studies on progression of heart failure and ventricular arrhythmias
	Toxic cardiomyopathy	Maling <i>et al</i> (Maling and Highman, 1958)	Left ventricular structural changes and arrhythmias

Chapter 3

Table 3.1 Common animal models of heart failure (continued)

Species	Model	Investigator	Functional features
Dog	Direct-current shock	Mehta <i>et al</i> (Mehta et al., 1978) McDonald <i>et al</i> (McDonald et al., 1994b, McDonald et al., 1992, McDonald et al., 1994a, McDonald et al., 1990)	Studies of remodelling, bioenergetics and therapeutic interventions
	Genetic	Calvert <i>et al</i> (Calvert et al., 1997b, Calvert et al., 1997a)	Spontaneous cardiomyopathy in Doberman Pinscher dogs
	Volume overload	Kleaveland <i>et al</i> (Kleaveland et al., 1988) McCullagh <i>et al</i> (McCullagh et al., 1972) Nagatsu <i>et al</i> (Nagatsu et al., 1994) Tsutsui <i>et al</i> (Tsutsui et al., 1994)	Aorto-caval fistula, mitral regurgitation

Chapter 3

Table 3.1 Common animal models of heart failure (continued)

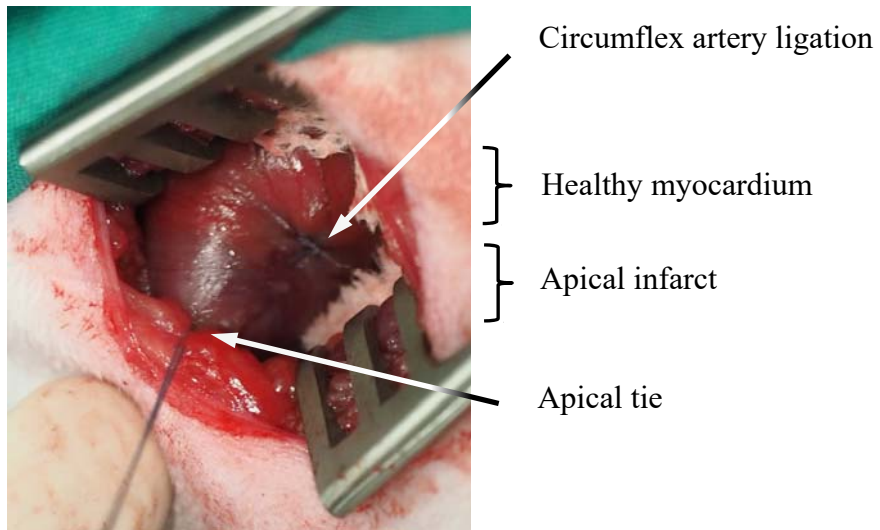
Species	Model	Investigator	Functional features
Dog	Vena caval constriction	Lischitz <i>et al</i> (Lischitz and Schrier, 1973) Underwood <i>et al</i> (Underwood et al., 1992)	Low output failure, neurohumoral changes

Chapter 3

Table 3.1 Common animal models of heart failure (continued)

Species	Model	Investigator	Functional features
Rabbit	Coronary ligation	Pye <i>et al</i> (Pye and Cobbe, 1996, Pye et al., 1996)	Studies of altered calcium cycling and altered electrophysiologic responses
	Volume and pressure overload	Magid <i>et al</i> (Magid et al., 1994) Ezzaher <i>et al</i> (Ezzaher et al., 1991, Ezzaher et al., 1992) Gilson <i>et al</i> (Gilson et al., 1990)	Myocardial alterations similar to failing human myocardium
	Pacing tachycardia	Murakami <i>et al</i> (Murakami et al., 1996) Liu <i>et al</i> (Liu and Zucker, 1999)	Neurohumoral alterations similar to failing human myocardium
	Toxic cardiomyopathy	Pye <i>et al</i> (Pye and Cobbe, 1996, Pye et al., 1996) Downing <i>et al</i> (Downing and Chen, 1985)	Studies of altered calcium cycling and altered electrophysiologic responses

Figure 3.1 Apical infarct following ligation of circumflex artery in rabbit heart



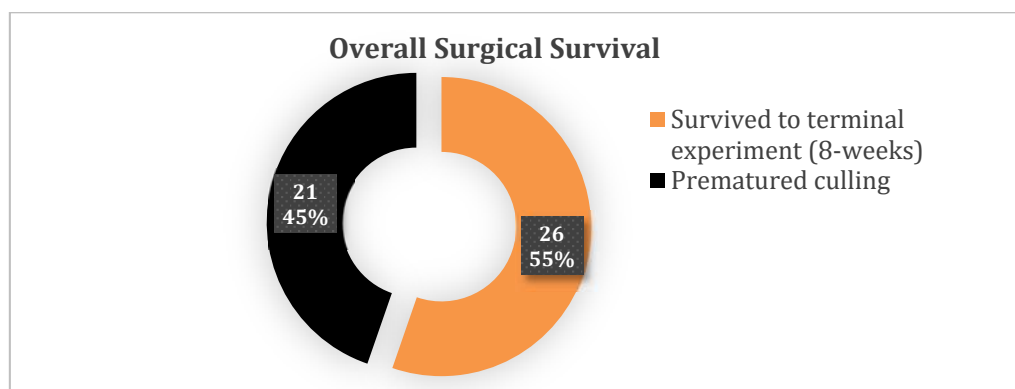
3.2 Challenges of Building a Leporine Heart Failure Model by Coronary Ligation

3.2.1 Background

This study represents a maiden attempt to create a heart failure rabbit model by coronary ligation at the Department of Cardiovascular Sciences in collaboration with Central Research Facility (CRF). This collaboration is instrumental as the CRF provides high-standard of pre-, intra- and post-operative care as well as welfare for rabbits undergoing this surgical procedure. All procedures were performed in strict accordance with the Animals (Scientific Procedures) Act 1986 and the current Guide for the Care and Use of Laboratory Animals published by the National Institute of Health (NIH Publication No. 85-23, revised 2011).

In total, forty-seven surgeries were performed in this study, 27 of which were coronary-ligation procedures, representing 58% of the total procedures over the study period. The overall surgical survival in this study is 55%, defined as rabbits surviving for 8 weeks post-operatively when the rabbits were sacrificed for terminal experiments (Figure 3.2). Twenty-one rabbits were prematurely culled due to various intra- and post-operative complications detailed in the following sections.

Figure 3.2 Overall survival in rabbits undergoing coronary ligation and sham procedures

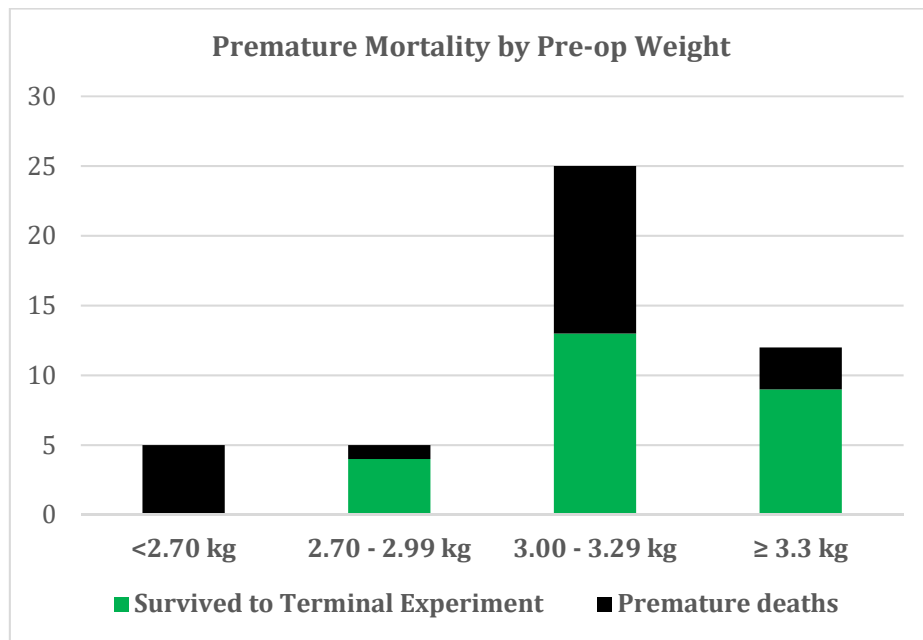


3.2.2 Pre-operative Animal Weight

In this study, rabbit weight at the time of surgery was 3.2 ± 0.1 kg. There was no statistical difference in pre-operative weight in rabbits undergoing coronary ligation (HF group) or sham procedures (SHM group).

The first 4 rabbits in this study had lower mean weight at 1.6 ± 0.1 kg at the time of surgery. All 4 rabbits died prematurely following surgery. As such, heavier rabbits were subsequently selected for this study. Further analysis revealed that rabbits with weights with at least 2.7 kg were required to ensure post-operative survival (Figure 3.3). Analysis of four different weight classes recorded a survival rate of 80% for rabbits weighing 2.70 – 2.99 kg, 52% for rabbits weighing 3.00 – 3.29 kg, and 75% for rabbits weighing at least 3.30 kg.

Figure 3.3 Premature mortality by pre-operative rabbit weight



3.2.3 Type of Surgeries: Coronary Ligation or Sham Procedures

In this study, 26 rabbits survived for 8 weeks until the terminal experiments. Of these rabbits, 14 underwent coronary ligation (HF group) (Figure 3.4). Meanwhile, 13 rabbits

in the HF group were culled prematurely, thereby indicating a lower survival rate in this group (Figure 3.5). Although this could suggest that coronary ligation per se carries a higher post-operative mortality, the contribution of heart failure progression to the mortality in HF group may play a part.

Figure 3.4 Overall survival of rabbits by procedure type

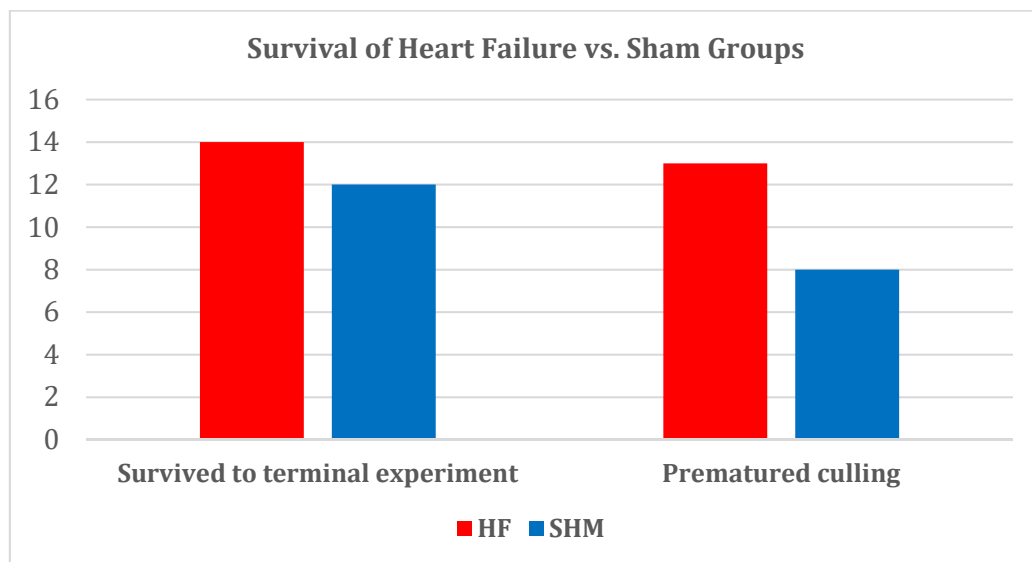
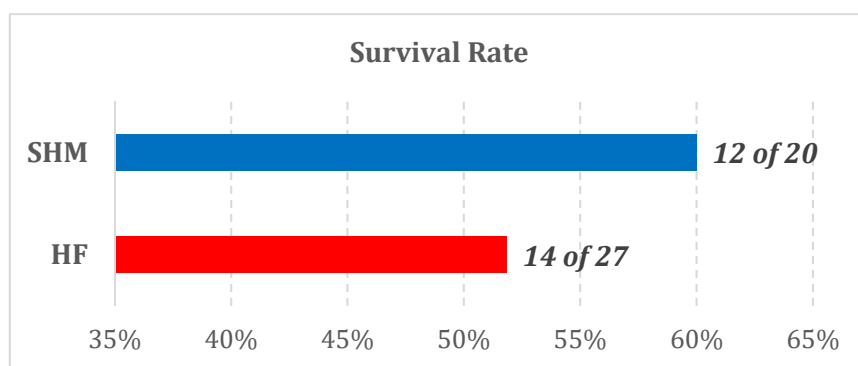


Figure 3.5 Survival rate of rabbits undergoing coronary ligation (HF) vs. sham (SHM) procedures

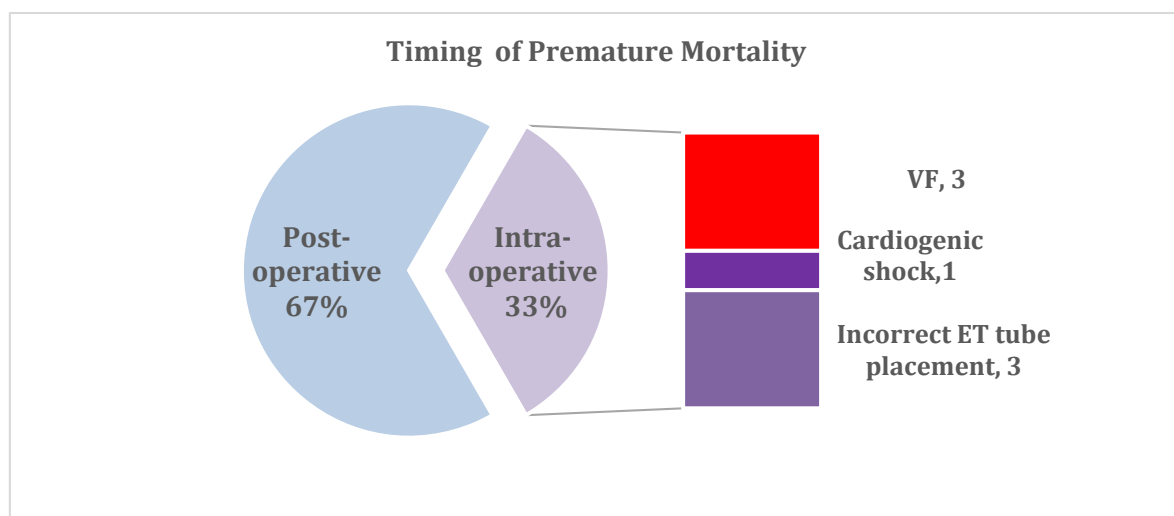


3.2.4 Premature Mortality

In this study, 21 rabbits died prematurely, 7 of which died during surgery. Intra-operative mortality was attributed to incorrect endotracheal tube placement, cardiogenic shock or ventricular fibrillation refractory to internal defibrillation (Figure 3.6).

Fourteen rabbits developed post-operative complications requiring premature culling. Of these 14 rabbits, post-mortem examination was performed on 12 rabbits. Organs comprising hearts, lungs, livers, lymph nodes as well as trachea with main bronchi were harvested and sent for histopathological analyses. Majority of the post-operative mortality was due to tracheitis with alveolar oedema and pneumonia seen in 23% of cases respectively (Figure 3.7). In most of these cases, complications occurred within 2 weeks following surgery culminating in premature culling (Figure 3.8). During this study, it was found that post-operative complications tended to occur around 7-10 days post-operatively.

Figure 3.6 Timing of premature mortality in rabbits



VF ventricular fibrillation; ET endotracheal

Figure 3.7 Histopathological findings in rabbits undergoing post-mortem examination following premature death

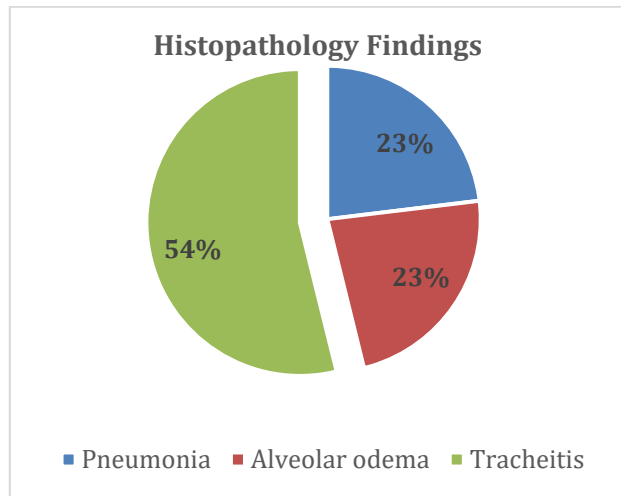
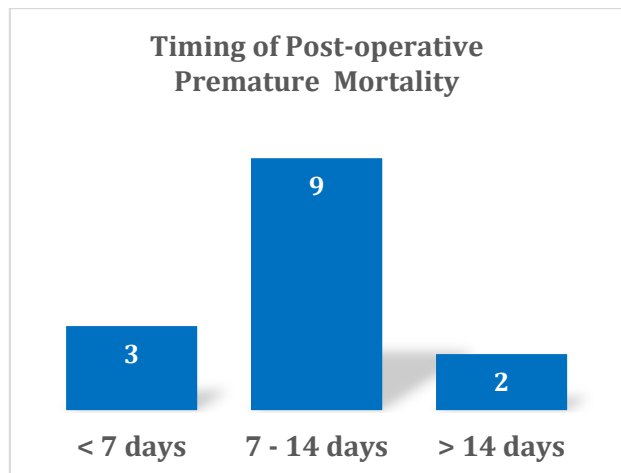


Figure 3.8 Timing of post-operative premature mortality in rabbits



3.2.5 Refinements and Learning Curve

The building of a surgical heart failure model in this study presented a unique and challenging learning journey. The principles of 3 “R”s, i.e. replacement, reduction and refinement, have been adhered to in an attempt to minimise intra- and post-operative mortality and ultimately permitting humane use of animals in research studies. In this respect, the rabbit heart failure model developed in this study is irreplaceable by another

experimental model that will afford comprehensive study of pathophysiological changes of whole heart and peripheral organs in heart failure. Nonetheless, the number of rabbit surgeries have been reduced to the minimum, allowing for meaningful data to be obtained at terminal experiments. Additionally, the initially high post-operative mortality provided valuable insights in developing refinements in pre-operative preparations, surgical and intubation techniques as well as post-operative care.

Various refinements were implemented throughout the study period, guided by advice from named veterinary surgeon at the CRF. These refinements were tabulated in chronological order in Table 3.2. These ranges from selecting appropriate pre-operative pre-medications and ventilator settings to post-operative analgesia and antibiotic prescription. In most cases of premature culling, post-mortem examinations were performed to inspect and obtain vital organ specimens to be sent for histopathological analyses, thus guiding specific refinements to be implemented throughout the study period (Figure 3.9).

The initial learning curve in the development of this surgical model of heart failure was steep, being evident from the high initial premature intra- and post-operative mortality. Nevertheless, the various targeted refinements act synergistically to eventually abolish any premature mortality in the last 3 months of the 24-month period when surgeries were carried out (Figure 3.10).

Chapter 3

Table 3.2 Refinements developed during the course of building a surgical heart failure model in rabbits

Date of Surgery	Refinements	Type of Refinements
25/11/13	<ol style="list-style-type: none"> 1. Premedication regime given as intramuscular injections based on traditional practices of Anaesthetic terminal experiments: <i>medetomidine, ketamine</i> and <i>butorphanol tartrate</i> 2. Eye cream following intubation 	Anaesthetic
27/01/14	<ol style="list-style-type: none"> 1. Isofluorane to maintain anaesthesia during intubation 2. Removing need for mattress sutures during skin closure 3. Use 5-0 Vicryl for skin closure 	Anaesthetic
09/07/14	Premedication regime changed to combination of <i>ketamine, xylazine</i> and <i>butorphanol tartrate</i>	Anaesthetic
16/07/14	<ol style="list-style-type: none"> 1. Premedication regime reverted back to <i>medetomidine, ketamine</i> and <i>butorphanol tartrate</i> 2. Duhacort (dexamethasone) injected into pericardial sac prior to rib closure to prevent adhesion/pericarditis 	Anaesthetic Surgical
08/12/14	Standardise use of post-op Baytril for 7-10 days	Infection control
11/02/15	<ol style="list-style-type: none"> 1. Premedications given as <i>subcutaneous</i> injections 2. Disposable laryngoscope with straighter, longer blade 3. Intubation BEFORE shaving to minimise risk of ET tube friction with trachea 	Anaesthetic Respiratory
11/03/15	<ol style="list-style-type: none"> 1. Routine post-op enrofloxacin (Baytril) changed to trimethoprim/sulfadiazine (Tribriissen) 2. Use of humidified air and steroid in the event of upper airway noise 	Infection control Respiratory

Chapter 3

Table 3.2 (continued)

Date of Surgery	Refinements	Type of Refinements
16/03/15	Lower limit of pre-op weight set at 2.7 kg (ideal weight: 3 kg ± 10%)	Surgical Respiratory
13/04/15	<ol style="list-style-type: none"> 1. Water-based jelly to lubricate end of ET tube 2. Inline humidifier attached to inflow tube 3. Reduce ventilator rate and tidal volume to ~ 40rpm and 20mL 4. Humidified air for 3-4 days post-operatively 	Respiratory
10/06/15	<ol style="list-style-type: none"> 1. Nebulised air through jet nebuliser in recovery room immediately post-surgery 2. Nebulised air for at least 1 hour every day for 7 days post-operatively 	Respiratory
01/07/15	<ol style="list-style-type: none"> 1. Connecting tube kit to avoid direct connection from vaporizer to ventilator – preventing pressure build up 2. Transparent cuffed ET tube to ensure ET tube in trachea (visualisation of condensation) 3. No humidifier to be used for next batch of surgeries 4. Wet hay for 10 days post-operatively 	Respiratory
06/07/15	<ol style="list-style-type: none"> 1. To prevent O₂ saturation desaturation <ul style="list-style-type: none"> - Intermittent re-inflation of left lung required during 20-minute waiting time - Minimise surgical time from skin incision to thoracotomy 2. Plastic cover to support rabbit (esp. neck) when transferring from pre-op room to theatre after intubation 	Respiratory

Chapter 3

Table 3.2 (continued)

Date of Surgery	Refinements	Type of Refinements
13/07/15	<ol style="list-style-type: none">1. Transparent <i>cuffed</i> ET tube size 2.5mm2. Successful re-inflation of left lung by inflating the cuff with 2.5 mL air and clamping outflow tube	Respiratory

Chapter 3

Figure 3.9 Temporal association of refinements with premature post-operative mortality in rabbits

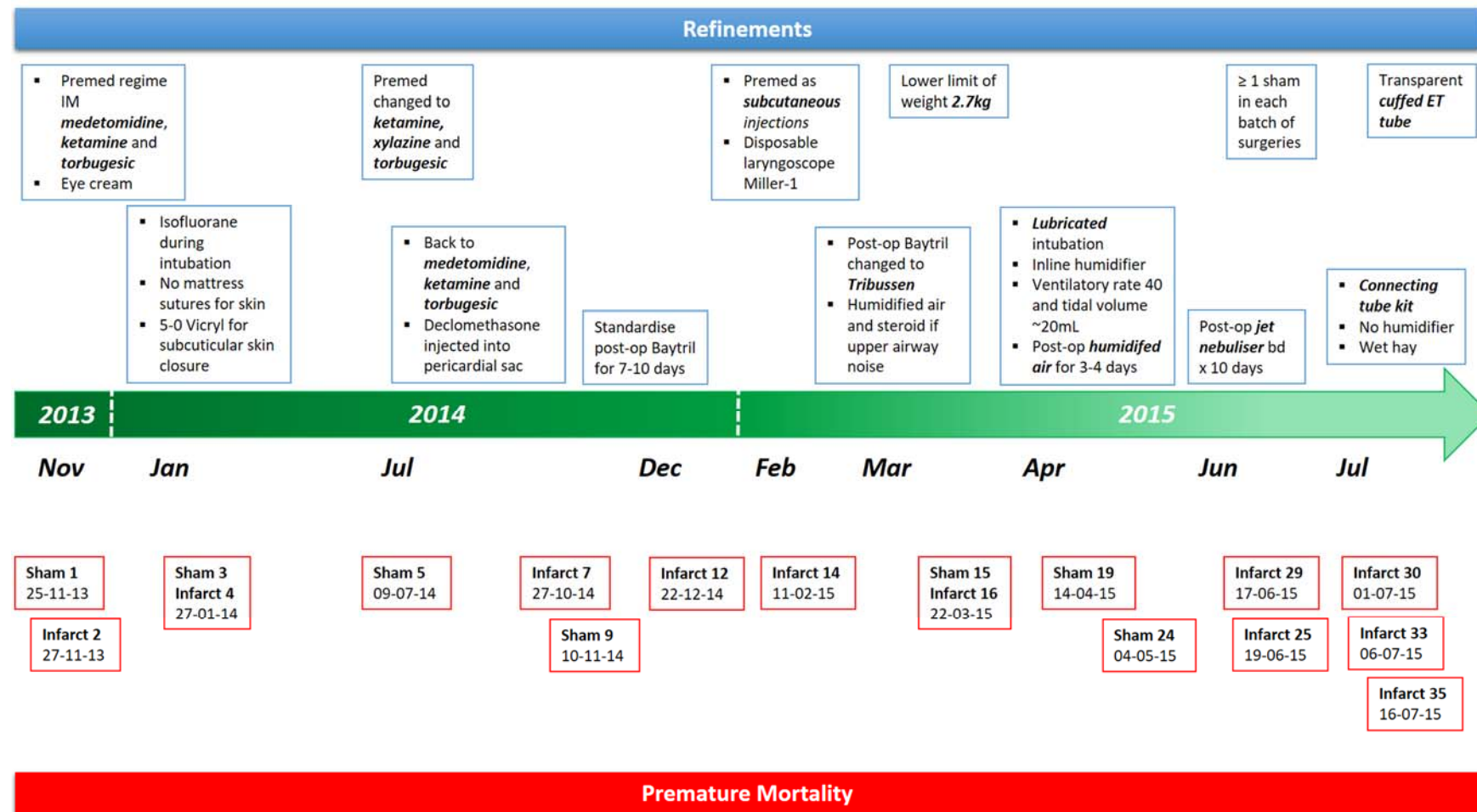
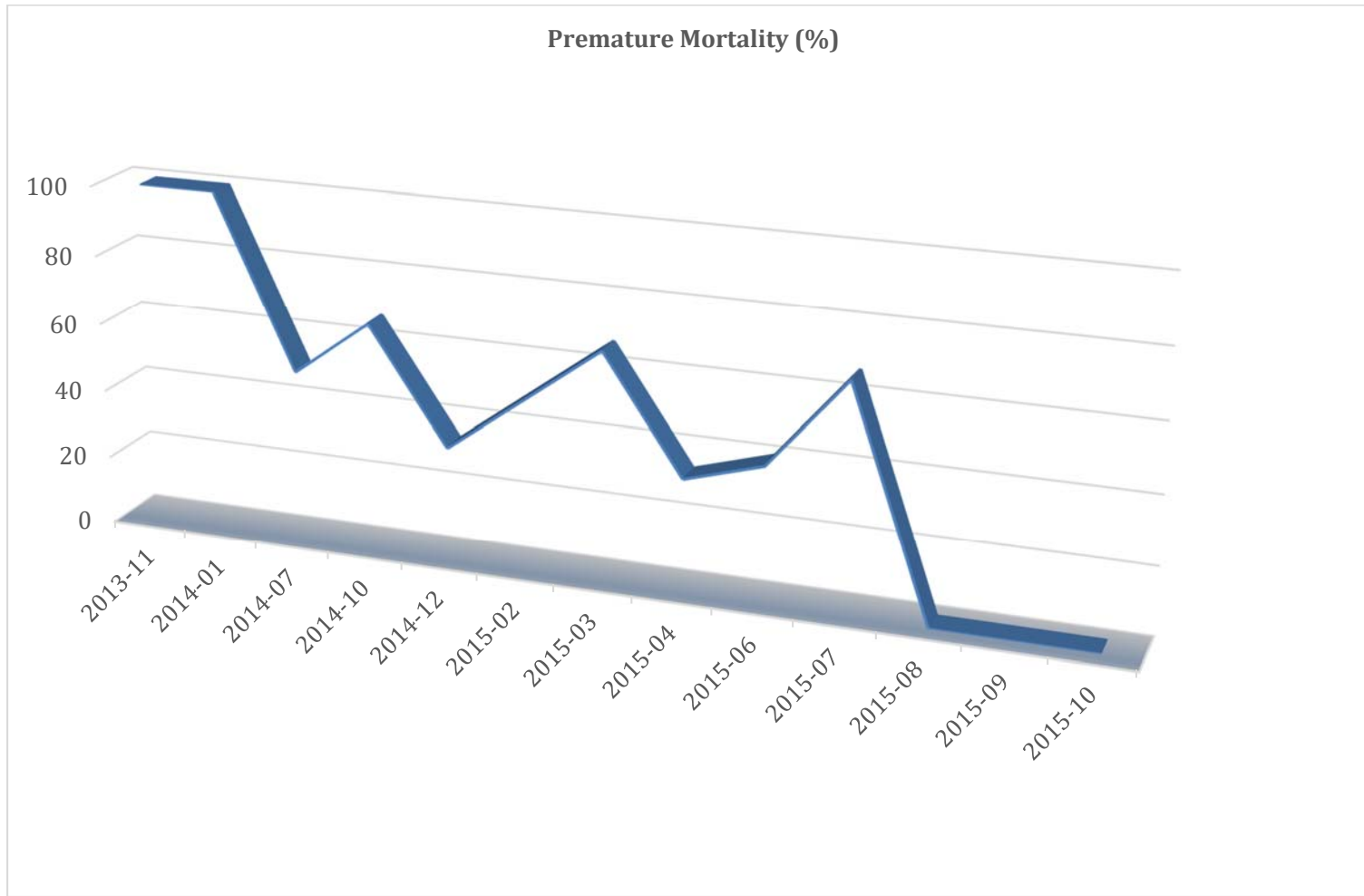


Figure 3.10 Time trend of percentage premature mortality in rabbits



3.3 Transthoracic Echocardiography

3.3.1 Background

Transthoracic echocardiography is a non-invasive imaging technique that employs ultrasound to establish diagnoses of various cardiovascular diseases through assessment of structural and functional status of the beating heart. The range of frequencies of the ultrasound wave utilised depends on the mode of studies, from 2 MHz in adult transthoracic studies to 7 MHz for harmonic imaging, transoesophageal studies and paediatric echocardiography. Generation of transthoracic echocardiographic images is accomplished by a transducer containing a layer of piezoelectric crystals capable of transmitting and receiving high-frequency ultrasound waves to and from the thoracic cavity, thereby detecting echoes reflected back from the heart and great vessels. The resulting electrical signals, generated by echoes from structures closest to the transducer to structures most distant to the latter, are amplified and transformed to convey spatial resolution of cardiac structures. On the other hand, temporal resolution is provided by multiple sweeps of ultrasound waves across a sector over time.

Historically the development of cardiac ultrasound is credited to Inge Edler and Mellmuth Hertz. The collaboration between Dr. Edler, a cardiologist, and Dr. Hertz, a physicist, was borne out of the interest in developing a diagnostic tool to evaluate patients with mitral stenosis prior to undergoing surgery at the time (Edler and Lindstrom, 2004). Eventually, with Hertz being the first human volunteer, they were the first to demonstrate movement of the “left atrial wall” with ultrasound, subsequently proven to be that of the anterior mitral valve leaflet through further cadaveric studies (Feigenbaum, 1996, Edler and Gustafson, 1957, Edler, 1961). Dr. Harvey Feigenbaum who was at that time interested in measuring left ventricular volumes and pressures for assessment of compliance, became the first physician to record the presence of pericardial effusion as echo-free space in a patient. These observations were subsequently validated by animal studies (Feigenbaum et al., 1966, Feigenbaum et al., 1965). Dr. Feigenbaum’s work in developing M-mode echocardiography for the measurement of left ventricular dimensions spearheaded clinical utility of echocardiography, with similar success being reported by other investigators (Popp and Harrison, 1970, Pombo et al., 1971,

Feigenbaum et al., 1972). Following the use of M-mode, two-dimensional echocardiography developed by Griffith and Henry (Griffith and Henry, 1974), conventional Doppler study by Baker et al (Rushmer et al., 1966, Baker et al., 1977), as well as colour Doppler flow imaging in the 1980's (Omoto et al., 1984, Helmcke et al., 1987) further expanded the clinical role of echocardiography.

Echocardiography plays a pivotal role in the diagnosis and management of heart failure. Among all modalities available for cardiac imaging, transthoracic echocardiography remains the modality of choice in all causes of heart failure due to its portability, safety and non-invasiveness. Systolic heart failure characterised by a dilated left ventricle and a reduced ejection fraction can therefore be reliably diagnosed by echocardiography. As early as 1975, left ventricular ejection fraction has been shown to provide important clinical and prognostic indicator for left ventricular performance (Nelson et al., 1975). Left ventricular volumes, namely end-diastolic, end-systolic and stroke volume, can be measured from two-dimensional echocardiography, providing a reliable estimation of ejection fraction in both canine (Buda and Zottz, 1986) and human studies (Stamm et al., 1982). Relevant to this thesis, echocardiography on normal healthy rabbits is proved to be feasible (Fontes-Sousa et al., 2006, Casamian-Sorrosal et al., 2014). More importantly, the rabbit heart failure model used in this thesis, originally established in the Department of Cardiology, Glasgow Royal Infirmary, have also been validated by transthoracic echocardiography to provide reliable information on structural changes and haemodynamic status of the left ventricle in heart failure induced by coronary ligation (Pye et al., 1996).

3.3.2 Method

Transthoracic echocardiography was conducted on the rabbits 1-2 week prior to euthanasia for terminal experimental studies of *ex vivo* assessment of electrophysiological performance. This was performed using a 5 MHz paediatric probe with a SoniVue sonograph. The rabbit was sedated with a subcutaneous injection containing a combination of Medetomidine Hydrochloride (Sedator, 0.2 mg/kg), Ketamine (Narketan, 10 mg/kg) and Butorphanol Tartrate (Torbugesic, 0.05 mg/kg). A small area of the anterior chest wall was shaved to allow for an optimal echocardiographic window. The

animal was positioned on a left lateral position. Transthoracic echocardiography generally required 40-45 minutes to obtain sufficient echocardiographic parameters and images for *post-hoc* analyses. During this period, oxygen saturation of the sedated rabbit was closely monitored with pulse oximetry. Upon completion of echocardiography, all rabbits were recovered from their sedation with Atipamezole Hydrochloride (Atipam, 1mg/kg).

The following echocardiographic parameters were obtained in the M-mode under parasternal long-axis view during end-systole and end-diastole (Figure 3.11a):-

1. left atrial systolic diameter (LAD)
2. end-diastolic (LVEDD) and end-systolic left ventricular internal diameter
3. interventricular septal thickness (IVS)
4. left ventricular posterior wall thickness (LVPW)

In parasternal short-axis view at a level just below the tips of the mitral valve leaflets, endocardial border was tracked and marked during the end-diastolic and end-systolic frame captured. This allows automatic computation of end-diastolic and end-systolic endocardial area (Figure 3.11b).

Using all the aforementioned echocardiographic parameters, fractional area change (FAC) and ejection fraction (EF) can be calculated, reflecting the percentage of left ventricular area and volume reduction respectively during systole in long and short axis.

Figure 3.11 Parasternal echocardiographic windows in rabbits illustrating long-axis view of mitral valve in M-mode (Figure 3.11a) and short axis view of basal left ventricle (Figure 3.11b)

Figure 3.11a

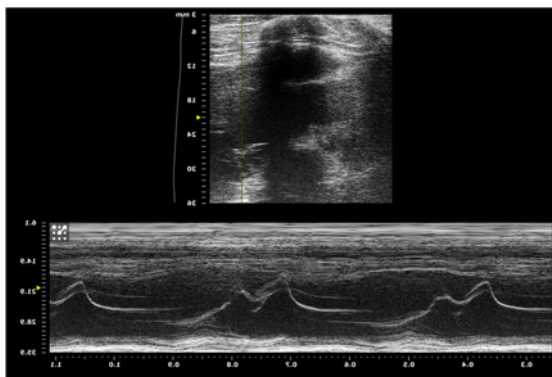


Figure 3.11b



3.4 Measurements of Ventricular Fibrillation Threshold and Ventricular Refractoriness in Langendorff-perfused Rabbit Hearts

3.4.1 Background

The Langendorff heart preparation was first pioneered in 1895 based on the observation by Oskar Langendorff that an excised mammalian heart which had stopped contracting could resume contraction for hours following a connection between its corresponding aorta with a reservoir of blood (Langendorff, 1895). This phenomenon was based on the premises that the pressure generated by the blood within the aorta closed the aortic valve, thereby directing blood through the coronary vasculature to maintain cardiac contractility. This experimental set-up has proven to be reproducible by means of appropriate cardiac preparation and equipment (Curtis and Hearse, 1989b). The underlying principle of Langendorff heart preparation involves cannulation of aorta to allow perfusate to enter coronary vasculature with either constant flow or constant pressure, thereby permitting measurement of either coronary vascular resistance or coronary flow respectively. The heart rate is determined by the sinoatrial node which reflects species variation (Johns and Olson, 1954). In both rats and mice, the *in vivo* heart rates (Mitchell et al., 1998, Curtis and Walker, 1986, Curtis et al., 1987, Curtis et al., 1985) were correspondingly higher than those in the Langendorff preparations (Curtis and Hearse, 1989b), (Yamada et al., 1990, Stables and Curtis, 2009, Nakata et al., 1990, Farkas and Curtis, 2002, Curtis and Hearse, 1989a, Bernier et al., 1989). In rabbits, the heart rate in the Langendorff preparation (Rees and Curtis, 1993a, Rees and Curtis, 1993b) is similar to that in conscious animals (Murakami et al., 1996), i.e. ~ 200 beats per minute. This is believed to be due to underlying species-dependent autonomic tone whereupon sympathetic removal occurs with Langendorff preparation and thus has less of an effect in rabbits than rodents owing to less sympathetic control on the baseline heart rate in the former.

In this study, isolated Langendorff perfused rabbit heart with intact autonomic innervation was used (Ng et al., 2001). This model overcomes several shortcomings compared to other models. First, it addressed the issue of *in vivo* heart performance being confounded by the influences of circulating catecholamines and haemodynamic reflexes

during direct autonomic nerve stimulations. Second, it exhibited a physiological cardiac response under corresponding autonomic nerve stimulation as compared to *in vitro* studies using exogenous pharmacological agents, such as isoproterenol, to mimic the autonomic nerve activity.

3.4.2 Method

3.4.2.1 Isolation of Heart with Intact Dual Autonomic Innervation

Isolation of rabbit heart with intact dual-innervated autonomic nerves was described in a previous study (Ng et al., 2001). Adult male New Zealand White rabbits were premedicated with subcutaneous injection of sedatives comprising a combination of Medetomidine Hydrochloride (Sedator, 0.2 mg/kg), Ketamine (Narketan, 10 mg/kg) and Butorphanol Tartrate (Torbugesic, 0.05 mg/kg). After 10 – 15 minutes, once the animal was fully sedated, the ear marginal vein was cannulated. One thousand IU heparin was given intravenously. The animal was shaved from neck to abdominal area. A midline cervical incision was made to isolate trachea. General anaesthesia was maintained by intravenous injections of Propofol. The trachea was intubated with a 5 mm plastic tube which was secured by Silk sutures. Positive pressure ventilation was initiated and maintained by a small-animal ventilator (Harvard Apparatus Ltd, Edenbridge, Kent, UK) with O₂-air mixture at 60 breaths min⁻¹. The common carotid arteries were identified, isolated and tied off with Silk sutures. The adjacent vagus nerves on each side were partially dissected at mid-cervical level. The midline neck incision was extended caudally to abdominal level to expose the ribcage, following which the pectoral muscles were dissected. Bilateral subclavian and internal jugular vessels were ligated with Silk sutures. The rabbit was euthanized with Pentobarbitone Sodium (160 mg/kg, Sagatal, Rhone Merieux, Harlow, UK) and 1000 IU heparin intravenously. Bilateral incisions were made at lower thorax just above the diaphragm level, allowing the anterior portion of the ribcage to be removed in order to expose the mediastinum. The pericardial sac was incised and ice-cold Tyrode solution was applied to the epicardial surface of the beating heart to reduce both temperature and metabolism. The descending aorta was isolated and cannulated with a custom-made flange-shaped plastic tube through which ice-cold Tyrode solution was injected. A small incision was made at the pulmonary artery,

allowing the Tyrode solution to escape from the right heart. Following the dissection of the vertebral column at the first cervical vertebra and the 12th thoracic vertebra, the whole-heart preparation extending from neck to the thorax inclusive of the residual ribcage were excised. The proximal dissection at the level of first cervical vertebral ensures this whole-heart preparation is a spinal specimen devoid of any brainstem activity, thereby eliminating the influence of afferent inputs and central modulation during autonomic nerve stimulations.

All procedures were undertaken in accordance with the Animals (Scientific Procedures) Act 1986 in the UK and the Guide for the Care and Use of Laboratory Animals published by the US National Institutes of Health (NIH Publication No. 85-23, revised 1996).

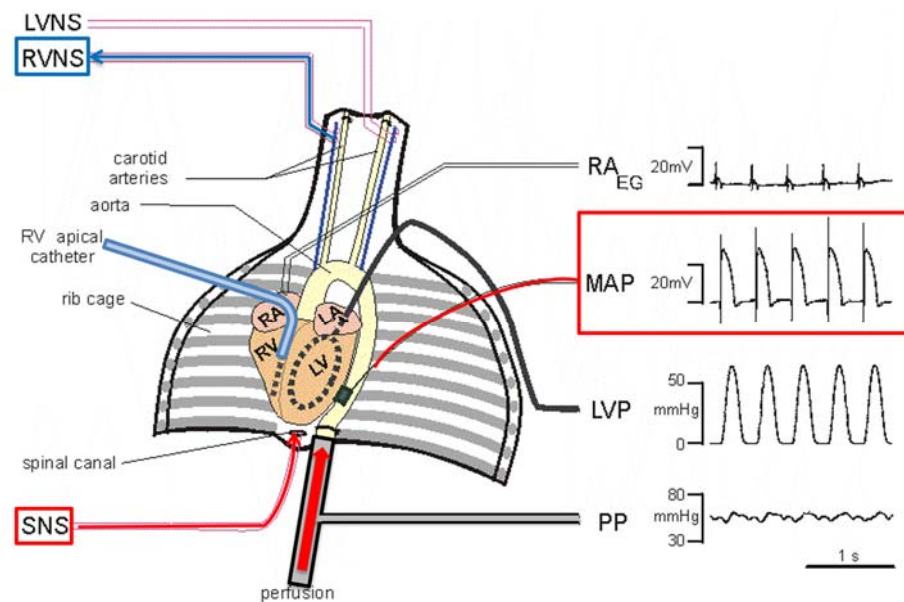
3.4.2.2 Langendorff Preparation Protocol and Cardiac Electrical Signal Recording

The plastic tube which was cannulated in the descending aorta was connected to the perfusion apparatus to deliver perfusate in modified Langendorff fashion using Tyrode solution comprising (in mM): 130 NaCl, 24 NaHCO₃, 1.0 CaCl₂, 1.0 MgCl₂, 4.0 KCl, 1.2 NaH₂PO₄ and 20 dextrose. Constant pH was achieved at 7.4 by gassing a mixture of 95% O₂ and 5% CO₂ whilst temperature was maintained constant at 37°C with a feedback control via a heating element in the bathing solution. A Gilson Minipuls 3 peristaltic pump was used to deliver Tyrode solution at a constant flow rate of 100mL/min thereby maintaining a constant perfusion pressure. A 3F polypropylene catheter (Portex, Kent, UK) was inserted using Seldinger technique through the left ventricular apex to allow for drainage of Thebesian venous effluent. Left ventricular pressure was measured by a pressure transducer (MTL0380, AD Instruments, Chalgrove, UK) using a water-filled latex balloon inserted through a small incision at the left atrium into the left ventricle. The volume of the balloon was adjusted to give rise to 0 – 5 end-diastolic pressure readings. Perfusion pressure was monitored with a separate pressure transducer connected in series with the aortic cannula.

Two pairs of platinum needle electrodes (Grass Instruments, Slough, UK) were used. One of the pairs was connected to the right atrial appendage for recording of atrial

electrograms whilst the second pair was connected to the right atrium and the rib cage to record a rudimentary electrocardiograph (ECG). To assess for atrio-ventricular delay, the electrodes used for recording of atrial electrograms were also used for atrial pacing. A spring-loaded mini-MAP electrode (Harvard Apparatus, Edenbridge, Kent, UK) was used to record monophasic action potentials (MAPs) from the epicardial surface of the left ventricular free wall simultaneously at the base and the apex using a DC-coupled high input impedance differential amplifier (Figure 3.12).

Figure 3.12 Langendorff-perfused rabbit heart preparation with intact dual-autonomic innervation



3.4.2.3 Autonomic Nerve Stimulation

The cervical vagus nerves were dissected from adjacent muscle fibres. Once isolated, individual nerve was supported by a pair of custom-made bipolar silver electrodes (Advent Research Materials, UK: 0.5 mm diameter). In contrast, bilateral sympathetic nerve stimulation was achieved by inserting a quadripolar catheter into the spinal canal at the 12th thoracic vertebra and advancing the catheter to the level of the 2nd thoracic vertebra. The electrodes for each branch of the autonomic nerves were connected to 2-channel constant voltage square pulse stimulators individually (S88, Grass Instruments),

the latter capable of stimulation over a range of frequencies (1 – 20 Hz) and strengths (1 – 20 V) at 2 ms pulse-width. This allows for both isolated and concurrent vagus and/or sympathetic nerve stimulations. A neuro-muscular blocking agent, decamethonium bromide (Sigma, UK, 5 µM) was added into Tyrode solution to prevent intercostal-muscle twitching caused by current spread to the spinal motor neurones during high-frequency sympathetic nerve stimulation.

3.4.2.4 Measurement of Atrial and Ventricular Electrophysiology

3.4.2.4.1 Measurement of Heart Rate and Atrio-ventricular Delay

All electrical signals, including heart rate and MAPs, as well as left ventricular and perfusion pressures were recorded with a PowerLab 800.s (ADIInstruments Ltd, UK) and subsequently digitalised at 1 kHz using LabChart Pro software (ADIInstruments Ltd, UK). Heart rate was recorded at steady state at baseline and following autonomic nerve stimulation. In addition, this was derived by measuring the beat-to-beat interval of the atrial electrograms. During atrial pacing with the needle electrodes originally used to record atrial electrograms, antegrade atrio-ventricular delay could be assessed by measuring the delay from the atrial stimulation spike to the beginning of the MAP measured from the left ventricular free wall.

3.4.2.4.2 Measurement of Ventricular Electrophysiology

A bipolar pacing electrode (EP Technologies, Sunnyvale, California, US) was inserted through the incision at the pulmonary artery into the right ventricular apex, and was connected to a constant current stimulator (DS7A, Digitimer, Welwyn Garden City, UK) to deliver a pacing current at twice the diastolic threshold with a 2 ms pulse width.

Ventricular fibrillation threshold (VFT) was measured with right ventricular burst pacing (30 stimuli, 30 ms interval) after a 20-beat drivetrain at 240 ms, and was determined by progressively increasing the pacing current at 0.5 mA steps. If no VF was induced, a 5-second rest period ensued before the next pacing train resumed. VFT was defined as the

minimum current required to induce sustained VF lasting for at least 10 seconds (Figure 3.13).

Both standard restitution and ventricular refractoriness were determined by right ventricular pacing using a 20-beat drive train (S_1 , 240ms cycle length) followed by an S_2 decrementing at 10 ms from 240 ms to 200 ms, and subsequently at 5 ms from 200 ms to ventricular effective refractory period (ERP). ERP was thus defined as the longest coupling interval that failed to capture the ventricles (Figure 3.14). Using a custom-written programme (Kettlewell et al., 2004), MAP duration was measured from the beginning of the signal to 90% repolarisation ($MAPD_{90}$), i.e. peak of the action potential to the isoelectric line. Restitution was prescribed by the relationship between S_2 - $MAPD_{90}$ and its preceding diastolic intervals (DI), the latter being measured by the interval between S_1 and S_2 -MAP signals minus S_1 - $MAPD_{90}$. A best-fitted exponential curve was created ($MAPD_{90} = MAPD_{90\max} [1 - e^{-DI/T}]$) with Microcal Origin (v9.1, Origin, San Diego, CA, US) where $MAPD_{90\max}$ was the maximum $MAPD_{90}$ and T was the time constant. Specifically, in adopting this mono-exponential growth function for curve fitting, maximum $MAPD_{90}$ and T are both constants obtained by the least squares fitting to the experimental values of $MAPD_{90}$ and DI (Hering, 1909). Analysis of the first derivative of this fitted curve yielded the maximum slope of action potential duration (APD) restitution, enabling the restitution hypothesis to be verified (Cao et al., 1999). It should be recognised that this maximum curve-fitting method used empirically to describe the data assumes that cardiac restitution will conform to such an exponential behaviour. In the clinical setting, this assumption may not always be true with the requirement of the maximum slope occurring at the shortest diastolic interval. Hence such a restrictive assumption may not be able to track data fluctuations in a physiological model. Furthermore, in the presence of regional heterogeneity, the fitting of a single function is not robust, resulting in large standard errors in the least-square estimates in the parameter values of the function. To overcome such shortcomings, an alternative method of calculating the least mean squares was proposed. This involves fitting the data by overlapping least-squares linear segments of 40 ms in diastolic intervals, calculating the means and the resultant standard errors. Indeed, the latter method of “least mean squares” have been validated in clinical studies to allow for a more physiological representation as well as to account for regional heterogeneity (Taggart et al., 2003, Nicolson et al., 2012).

For the Langendorff's preparation used in this thesis, the focus of the study is the maximum slopes and therefore an exponential function is assumed.

Throughout this thesis, standard APD restitution was measured using the aforementioned S1-S2 protocol which affords measurements of ventricular ERP. It is however important to recognise that APD restitution is not the only mechanism that can give rise to APD alternans. Conduction velocity (CV) restitution plays a similarly important influence in the induction of alternans. Specifically, the probability of discordant alternans formation has been shown to be inversely proportional to c'/c^2 , where c is CV and c' is the slope of the CV restitution curve (Echebarria and Karma, 2002). Discordant alternans therefore forms more easily when the gradient CV restitution curve is extremely steep. However, the measurement of CV restitution has inherently similar challenges as that of APD restitution due to its dependency of DIs. Furthermore, in anisotropic cardiac tissue, the longitudinal and transverse propagation directions may not be easy to determine due to the complex myocardial fibres alignment, contributing to not only spatial but also temporal variation in CV especially during alternans. In small animal models, CV measurements pose a greater experimental uncertainty due to measurement of two very close sites which results in a small difference in time.

Figure 3.13 An example of MAP Recording with VF induction by burst pacing following a drive train at 240 ms cycle length

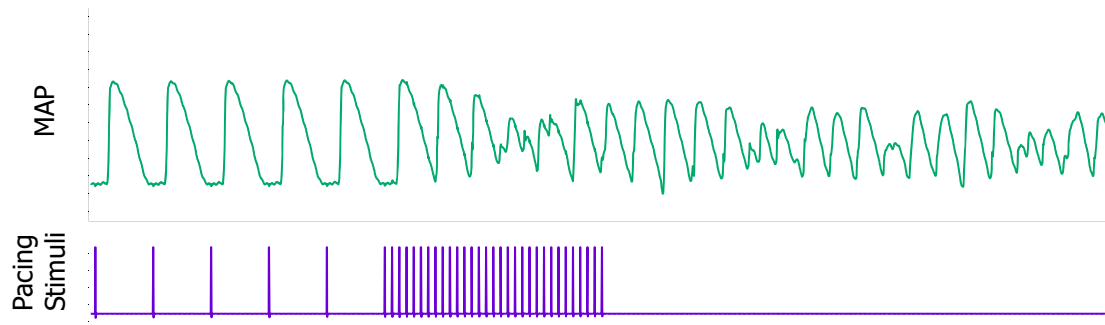


Figure 3.14 MAP recordings during an S1-S2 protocol at 240 ms S1 cycle length, with S2 capturing the ventricle in one drive train (Figure 3.14a) but failing to capture the ventricle in the next drive train (Figure 3.14b)

Figure 3.14a

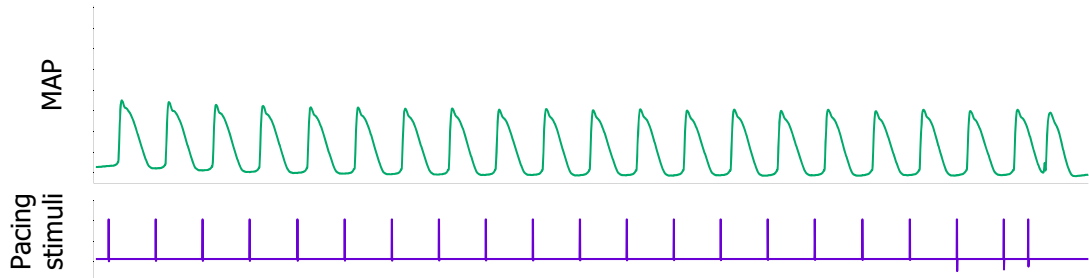
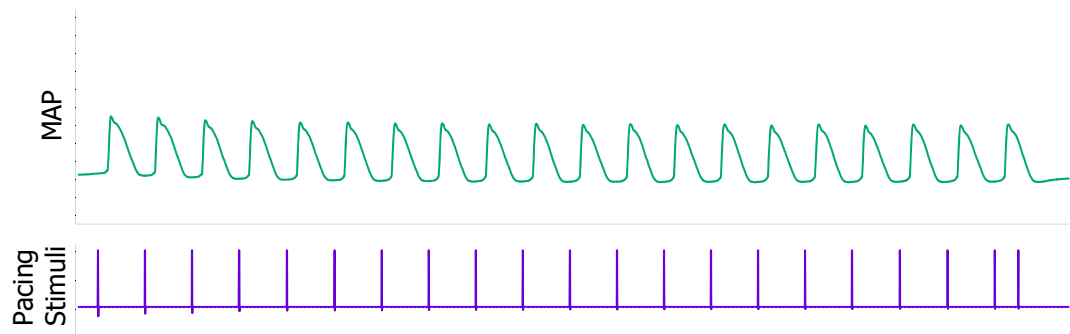


Figure 3.14b



3.5 Cardiac Remodelling and Organ Congestion

3.5.1 Background

Following myocardial infarction, significant structural changes occur to the ventricles as seen in both animals (Pfeffer, 1991) and humans (McKay et al., 1986). This process of structural change was coined *remodelling*, describing significant degree of hypertrophy as a compensatory response to impaired contractile performance as a result of myocardial infarction (Braunwald and Pfeffer, 1991). Specifically left ventricular remodelling encompasses changes in mass, volume, geometry and cellular composition in the left ventricle in response to mechanical stress and/or systemic neurohumoral activation (Sutton and Sharpe, 2000).

Adverse phenotypic changes to the heart following myocardial infarction contributes to peripheral organ congestion, creating the well-recognised clinical syndrome of chronic heart failure (Katz et al., 1960). Conceptually contractile dysfunction of a pumping chamber leads to back-pressure in the vasculature and corresponding organs proximal to the chamber in question. As such, left ventricular failure results in pulmonary congestion whereas right ventricular failure leads to raised systemic venous pressure and hence hepatic congestion and peripheral fluid retention. Ultimately longstanding pulmonary congestion contributes to pulmonary hypertension and right ventricular overload. Hence the leading cause of right ventricular failure is left ventricular failure.

3.5.2 Method

3.5.2.1 Measurement of Wet and Dry Organ Weights

In order to assess the degree of compensatory cardiac remodelling and organ congestion in the coronary ligation model of rabbit heart failure, livers and lungs were excised from the animals at the time of euthanasia, blotted to remove excess blood, and weighed to record their wet weights. At the end of each experiment, each heart was carefully excised from the residual ribcage, preserving its great vessels. The heart was blotted and the wet

weight was measured. All organs were dried in an oven heated to 70 °C until their corresponding dry weights plateau.

3.5.2.2 Ex-vivo Cardiac Magnetic Resonance Imaging

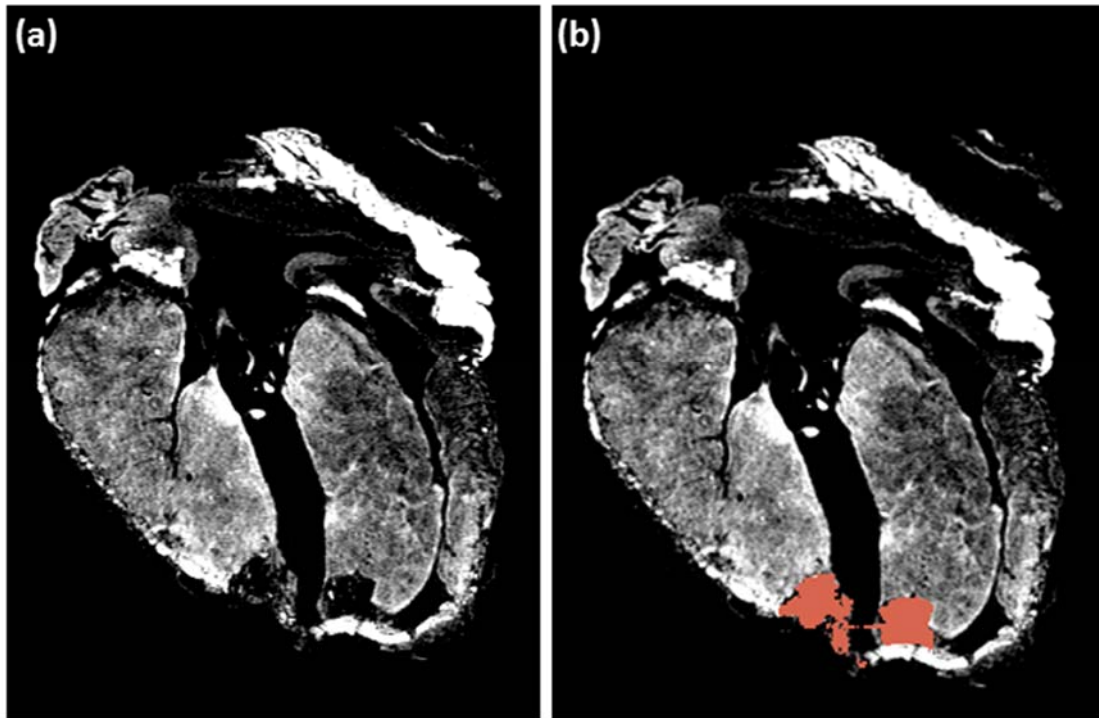
In some cases, at the end of a terminal experiment, the heart was excised from the residual ribcage, with its great vessels preserved. The whole heart was fixed with 4% paraformaldehyde overnight. On the next day, the heart was placed in a test tube containing proton-free fluid, Fomblin-Y (Silma Aldrich). Fomblin-Y was used as it is devoid of magnetic resonance imaging (MRI) signal in addition to being susceptibility-matched to tissue.

MRI scanning was performed on a 9.4T Agilent scanner (Agilent Technologies, Santa Clare, CA, USA) with a 310mm bore diameter and 6cm inner-diameter gradient coil (1000 mT/m maximum gradient strength), interfaced with a DirectDrive Console. Radio frequency transmission and reception was achieved with a 40mm millipede transmit/receive RF coil. The rabbit hearts were positioned at the isocenter of the magnet and located with fast gradient echo scan. 3D gradient echo shimming of first and second order shims was performed over the entire heart and shim quality was confirmed using point resolved spectroscopy (PRESS) of the water peak.

T2-weighted images were acquired using a fast spin echo (FSE) sequence with TR/TE = 3000/40ms, 30 x 30mm field of view (256 x 256 matrix), 36 x 1mm coronal slices and 3 signal averages (scan duration = 9mins 42sec). The resultant images were used to generate 2D slice montage representations of the heart (Figure 3.15).

For accurate quantification of scar volume, T1-weighted images were acquired using a 3-dimensional magnetization prepared rapid gradient-echo (MP-RAGE) sequence with TR/TE = 6.5/3.3ms, 40 x 30 x 30mm field of view (256 x 192 x 192 matrix) and 2 signal averages (scan duration = 57mins 39sec). Scar volume was calculated using manual ROI analysis in 3D Slicer (<http://www.slicer.org>).

Figure 3.15 Sagittal representation of rabbit heart taken from 3D T1-weighted MP-RAGE scan (a) with superimposed scar region (b) (highlighted red) generated by semi-automated region growing analysis in 3D Slicer



3.6 Data Presentation and Statistical Analysis

All experimental data presented in the following chapters are expressed as mean \pm standard error. Comparison between groups of data was made with either Student's t-test or with repeated measures of ANOVA if appropriate. A two-tailed P value of less than 0.05 was considered significant. All P values were represented by asterisks in graphs, whereby * denotes $P \leq 0.05$, ** denotes $P \leq 0.01$, and *** denotes $P \leq 0.001$.

3.7 References

- ANVERSA, P., KAJSTURA, J., REISS, K., QUAINI, F., BALDINI, A., OLIVETTI, G. & SONNENBLICK, E. H. 1995. Ischemic cardiomyopathy: myocyte cell loss, myocyte cellular hypertrophy, and myocyte cellular hyperplasia. *Ann N Y Acad Sci*, 752, 47-64.
- ANVERSA, P., ZHANG, X., LI, P. & CAPASSO, J. M. 1992. Chronic coronary artery constriction leads to moderate myocyte loss and left ventricular dysfunction and failure in rats. *J Clin Invest*, 89, 618-29.
- BAKER, D. W., RUBENSTEIN, S. A. & LORCH, G. S. 1977. Pulsed Doppler echocardiography: principles and applications. *Am J Med*, 63, 69-80.
- BERNIER, M., CURTIS, M. J. & HEARSE, D. J. 1989. Ischemia-induced and reperfusion-induced arrhythmias: importance of heart rate. *Am J Physiol*, 256, H21-31.
- BING, O. H., BROOKS, W. W., CONRAD, C. H., SEN, S., PERREAUULT, C. L. & MORGAN, J. P. 1991. Intracellular calcium transients in myocardium from spontaneously hypertensive rats during the transition to heart failure. *Circ Res*, 68, 1390-400.
- BOLUYT, M. O., O'NEILL, L., MEREDITH, A. L., BING, O. H., BROOKS, W. W., CONRAD, C. H., CROW, M. T. & LAKATTA, E. G. 1994. Alterations in cardiac gene expression during the transition from stable hypertrophy to heart failure. Marked upregulation of genes encoding extracellular matrix components. *Circ Res*, 75, 23-32.
- BRAUNWALD, E. & PFEFFER, M. A. 1991. Ventricular enlargement and remodeling following acute myocardial infarction: mechanisms and management. *Am J Cardiol*, 68, 1D-6D.
- BUDA, A. J. & ZOTZ, R. J. 1986. Serial assessment of circumferential regional left ventricular function following complete coronary occlusion. *Am Heart J*, 112, 447-52.
- CALVERT, C. A., HALL, G., JACOBS, G. & PICKUS, C. 1997a. Clinical and pathologic findings in Doberman pinschers with occult cardiomyopathy that died suddenly or developed congestive heart failure: 54 cases (1984-1991). *J Am Vet Med Assoc*, 210, 505-11.
- CALVERT, C. A., PICKUS, C. W., JACOBS, G. J. & BROWN, J. 1997b. Signalment, survival, and prognostic factors in Doberman pinschers with end-stage cardiomyopathy. *J Vet Intern Med*, 11, 323-6.
- CAO, J. M., QU, Z., KIM, Y. H., WU, T. J., GARFINKEL, A., WEISS, J. N., KARAGUEUZIAN, H. S. & CHEN, P. S. 1999. Spatiotemporal heterogeneity in the induction of ventricular fibrillation by rapid pacing: importance of cardiac restitution properties. *Circ Res*, 84, 1318-31.
- CASAMIAN-SORROSAL, D., SAUNDERS, R., BROWNE, W. J., ELLIOTT, S. & FONFARA, S. 2014. M-mode, two-dimensional and Doppler echocardiographic findings in 40 healthy domestic pet rabbits. *J Vet Cardiol*, 16, 101-8.
- CURTIS, M. J. & HEARSE, D. J. 1989a. Ischaemia-induced and reperfusion-induced arrhythmias differ in their sensitivity to potassium: implications for mechanisms of initiation and maintenance of ventricular fibrillation. *J Mol Cell Cardiol*, 21, 21-40.

- CURTIS, M. J. & HEARSE, D. J. 1989b. Reperfusion-induced arrhythmias are critically dependent upon occluded zone size: relevance to the mechanism of arrhythmogenesis. *J Mol Cell Cardiol*, 21, 625-37.
- CURTIS, M. J., JOHNSTON, K. M., MACLEOD, B. A. & WALKER, M. J. 1985. The actions of felodipine on arrhythmias and other responses to myocardial ischaemia in conscious rats. *Eur J Pharmacol*, 117, 169-78.
- CURTIS, M. J., MACLEOD, B. A. & WALKER, M. J. 1987. Models for the study of arrhythmias in myocardial ischaemia and infarction: the use of the rat. *J Mol Cell Cardiol*, 19, 399-419.
- CURTIS, M. J. & WALKER, M. J. 1986. The mechanism of action of the optical enantiomers of verapamil against ischaemia-induced arrhythmias in the conscious rat. *Br J Pharmacol*, 89, 137-47.
- DAHL, L. K., HEINE, M. & TASSINARI, L. 1962. Role of genetic factors in susceptibility to experimental hypertension due to chronic excess salt ingestion. *Nature*, 194, 480-2.
- DOWNING, S. E. & CHEN, V. 1985. Myocardial injury following endogenous catecholamine release in rabbits. *J Mol Cell Cardiol*, 17, 377-87.
- ECHEBARRIA, B. & KARMA, A. 2002. Instability and spatiotemporal dynamics of alternans in paced cardiac tissue. *Phys Rev Lett*, 88, 208101.
- EDLER, I. 1961. Atrioventricular valve motility in the living human heart recorded by ultrasound. *Acta Med Scand Suppl*, 370, 83-124.
- EDLER, I. & GUSTAFSON, A. 1957. Ultrasonic cardiogram in mitral stenosis; preliminary communication. *Acta Med Scand*, 159, 85-90.
- EDLER, I. & LINDSTROM, K. 2004. The history of echocardiography. *Ultrasound Med Biol*, 30, 1565-644.
- EZZAHER, A., EL HOUDA BOUANANI, N. & CROZATIER, B. 1992. Force-frequency relations and response to ryanodine in failing rabbit hearts. *Am J Physiol*, 263, H1710-5.
- EZZAHER, A., EL HOUDA BOUANANI, N., SU, J. B., HITTINGER, L. & CROZATIER, B. 1991. Increased negative inotropic effect of calcium-channel blockers in hypertrophied and failing rabbit heart. *J Pharmacol Exp Ther*, 257, 466-71.
- FARKAS, A. & CURTIS, M. J. 2002. Limited antifibrillatory effectiveness of clinically relevant concentrations of class I antiarrhythmics in isolated perfused rat hearts. *J Cardiovasc Pharmacol*, 39, 412-24.
- FEIGENBAUM, H. 1996. Evolution of echocardiography. *Circulation*, 93, 1321-7.
- FEIGENBAUM, H., POPP, R. L., WOLFE, S. B., TROY, B. L., POMBO, J. F., HAINE, C. L. & DODGE, H. T. 1972. Ultrasound measurements of the left ventricle. A correlative study with angiography. *Arch Intern Med*, 129, 461-7.
- FEIGENBAUM, H., WALDHAUSEN, J. A. & HYDE, L. P. 1965. Ultrasound Diagnosis of Pericardial Effusion. *JAMA*, 191, 711-4.
- FEIGENBAUM, H., ZAKY, A. & WALDHAUSEN, J. A. 1966. Use of ultrasound in the diagnosis of pericardial effusion. *Ann Intern Med*, 65, 443-52.
- FELDMAN, A. M., WEINBERG, E. O., RAY, P. E. & LORELL, B. H. 1993. Selective changes in cardiac gene expression during compensated hypertrophy and the transition to cardiac decompensation in rats with chronic aortic banding. *Circ Res*, 73, 184-92.
- FONTES-SOUZA, A. P., BRAS-SILVA, C., MOURA, C., AREIAS, J. C. & LEITE-MOREIRA, A. F. 2006. M-mode and Doppler echocardiographic reference values for male New Zealand white rabbits. *Am J Vet Res*, 67, 1725-9.

- GARCIA, R. & DIEBOLD, S. 1990. Simple, rapid, and effective method of producing aortocaval shunts in the rat. *Cardiovasc Res*, 24, 430-2.
- GILSON, N., EL HOUDA BOUANANI, N., CORSIN, A. & CROZATIER, B. 1990. Left ventricular function and beta-adrenoceptors in rabbit failing heart. *Am J Physiol*, 258, H634-41.
- GOMEZ, A. M., VALDIVIA, H. H., CHENG, H., LEDERER, M. R., SANTANA, L. F., CANNELL, M. B., MCCUNE, S. A., ALTSCHULD, R. A. & LEDERER, W. J. 1997. Defective excitation-contraction coupling in experimental cardiac hypertrophy and heart failure. *Science*, 276, 800-6.
- GRIFFITH, J. M. & HENRY, W. L. 1974. A sector scanner for real time two-dimensional echocardiography. *Circulation*, 49, 1147-52.
- GRIMA, E. A., MOE, G. W., HOWARD, R. J. & ARMSTRONG, P. W. 1994. Recovery of attenuated baroreflex sensitivity in conscious dogs after reversal of pacing induced heart failure. *Cardiovasc Res*, 28, 384-90.
- HASENFUSS, G. 1998. Animal models of human cardiovascular disease, heart failure and hypertrophy. *Cardiovasc Res*, 39, 60-76.
- HELMCKE, F., NANDA, N. C., HSIUNG, M. C., SOTO, B., ADEY, C. K., GOYAL, R. G. & GATEWOOD, R. P., JR. 1987. Color Doppler assessment of mitral regurgitation with orthogonal planes. *Circulation*, 75, 175-83.
- HERING, H. E. 1909. Experimentelle studien an saugethieren uber das electrocardiogram. *Z Exp Pathol Ther*, 7, 363-378.
- HOLYCROSS, B. J., SUMMERS, B. M., DUNN, R. B. & MCCUNE, S. A. 1997. Plasma renin activity in heart failure-prone SHHF/Mcc-facp rats. *Am J Physiol*, 273, H228-33.
- HUNTINGTON, K., PICARD, P., MOE, G., STEWART, D. J., ALBERNAZ, A. & MONGE, J. C. 1998. Increased cardiac and pulmonary endothelin-1 mRNA expression in canine pacing-induced heart failure. *J Cardiovasc Pharmacol*, 31 Suppl 1, S424-6.
- INOKO, M., KIHARA, Y., MORII, I., FUJIWARA, H. & SASAYAMA, S. 1994. Transition from compensatory hypertrophy to dilated, failing left ventricles in Dahl salt-sensitive rats. *Am J Physiol*, 267, H2471-82.
- JOHNS, T. N. & OLSON, B. J. 1954. Experimental myocardial infarction. I. A method of coronary occlusion in small animals. *Ann Surg*, 140, 675-82.
- KAJSTURA, J., ZHANG, X., REISS, K., SZOKE, E., LI, P., LAGRASTA, C., CHENG, W., DARZYNKIEWICZ, Z., OLIVETTI, G. & ANVERSA, P. 1994. Myocyte cellular hyperplasia and myocyte cellular hypertrophy contribute to chronic ventricular remodeling in coronary artery narrowing-induced cardiomyopathy in rats. *Circ Res*, 74, 383-400.
- KATZ, L. N., FEINBERG, H. & SHAFFER, A. B. 1960. Hemodynamic aspects of congestive heart failure. *Circulation*, 21, 95-111.
- KETTLEWELL, S., WALKER, N. L., COBBE, S. M., BURTON, F. L. & SMITH, G. L. 2004. The electrophysiological and mechanical effects of 2,3-butane-dione monoxime and cytochalasin-D in the Langendorff perfused rabbit heart. *Exp Physiol*, 89, 163-72.
- KHADOUR, F. H., KAO, R. H., PARK, S., ARMSTRONG, P. W., HOLYCROSS, B. J. & SCHULZ, R. 1997. Age-dependent augmentation of cardiac endothelial NOS in a genetic rat model of heart failure. *Am J Physiol*, 273, H1223-30.

- KLEAVELAND, J. P., KUSSMAUL, W. G., VINCIGUERRA, T., DITERS, R. & CARABELLO, B. A. 1988. Volume overload hypertrophy in a closed-chest model of mitral regurgitation. *Am J Physiol*, 254, H1034-41.
- KRENEK, P., KMECOVA, J., KUCEROVA, D., BAJUSZOVA, Z., MUSIL, P., GAZOVA, A., OCHODNICKY, P., KLIMAS, J. & KYSELOVIC, J. 2009. Isoproterenol-induced heart failure in the rat is associated with nitric oxide-dependent functional alterations of cardiac function. *Eur J Heart Fail*, 11, 140-6.
- LANGENDORFF, O. 1895. Untersuchen am überlebenden Säugetierherzen. *Pflugers Arch*, 66, 291-332.
- LI, Z., BING, O. H., LONG, X., ROBINSON, K. G. & LAKATTA, E. G. 1997. Increased cardiomyocyte apoptosis during the transition to heart failure in the spontaneously hypertensive rat. *Am J Physiol*, 272, H2313-9.
- LIFSCHITZ, M. D. & SCHRIER, R. W. 1973. Alterations in cardiac output with chronic constriction of thoracic inferior vena cava. *Am J Physiol*, 225, 1364-70.
- LIU, J. L. & ZUCKER, I. H. 1999. Regulation of sympathetic nerve activity in heart failure: a role for nitric oxide and angiotensin II. *Circ Res*, 84, 417-23.
- LIU, Z., HILBELINK, D. R. & GERDES, A. M. 1991. Regional changes in hemodynamics and cardiac myocyte size in rats with aortocaval fistulas. 2. Long-term effects. *Circ Res*, 69, 59-65.
- MAGID, N. M., OPIO, G., WALLERSON, D. C., YOUNG, M. S. & BORER, J. S. 1994. Heart failure due to chronic experimental aortic regurgitation. *Am J Physiol*, 267, H556-62.
- MALING, H. M. & HIGHMAN, B. 1958. Exaggerated ventricular arrhythmias and myocardial fatty changes after large doses of norepinephrine and epinephrine in unanesthetized dogs. *Am J Physiol*, 194, 590-6.
- MAXWELL, M. P., HEARSE, D. J. & YELLON, D. M. 1987. Species variation in the coronary collateral circulation during regional myocardial ischaemia: a critical determinant of the rate of evolution and extent of myocardial infarction. *Cardiovasc Res*, 21, 737-46.
- MCCULLAGH, W. H., COVELL, J. W. & ROSS, J., JR. 1972. Left ventricular dilatation and diastolic compliance changes during chronic volume overloading. *Circulation*, 45, 943-51.
- MCDONALD, K. M., CARLYLE, P. F., MATTHEWS, J., HAUER, K., ELBERS, T., HUNTER, D. & COHN, J. N. 1990. Early ventricular remodeling after myocardial damage and its attenuation by converting enzyme inhibition. *Trans Assoc Am Physicians*, 103, 229-35.
- MCDONALD, K. M., FRANCIS, G. S., CARLYLE, P. F., HAUER, K., MATTHEWS, J., HUNTER, D. W. & COHN, J. N. 1992. Hemodynamic, left ventricular structural and hormonal changes after discrete myocardial damage in the dog. *J Am Coll Cardiol*, 19, 460-7.
- MCDONALD, K. M., GARR, M., CARLYLE, P. F., FRANCIS, G. S., HAUER, K., HUNTER, D. W., PARISH, T., STILLMAN, A. & COHN, J. N. 1994a. Relative effects of alpha 1-adrenoceptor blockade, converting enzyme inhibitor therapy, and angiotensin II subtype 1 receptor blockade on ventricular remodeling in the dog. *Circulation*, 90, 3034-46.
- MCDONALD, K. M., YOSHIYAMA, M., FRANCIS, G. S., UGURBIL, K., COHN, J. N. & ZHANG, J. 1994b. Myocardial bioenergetic abnormalities in a canine model of left ventricular dysfunction. *J Am Coll Cardiol*, 23, 786-93.

- MCKAY, R. G., PFEFFER, M. A., PASTERNAK, R. C., MARKIS, J. E., COME, P. C., NAKAO, S., ALDERMAN, J. D., FERGUSON, J. J., SAFIAN, R. D. & GROSSMAN, W. 1986. Left ventricular remodeling after myocardial infarction: a corollary to infarct expansion. *Circulation*, 74, 693-702.
- MEHTA, J., RUNGE, W., COHN, J. N. & CARLYLE, P. 1978. Myocardial damage after repetitive direct current shock in the dog: correlation between left ventricular end-diastolic pressure and extent of myocardial necrosis. *J Lab Clin Med*, 91, 272-89.
- MITCHELL, G. F., JERON, A. & KOREN, G. 1998. Measurement of heart rate and Q-T interval in the conscious mouse. *Am J Physiol*, 274, H747-51.
- MOE, G. W. & ARMSTRONG, P. 1999. Pacing-induced heart failure: a model to study the mechanism of disease progression and novel therapy in heart failure. *Cardiovasc Res*, 42, 591-9.
- MOE, G. W., MONTGOMERY, C., HOWARD, R. J., GRIMA, E. A. & ARMSTRONG, P. W. 1993. Left ventricular myocardial blood flow, metabolism, and effects of treatment with enalapril: further insights into the mechanisms of canine experimental pacing-induced heart failure. *J Lab Clin Med*, 121, 294-301.
- MURAKAMI, H., LIU, J. L. & ZUCKER, I. H. 1996. Blockade of AT1 receptors enhances baroreflex control of heart rate in conscious rabbits with heart failure. *Am J Physiol*, 271, R303-9.
- NAGATSU, M., ZILE, M. R., TSUTSUI, H., SCHMID, P. G., DEFREYTE, G., COOPER, G. T. & CARABELLO, B. A. 1994. Native beta-adrenergic support for left ventricular dysfunction in experimental mitral regurgitation normalizes indexes of pump and contractile function. *Circulation*, 89, 818-26.
- NAKATA, T., HEARSE, D. J. & CURTIS, M. J. 1990. Are reperfusion-induced arrhythmias caused by disinhibition of an arrhythmogenic component of ischemia? *J Mol Cell Cardiol*, 22, 843-58.
- NELSON, G. R., COHN, P. F. & GORLIN, R. 1975. Prognosis in medically-treated coronary artery disease: influence of ejection fraction compared to other parameters. *Circulation*, 52, 408-12.
- NG, G. A., BRACK, K. E. & COOTE, J. H. 2001. Effects of direct sympathetic and vagus nerve stimulation on the physiology of the whole heart--a novel model of isolated Langendorff perfused rabbit heart with intact dual autonomic innervation. *Exp Physiol*, 86, 319-29.
- NICOLSON, W. B., MCCANN, G. P., BROWN, P. D., SANDILANDS, A. J., STAFFORD, P. J., SCHLINDWEIN, F. S., SAMANI, N. J. & NG, G. A. 2012. A novel surface electrocardiogram-based marker of ventricular arrhythmia risk in patients with ischemic cardiomyopathy. *J Am Heart Assoc*, 1, e001552.
- OMOTO, R., YOKOTE, Y., TAKAMOTO, S., KYO, S., UEDA, K., ASANO, H., NAMEKAWA, K., KASAI, C., KONDO, Y. & KOYANO, A. 1984. The development of real-time two-dimensional Doppler echocardiography and its clinical significance in acquired valvular diseases. With special reference to the evaluation of valvular regurgitation. *Jpn Heart J*, 25, 325-40.
- PFEFFER, J. M. 1991. Progressive ventricular dilation in experimental myocardial infarction and its attenuation by angiotensin-converting enzyme inhibition. *Am J Cardiol*, 68, 17D-25D.
- PFEFFER, M. A., PFEFFER, J. M., FISHBEIN, M. C., FLETCHER, P. J., SPADARO, J., KLONER, R. A. & BRAUNWALD, E. 1979. Myocardial infarct size and ventricular function in rats. *Circ Res*, 44, 503-12.

- POMBO, J. F., TROY, B. L. & RUSSELL, R. O., JR. 1971. Left ventricular volumes and ejection fraction by echocardiography. *Circulation*, 43, 480-90.
- POPP, R. L. & HARRISON, D. C. 1970. Ultrasonic cardiac echography for determining stroke volume and valvular regurgitation. *Circulation*, 41, 493-502.
- PYE, M. P., BLACK, M. & COBBE, S. M. 1996. Comparison of in vivo and in vitro haemodynamic function in experimental heart failure: use of echocardiography. *Cardiovasc Res*, 31, 873-81.
- PYE, M. P. & COBBE, S. M. 1996. Arrhythmogenesis in experimental models of heart failure: the role of increased load. *Cardiovasc Res*, 32, 248-57.
- REES, S. A. & CURTIS, M. J. 1993a. Selective IK blockade as an antiarrhythmic mechanism: effects of UK66,914 on ischaemia and reperfusion arrhythmias in rat and rabbit hearts. *Br J Pharmacol*, 108, 139-45.
- REES, S. A. & CURTIS, M. J. 1993b. Specific IK₁ blockade: a new antiarrhythmic mechanism? Effect of RP58866 on ventricular arrhythmias in rat, rabbit, and primate. *Circulation*, 87, 1979-89.
- RUSHMER, R. F., BAKER, D. W. & STEGALL, H. F. 1966. Transcutaneous Doppler flow detection as a nondestructive technique. *J Appl Physiol*, 21, 554-66.
- SABBAH, H. N., STEIN, P. D., KONO, T., GHEORGHIADE, M., LEVINE, T. B., JAFRI, S., HAWKINS, E. T. & GOLDSTEIN, S. 1991. A canine model of chronic heart failure produced by multiple sequential coronary microembolizations. *Am J Physiol*, 260, H1379-84.
- SCHWARTZ, P. J. & STONE, H. L. 1980. Left stellectomy in the prevention of ventricular fibrillation caused by acute myocardial ischemia in conscious dogs with anterior myocardial infarction. *Circulation*, 62, 1256-65.
- STABLES, C. L. & CURTIS, M. J. 2009. Development and characterization of a mouse in vitro model of ischaemia-induced ventricular fibrillation. *Cardiovasc Res*, 83, 397-404.
- STAMM, R. B., CARABELLO, B. A., MAYERS, D. L. & MARTIN, R. P. 1982. Two-dimensional echocardiographic measurement of left ventricular ejection fraction: prospective analysis of what constitutes an adequate determination. *Am Heart J*, 104, 136-44.
- SUTTON, M. G. & SHARPE, N. 2000. Left ventricular remodeling after myocardial infarction: pathophysiology and therapy. *Circulation*, 101, 2981-8.
- SWYNGHEDAUW, B. 1986. Developmental and functional adaptation of contractile proteins in cardiac and skeletal muscles. *Physiol Rev*, 66, 710-71.
- SZABO, J., CSAKY, L. & SZEGI, J. 1975. Experimental cardiac hypertrophy induced by isoproterenol in the rat. *Acta Physiol Acad Sci Hung*, 46, 281-5.
- TAGGART, P., SUTTON, P., CHALABI, Z., BOYETT, M. R., SIMON, R., ELLIOTT, D. & GILL, J. S. 2003. Effect of adrenergic stimulation on action potential duration restitution in humans. *Circulation*, 107, 285-9.
- TEERLINK, J. R., LOFFLER, B. M., HESS, P., MAIRE, J. P., CLOZEL, M. & CLOZEL, J. P. 1994. Role of endothelin in the maintenance of blood pressure in conscious rats with chronic heart failure. Acute effects of the endothelin receptor antagonist Ro 47-0203 (bosentan). *Circulation*, 90, 2510-8.
- TSUTSUI, H., SPINALE, F. G., NAGATSU, M., SCHMID, P. G., ISHIHARA, K., DEFREYTE, G., COOPER, G. T. & CARABELLO, B. A. 1994. Effects of chronic beta-adrenergic blockade on the left ventricular and cardiocyte abnormalities of chronic canine mitral regurgitation. *J Clin Invest*, 93, 2639-48.

- UNDERWOOD, R. D., AARHUS, L. L., HEUBLEIN, D. M. & BURNETT, J. C., JR. 1992. Endothelin in thoracic inferior vena caval constriction model of heart failure. *Am J Physiol*, 263, H951-5.
- VAN VELDHUISEN, D. J., VAN GILST, W. H., DE SMET, B. J., DE GRAEFF, P. A., SCHOLTENS, E., BUIKEMA, H., GIRBES, A. R., WESSELING, H. & LIE, K. I. 1994. Neurohumoral and hemodynamic effects of ibopamine in a rat model of chronic myocardial infarction and heart failure. *Cardiovasc Drugs Ther*, 8, 245-50.
- VANOLI, E., DE FERRARI, G. M., STRAMBA-BADIALE, M., HULL, S. S., JR., FOREMAN, R. D. & SCHWARTZ, P. J. 1991. Vagal stimulation and prevention of sudden death in conscious dogs with a healed myocardial infarction. *Circ Res*, 68, 1471-81.
- VARRO, A., LATHROP, D. A., HESTER, S. B., NANASI, P. P. & PAPP, J. G. 1993. Ionic currents and action potentials in rabbit, rat, and guinea pig ventricular myocytes. *Basic Res Cardiol*, 88, 93-102.
- WEINBERG, E. O., SCHOEN, F. J., GEORGE, D., KAGAYA, Y., DOUGLAS, P. S., LITWIN, S. E., SCHUNKERT, H., BENEDICT, C. R. & LORELL, B. H. 1994. Angiotensin-converting enzyme inhibition prolongs survival and modifies the transition to heart failure in rats with pressure overload hypertrophy due to ascending aortic stenosis. *Circulation*, 90, 1410-22.
- WHIPPLE, G., SHEFFIELD, L., WOODMAN, E., THOEPHILIS, C. & S, F. Reversible congestive heart failure due to rapid stimulation of the normal heart. Proc New Engl Cardiovasc Soc, 1961-1962. 39-40.
- YAMADA, M., HEARSE, D. J. & CURTIS, M. J. 1990. Reperfusion and readmission of oxygen. Pathophysiological relevance of oxygen-derived free radicals to arrhythmogenesis. *Circ Res*, 67, 1211-24.

Chapter 4

Sympatho-vagal Interaction in Isolated Dual-innervated, Langendorff-perfused Rabbit's Heart

Under Review for Consideration for Publication

Autonomic Modulation in a Rabbit Model of Heart Failure

Chapter 4: Sympatho-vagal Interaction in Isolated Dual-innervated, Langendorff-perfused Rabbit's Heart

4.1 Introduction

The effect of autonomic nerve activity on heart rate (HR) control is well recognised. Sympathetic nerve stimulation leads to an increase in HR (positive chronotropy) whereas vagus nerve stimulation results in a reduction in HR (negative chronotropy) (Levy and Zieske, 1969). This is believed to be modulated at the molecular level by neurotransmitters, namely catecholamines and acetylcholine on the intrinsic pacemakers, typically at the sino-atrial node (Levy, 1997). Additionally, the effect on HR changes is shown to increase with the strength and frequency of the corresponding autonomic nerve stimulations up to a maximal limit (Ng et al., 2001). In spite of this clear dichotomy in HR control, physiologically sympathetic and vagus nerves exhibit complex interaction with studies depicting a picture of vagal dominance in overall HR control during sympatho-vagal interaction (Brack et al., 2004, Uijtdehaage and Thayer, 2000, Mizuno et al., 2008, Yang and Levy, 1992, Levy, 1971). This phenomenon has been coined *accentuated antagonism*, describing the inhibition of sympathetic nerve activity on cardiac functions in the presence of vagus nerve stimulation (Levy, 1971).

Importantly, the influence of autonomic nerve activity extends beyond chronotropic control and has been shown to be a prognostic marker of ventricular arrhythmias in cardiac patients, in particular those with heart failure (Nolan et al., 1998) or prior myocardial infarction (La Rovere et al., 1998). Abnormal autonomic nerve activity leading to increased susceptibility life-threatening ventricular arrhythmias contributes to increased mortality in patients in these cardiac conditions (Schwartz, 1998). Although the direct mechanism between impaired autonomic nerve activity and increased ventricular arrhythmias is poorly understood, one possible mechanistic route involves autonomic modulation of cardiac electrical restitution.

Cardiac electrical restitution (RT) explains the non-linear relationship between action potential duration (APD) with its preceding diastolic intervals (DI). Ventricular fibrillation (VF) initiation is believed to be associated with break-up of rotors or spiral

waves to multiple disorganised wavelets and oscillations (Weiss et al., 2000). The restitution hypothesis proposed that as the slopes of APD restitution curves become steeper, typically beyond 1, oscillations, and hence VF initiation, are facilitated (Cao et al., 1999). Autonomic modulation of RT with sympathetic nerve steepening the slope and vagus nerve flattening the slope, have been demonstrated to exert opposing effects on ventricular electrophysiology – the former reducing the ventricular fibrillation threshold (VFT) and shortening ventricular effective refractory period (ERP) whereas the latter raising the VFT and prolonging the ERP (Ng et al., 2007).

In this study, isolated dual-innervated Langendorff-perfused rabbit hearts were used to examine the effect of concurrent sympathetic and vagus nerve stimulation on HR and ventricular electrophysiology, i.e. VFT, ERP and RT.

4.2 Aim

The aim of this study was as follow:-

- 1) To assess presence of accentuated antagonism in VFT, ERP and RT slopes.
- 2) To establish the frequency response on HR, VFT, ERP and RT at baseline (BL) and in the presence of background opposing autonomic nerve stimulations.

4.3 Method

4.3.1 Isolated Rabbit Heart Preparation with Intact Dual Autonomic Nerve Innervation

Adult male New Zealand White rabbits (2.8 – 3.7 kg, $n = 18$) were sedated with a subcutaneous injection containing a mixture of Medetomidine Hydrochloride (Sedator, 0.2 mg/kg), Ketamine (Narketan, 10 mg/kg) and Butorphanol (Torbugesic, 0.05 mg/kg). After 15 minutes of waiting, surgery was performed to isolate rabbit heart with intact dual autonomic innervation as described in detail in the previous chapter (Chapter 3.4.2.1).

4.3.2 Langendorff Perfusion

Once isolated, rabbit hearts were perfused in modified Langendorff mode with Tyrode solution in an experimental set up as described in Chapter 3.4.2.2. Relevantly atrial electrogram was recorded through a pair of platinum needle electrodes attached to the right atrial appendage to allow for derivation of instantaneous HR.

4.3.3 Autonomic Nerve Stimulation

As described in Chapter 3.4.2.3 in detail, the right cervical vagus nerve was supported and stimulated by a pair of custom-made bipolar silver electrodes. Bilateral sympathetic nerve stimulation was achieved by insertion of a quadripolar catheter into the spinal canal to the level of stellate ganglia.

For each of the autonomic nerves, a voltage response curve was constructed by assessing the HR response during sympathetic (SNS)/vagus nerve stimulation (VNS) with varying strength from 1 – 10 V. The optimal voltage required by each nerve to induce 80% of maximal HR changes was determined and used to assess the frequency response of the corresponding autonomic nerves.

In this study, low-frequency SNS (LS) was defined as the frequency which produced an elevated intrinsic HR of around 180 – 200 bpm whereas high-frequency SNS (HS) gave rise to a HR of around 230 – 250 bpm. Low-frequency VNS (LV) was determined as the frequency which led to a bradycardia of around 90 – 100 bpm whilst high-frequency VNS (HV) a HR of around 60 – 70 bpm.

This study was designed in two protocols. In Protocol 1 (VNS-SNS), the effects of low-(LS) and high-frequency SNS (HS) were assessed at baseline (BL) and in the presence of background high-frequency VNS (HV). In Protocol 2 (SNS-VNS), the sequence of nerve stimulation was reversed, i.e. the effects of low- (LV) and high-frequency VNS (HV) were examined at BL and in the presence of high-frequency SNS (HS).

4.3.4 Cardiac Electrical Recording and Pacing

A spring-loaded mini-MAP electrode was placed at the epicardial surface of left ventricular free wall for recording of monophasic action potential (MAP) using a DC-coupled high-input impedance differential amplifier as described in Chapter 3.4.2.2. A bipolar pacing electrode was inserted into the right ventricular apex for ventricular pacing manoeuvres required for measurement of VFT and ERP.

4.3.5 Measurement of Ventricular Electrophysiology: VFT, ERP and RT

VFT and ERP were determined by specific pacing protocols as described in Chapter 3.3.2.4. RT was derived from measurements of MAP duration during S1 – S2 protocol used for ERP measurement. The specifics of RT calculations were explained in Chapter 3.4.2.4. In both pacing protocols, relevant autonomic nerve stimulations were performed and steady-state HR was ensured before commencing the appropriate pacing protocols.

4.4 Results

4.4.1 Effects of Sympatho-vagal Interaction on Heart Rate

4.4.1.1 Effects of Background High-frequency Vagus Nerve Stimulation on Heart Rate Response during Low and High-frequency Sympathetic Nerve Stimulations

In Protocol 1, HR response was first assessed with low (LS) and high-frequency SNS (HS) correspondingly. Steady-state HR was recorded from atrial electrogram following SNS-induced tachycardia. The protocol was then repeated by introducing high-frequency VNS (HV) in the background, ensuring a steady state HR was reached prior to commencing either low or high-frequency SNS. After a new steady state HR was reached following stimulation of two sets of autonomic nerves, pacing protocol was commenced to measure VFT. Figure 4.1 illustrates HR changes during Protocol 1 in a typical experiment. LS increased the HR to about 170 bpm whereas HS led to a tachycardia of 230 bpm (Figure 4.1A) from an initial HR of 145 bpm. This protocol was repeated with

introduction of background HV resulting in a bradycardia of 50 bpm with concomitant LS and HS increasing the HR to around 85 bpm and 110 bpm correspondingly (Figure 4.1B).

The mean data ($n = 12$) for the HR response of SNS at BL and in the presence of background VNS is illustrated in Figure 4.2A. In this protocol, mean HR was 140.7 ± 7.0 bpm. SNS exerted a frequency-dependent tachycardia effect with LS (2.5 ± 0.2 Hz) increasing the HR to 180.1 ± 5.7 bpm whilst HS (9.3 ± 0.8 Hz) raising the HR to 224.8 ± 3.8 bpm. Background HV (9.9 ± 0.6 Hz) reduced the HR to 59.3 ± 5.3 bpm and attenuated concurrent SNS-induced tachycardia in a frequency-responsive manner. Specifically, HV-LS led to a mean HR of 90.0 ± 6.9 bpm and HV-HS a mean HR of 112.4 ± 9.8 bpm. These findings were further supported when absolute change in HR was calculated under the aforementioned SNS and VNS combinations (Figure 4.2B). At BL, HR increased by 48.7 ± 5.5 bpm and 93.6 ± 5.0 bpm under LS and HS correspondingly. Background HV attenuated the positive chronotropic effect of SNS in a frequency-dependent effect with the HR increments being 28.9 ± 5.8 bpm ($p = 0.0416$) and 46.5 ± 8.4 bpm ($p = 0.0003$) for HV-LS and HV-HS correspondingly.

Figure 4.1 An example of intrinsic heart rate changes following low- or high-frequency sympathetic nerve stimulation at baseline (Figure 4.1A) and with concurrent high-frequency vagus nerve stimulation (Figure 4.1B)

Figure 4.1A

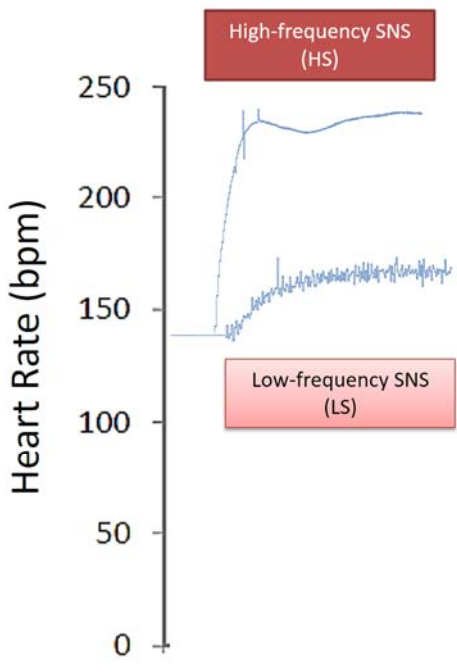


Figure 4.1B

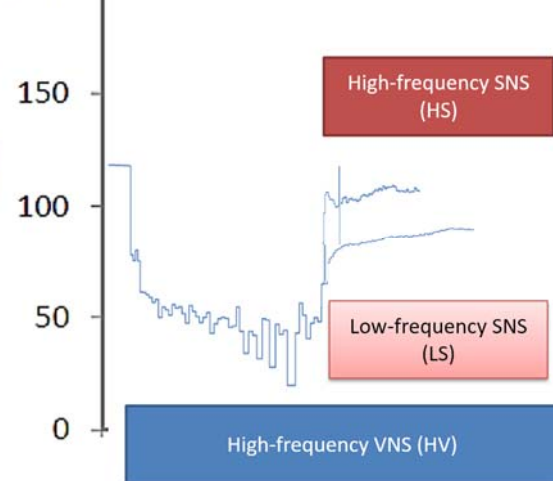
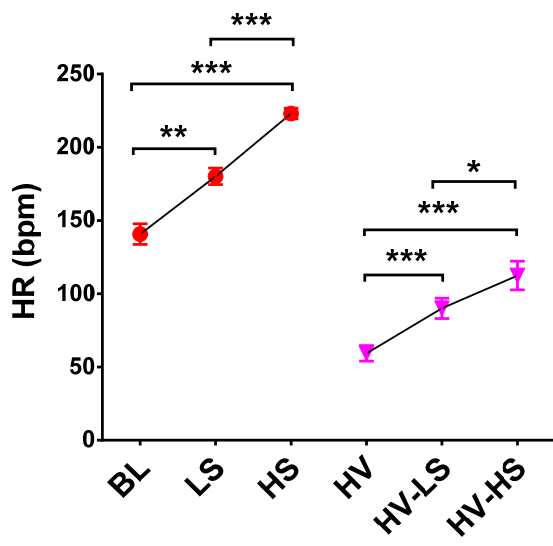
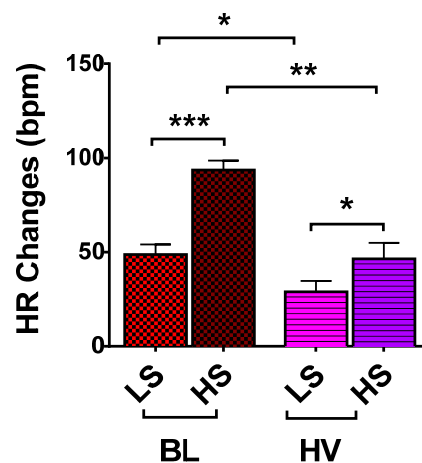


Figure 4.2 Absolute heart rate (Figure 4.2A) and relative heart rate changes (Figure 4.2B) following low- (LS) and high-frequency (HS) sympathetic stimulation at baseline (BL), as well as following low- (HV-LS) and high-frequency (HV-HS) sympathetic stimulation with concurrent high-frequency vagal stimulation (HV)

Figure 4.2A**Figure 4.2B**

4.4.1.2 Effects of Background High-frequency Sympathetic Nerve Stimulation on Heart Rate Response during Low and High-frequency Vagus Nerve Stimulations

In Protocol 2, HR response was initially assessed with low (LV) and high-frequency VNS (HV) by derivative measurements from atrial electrogram. This was then repeated by introducing background high-frequency SNS (HS), ensuring a steady state HR was achieved before initiating low or high-frequency VNS. Figure 4.3 illustrated an example of Protocol 2 when HR was reduced from around 140 bpm to 100 bpm and 50 bpm by LV and HV correspondingly. Background HS increased the HR to about 225 bpm with concurrent VNS reducing the HR to 160 bpm and 110 bpm at low and high frequency of stimulations.

Mean HR data ($n = 13$) for Protocol 2 was illustrated in Figure 4.4A. At BL, HR was recorded at 130.6 ± 5.7 bpm. VNS led to a frequency-dependent bradycardia, lowering

the HR to 101.4 ± 4.0 bpm and 69.7 ± 5.7 bpm with LV (3.2 ± 0.5 Hz) and HV (9.9 ± 0.6 Hz) respectively. Background HS resulted in a tachycardia of 224.1 ± 3.5 bpm with concurrent LV (HS-LV) and HV (HS-HV) reducing the HR to 143.8 ± 6.1 bpm and 94.7 ± 5.5 bpm respectively. At both BL and during background HS, there was a frequency-dependent effect on vagal-induced bradycardia. Furthermore, the effect of vagal bradycardia was potentiated in the presence of background SNS. Both these phenomena were illustrated in Figure 4.4B demonstrating absolute HR reduction by VNS at BL and during SNS. At BL, LV gave rise to a HR reduction of 28.7 ± 3.9 bpm whereas HV led to a greater HR reduction of 58.8 ± 6.4 bpm. In the presence of SNS, the negative chronotropic response by VNS was enhanced in a frequency-dependent manner with HS-LV leading to a HR reduction of 72.3 ± 7.8 bpm ($p = 0.0002$) whilst HS-HV a HR reduction of 120.6 ± 9.4 bpm ($p = 0.0003$).

Figure 4.3 An example of intrinsic heart rate changes following low- or high-frequency vagus nerve stimulation at baseline (Figure 4.3A) and with concurrent high-frequency sympathetic nerve stimulation (Figure 4.3B)

Figure 4.3A

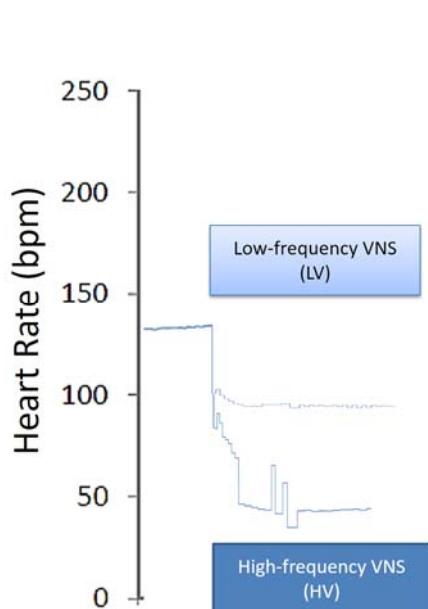


Figure 4.3B

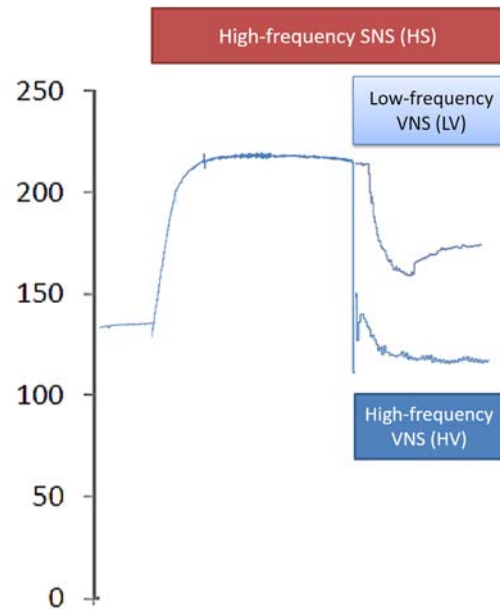
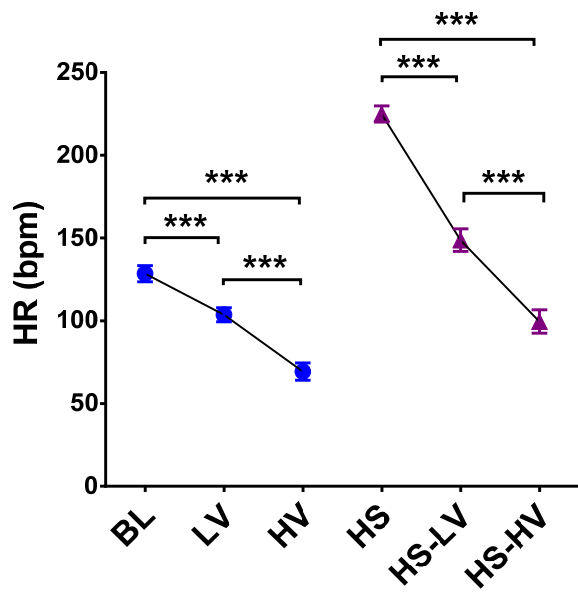
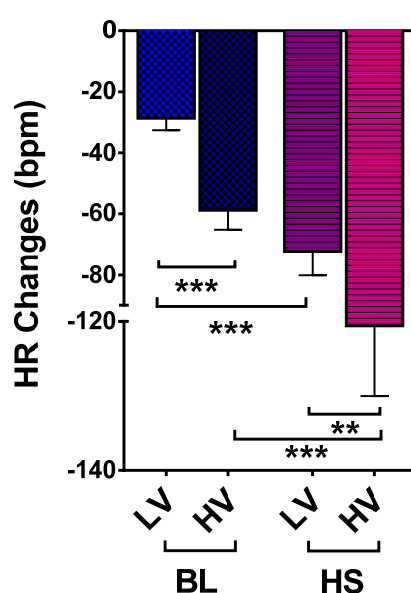


Figure 4.4 Absolute heart rate (Figure 4.4A) and relative heart rate changes (Figure 4.4B) following low- (LV) and high-frequency (HV) vagal stimulation at baseline (BL), as well as following low- (HS-LV) and high-frequency (HS-HV) vagal stimulation with concurrent high-frequency sympathetic stimulation (HS)

Figure 4.4A**Figure 4.4B**

4.4.1.3 Algebraic Sum of Heart Rate Changes with Sympathetic and Vagus Nerve Stimulation

To investigate the possible interaction between the two branches of autonomic nerves on chronotropic response, the HR changes by SNS and VNS individually were analysed by simple addition, i.e. algebraic sum. A comparison between these algebraic sums and the actual HR changes occurring during sympatho-vagal interaction was made for Protocol 1 (Figure 4.5A) and Protocol 2 (Figure 4.5B). The algebraic sum (expected) and the actual (observed) HR changes differed significantly irrespectively of both the frequency and the sequence of nerve stimulations. Notably the observed HR changes were lower than those expected in both protocols.

Figure 4.5 Comparison of expected (algebraic summed) and observed heart rate changes during sympatho-vagal interaction

Figure 4.5A

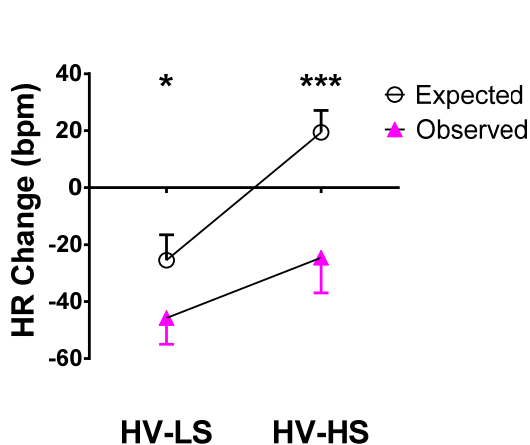
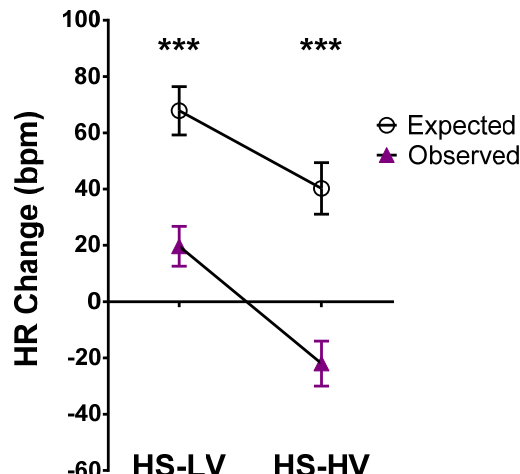


Figure 4.5B



4.4.2 Effects of Sympatho-vagal Interaction on Ventricular Fibrillation Threshold

4.4.2.1 Effects of Background High-frequency Vagus Nerve Stimulation on Ventricular Fibrillation Threshold during Low and High-frequency Sympathetic Nerve Stimulations

In Protocol 1, ventricular fibrillation threshold (VFT) was assessed by burst pacing protocol as described previously. Figure 4.6A illustrated the mean VFT data ($n = 12$). In the absence of any autonomic nerve stimulation, baseline (BL) VFT was 4.2 ± 0.4 mA. SNS led to a reduction in VFT of differing degree depending on frequency of stimulation. LS resulted in a lower VFT of 2.3 ± 0.4 mA whereas HS led to an even lower VFT of 1.6 ± 0.3 mA. A repeat of Protocol 1 by introducing background high-frequency VNS (HV) raised the VFT from 4.2 ± 0.4 mA to 8.0 ± 0.9 mA. Concurrent SNS in the presence of HV reduced VFT in a frequency-dependent manner, i.e. 5.2 ± 0.7 mA for HV-LS and 4.0 ± 0.6 mA for HV-HS.

The preservation of frequency-sensitive nature in VFT, as seen in HR responses, is further supported in Figure 4.6B. When absolute VFT changes were calculated, LS reduced VFT by 1.9 ± 0.3 mA from VFT at BL whereas HS led to a statistically significant VFT reduction of 2.6 ± 0.3 mA. This phenomenon of frequency response persisted in the presence of background VNS. HV-LS reduced VFT by 2.8 ± 0.8 mA from a HV-induced VFT level of 8.0 ± 0.9 mA. During HV-HS, there was greater VFT reduction of 4.0 ± 0.9 mA. Compared to BL, background HV did not affect the VFT-lowering effect of SNS with the VFT reduction being 2.8 ± 0.8 mA ($p = 0.1852$) and 4.0 ± 0.9 mA ($p = 0.1356$) for HV-LS and HV-HS correspondingly.

Figure 4.6 Absolute ventricular fibrillation threshold (VFT) (Figure 4.6A) and relative VFT changes (Figure 4.6B) at baseline (BL), following low- (LS) and high-frequency (HS) sympathetic stimulation, high-frequency vagal stimulation (HV) and during vago-sympathetic interaction (HV-LS, HV-HS)

Figure 4.6A

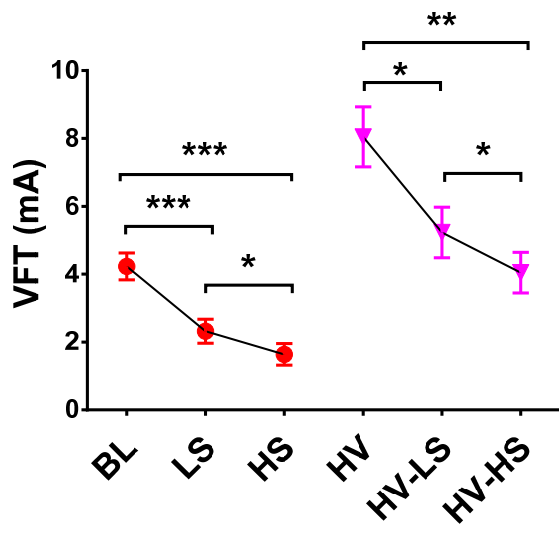
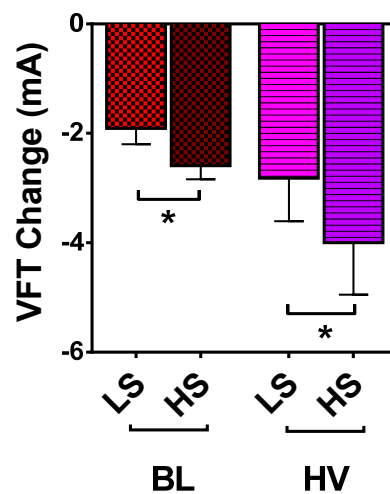


Figure 4.6B

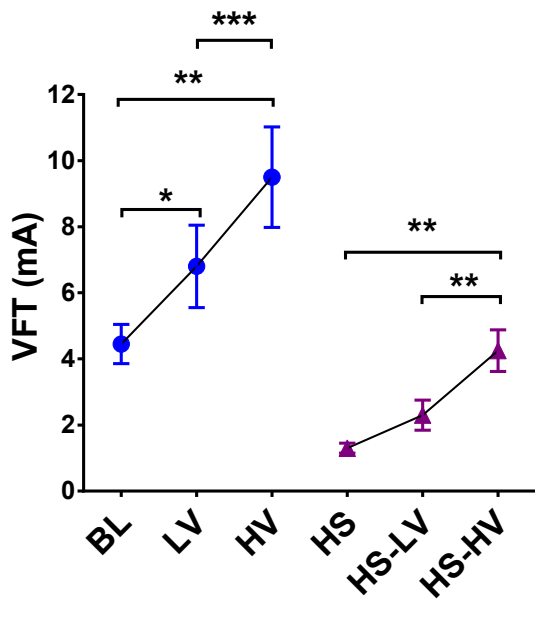
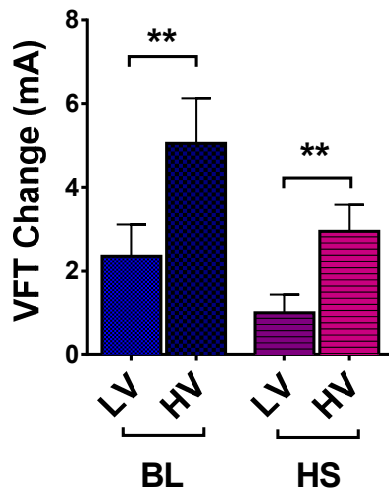


4.4.2.2 Effects of Background High-frequency Sympathetic Nerve Stimulation on Ventricular Fibrillation Threshold during Low and High-frequency Vagus Nerve Stimulations

In Protocol 2, the effect of differing frequency of VNS on VFT at BL and in the presence of high-frequency SNS (HS) was assessed. Figure 4.7A illustrated the mean VFT data ($n = 13$). VFT was measured to be 4.5 ± 0.6 mA at BL. VNS raised VFT in a frequency-dependent manner, with LV leading to VFT of 6.8 ± 1.2 mA and HV resulting in VFT of 9.5 ± 1.5 mA. HS lowered VFT from the baseline value of 4.5 ± 0.6 mA to 1.3 ± 0.2 mA. Concurrent VNS in the presence of HS increased VFT in a frequency-responsive manner. VFT was measured as 2.3 ± 0.5 mA and 4.3 ± 0.6 mA during HS-LV and HS-HV correspondingly.

Figure 4.7B illustrated absolute VFT changes of LV and HV when compared to VFT at baseline and that during HS. As previously shown for frequency response of SNS in Protocol 1 (Figure 4.6B), the frequency response of VNS on VFT in Protocol 2 was preserved. At BL, LV increased VFT by 2.4 ± 0.8 mA whereas HV led to a greater increment in VFT by 5.1 ± 1.1 mA. In the presence of background SNS, the effect of VNS-induced VFT elevation was less although the frequency response of VNS remained. HS-LV elevated VFT by 1.0 ± 0.4 mA from 1.3 ± 0.2 mA (HS) whereas HS-HV led to a greater VFT increment by 3.0 ± 0.6 mA. Compared to BL, the degree of VNS-induced VFT increment in the presence of background SNS is similar for both HV-LS ($p = 0.1860$) and HV-HS ($p = 0.0842$).

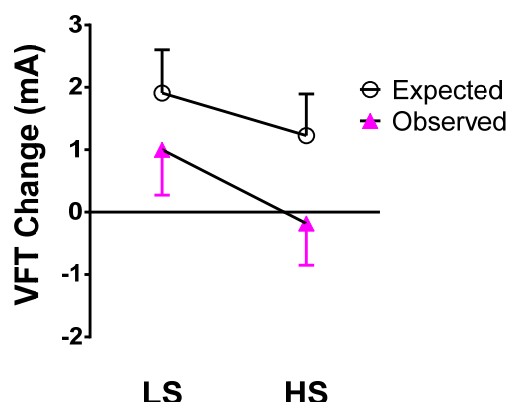
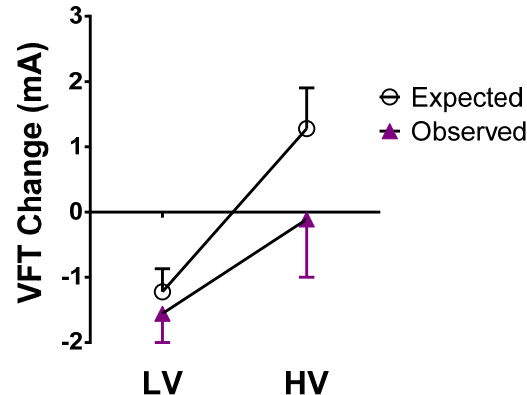
Figure 4.7 Absolute ventricular fibrillation threshold (VFT) (Figure 4.7A) and relative VFT changes (Figure 4.7B) at baseline (BL), following low- (LV) and high-frequency (HV) vagal stimulation, high-frequency sympathetic stimulation (HS) and during sympatho-vagal interaction (HS-LV, HS-HV)

Figure 4.7A**Figure 4.7B**

4.4.2.3 Algebraic Sum of Ventricular Fibrillation Threshold Changes with Sympathetic and Vagus Nerve Stimulation

The observed and expected VFT changes were examined during sympatho-vagal interaction in Protocol 1 (Figure 4.8A) and Protocol 2 (Figure 4.8B). As described previously (see Chapter 4.4.1.3), the expected VFT changes were derived by algebraic summation of VFT change by individual nerves in the corresponding protocols. Irrespective of the frequency or sequence of autonomic nerve stimulation, there is a lack of sympatho-vagal interaction for VFT as evident from the lack of significant difference between the observed and expected VFT changes.

Figure 4.8 Comparison of expected (algebraic summed) and observed ventricular fibrillation threshold (VFT) changes during vago-sympathetic (Figure 4.8A) and sympatho-vagal interactions (Figure 4.8B)

Figure 4.8A**Figure 4.8B**

4.4.3 Effects of Sympatho-vagal Interaction on Action Potential Duration Restitution

4.4.3.1 Effects of Background High-frequency Vagus Nerve Stimulation on Cardiac Restitution during Low and High-frequency Sympathetic Nerve Stimulations

Cardiac electrical restitution (RT) was assessed by measuring action potential duration (APD_{90}) during an extrastimulus pacing protocol, and by measuring the steepest gradient of the restitution slope (r) when APD_{90} was plotted against its preceding diastolic interval (DI). Figure 4.9 demonstrated the restitution curves obtained in a typical experiment at BL (Figure 4.9A) and in the presence of HV (Figure 4.9B). In this example, baseline restitution slope was increased by SNS from 1.22 to 2.92 and 3.14 during LS and HS correspondingly (Figure 4.9A). Background HV flattened the restitution curve to 0.75 with concurrent SNS steepening RT slopes to 2.30 and 2.74 during low- and high-frequency SNS correspondingly (Figure 4.9B).

Figure 4.10A illustrated mean RT data ($n = 13$) obtained during Protocol 1. Baseline restitution slopes were calculated as 1.28 ± 0.11 . LS steepened the restitution slopes to 2.97 ± 0.27 whilst HS produced an even steeper restitution gradient of 3.41 ± 0.34 . Background VNS flattened restitution slopes to 0.71 ± 0.08 with concurrent LS and HS steepening restitution slopes to 2.03 ± 0.19 and 2.43 ± 0.24 .

Relative RT changes by LS and HS were calculated at both baseline and during VNS (Figure 4.10B). SNS exhibited a frequency-dependent response in increasing RT in both situations. At BL, LS increased RT by $142.76 \pm 25.81\%$ whilst the increment in RT by HS was greater at $177.09 \pm 33.23\%$. In the presence of background HV, the effect of SNS in steepening RT slopes persisted in a frequency-sensitive manner despite HV flattening RT slopes. HV-LS led to an increase of $223.54 \pm 37.41\%$ in RT while HV-HS an increase of $295.20 \pm 60.86\%$.

Figure 4.9 An example of action potential duration (APD)-restitution (RT) curves with steepest slope gradients (r) measured at baseline (BL), following low- (LS) and high-frequency (HS) sympathetic stimulation (Figure 4.9A) as well as during vago-sympathetic interaction (Figure 4.9B) with concurrent high-frequency vagal stimulation (HV)

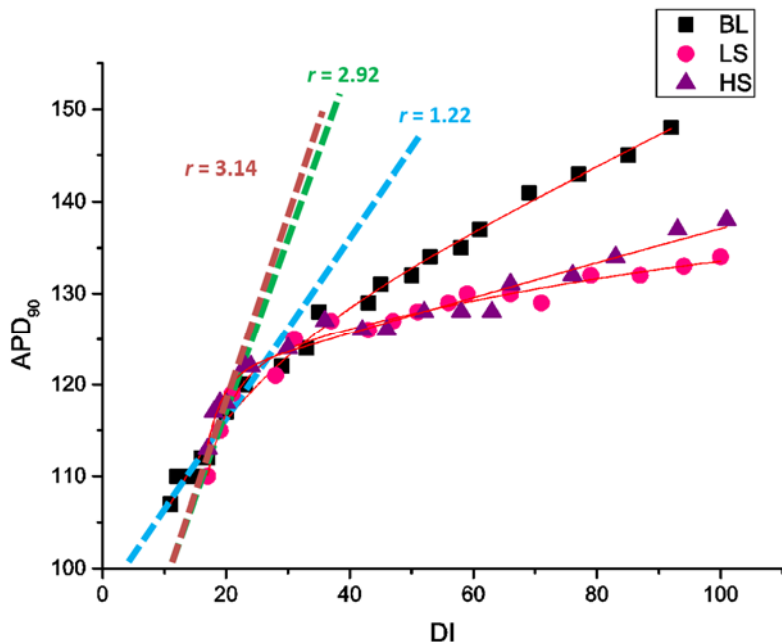
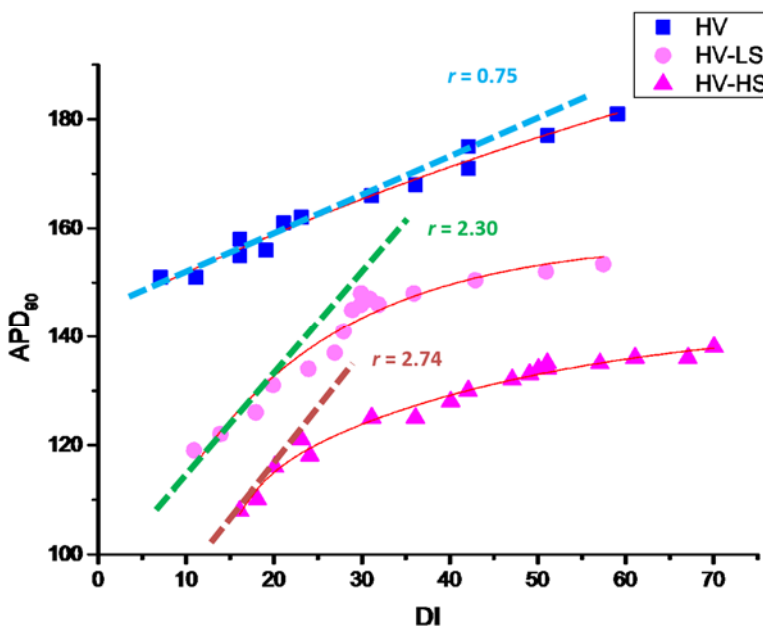
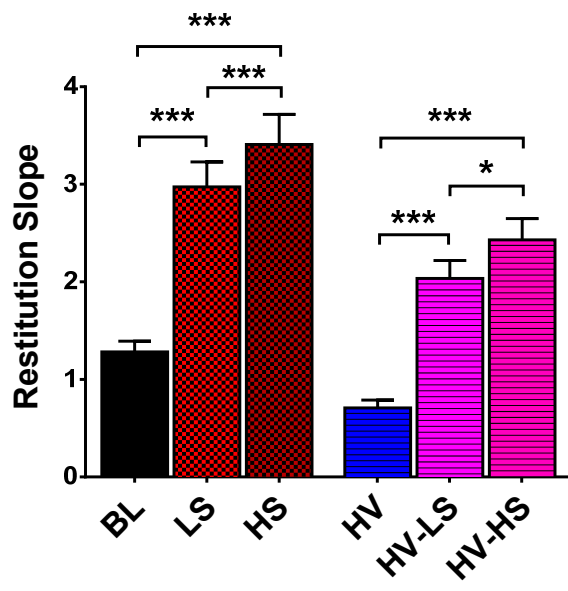
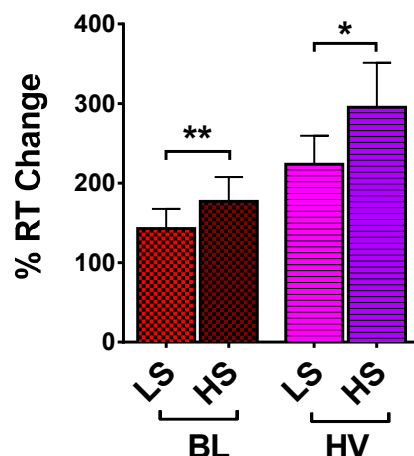
Figure 4.9A**Figure 4.9B**

Figure 4.10 Absolute restitution slope gradients (Figure 4.10A) and relative changes (Figure 4.10B) at baseline (BL), following low- (LS) and high-frequency (HS) sympathetic stimulation, high-frequency (HV) vagal stimulation and during vago-sympathetic interactions (HV-LS, HV-HS)

Figure 4.10A**Figure 4.10B**

4.4.3.2 Effects of Background High-frequency Sympathetic Nerve Stimulation on Cardiac Restitution during Low and High-frequency Vagus Nerve Stimulations

RT was measured using an extrastimulus pacing protocol as previously described to assess the effect of VNS on RT at BL and during background SNS. Figure 4.11 illustrated RT curves obtained in a typical experiment using Protocol 2. At baseline, maximum RT slope gradient (r) was 1.38. VNS flattened RT slopes to 0.92 and 0.72 by low- and high-frequency stimulations respectively (Figure 4.11A). Background SNS at high frequency stimulation steepened the slope to 3.14 (Figure 4.11B). Concurrent VNS reduced RT slopes to 2.15 (HS-LV) and 2.09 (HS-HV).

Mean RT data for Protocol 2 ($n = 14$) was illustrated in Figure 4.12A. Low- and high-frequency VNS flattened RT slopes from a baseline of 1.39 ± 0.13 to 0.81 ± 0.13 and 0.72

± 0.11 correspondingly. Background HS steepened RT slope to 3.60 ± 0.37 with concurrent VNS flattening the RT slopes. HS-LV led to a mean RT slope of 2.31 ± 0.22 whereas HS-HV resulted in a mean RT slope of 2.13 ± 0.23 .

Relative change in RT was calculated and illustrated in Figure 4.12B. VNS did not exhibit statistically significant frequency response in RT slope flattening. At BL, LV and HV flattened RT slope by $42.69 \pm 5.28\%$ and $49.48 \pm 5.18\%$ respectively. In the presence of background HS, the effect of concurrent VNS on RT slope flattening was less compared to BL although this did not reach statistical significance. HS-LV reduced the RT slope gradient by $32.40 \pm 4.97\%$ whereas HS-HV flattened the slope by $38.07 \pm 6.37\%$.

Figure 4.11 An example of action potential duration (APD)-restitution (RT) curves with steepest slope gradients (r) measured at baseline (BL), following low- (LV) and high-frequency (HV) vagal stimulation (Figure 411A) as well as during sympatho-vagal interaction (Figure 411B) with concurrent high-frequency sympathetic stimulation (HS)

Figure 4.11A

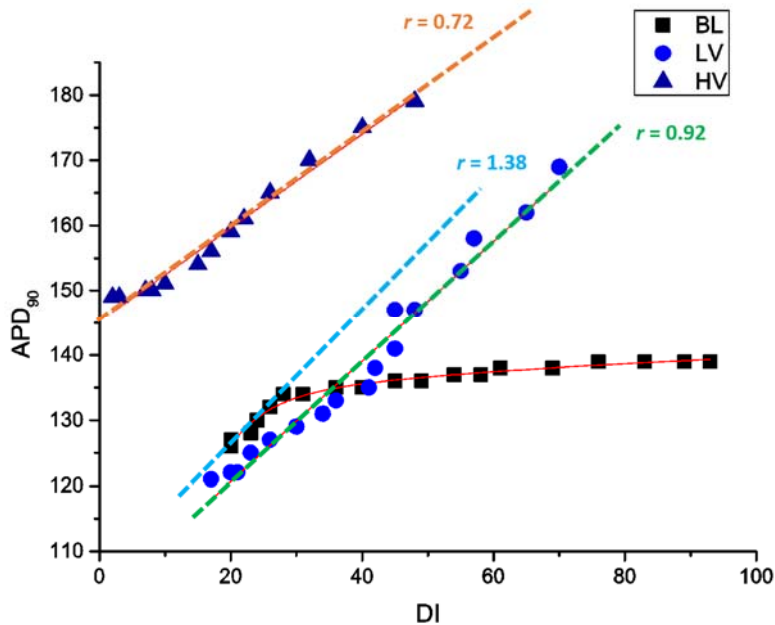


Figure 4.11B

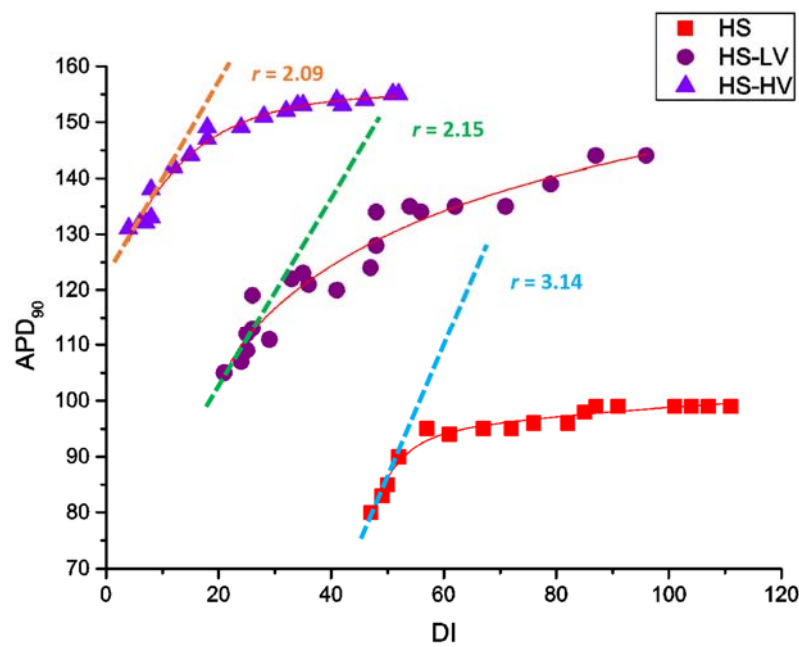
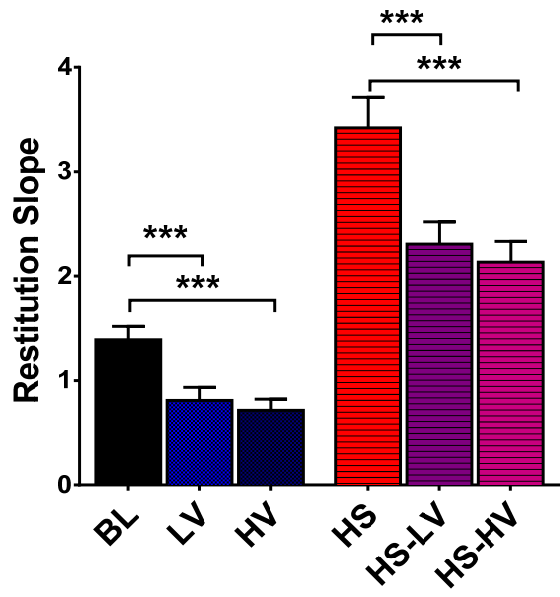
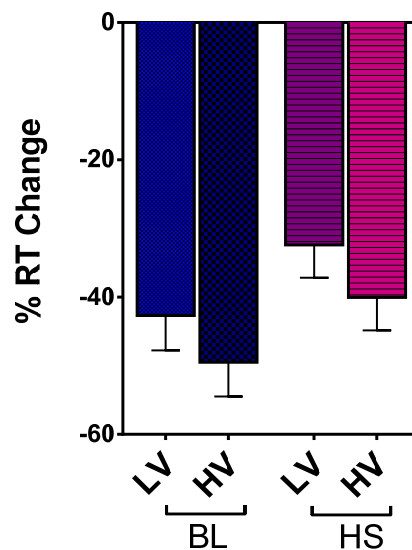


Figure 4.12 Absolute restitution slope gradients (Figure 4.12A) and relative changes (Figure 4.12B) at baseline (BL), following low- (LV) and high-frequency (HV) vagal stimulation, high-frequency (HS) sympathetic stimulation and during sympatho-vagal interactions (HS-LV, HS-HV)

Figure 4.12A**Figure 4.12B**

4.4.4 Effects of Sympatho-vagal Interaction on Ventricular Effective Refractory Period

4.4.4.1 Effects of Background High-frequency Vagus Nerve Stimulation on Ventricular Effective Refractory Period during Low and High-frequency Sympathetic Nerve Stimulations

In this study, ventricular refractoriness was assessed by measuring effective refractory period (ERP) through an extrastimulus pacing protocol during which APD₉₀ was also measured to derive RT values described in the previous sections. Briefly, ERP was defined as the longest S₁-S₂ interval that captured the ventricles. Figure 4.13A illustrates the mean ERP data ($n = 13$) obtained in Protocol 1. At baseline, ventricular ERP was 140.7 ± 4.1 ms. This was shortened during SNS and prolonged during VNS. Low and high-frequency SNS shortened ERP to 128.0 ± 4.4 ms and 121.1 ± 4.4 ms

correspondingly. Introduction of background high-frequency VNS resulted in ERP prolongation to 158.7 ± 6.7 ms which was shortened by concurrent LS and HS to 144.3 ± 5.0 ms and 140.0 ± 4.7 ms respectively.

In spite of the general trend of SNS shortening ERP at baseline and during background VNS, there is no significant difference in ERP shortening between low and high-frequency SNS in either condition (Figure 4.13B). At BL, LS shortened ERP by 12.7 ± 3.3 ms whereas HS shortened the ERP by 19.6 ± 3.0 ms. Additionally, the effect of SNS in shortening ERP persisted in the presence of background HV with HV-LS shortening the ERP by 14.3 ± 5.0 ms and, in the case of HV-HS, by 19.6 ± 7.1 ms.

Figure 4.13 Absolute ventricular effective refractory period (ERP) (Figure 4.13A) and ERP changes (Figure 4.13B) at baseline (BL), following low- (LS) and high-frequency (HS) sympathetic stimulation, high-frequency vagal stimulation (HV) and during vago-sympathetic interaction (HV-LS, HV-HS)

Figure 4.13A

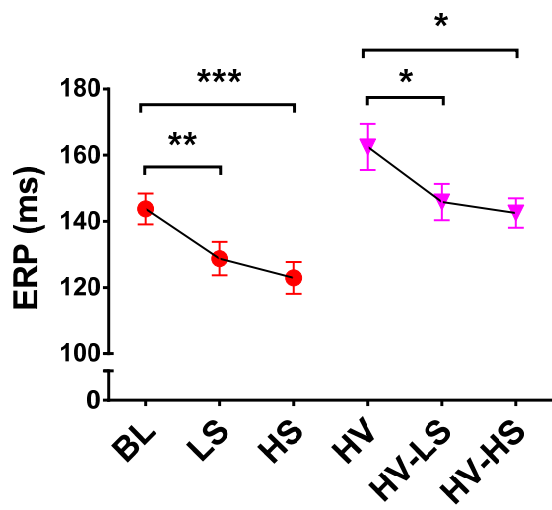
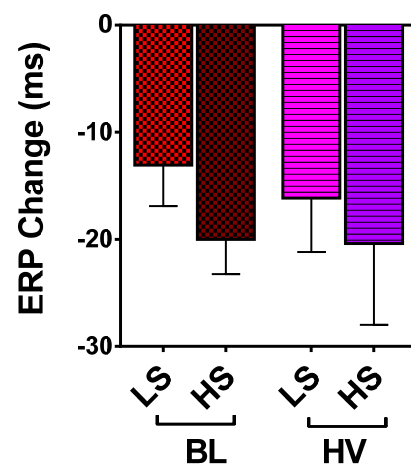


Figure 4.13B

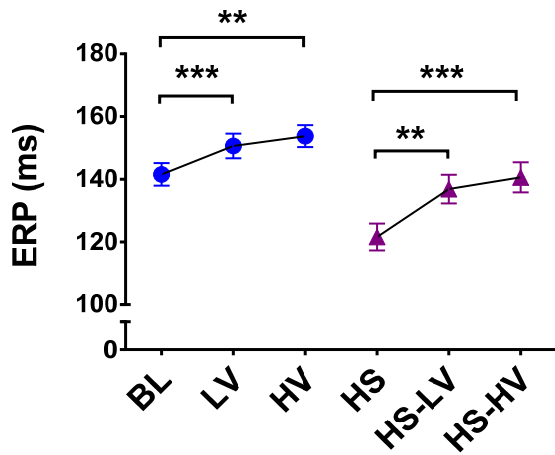
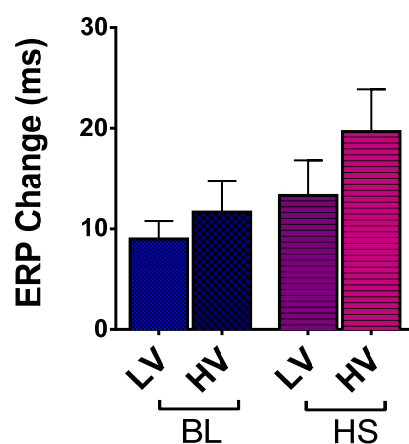


4.4.4.2 Effects of Background High-frequency Sympathetic Nerve Stimulation on Ventricular Effective Refractory Period during Low and High-frequency Vagus Nerve Stimulations

Mean ERP data ($n = 14$) obtained in Protocol 2 was illustrated in Figure 4.14A. Baseline ventricular ERP was 143.0 ± 3.5 ms. Overall, VNS prolonged ERP with LV prolonging ERP to 152.0 ± 3.9 ms whilst HV giving rise to a prolonged ERP of 154.7 ± 3.6 ms. Background high-frequency SNS (HS) shortened baseline ERP to 122.3 ± 4.7 ms. However concurrent LV and HV during SNS prolonged ERP to 135.3 ± 4.6 ms and 141.3 ± 5.0 ms respectively.

The persistent effect of VNS in ERP prolongation whether at baseline or in the presence of SNS was further illustrated in Figure 4.14B. At BL, VNS prolonged ERP by 9.0 ± 1.8 ms and 11.7 ± 3.1 ms during low and high-frequency stimulation. Whereas in the presence of HS, HS-LV and HS-HV continued to prolong ERP by 13.0 ± 3.6 ms and 19.0 ± 4.5 ms respectively. Similar to what was observed in Protocol 1, there was a lack of frequency response in ERP.

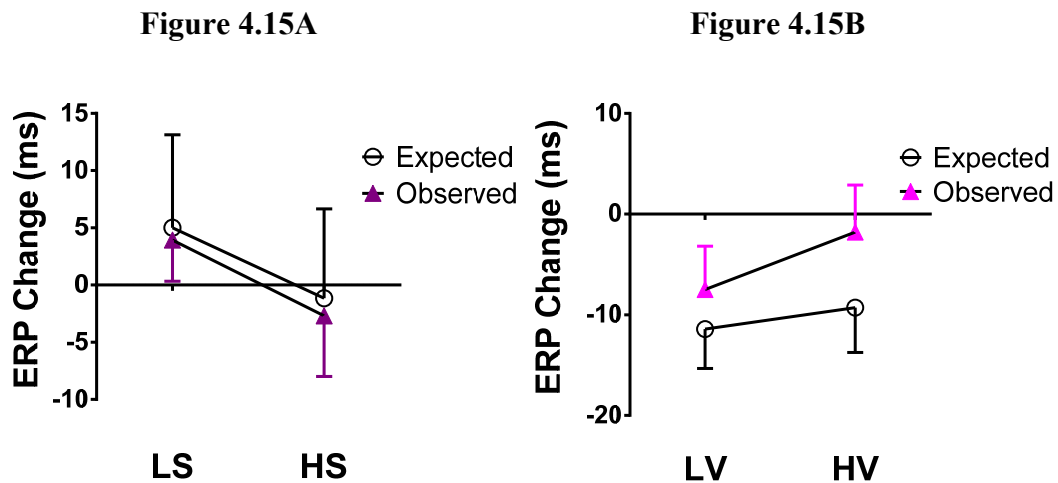
Figure 4.14 Absolute ventricular effective refractory period (ERP) (Figure 4.14A) and ERP changes (Figure 4.14B) at baseline (BL), following low- (LV) and high-frequency (HV) vagal stimulation, high-frequency sympathetic stimulation (HS) and during sympatho-vagal interaction (HS-LV, HS-HV)

Figure 4.14A**Figure 4.14B**

4.4.4.3 Algebraic Sum of Ventricular Effective Refractory Period Changes with Sympathetic and Vagus Nerve Stimulations

To investigate for possible sympatho-vagal interaction in ERP, the observed and expected ERP changes during sympatho-vagal interaction in Protocol 1 (Figure 4.15A) and Protocol 2 (Figure 4.15B) were compared. As described previously (see Chapter 4.4.1.3), the expected ERP changes were calculated by algebraic summation of ERP change for individual nerves. Irrespective of the sequence and frequency of nerve stimulation, there is a lack of sympatho-vagal interaction in ERP as reflected by the similarity between the expected and the observed values.

Figure 4.15 Comparison of expected (algebraic summed) and observed ventricular effective refractory period (VFT) changes during vago-sympathetic (Figure 4.15A) and sympatho-vagal interactions (Figure 4.15B)



4.5 Discussion

This study represents a first attempt at establishing the effect of sympatho-vagal interaction on both atrial and ventricular electrophysiology in isolated Langendorff-perfused rabbit hearts with dual-intact autonomic nerves. It validates the phenomenon of accentuated antagonism in HR response during concurrent sympatho-vagal nerve stimulation. More importantly, it demonstrates the absence of accentuated antagonism in ventricular electrophysiology including action potential duration restitution, ventricular fibrillation thresholds as well as ventricular refractoriness.

Additionally, HR changes are sensitive to the frequencies of nerve stimulation during isolated and combined sympatho-vagal nerve stimulations. Interestingly, this frequency response can be observed in ventricular electrophysiology as well.

4.5.1 Effect of Sympatho-vagal Interaction on Intrinsic Heart Rate

4.5.1.1 Frequency-dependent Heart Rate Response during Autonomic Nerve Stimulation

The effect of direct sympathetic and vagal nerve stimulations individually on intrinsic HR response has been well described (Ng et al., 2001). The positive chronotropic effect of sympathetic nerve stimulation and the negative chronotropic effect of vagus nerve stimulation reflects autonomic modulation on the spontaneous firing of the sino-atrial node. The altered automaticity of sino-atrial node translates into augmentation of intrinsic HR by sympathetic and conversely attenuation in vagus nerve stimulation.

At the cellular level, the neurotransmitters released from sympathetic and vagus nerve endings are responsible for the observed HR changes. Noradrenaline released from stimulation of sympathetic nerve endings activates cardiac β -adrenoreceptors, thereby increasing L-type Ca^{2+} current and I_f current (the “pacemaker” current), leading to an increased rate of depolarization (Hartzell, 1988). Compared to vagus nerve stimulation, HR increment during sympathetic nerve stimulation is gradual (Figure 4.1A), especially evident during low-frequency stimulation. This latency is accountable by the noradrenaline being slowly released from sympathetic nerve endings (Levy et al., 1993).

The negative chronotropic effect of vagus nerve stimulation is attributable to acetylcholine released from vagus nerve ending and its subsequent action upon binding to muscarinic receptors in the heart. In contrast to the latency observed in HR increment during sympathetic nerve stimulation, the reduction in HR during vagus nerve stimulation is instantaneous (Figure 4.3A) even at low-frequency stimulation. This is attributable to the rapid activation of muscarinic receptors by acetylcholine during vagus nerve stimulation (Levy, 1996). Stimulation of unmyelinated C fibres can theoretically lead to slow response in HR reduction (Ford and McWilliam, 1986) but in this study, this phenomenon was not observed suggesting that either the C fibres were not stimulated by the chosen strength of stimulation giving rise to 80% of maximal HR response. Alternatively, the contribution of vagal C fibres to HR response is insignificant in this study (Jones et al., 1995).

The use of low and high-frequency nerve stimulation affords demonstration of the effect of nerve fibre firing rate on intrinsic HR. In this study, both sympathetic and vagus nerve demonstrated distinctively frequency-dependent HR increment and reduction respectively. This is in agreement with the excitatory response of nerve cells historically documented by Eccles (Eccles, 1957).

4.5.1.2 Accentuated Antagonism

Both sympathetic and vagus nerves are tonically active *in vivo* (Gizzatullin et al., 2007). Although both nerves produced opposing HR changes, Saman observed a vagal-dominant effect in HR changes during concurrent sympatho-vagal nerve stimulations (Samaan, 1935). This phenomenon was subsequently termed *accentuated antagonism* (Levy, 1971). Although the initial sympatho-vagal interaction was investigated in *in vivo* studies, this study allows such an investigation to be performed in an *in vitro* setting to dissect the effect of neurotransmitters released during sympatho-vagal interaction from the potential confounding effect of circulating humoral factors and autonomic reflexes.

Protocol 1 demonstrated the attenuation of positive chronotropic effect of sympathetic nerve stimulation by background high-frequency vagus nerve stimulation. This was illustrated by the significant difference between algebraic sum of HR changes by individual nerves when compared to the observed HR changes, confirming significant vagal dominance, i.e. *accentuated antagonism*. Furthermore, the higher the frequency of sympathetic nerve stimulation, the greater the diminishing effect on HR increment in the presence of background vagus nerve stimulation. This antagonistic results can occur at pre- and post-synaptic levels (Levy, 1971). Acetylcholine released by background vagus nerve stimulation can bind to M₃ receptors at the presynaptic sympathetic nerve terminals, thereby reducing noradrenaline that can be released during sympathetic nerve stimulation (Loffelholz and Muscholl, 1969). Meanwhile post-synaptically, activation of muscarinic receptors facilitates the inhibitory action of G-protein, Gi on adenyl cyclase, preventing cAMP-mediated phosphorylation of the pacemaker current (I_f), the L-type calcium current (I_{CaL}) and the delayed rectifier current (I_{Kr}). The inhibitory effects on these ion currents ultimately have a negative effect on the sino-atrial node firing rate, and

ultimately the HR (Irisawa et al., 1993). Finally, acetylcholine released during vagus nerve stimulation exerts a direct electrophysiological effect on resting membrane potential of sino-atrial node by activating the acetylcholine-activated potassium current [$I_{K(ACh)}$] (Medina et al., 2000).

In contrast to the attenuation of sympathetic-driven positive chronotropic effect by background vagus nerve stimulation, the reverse was not observed in Protocol 2. Indeed, the negative chronotropic effect of vagus nerve stimulation was augmented in the presence of concurrent sympathetic nerve stimulation, further cementing the notion of *accentuated antagonism*. This is in coherence with the previous findings demonstrating the vagal dominant effect during sympatho-vagal interaction studies (Yang et al., 1994, Revington and McCloskey, 1990). On the other hand, other *in vivo* studies with anaesthetized dogs demonstrated the attenuation of vagally-driven negative chronotropic effect and its instantaneous action by sympathetic stimulation. This was subsequently alluded to neuropeptide Y (Warner and Levy, 1989) binding to neuropeptide Y2 receptors located on pre-synaptic vagal nerve terminals (Warner and Levy, 1989), thereby inhibiting the release of acetylcholine (Potter, 1987). The abolishment of vagal effect during sympathetic stimulation was not observed in this study, thereby implying negligible, if not absent, role of neuropeptide Y. This phenomenon can be confirmed in future studies by using neuropeptide Y2 analogues to assess its effect on the vagal dominant effect observed during sympatho-vagal stimulation in this model. In spite of the presence of background high-frequency sympathetic nerve stimulation, the negative chronotropic effect of vagus nerve was potentiated by high-frequency sympathetic stimulation (Figure 4.5B). The lack of neuropeptide Y effect can be explained by the overpowering combined effects of G_i protein on phosphorylation of various ion channels, the direct electrophysiologic effect of $I_{K(ACh)}$ and possible inhibition of acetylcholine on neuropeptide Y release during continuous vagal stimulation (Yang et al., 1994). It is also conceivable that the strength of sympathetic nerve stimulation in Protocol 2 is not sufficiently high (Potter, 1985, Potter, 1987) to induce neuropeptide Y release (Lundberg and Hokfelt, 1986) when compared to studies which observed the aforementioned neuropeptide Y effect. Future sympatho-vagal interaction studies to investigate chronotropic changes in the presence of neuropeptide Y inhibitor for clarification of involvement of this co-transmitter would be enlightening (Herring et al., 2008).

4.5.2 Effect of Sympatho-vagal Interaction on Ventricular Fibrillation Threshold

The arrhythmogenic effect of sympathetic nerve stimulation (Schwartz and Stone, 1980, Schwartz et al., 1976, Schwartz and Malliani, 1975) and the protective effect of vagus nerve stimulation (Cerati and Schwartz, 1991, Vanoli et al., 1991) are well known. Previous *in vitro* study involving direct individual sympathetic and vagus nerve stimulations validates the historical studies. Direct sympathetic nerve stimulation lowers ventricular fibrillation threshold whilst vagus nerve stimulation exerts a protective effect against arrhythmogenesis by raising ventricular fibrillation threshold (Ng et al., 2007).

In this study, the effect of sympatho-vagal interaction on ventricular fibrillation inducibility in an *in vitro* model was assessed. In Protocol 1, low and high-frequency sympathetic nerve stimulation resulted in lowering of ventricular fibrillation thresholds expectedly in a frequency-sensitive manner, affirming the temporal summation pattern of autonomic nerve firing for the arrhythmogenic effect of sympathetic nerve stimulation. In the presence of background high-frequency vagus nerve stimulation, there was a reduced susceptibility to ventricular fibrillation as evident from the higher ventricular fibrillation threshold when compared to that at baseline. Concurrent sympathetic nerve stimulation, however, led to continual lowering of ventricular fibrillation threshold despite background persistent vagus nerve stimulation. Indeed, the degree of ventricular fibrillation susceptibility produced by sympathetic nerve stimulation increased insignificantly in the presence of background vagus nerve stimulation (Figure 4.6B). In Protocol 2, vagus nerve stimulation confers protection against ventricular fibrillation by raising the ventricular fibrillation threshold. Whilst concurrent sympathetic nerve stimulation lowered the ventricular fibrillation threshold from the baseline level, vagal stimulation maintained its protective effect of raising VFT but this effect is somewhat attenuated in the presence of background sympathetic nerve stimulation.

In essence, this study demonstrated that at ventricular level, the arrhythmogenic effect of sympathetic nerve stimulation is unperturbed by the presence of concurrent vagal stimulation irrespective of the sequence of nerve stimulation. The lack of difference between the expected summation of VFT change compared to the observed VFT change

during sympatho-vagal interaction confirms the absence of vagal dominance that was observed in HR response. This is in contrast with studies on healthy canine models in which repetitive extrasystole threshold was used as a reliable surrogate marker for VFT. Kohman et al demonstrated that the antifibrillatory effect of vagus nerve stimulation is significantly related to the prevailing level of adrenaline tone (Kolman et al., 1976). In a subsequent study, methacholine, a selective muscarinic agent, did not confer additional increment in repetitive extrasystole threshold in propranolol-treated dogs beyond that resulting from propranolol alone. On the other hand, vagal stimulation abolished the lowering of repetitive extrasystole threshold by norepinephrine infusion in the same study (Rabinowitz et al., 1976). Although these studies involved using pharmacological analogues, there have been study using direct nerve stimulation to echo these findings. In another study, the antifibrillatory effect of direct vagal nerve stimulation was demonstrated by the reversal of adverse ventricular electrophysiological changes in the presence of sympathetic hyperactivity (Huang et al., 2015). This is in agreement with the present study in which VNS increased VFT in a frequency-dependent manner in the presence of background high-frequency SNS. However, the degree of VFT-raising effect by VNS is similar at BL and during concurrent SNS, suggesting the absence of accentuated antagonism in VFT changes. In contrast to other studies, this study demonstrated that the pro-arrhythmic effect of SNS prevailed despite the presence of background VNS.

4.5.3 Effect of Sympatho-vagal Interaction on Action Potential Duration Restitution Slopes

Autonomic modulation of APD restitution was first demonstrated using adrenergic analogues in *in vivo* studies in porcine models (Taggart et al., 1990) and in humans (Taggart et al., 2003). Adrenergic activation resulted in a downward shift (i.e. shortening of APD) in addition to increasing the maximum slope of the restitution curve. The findings were subsequently validated in *in vitro* studies with direct sympathetic nerve stimulation (Ng et al., 2007). In Protocol 1, this study demonstrated a similar trend with sympathetic stimulation leading to shortening of APD compared to baseline and steepening of the maximum slope of the restitution curve (Figure 4.9A). Additionally, the degree of downward shift and increase in maximum restitution slope is modulated by

the frequency of sympathetic nerve stimulation (Figures 4.9A and 4.10). This is the first study which demonstrated a frequency response in maximal restitution slope under sympathetic stimulation.

Conversely, vagus nerve stimulation produced an upward shift of the restitution curve (i.e. APD prolongation) with a reduction in the maximum slope of the restitution curve. This was first described in an *in vitro* model using direct vagus nerve stimulation on Langendorff-perfused rabbit hearts (Ng et al., 2007). No study was found using cholinergic agonist to investigate its effect on electrical restitution. Protocol 2 in this study reaffirms the effect of vagus nerve stimulation in causing an upward shift of the restitution curve in addition to flattening the maximal slope of the restitution curves (Figure 4.11A and 4.12). More importantly, in accord to the findings in Protocol 1, the study represents the first attempt to describe a direct relationship between *temporal* summation of autonomic nerve stimulation (i.e. frequency of stimulation) with maximal restitution slopes (Figure 4.12).

During concurrent sympathetic and vagal stimulations, sympathetic effect of steepening maximal APD restitution slope was not perturbed in the presence of vagal stimulation irrespective of the sequence of nerve stimulation. In Protocol 1, background vagus nerve stimulation led to a flattening of maximal restitution slope from that at baseline. However concurrent sympathetic nerve stimulation abolished this vagal effect and steepened the restitution slope. In Protocol 2, background sympathetic nerve stimulation steepened the restitution slope with concurrent vagal stimulation flattening the restitution slopes. However, the degree of slope flattening by vagus nerve stimulation was attenuated in the presence of background sympathetic nerve stimulation (Figure 4.12B).

The prevailing sympathetic effect in steepening APD restitution slopes during sympatho-vagal interaction mirrors its continual effect in lowering VFT in the presence of vagal stimulation within the same study. The plausible relationship between VFT initiation and APD restitution slopes was first proposed by Weiss et al (Weiss et al., 2000). VFT initiation is regarded as a “first wave break” which in turn is dependent on APD and conduction velocity of the preceding diastolic interval (i.e. APD restitution slope). Autonomic modulation of electrical restitution and VFT has been well described but

studies on sympatho-vagal interaction on these electrophysiological aspects are scarce. In an *in vivo* canine model, vagus nerve stimulation for 2 hours was shown to flatten APD restitution slope with associated increase in VFT following a hypersympathetic state induced by left stellate ganglion stimulation for 2 hours beforehand (Huang et al., 2015). In this study, APD restitution were measured at the bases of the LV epicardial surfaces with distinctive changes in its gradients during isolated and combined sympatho-vagal stimulations. It is probable that similar changes in restitution slopes may be observed in mid-wall and apices of LV epicardial surfaces although regional heterogeneity may exist especially in the context of endocardial apical pacing (Pitruzzello et al., 2007).

4.5.4 Effect of Sympatho-vagal Interaction on Ventricular Refractoriness

The findings of ventricular ERP shortening during sympathetic nerve stimulation in Protocol 1 is in agreement with previous *in vivo* data demonstrating shorter APD and ERP under sympathetic influence (Martins and Zipes, 1980). Introduction of background high-frequency vagal stimulation resulted in ERP prolongation from baseline level, in accordance to previous *in vivo and in vitro* studies (Martins and Zipes, 1980, Ng et al., 2007). However, in the presence of vagus nerve stimulation, concurrent sympathetic nerve stimulation produced similar degree of ERP shortening as that observed in the absence of background vagal stimulation (Figure 4.13B).

In Protocol 2, vagus nerve stimulation led to ERP prolongation at baseline expectedly. Background sympathetic stimulation resulted in ERP shortening from baseline level with concurrent vagal stimulation reversing the effect by ERP prolongation.

The findings in Protocol 2 demonstrating the vagal reversal effect on ERP prolongation following sympathetic stimulation is in congruent with previous studies in dogs (Huang et al., 2015, Ophof et al., 1993, Schwartz et al., 1977) and humans (Morady et al., 1988). However, this cannot explain the findings in Protocol 1 in which sympathetic-induced ERP shortening persisted in the presence of background vagal stimulation. As the ultimate ERP changes seem to follow the final autonomic nerve involved in whichever sequence of nerve stimulation, a more plausible and unifying explanation would be the lack of sympatho-vagal interaction in ventricular refractoriness. The absence of any

significant difference between the expected summation ERP change of individual nerves compared to the observed ERP change further validates the lack of accentuated antagonism (Figure 4.15). In addition, no frequency response was seen in ERP in contrast to VFT and APD restitution slopes.

4.5.5 Absence of Accentuated Antagonism in Ventricular Electrophysiology during Sympatho-vagal Interaction

Beyond the characteristic changes in HR response (i.e. chronotropy), sympatho-vagal interaction has demonstrated a vagal dominant effect in dromotropy (Hoyano et al., 1997) and some aspects of ventricular performances (Brack et al., 2010). This study was designed to investigate primarily the effect of sympatho-vagal interaction on ventricular electrophysiology. Vagal dominance was observed in HR changes during sympatho-vagal interaction, affirming the findings of accentuated antagonism described by other studies. This finding provides a reliable neuro-electrophysiologic baseline for investigating different aspects of ventricular electrophysiology. This reveals a lack of accentuated antagonism in ventricular electrophysiology. Specifically, whilst sympatho-vagal interaction appears to be absent in ventricular refractoriness, the sympathetic effect of increased ventricular fibrillation inducibility and maximal restitution slope prevails in the presence of vagus nerve stimulation. As such, the vagal dominant effect observed in HR changes driven by presynaptic action of acetylcholine at atrial level is absent at the ventricular level. The dichotomy between atrial and ventricular electrophysiologic findings are unlikely to be due to the effect of central modulation at either location due to the Langendorff heart preparation being a spinal specimen severed from the brainstem at the level of the first cervical vertebra. However, other co-transmitters may be at play at the ganglia in the ventricles. Specifically, neuropeptide Y, and to lesser extent, galanin, released during sympathetic stimulation may act synergistically to suppress a degree of vagal activity hence nullifying the accentuated antagonism observed at the atrial level although the latter phenomenon is only observed in guinea pig models (Herring et al., 2008). The inhibitory effect on vagal activity during sympathetic stimulations by neuropeptide Y and galanin are mediated through neuropeptide Y2 receptors and galanin receptors located at the presynaptic vagal terminals. Future studies using neuropeptide Y2 receptor blocker as well as galanin receptor antagonist may shed light on the role of

these co-transmitters in ventricular electrophysiology during sympatho-vagal interaction. Although historically pharmacological analogues of norepinephrine and muscarinic agents have been used for sympatho-vagal interaction studies, no study to date utilise a cardio-selective β -blockers to dissect the mechanism of sympatho-vagal interaction. Additionally genetic knock-out models of relevant receptors, i.e. muscarinic M₂ and M₃ receptors, β -adrenoreceptors, neuropeptide Y₂ receptors as well as galanin receptors should be considered as part of the wide research repertoire available to further dissect the mechanism for the observed electrophysiologic changes during sympatho-vagal interaction.

4.6 Conclusion

This study demonstrated accentuated antagonism in heart rate response but not in ventricular electrophysiology during sympatho-vagal interaction. The absence of vagal dominant effect at the ventricular level suggested a different mechanism at play during sympatho-vagal interaction. Future works on ion channel distribution and nerve distribution at the ventricular level are required.

4.7 References

- BRACK, K. E., COOTE, J. H. & NG, G. A. 2004. Interaction between direct sympathetic and vagus nerve stimulation on heart rate in the isolated rabbit heart. *Exp Physiol*, 89, 128-39.
- BRACK, K. E., COOTE, J. H. & NG, G. A. 2010. Vagus nerve stimulation inhibits the increase in Ca²⁺ transient and left ventricular force caused by sympathetic nerve stimulation but has no direct effects alone--epicardial Ca²⁺ fluorescence studies using fura-2 AM in the isolated innervated beating rabbit heart. *Exp Physiol*, 95, 80-92.
- CAO, J. M., QU, Z., KIM, Y. H., WU, T. J., GARFINKEL, A., WEISS, J. N., KARAGUEUZIAN, H. S. & CHEN, P. S. 1999. Spatiotemporal heterogeneity in the induction of ventricular fibrillation by rapid pacing: importance of cardiac restitution properties. *Circ Res*, 84, 1318-31.
- CERATI, D. & SCHWARTZ, P. J. 1991. Single cardiac vagal fiber activity, acute myocardial ischemia, and risk for sudden death. *Circ Res*, 69, 1389-401.
- ECCLES, J. C. 1957. The excitatory reactions of nerve cells. *The Physiology of Nerve Cells*. Baltimore, USA: The Johns Hopkins Press.
- FORD, T. W. & MCWILLIAM, P. N. 1986. The effects of electrical stimulation of myelinated and non-myelinated vagal fibres on heart rate in the rabbit. *J Physiol*, 380, 341-7.

- GIZZATULLIN, A. R., GILMUTDINOVA, R. I., MINNAHMETOV, R. R., SITDIKOV, F. G. & CHIGLINTCEV, V. M. 2007. Parasympathetic cardiac effects in sympathectomized rats. *Bull Exp Biol Med*, 144, 166-70.
- HARTZELL, H. C. 1988. Regulation of cardiac ion channels by catecholamines, acetylcholine and second messenger systems. *Prog Biophys Mol Biol*, 52, 165-247.
- HERRING, N., LOKALE, M. N., DANSON, E. J., HEATON, D. A. & PATERSON, D. J. 2008. Neuropeptide Y reduces acetylcholine release and vagal bradycardia via a Y₂ receptor-mediated, protein kinase C-dependent pathway. *J Mol Cell Cardiol*, 44, 477-85.
- HOYANO, Y., FURUKAWA, Y., KASAMA, M. & CHIBA, S. 1997. Parasympathetic inhibition of sympathetic effects on atrioventricular conduction in anesthetized dogs. *Am J Physiol*, 273, H1800-6.
- HUANG, J., QIAN, J., YAO, W., WANG, N., ZHANG, Z., CAO, C., SONG, B. & ZHANG, Z. 2015. Vagus nerve stimulation reverses ventricular electrophysiological changes induced by hypersympathetic nerve activity. *Exp Physiol*, 100, 239-48.
- IRISAWA, H., BROWN, H. F. & GILES, W. 1993. Cardiac pacemaking in the sinoatrial node. *Physiol Rev*, 73, 197-227.
- JONES, J. F., WANG, Y. & JORDAN, D. 1995. Heart rate responses to selective stimulation of cardiac vagal C fibres in anaesthetized cats, rats and rabbits. *J Physiol*, 489 (Pt 1), 203-14.
- KOLMAN, B. S., VERRIER, R. L. & LOWN, B. 1976. Effect of vagus nerve stimulation upon excitability of the canine ventricle. Role of sympathetic-parasympathetic interactions. *Am J Cardiol*, 37, 1041-5.
- LA ROVERE, M. T., BIGGER, J. T., JR., MARCUS, F. I., MORTARA, A. & SCHWARTZ, P. J. 1998. Baroreflex sensitivity and heart-rate variability in prediction of total cardiac mortality after myocardial infarction. ATRAMI (Autonomic Tone and Reflexes After Myocardial Infarction) Investigators. *Lancet*, 351, 478-84.
- LEVY, M. N. 1971. Sympathetic-parasympathetic interactions in the heart. *Circ Res*, 29, 437-45.
- LEVY, M. N. 1997. Neural control of cardiac function. *Baillieres Clin Neurol*, 6, 227-44.
- LEVY, M. N., YANG, T. & WALLICK, D. W. 1993. Assessment of beat-by-beat control of heart rate by the autonomic nervous system: molecular biology technique are necessary, but not sufficient. *J Cardiovasc Electrophysiol*, 4, 183-93.
- LEVY, M. N. & ZIESKE, H. 1969. Autonomic control of cardiac pacemaker activity and atrioventricular transmission. *J Appl Physiol*, 27, 465-70.
- LEVY, M. N. M., P.J. 1996. *Nervous Control of the Heart*, Amsterdam, Harwood Academic Publishers GmbH.
- LOFFELHOLZ, K. & MUSCHOLL, E. 1969. A muscarinic inhibition of the noradrenaline release evoked by postganglionic sympathetic nerve stimulation. *Naunyn Schmiedebergs Arch Pharmakol*, 265, 1-15.
- LUNDBERG, J. M. & HOKFELT, T. 1986. Multiple co-existence of peptides and classical transmitters in peripheral autonomic and sensory neurons--functional and pharmacological implications. *Prog Brain Res*, 68, 241-62.
- MARTINS, J. B. & ZIPES, D. P. 1980. Effects of sympathetic and vagal nerves on recovery properties of the endocardium and epicardium of the canine left ventricle. *Circ Res*, 46, 100-10.

- MEDINA, I., KRAPIVINSKY, G., ARNOLD, S., KOVOOR, P., KRAPIVINSKY, L. & CLAPHAM, D. E. 2000. A switch mechanism for G beta gamma activation of I(KACh). *J Biol Chem*, 275, 29709-16.
- MIZUNO, M., KAMIYA, A., KAWADA, T., MIYAMOTO, T., SHIMIZU, S., SHISHIDO, T. & SUGIMACHI, M. 2008. Accentuated antagonism in vagal heart rate control mediated through muscarinic potassium channels. *J Physiol Sci*, 58, 381-8.
- MORADY, F., KOU, W. H., NELSON, S. D., DE BUITLEIR, M., SCHMALTZ, S., KADISH, A. H., TOIVONEN, L. K. & KUSHNER, J. A. 1988. Accentuated antagonism between beta-adrenergic and vagal effects on ventricular refractoriness in humans. *Circulation*, 77, 289-97.
- NG, G. A., BRACK, K. E. & COOTE, J. H. 2001. Effects of direct sympathetic and vagus nerve stimulation on the physiology of the whole heart--a novel model of isolated Langendorff perfused rabbit heart with intact dual autonomic innervation. *Exp Physiol*, 86, 319-29.
- NG, G. A., BRACK, K. E., PATEL, V. H. & COOTE, J. H. 2007. Autonomic modulation of electrical restitution, alternans and ventricular fibrillation initiation in the isolated heart. *Cardiovasc Res*, 73, 750-60.
- NOLAN, J., BATIN, P. D., ANDREWS, R., LINDSAY, S. J., BROOKSBY, P., MULLEN, M., BAIG, W., FLAPAN, A. D., COWLEY, A., PRESCOTT, R. J., NEILSON, J. M. & FOX, K. A. 1998. Prospective study of heart rate variability and mortality in chronic heart failure: results of the United Kingdom heart failure evaluation and assessment of risk trial (UK-heart). *Circulation*, 98, 1510-6.
- OPTHOF, T., DEKKER, L. R., CORONEL, R., VERMEULEN, J. T., VAN CAPELLE, F. J. & JANSE, M. J. 1993. Interaction of sympathetic and parasympathetic nervous system on ventricular refractoriness assessed by local fibrillation intervals in the canine heart. *Cardiovasc Res*, 27, 753-9.
- PITRUZZELLO, A. M., KRASSOWSKA, W. & IDRISI, S. F. 2007. Spatial heterogeneity of the restitution portrait in rabbit epicardium. *Am J Physiol Heart Circ Physiol*, 292, H1568-78.
- POTTER, E. 1987. Presynaptic inhibition of cardiac vagal postganglionic nerves by neuropeptide Y. *Neurosci Lett*, 83, 101-6.
- POTTER, E. K. 1985. Prolonged non-adrenergic inhibition of cardiac vagal action following sympathetic stimulation: neuromodulation by neuropeptide Y? *Neurosci Lett*, 54, 117-21.
- RABINOWITZ, S. H., VERRIER, R. L. & LOWN, B. 1976. Muscarinic effects of vago-sympathetic trunk stimulation on the repetitive extrasystole (RE) threshold. *Circulation*, 53, 622-7.
- REVINGTON, M. L. & MCCLOSKEY, D. I. 1990. Sympathetic-parasympathetic interactions at the heart, possibly involving neuropeptide Y, in anaesthetized dogs. *J Physiol*, 428, 359-70.
- SAMAAN, A. 1935. The antagonistic cardiac nerves and heart rate. *J Physiol*, 83, 332-40.
- SCHWARTZ, P. J. 1998. The autonomic nervous system and sudden death. *Eur Heart J*, 19 Suppl F, F72-80.
- SCHWARTZ, P. J. & MALLIANI, A. 1975. Electrical alternation of the T-wave: clinical and experimental evidence of its relationship with the sympathetic nervous system and with the long Q-T syndrome. *Am Heart J*, 89, 45-50.

- SCHWARTZ, P. J., SNEBOLD, N. G. & BROWN, A. M. 1976. Effects of unilateral cardiac sympathetic denervation on the ventricular fibrillation threshold. *Am J Cardiol*, 37, 1034-40.
- SCHWARTZ, P. J. & STONE, H. L. 1980. Left stellectomy in the prevention of ventricular fibrillation caused by acute myocardial ischemia in conscious dogs with anterior myocardial infarction. *Circulation*, 62, 1256-65.
- SCHWARTZ, P. J., VERRIER, R. L. & LOWN, B. 1977. Effect of stellectomy and vagotomy on ventricular refractoriness in dogs. *Circ Res*, 40, 536-40.
- TAGGART, P., SUTTON, P., CHALABI, Z., BOYETT, M. R., SIMON, R., ELLIOTT, D. & GILL, J. S. 2003. Effect of adrenergic stimulation on action potential duration restitution in humans. *Circulation*, 107, 285-9.
- TAGGART, P., SUTTON, P., LAB, M., DEAN, J. & HARRISON, F. 1990. Interplay between adrenaline and interbeat interval on ventricular repolarisation in intact heart in vivo. *Cardiovasc Res*, 24, 884-95.
- UIJTDEHAAGE, S. H. & THAYER, J. F. 2000. Accentuated antagonism in the control of human heart rate. *Clin Auton Res*, 10, 107-10.
- VANOLI, E., DE FERRARI, G. M., STRAMBA-BADIALE, M., HULL, S. S., JR., FOREMAN, R. D. & SCHWARTZ, P. J. 1991. Vagal stimulation and prevention of sudden death in conscious dogs with a healed myocardial infarction. *Circ Res*, 68, 1471-81.
- WARNER, M. R. & LEVY, M. N. 1989. Inhibition of cardiac vagal effects by neurally released and exogenous neuropeptide Y. *Circ Res*, 65, 1536-46.
- WEISS, J. N., CHEN, P. S., QU, Z., KARAGUEUZIAN, H. S. & GARFINKEL, A. 2000. Ventricular fibrillation: how do we stop the waves from breaking? *Circ Res*, 87, 1103-7.
- YANG, T. & LEVY, M. N. 1992. Sequence of excitation as a factor in sympathetic-parasympathetic interactions in the heart. *Circ Res*, 71, 898-905.
- YANG, T., SENTURIA, J. B. & LEVY, M. N. 1994. Antecedent sympathetic stimulation alters time course of chronotropic response to vagal stimulation in dogs. *Am J Physiol*, 266, H1339-47.

Chapter 5

Beta-blocker Modulation of Heart Rate and Ventricular Electrophysiology in Sympatho-vagal Interaction: Potential Mechanisms

Under Review for Consideration for Publication

Autonomic Modulation in a Rabbit Model of Heart Failure

Chapter 5: Beta-blocker Modulation of Heart Rate and Ventricular Electrophysiology in Sympatho-vagal Interaction – Potential Mechanisms

5.1 Introduction

Sympathetic nervous system hyperactivity has long been regarded as a key clinical and epidemiological link to increased mortality, most of which due to increased arrhythmic death from ventricular tachyarrhythmias (Schwartz, 1998, Meredith et al., 1991). As such, β -blockade proves to be an invaluable therapeutic strategy to attenuate this hyperadrenergic effect. β -blockers have been shown to reduce arrhythmic deaths by reducing the incidence of myocardial infarction (MI). These effects were particularly prominent in patients in certain cardiac conditions, including ischaemic heart disease, recent MI and heart failure where a reduction in sudden death by more than 40% was observed (Packer, 2001, Hjalmarson et al., 2000, CIBIS-II Investigators and Committees, 1999).

Historically propranolol was the first β -blocker developed in 1962 with the original intention of being used to ameliorate angina pectoris. Over the ensuing decade, experimental studies demonstrated consistently the ability of β -blockers to suppress ventricular arrhythmias induced by supratherapeutic dosage of cardiac glycosides. The initial uptake on the antifibrillatory and antiarrhythmic properties of β -blockers were gradual not only due to the preconception of its therapeutic role as an antianginal agent but also the preoccupation of assessing potency of anti-arrhythmic properties through suppression of premature ventricular beats and ventricular tachycardias induced by programmed electrical stimulation. The latter methodology ended with the Cardiac Arrhythmia Suppression Trial (CAST) (The CAST Investigators, 1989).

Broadly, β -blockers mediate their antifibrillatory and antiarrhythmic properties by competitively antagonising myocardial β -adrenoreceptors, thereby attenuating the electrophysiologic effects of sympathetic hyperactivity. During hyperadrenergic state, these electrophysiologic effects include shortened ventricular action potential duration (and hence effective refractory period), increased conduction velocity, increased ventricular triggered automaticity, reduced ventricular tachycardia and fibrillation

(VFT) thresholds, attenuated vagal activity, as well as increased dispersion of ventricular refractoriness (Dorian, 2005).

In Chapter 4, the effect of sympathetic nerve stimulation (SNS) was noted to prevail in VFT as well as cardiac restitution during sympatho-vagal interaction studies, in contrast to heart rate changes which reflect vagal dominance, affirming the lack of accentuated antagonism in the ventricle. In this chapter, the effect of β -blockers was investigated beyond their known effect in isolated sympathetic hyperactivity state through sympatho-vagal interaction studies described in the earlier chapter.

5.2 Aim

The study serves to fulfil the primary objective of assessing the effect of metoprolol tartrate on heart rate (HR) and ventricular electrophysiology namely VFT, ventricular effective refractory period (ERP) and cardiac restitution (RT) during sympatho-vagal interaction. A secondary objective was established to investigate for possible role of sodium acetate in accounting for the effect of metoprolol on ventricular electrophysiology.

5.3 Method

5.3.1 Isolated Rabbit Heart Preparation with Intact Dual Autonomic Innervation

Adult male New Zealand White rabbits (2.9 – 3.1 kg, $n = 18$) were sedated with a subcutaneous injection containing a mixture of Medetomidine Hydrochloride (Sedator, 0.2 mg/kg), Ketamine (Narketan, 10 mg/kg) and Butorphanol Tartrate (Torbugesic, 0.05 mg/kg). Once the animal was suitably sedated, surgery was performed to isolate rabbit heart with intact dual autonomic innervation as described in detail in the previous chapter (Chapter 3.4.2.1).

5.3.2 Langendorff Perfusion with Acetate-free and Acetate-containing Tyrode solutions

Rabbit hearts were perfused in modified Langendorff mode (Chapter 3.4.2.2) with two different compositions of Tyrode solution. The first series of experiments ($n = 8$) were performed with *acetate-free* Tyrode solution (in mM): 130.0 NaCl, 24.0 NaHCO₃, 1.0 CaCl₂, 1.0 MgCl₂, 4.0 KCl, 1.2 NaH₂PO₄ and 20.0 dextrose. To fulfil the secondary objective, experiments ($n = 5$) were repeated using *acetate-containing* Tyrode solution (in mM): 138.0 NaCl, 24.0 NaHCO₃, 1.8 CaCl₂, 1.0 MgCl₂, 4.0 KCl, 0.4 NaH₂PO₄, 11.0 dextrose and 20.0 sodium acetate.

5.3.3 Autonomic Nerve Stimulation

As described in Chapter 3.4.2.3 in detail, the right cervical vagus nerve was supported and stimulated by a pair of custom-made bipolar silver electrodes. Bilateral sympathetic nerve stimulation was achieved by insertion of a quadripolar catheter into the spinal canal to the level of stellate ganglia.

For each of the autonomic nerves, a voltage response curve was constructed by assessing the heart rate response during sympathetic (SNS)/vagus nerve stimulation (VNS) with varying strength from 1 – 10 V. The optimal voltage required by each nerve to induce 80% of maximal heart rate changes was determined and used to assess the frequency response of the corresponding autonomic nerves.

In this study, high-frequency SNS (HS) was defined by the frequency that gave rise to an SNS-induced tachycardia of around 230 – 250 bpm. Low-frequency VNS (LV) was determined as the frequency with a resulting bradycardia of around 90 – 100 bpm whilst high-frequency VNS (HV) a heart rate of around 60 – 70 bpm.

This study was carried out in three phases. In the first phase, the effects of low- (LV) and high-frequency VNS (HV) were examined at BL and in the presence of high-frequency SNS (HS). In the second phase, an identical sequence of autonomic nerve

stimulation was re-examined in the presence of metoprolol tartrate, a β_1 -adrenoreceptor antagonist ($1.8 \mu\text{M}$, Sigma-Aldrich, Gillingham, UK). The third phase comprises a repeat of the protocol following a washout period of 30 minutes.

5.3.4 Cardiac Electrical Recording and Pacing

A spring-loaded mini-MAP electrode was placed at the epicardial surface of left ventricular free wall for recording of monophasic action potential (MAP) using a DC-coupled high-input impedance differential amplifier as described in Chapter 3.4.2.2. A bipolar pacing electrode was inserted into the right ventricular apex for ventricular pacing manoeuvres required for measurement of VFT and ERP.

5.3.5 Measurement of Ventricular Electrophysiology: VFT, ERP and RT

VFT and ERP were determined by specific pacing protocols as described in Chapter 3.4.2.4. RT was derived from measurements of MAP duration during S1 – S2 protocol used for ERP measurement. The specifics of RT calculations were explained in Chapter 3.4.2.4. Steady-state HR was determined prior to commencing the pacing protocols in interest.

5.4 Results

5.4.1 Effect of Metoprolol on Sympatho-vagal Interaction of Heart Rate

Steady state heart rate was determined by derivation of atrial electrogram recordings prior to commencing VFT (Figure 5.1A) and ERP (Figure 5.1B) protocols. At baseline, heart rates were $146.2 \pm 10.6 \text{ bpm}$ ($n = 5$) and $152.6 \pm 6.9 \text{ bpm}$ ($n = 8$) respectively for VFT and ERP protocols. In both protocols, VNS led to heart rate reduction in a frequency-dependent manner as described in Chapter 4. In the presence of metoprolol (denoted as *red* line graphs), heart rate changes were similar to those at control (denoted as *black* line graphs) and washout (denoted as *blue* line graphs) conditions. In the VFT protocol during metoprolol infusion, low and high-frequency VNS reduced the heart rate to $105.0 \pm 8.5 \text{ bpm}$ and $58.5 \pm 11.3 \text{ bpm}$ respectively whereas in the ERP protocol,

the heart rate reduction was from 152.6 ± 6.9 bpm to 106.8 ± 5.7 bpm and 60.6 ± 4.6 bpm correspondingly (Figure 5.1).

In the presence of background high-frequency SNS, heart rate increased to 231.2 ± 6.2 bpm and 243.4 ± 2.1 bpm in VFT and ERP protocols correspondingly with concurrent VNS leading to exaggerated heart rate reduction in a frequency-sensitive manner as observed in Chapter 4, consistent with the phenomenon of accentuated antagonism. The presence of metoprolol however abolishes this phenomenon such that the concurrent vagally-induced bradycardic responses were similar to those observed at baseline. The initial HS-induced tachycardia observed in the control conditions were abolished by metoprolol, leading to a heart rate of 140.2 ± 10.3 bpm and 160.0 ± 5.5 bpm in the VFT and ERP protocols respectively. Following a washout period, the vagal dominant effect of heart rate reduction during background SNS was observed as seen in the initial control condition. An example of typical recordings of left ventricular systolic pressure (LVP), MAP and heart rate during high-frequency vagal stimulation at baseline and during sympatho-vagal interaction with or without metoprolol is illustrated in Figure 5.2

Figure 5.1 Intrinsic heart rate at baseline (BL), during low- (LV) and high-frequency (HV) vagal stimulation, high-frequency sympathetic stimulation (HS) and sympatho-vagal interaction (HS-LV, HS-HV) prior to commencing burst pacing (Figure 5.1A) or S1-S2 pacing protocol (Figure 5.1B) in control condition, during metoprolol infusion and following washout

Figure 5.1A

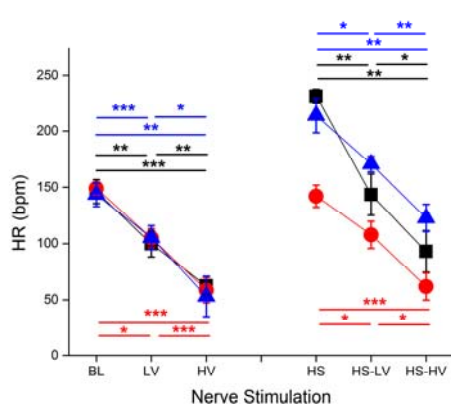


Figure 5.1B

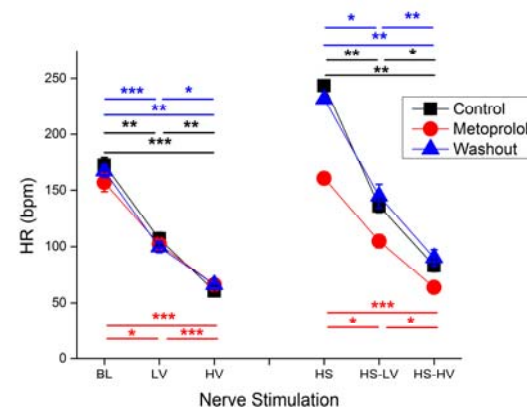


Figure 5.2 Intrinsic heart rate at baseline, during high-frequency vagal stimulation (VNS)(Figure 5.2A) and sympatho-vagal interaction (Figure 5.2B) with and without metoprolol in a typical experiment

Figure 5.2A

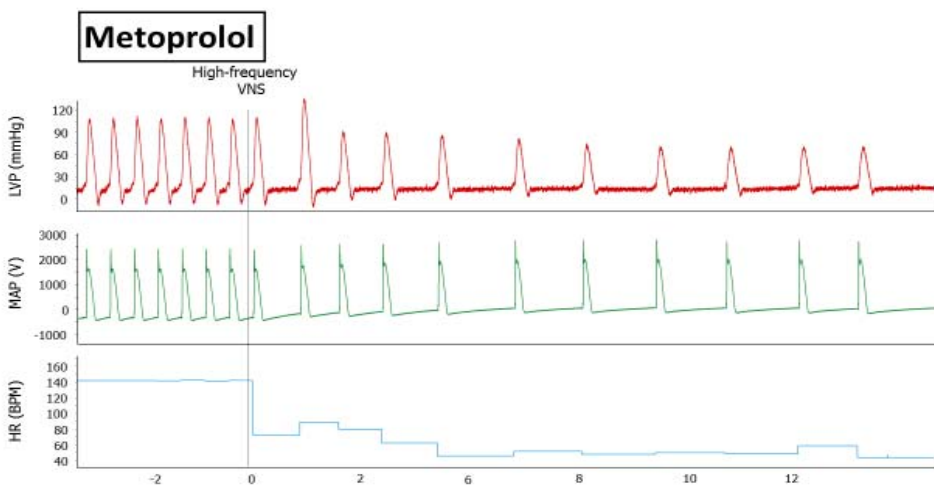
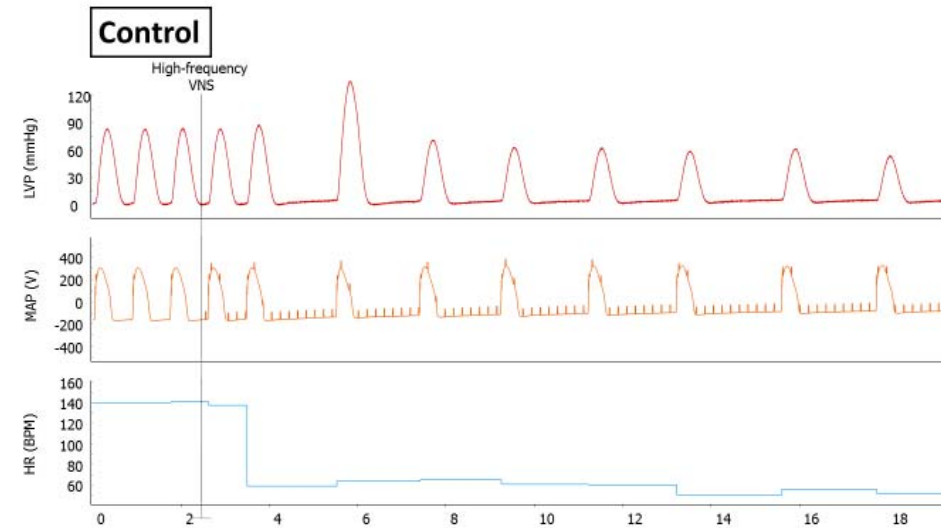
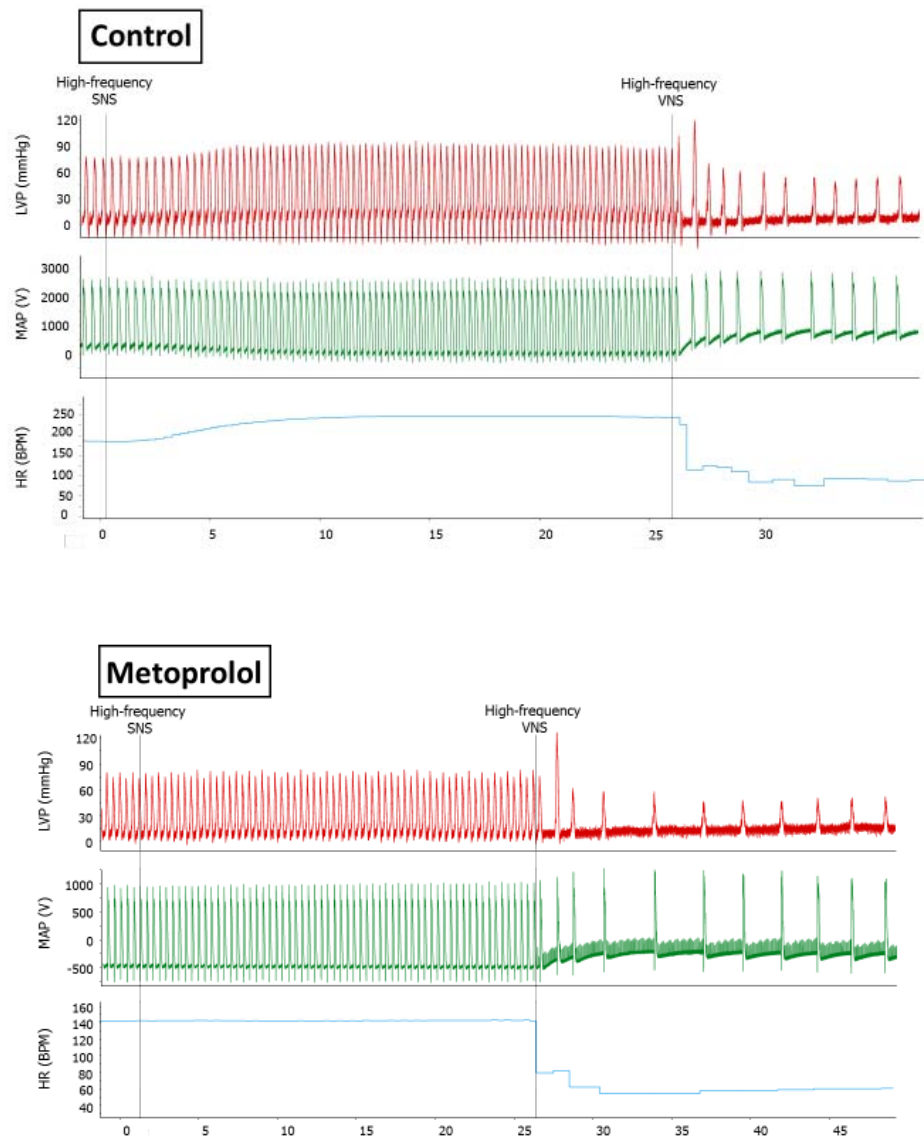


Figure 5.2B

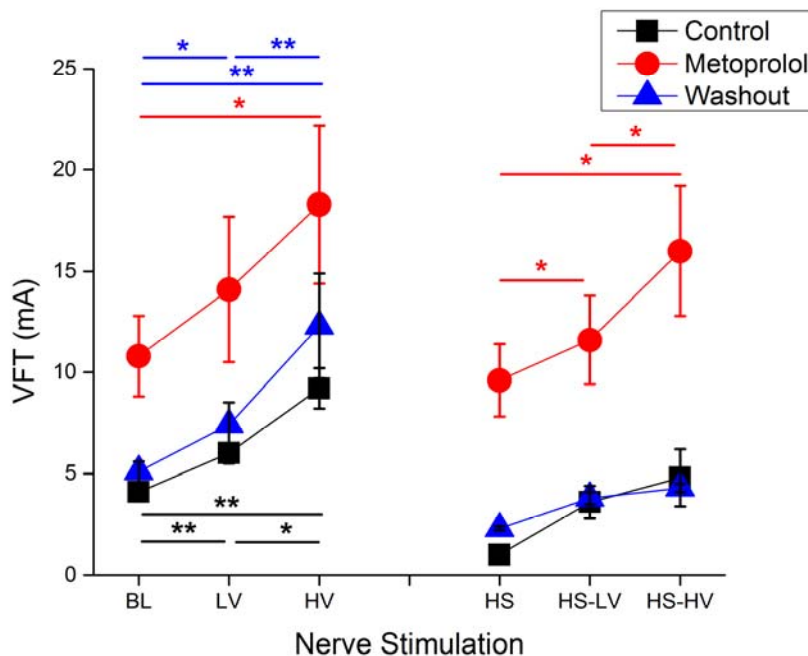
5.4.2 Effect of Metoprolol on Sympatho-vagal Interaction of Ventricular Fibrillation Inducibility

In this study, baseline VFT ($n = 5$) was 4.1 ± 0.4 mA. Under the control condition, VNS conferred protection, raising VFT to 6.0 ± 0.5 mA and 9.2 ± 0.1 mA during low- and high-frequency stimulations. In the presence of metoprolol, baseline VFT was higher than that in control condition at 10.8 ± 2.0 mA. The protective effect of VNS was maintained at this higher baseline VFT, with VFT being further elevated to 14.1 ± 3.6 mA and 18.3 ± 3.9 mA by low- and high-frequency VNS.

In the control condition, background high-frequency SNS led to a lower VFT at 1.0 ± 0.0 mA with concurrent VNS exerting significant effect on VFT, raising the VFT to 3.6 ± 0.8 mA during HS-LV, and to 4.8 ± 1.4 mA during HS-HV. In the presence of metoprolol, SNS failed to lower VFT, leading to a VFT of 9.6 ± 1.8 mA with further elevation of VFT by concurrent low- and high-frequency VNS to 11.6 ± 2.2 mA and 16.0 ± 3.2 mA correspondingly.

After a washout period of 30 minutes, baseline VFT reverted to a lower level of 5.1 ± 0.5 mA similar to that seen at control condition. Low- and high-frequency VNS increased the VFT to 7.4 ± 1.1 mA and 12.3 ± 2.6 mA respectively. Adequate washout of metoprolol was further validated with SNS-induced VFT reduction to 2.3 ± 0.1 mA with concurrent VNS increasing the VFT insignificantly to 3.8 ± 0.3 mA and 4.3 ± 0.2 mA during HS-LV and HS-HV, the changes of which were similar to those observed in the control condition.

Figure 5.3 Ventricular fibrillation threshold (VFT) at baseline (BL), during low-(LV) and high-frequency (HV) vagal stimulation, high-frequency sympathetic stimulation (HS) and sympatho-vagal interaction (HS-LV, HS-HV) in control condition, during metoprolol infusion and following washout



5.4.3 Effect of Metoprolol on Sympatho-vagal Interaction of Ventricular Restitution

Maximum RT slope was derived from ERP protocols ($n = 8$) with a baseline RT slope measurement of 2.6 ± 0.1 . Under control condition, VNS flattened the RT slopes to 0.9 ± 0.1 and 0.8 ± 0.2 during low- and high-frequency stimulations (Figure 5.4 A). SNS led to a steepening of the RT slope at 3.9 ± 0.1 with concurrent VNS producing flatter RT slopes of 2.7 ± 0.2 (HS-LV) and 2.5 ± 0.1 (HS-HV) (Figure 5.4A). Figure 5.5A demonstrated that VNS flattened the baseline maximum RT slope by $64.5 \pm 5.1\%$ and $70.6 \pm 6.0\%$ during low- and high-frequency stimulations whereas in the presence of background SNS, the effect of concurrent VNS on flattening RT slopes was attenuated to $30.2 \pm 4.3\%$ (HS-LV) and $36.6 \pm 3.5\%$ (HS-HV).

In the presence of metoprolol, RT slopes were attenuated globally (Figure 5.4B). Baseline RT slope was 1.3 ± 0.2 with VNS flattening the RT slopes to 0.5 ± 0.1 and 0.4 ± 0.1 during LV and HV correspondingly. The effect size of VNS-induced RT flattening was similar to that observed in the control condition at $63.1 \pm 6.4\%$ (LV) and $68.2 \pm 3.4\%$ (HV) (Figure 5.5B). Background SNS failed to steepen the RT slope in the presence of metoprolol, giving rise to a maximum RT slope of 1.9 ± 0.2 as opposed to 3.9 ± 0.1 in the control condition (Figure 5.4B). Concurrent VNS preserved its effect on flattening the RT slopes with HS-LV giving rise to a maximum RT slope of 0.9 ± 0.1 and HS-HV a maximum RT slope of 0.8 ± 0.1 . In contrast to the observations in the control condition, concurrent VNS during background SNS maintained its impact of RT slope flattening in the presence of metoprolol at $48.3 \pm 8.5\%$ (HS-LV) and $55.2 \pm 5.6\%$ (HS-HV) (Figure 5.5B).

Figure 5.4 Maximum action-potential duration restitution (RT) slope gradients at baseline (BL), during low- (LV) and high-frequency (HV) vagal stimulation, high-frequency sympathetic stimulation (HS) and sympatho-vagal interaction (HS-LV, HS-HV) in control condition and during metoprolol infusion

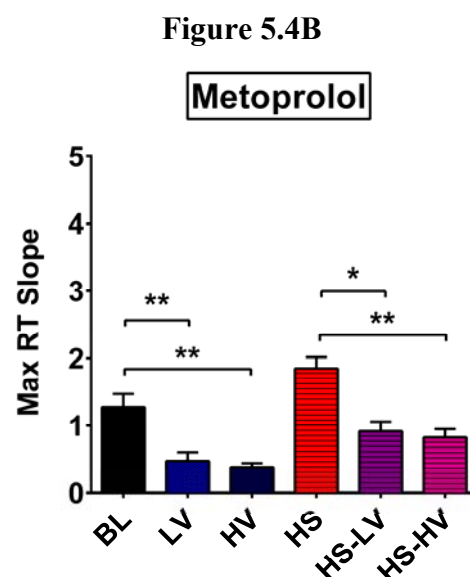
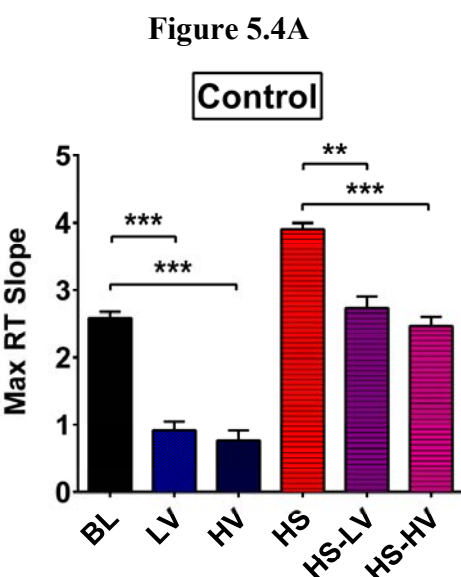
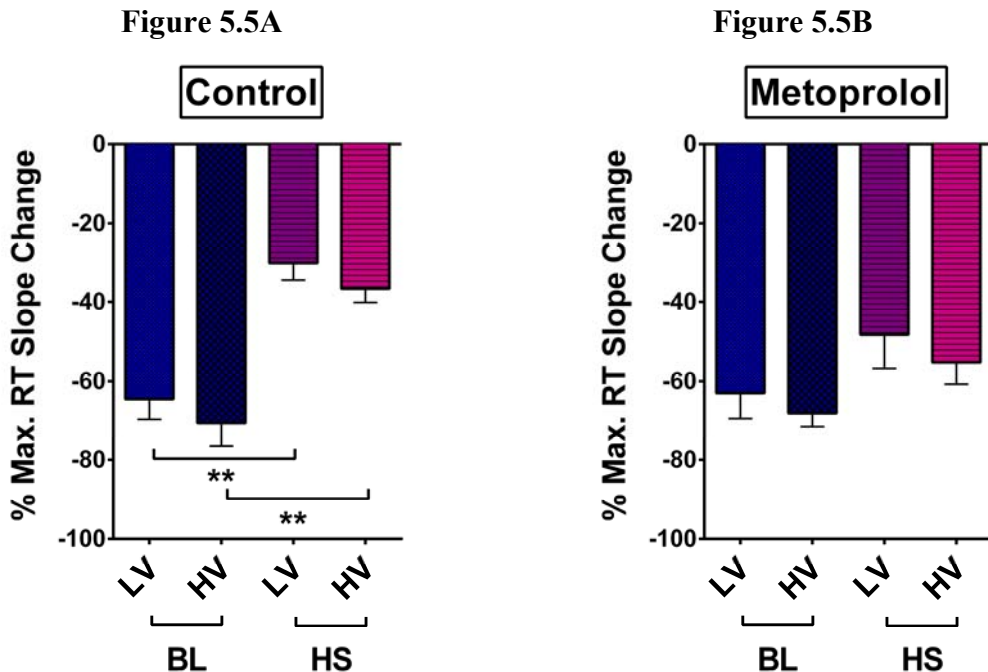


Figure 5.5 Relative changes in maximum restitution (RT) slope gradients from baseline values during vagal stimulation and sympatho-vagal interactions in control condition and following metoprolol infusion



5.4.4 Effect of Metoprolol on Sympatho-vagal Interaction of Ventricular Refractoriness

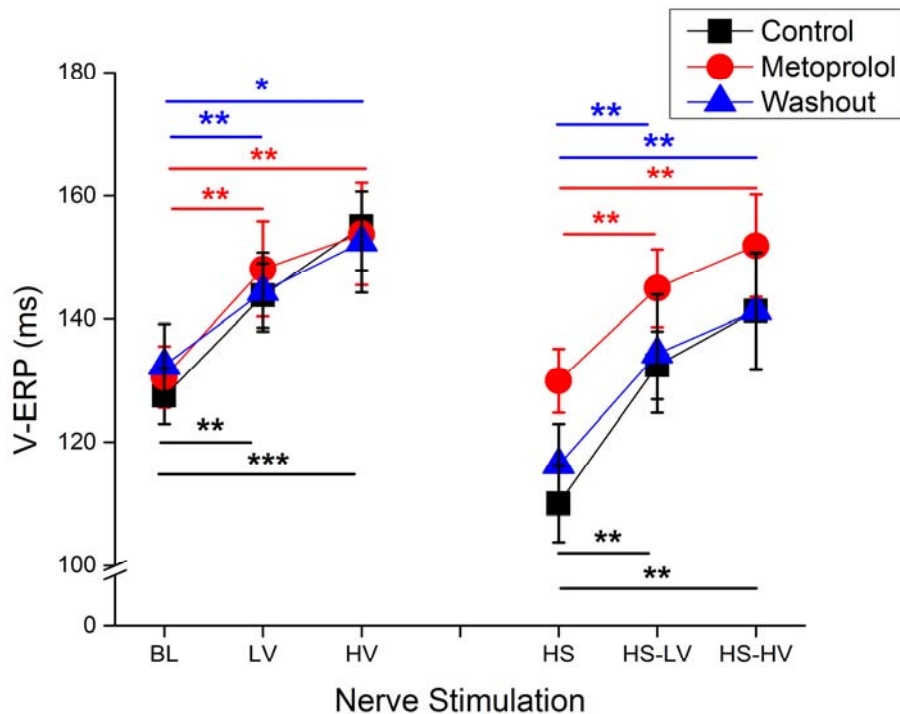
Baseline ventricular ERP (V-ERP) in this study ($n = 8$) was 127.5 ± 4.5 ms with VNS prolonging ERP to 143.8 ± 5.2 ms and 155.0 ± 7.1 ms during low- and high-frequency stimulations correspondingly (Figure 5.5). Background high-frequency SNS shortened V-ERP to 110.0 ± 6.2 ms with concurrent low- and high-frequency VNS maintaining its effect of V-ERP prolongation to 132.5 ± 5.5 ms (HS-LV) and 141.3 ± 9.4 ms (HS-HV) respectively (Figure 5.6).

In the presence of metoprolol, VNS exerted a similar effect on V-ERP prolongation, increasing the V-ERPs from 130.6 ± 5.0 ms to 148.1 ± 7.7 (LV) and 153.8 ± 8.3 ms (HV). However, metoprolol abolished SNS-induced ERP shortening, giving rise to a V-ERP of 130.0 ± 5.2 , similar to the baseline V-ERP measurement. Subsequent concurrent VNS effect on ERP prolongation was unaffected in the presence of

background SNS, leading to V-ERP of 145.0 ± 6.3 ms (HS-LV) and 151.9 ± 8.3 ms (HS-HV). In short, sympatho-vagal interaction of V-ERP in the presence of metoprolol mirrored the V-ERP changes at baseline.

Following a washout period, V-ERP changes reverted to those observed under the control condition, in particular the effect of SNS on ERP shortening re-emerged (116.3 ± 6.7 ms) with concurrent VNS prolonging the V-ERPs to 134.4 ± 9.6 ms (HS-LV) and 141.3 ± 9.5 ms (HS-HV).

Figure 5.6 Ventricular effective refractory period (V-ERP) at baseline (BL), during low- (LV) and high-frequency (HV) vagal stimulation, high-frequency sympathetic stimulation (HS) and sympatho-vagal interaction (HS-LV, HS-HV) in control condition, during metoprolol infusion and following washout



5.4.5 Effect of Sodium Acetate on Metoprolol-induced Heart Rate Changes and Metoprolol-conferred Protective Effect of Ventricular Fibrillation Inducibility

In order to further elucidate the effect of metoprolol on ventricular fibrillation inducibility, VFT protocol was repeated ($n = 5$) substituting acetate-containing Tyrode solution for the standard Tyrode solution as Langendorff perfusate. Baseline heart rate was 164.6 ± 13.9 bpm (Figure 5.7). In control condition, VNS produced a frequency-dependent bradycardic response, reducing the heart rate by 59.2 ± 4.4 bpm and by 84.6 ± 8.0 bpm during low- and high-frequency stimulations (Figure 5.8A). A similar magnitude of bradycardic response was seen in the presence of metoprolol when a baseline heart rate of 149.6 ± 2.4 bpm (Figure 5.7) decreased during low- and high-frequency VNS (Figure 5.8B). Background high-frequency SNS produced an increased heart rate of 236.2 ± 8.5 bpm (Figure 5.7) with concurrent low- and high-frequency VNS producing exaggerated bradycardic responses of -72.6 ± 7.7 bpm and -111.4 ± 9.3 bpm respectively. Metoprolol abolished SNS-induced tachycardia, giving rise to a heart rate of 146.8 ± 1.8 bpm, i.e. similar to the baseline heart rate of 149.6 ± 2.4 bpm (Figure 5.7) whilst concurrent low- and high-frequency VNS produced a similar magnitude of bradycardic responses as those at baseline (Figure 5.8B). Briefly, the accentuated antagonism of heart rate responses seen in control condition (Figure 5.8A) was abolished in the presence of metoprolol.

In control condition, baseline VFT measured to be 4.3 ± 0.5 mA whereas in the presence of metoprolol, baseline VFT was higher at 7.8 ± 1.5 mA (Figure 5.9). VNS conferred a protective effect, raising the VFT in a frequency-dependent manner (Figure 5.9). In the absence of metoprolol, VFT increased by 1.2 ± 0.1 mA and 3.4 ± 0.4 mA during low- and high-frequency VNS (Figure 5.9A) whilst in the presence of metoprolol, a greater increase in VFT was observed at 3.8 ± 0.8 mA and 7.6 ± 1.8 mA (Figure 5.10B). SNS lowered the VFT to 1.1 ± 0.1 mA in control condition (Figure 5.9) with concurrent low- and high-frequency VNS raising the VFT by 1.3 ± 0.2 mA and 2.5 ± 0.6 mA (Figure 5.10A). In contrast, in the presence of metoprolol, SNS failed to reduce VFT, leading to a VFT measurement of 6.7 ± 0.5 not dissimilar to the baseline VFT of 7.8 ± 1.5 mA (Figure 5.9). Concurrent low- and high-frequency VNS elevated

the VFT by 3.6 ± 1.1 mA and 6.3 ± 1.4 mA, a protective effect similar in magnitude at baseline (Figure 5.10B).

Overall, two-way ANOVA tests revealed no statistical significance in the heart rate and VFT data between Acetate-free and Acetate-containing Tyrode solutions (Figure 5.11). In regards to heart rate changes, in spite of significant heart rate variation between the different autonomic nerve stimulations ($p < 0.0001$), no significant difference in heart rate was noted between acetate-free (red bars) and acetate-containing (blue bars) Tyrode solutions during the control ($p = 0.2037$), Metoprolol ($p = 0.1841$) and washout ($p = 0.7648$) phases. Similarly, when comparing the VFT data, despite the varied VFT data between the different autonomic nerve stimulations ($p < 0.0001$), sodium acetate did not produce significant variation in VFT for each autonomic nerve stimulation compared to its acetate-free counterpart during the control ($p = 0.4246$), Metoprolol ($p = 0.4085$) and washout ($p = 0.841$) phases.

Figure 5.7 Intrinsic heart rate at baseline (BL), during low- (LV) and high-frequency (HV) vagal stimulation, high-frequency sympathetic stimulation (HS) and sympatho-vagal interaction (HS-LV, HS-HV) in control condition, during metoprolol infusion and following washout in Langendorff rabbit's heart preparation perfused with acetate-containing Tyrode solution

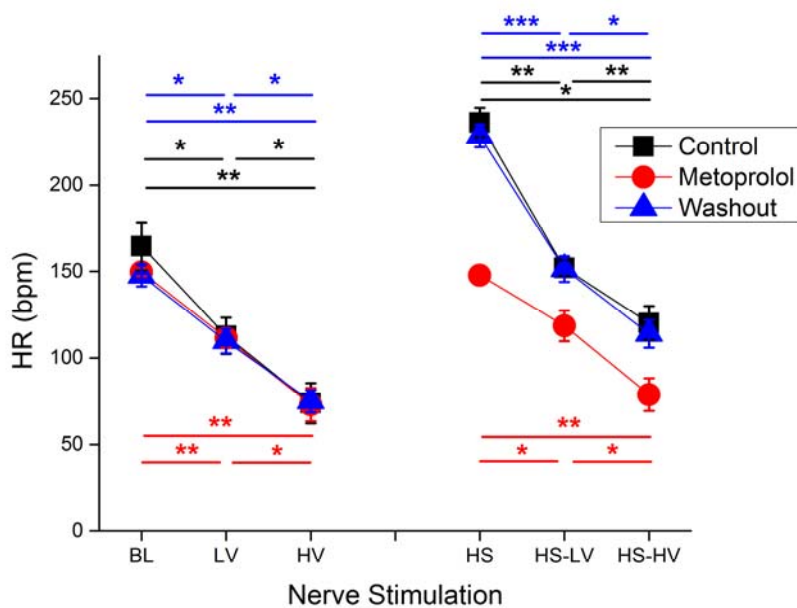


Figure 5.8 Absolute heart rate changes during low- (LV) and high-frequency (HV) vagal stimulation at baseline (BL) and with concurrent high-frequency sympathetic stimulation (HS) in control condition (Figure 5.7A) and during metoprolol infusion (Figure 5.7B) in Langendorff rabbit's heart preparation perfused with acetate-containing Tyrode solution

Figure 5.8A

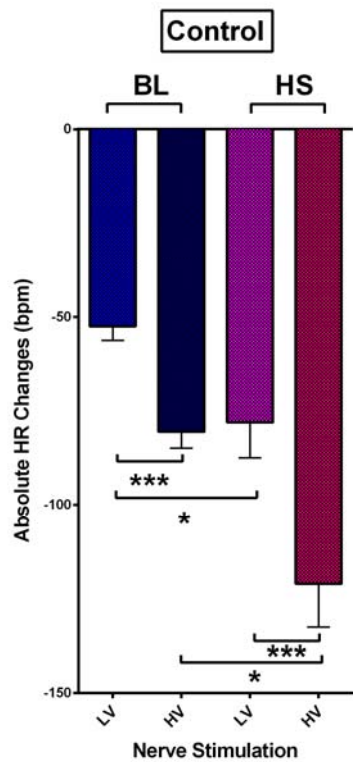


Figure 5.8B

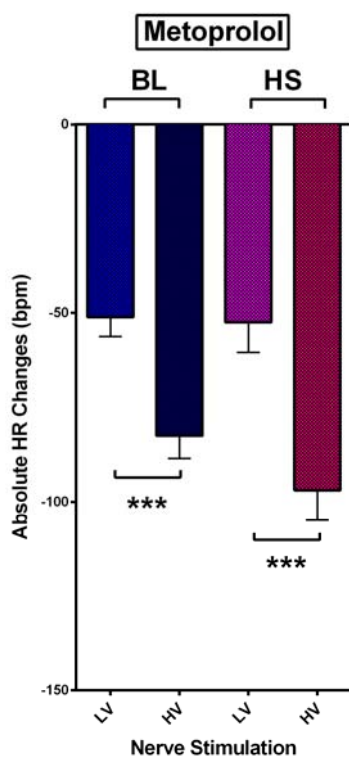


Figure 5.9 Ventricular fibrillation thresholds (VFT) at baseline (BL), during low-(LV) and high-frequency (HV) vagal stimulation, high-frequency sympathetic stimulation (HS) and sympatho-vagal interaction (HS-LV, HS-HV) in control condition, during metoprolol infusion and following washout in Langendorff rabbit's heart preparation perfused with acetate-containing Tyrode solution

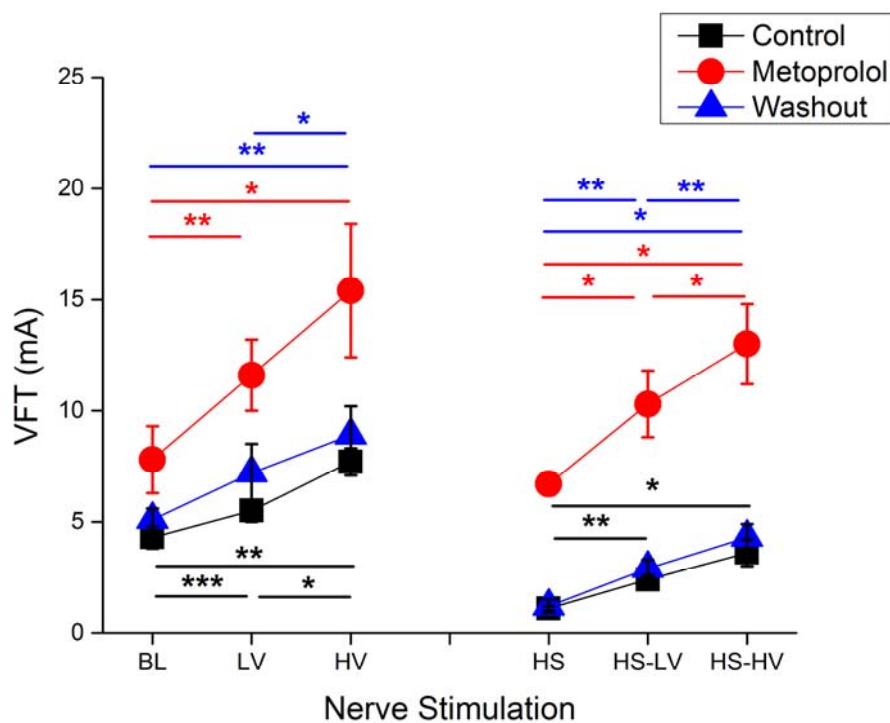


Figure 5.10 Absolute changes in ventricular fibrillation threshold (VFT) during low- (LV) and high-frequency (HV) vagal stimulation at baseline (BL) and with concurrent high-frequency sympathetic stimulation (HS) in control condition (Figure 5.7A) as well as during metoprolol infusion (Figure 5.7B) in Langendorff rabbit's heart preparation perfused with acetate-containing Tyrode solution

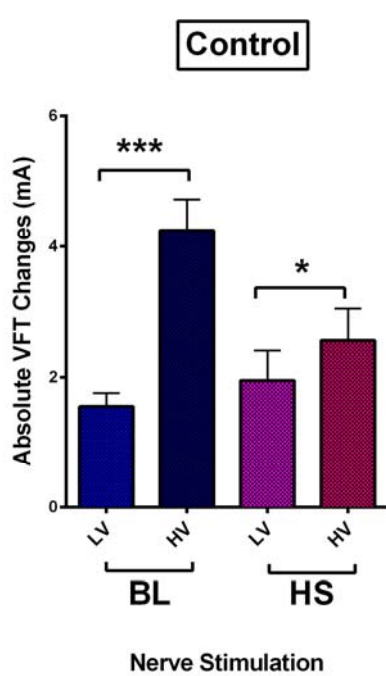
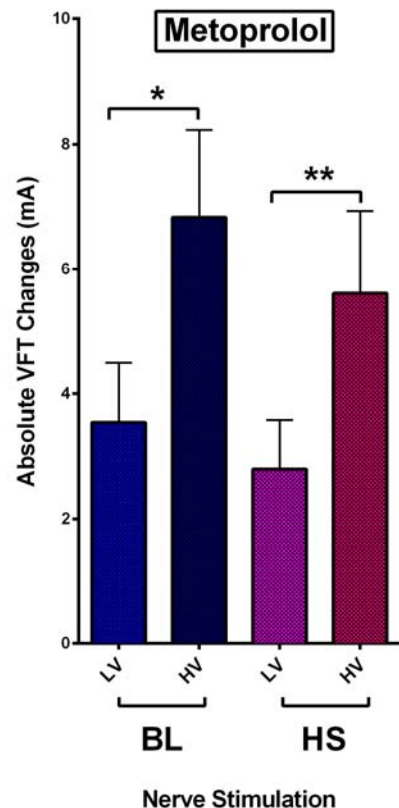
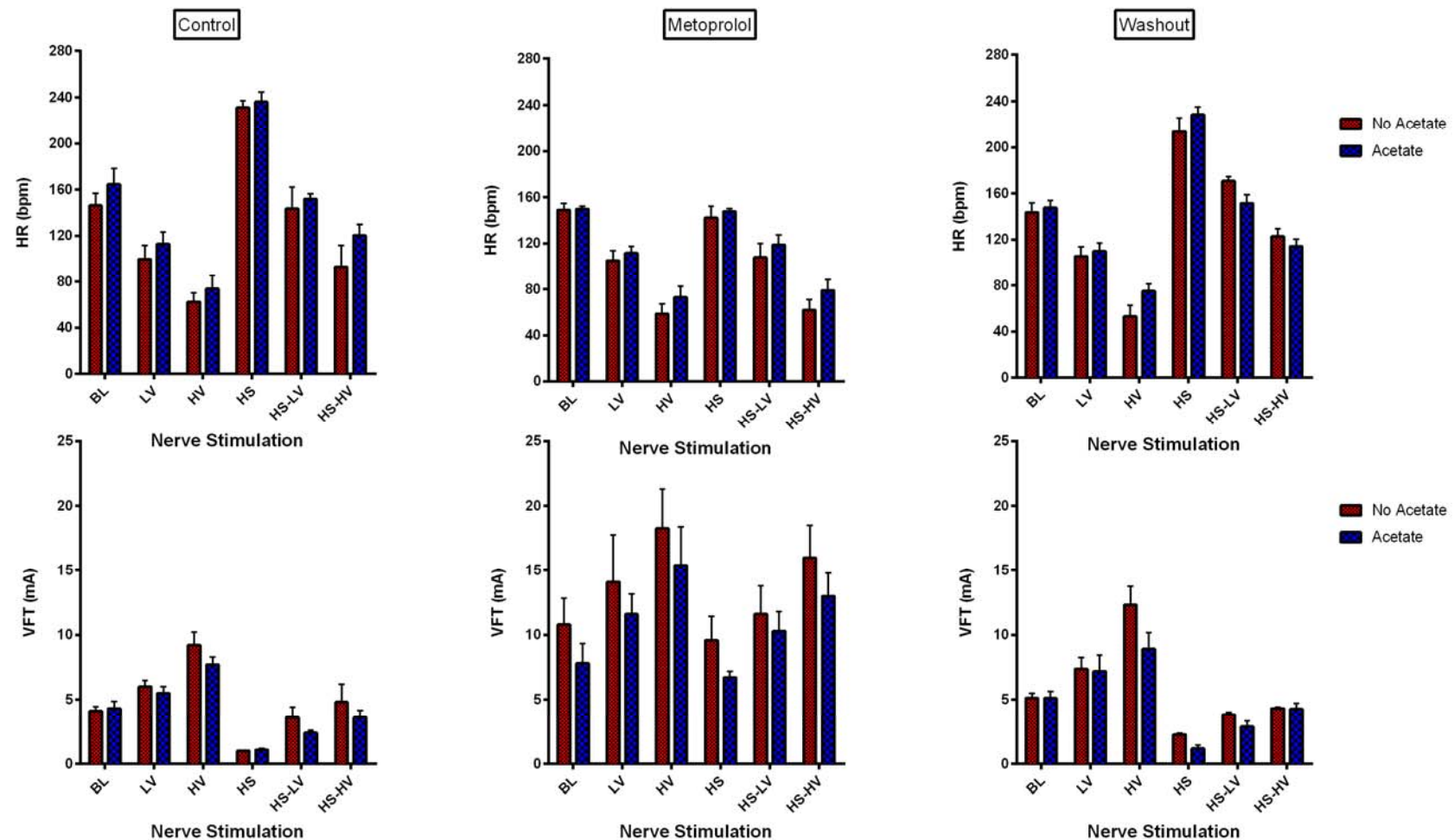
Figure 5.10A**Figure 5.10B**

Figure 5.11 Comparison of heart rate and ventricular fibrillation threshold between acetate-containing and acetate-free Tyrode solutions at control condition, during metoprolol infusion and following washout



5.5 Discussion

This study was designed as a follow-up study detailed in Chapter 4 revealing the prevailing effect of sympathetic nerve stimulation on ventricular fibrillation inducibility and electrical restitution in the presence of vagal stimulation. The use of metoprolol for adrenergic blockade allows the sympatho-vagal relationship to be dissected. The findings of this study are (1) metoprolol increases the overall VFT, i.e. not only that during sympathetic stimulation, but also those at baseline and during vagus nerve stimulation. (2) metoprolol reduces the overall maximal slopes of APD-RT curves including that at baseline and during autonomic nerve stimulations. (3) vagal stimulation confers additional anti-arrhythmic effects by raising VFT and flattening APD-RT curves even in the presence of metoprolol. (4) metoprolol abolishes ERP-shortening effect of sympathetic stimulation but does not alter baseline ERP and vagal-induced ERP prolongation. (5) Sodium acetate does not alter the overall findings in this study.

5.5.1 Effect of Metoprolol on VFT during Sympatho-vagal Interaction

Hypersympathetic activity and ventricular arrhythmias have long shared a clinical and epidemiological link (Anderson, 2003). The cellular link between these 2 components are not as straight forwarded, being confounded by spatial and temporal heterogeneity of adrenoreceptors in different cardiac diseases. In general, β_1 , β_2 and α_1 adrenoreceptors are found in the hearts with β_1 adrenoreceptors contributing to the effect of adrenergic stimulation on the ventricles. At cellular level, sympathetic stimulation results in activation of the stimulatory G (G_s) protein, initiating an activation cascade from adenyl cyclase to increased cAMP levels and enhanced protein kinase A (PKA) activity. Increased PKA produces a phosphorylation cascade to act on various downstream targets including sarcolemmal calcium release and other membrane-bound ion channels and currents. Hence the inward L-type Ca^{2+} current is increased during adrenergic stimulation, leading to increased contractility (Koch et al., 2000). Although increased L-type Ca^{2+} current prolongs APD, β_1 -adrenergic stimulation also increases the depolarising current, I_{Na} , thereby increasing conduction velocity (Murphy et al., 1996, Lu et al., 1999). Outward currents including I_{Ks} , chloride currents, I_{to} and variably I_{Kr} are also increased (Lo and Numann, 1998, Zhang et al., 2002, Thomas et al., 2004, Murphy et al., 1996, Lu et al., 1999, Koch et al., 2000, Ophof et al., 1993, Meszaros et al.,

1996, Dixon et al., 1996). Furthermore, isoproterenol has also been shown to reduce I_{K1} contributing to triggered activity which is responsible for ventricular arrhythmias caused by delayed afterdepolarization (Zhang et al., 2002). All these ionic remodelling coupled with electrophysiologic changes of increased automaticity, increased conduction velocity, reduced refractoriness as well as shortened APD promotes ventricular arrhythmias. As most of these effects are driven by β_1 -adrenoreceptors, metoprolol tartrate, being a selective β_1 beta-blocker, was used in this study.

In this study, metoprolol was found to not only suppress sympathetic effect of lowering VFT, but the overall VFTs at baseline and during vagal stimulation have been raised (Figure 5.3). The prevailing sympathetic effect on lowering VFT during sympatho-vagal interaction (Chapter 4) has also been abolished in the presence of metoprolol. Although this effect can be explained by pure adrenergic blockade by metoprolol, the raised overall VFT profiles remains a novel and reversible finding as evident from the washout data. Since metoprolol increased VFT at baseline, this raises the question of either the presence of tonic sympathetic activity or local adrenaline release. The possibility of tonic sympathetic activity seems implausible given that the heart rate at baseline did not change during metoprolol infusion and washout. However, the possibility of local release of norepinephrine at the pacing site could not be excluded in this study especially in the context of high-frequency pacing (Masuda and Levy, 1985). Furthermore, it is also conceivable that metoprolol may possess an unrecognised effect on ion channels at the ventricular level to account for the higher VFT at baseline. Additional antiarrhythmic effects of beta-blockers beyond adrenergic blockade have been reported for propranolol, nadolol, sotalol and atenolol in studies of mammalian hearts (Patterson and Lucchesi, 1984, Almotrefi et al., 1989). Apart from the reported membrane-stabilising (class I) and APD-prolonging (class III) effects (Nakaya et al., 1984), other additional antiarrhythmic effects of beta-blockers remain to be explored (Patterson and Lucchesi, 1984). Furthermore, variable protective effects against ventricular fibrillation by different beta-blockers have been reported, with metoprolol exerting more potent VFT-raising effect than other beta-blockers (Coram et al., 1987). The beta-blockade effect on ventricular arrhythmias also appears to be species-dependent. In rabbits, propranolol was shown to alter ventricular fibrillation dynamics, reducing wave breaks and converting ventricular fibrillation to ventricular tachycardia during the subacute phase following myocardial infarction (Chou et al., 2007). In contrast, metoprolol failed to prevent VFT reduction following SNS in rats

(Kalla et al.). In spite of previous studies demonstrating variable effects on VFT by β -blockers including that during SNS, this study demonstrated that the anti-fibrillatory effect by VNS remains unperturbed in the presence of metoprolol as compared to baseline (Figure 5.3).

5.5.2 Effect of Metoprolol on APD Restitution Slopes during Sympatho-vagal Interaction

Ventricular fibrillation is a chaotic lethal rhythm the initiation of which has been characterised in both computational and animal models to be due to a “wave break” of re-entrant wave fronts (Weiss et al., 2002, Fenton et al., 2002). This occurs when depolarising wave fronts are continually split into multiple other wave fronts meandering through the ventricles, thereby manifesting electrically as ventricular fibrillation. Two alternative hypotheses arise from this concept of initiation of ventricular fibrillation. The focal hypothesis presumes a stable mother rotor. In this case, a wave break can be due to tissue heterogeneity adjacent to the motor rotor, or abrupt changes of the core size and frequency of the rotor itself. This hypothesis is supported by studies showing organization of ventricular fibrillation into ventricular tachycardia via modulation of core size and frequency of the mother rotor with drugs such as verapamil (Samie et al., 2000, Jalife, 2000). The alternative hypothesis, the wavelet hypothesis, speculates that ventricular fibrillation is driven by the occurrence of multiple wavelets propagating, colliding and extinguishing one another, thereby obviating the need for a stable mother rotor. Wave breaks can occur due to static factors such as anatomical barriers, scars or fibrosis but can also be a result of dynamic changes in electrophysiologic properties such as conduction velocity and APD restitution (Cao et al., 1999, Fenton and Karma, 1998, Weiss et al., 2002). Therefore, a steep APD restitution slope will magnify oscillations of wavelengths, creating large gradients of wave breaks to facilitate the initiation of ventricular fibrillation.

Modulation of APD restitution slopes by different pharmacological agents have been shown to exert pro- and antiarrhythmic properties. Isoproterenol and norepinephrine facilitates initiation of ventricular fibrillation by increasing the slopes of APD restitution curves (Taggart et al., 2003). On the contrary, drugs which flattens APD restitution slope are shown to protect against ventricular fibrillation in *in vivo*, *ex vivo* and computational models, not only organizing ventricular fibrillation into stable ventricular tachycardia, but also preventing

degeneration of ventricular tachycardia into ventricular fibrillation. These pharmacological agents include amiodarone (Omichi et al., 2002), bretylium (Garfinkel et al., 2000), esmolol (Hao et al., 2004), propranolol (Endresen and Amlie, 1990), verapamil (Riccio et al., 1999) and diacetyl monoxime (Riccio et al., 1999, Lee et al., 2001). Physiologically direct autonomic nerve stimulation has been shown to have a modulating influence on APD restitution slopes with sympathetic stimulation promoting ventricular fibrillation by steepening restitution slope and conversely vagal stimulation mitigating ventricular fibrillation via flattening of restitution slope (Ng et al., 2007).

This study represents the first attempt to investigate the combined effects of autonomic modulations and beta-blockade on restitution slopes. Whilst at baseline, vagal stimulation led to flattening of restitution slope in a frequency-dependent manner, sympathetic stimulation steepened restitution slope compared to that at baseline. Subsequent concurrent vagal stimulation in the presence of sympathetic stimulation flattened restitution slopes modestly compared to its effect at baseline, suggesting the prevailing sympathetic effect on restitution slopes (Figure 5.4A and 5.5A). Interestingly, metoprolol confers additional antiarrhythmic effect by flattening restitution slopes in all conditions, including during vagal stimulations. This additional protective effect is not accountable by mere adrenergic blockade since the restitution slope during sympathetic stimulation was flattened by metoprolol such that its gradient (1.85 ± 0.17) is less than that of baseline restitution slope without metoprolol (2.59 ± 0.09) (Figure 5.3). A closer scrutiny of the relative change in restitution slopes indicates that metoprolol does not alter vagal flattening of restitution slope at baseline compared to the controls but does abolish the prevailing sympathetic effect during sympatho-vagal interaction such that the vagal effect of flattening restitution slopes was similar to that at baseline (Figure 5.5). Future studies on additional antiarrhythmic mechanism of metoprolol are required.

5.5.3 Effect of Metoprolol on Ventricular Refractoriness during Sympatho-vagal Interaction

The antagonistic effect of sympathetic and vagal stimulation on ventricular ERP was well known. Sympathetic stimulation and adrenergic analogues have been shown to reduce both APD and ERP in experimental and human studies (Martins and Zipes, 1980, Nattel et al.,

1981, Morady et al., 1988b, Ng et al., 2007). Conversely, vagal stimulation and cholinergic analogues prolonged APD and ERP in rabbit and canine models (Martins and Zipes, 1980, Ng et al., 2007, Inoue and Zipes, 1987) as well as in humans (Ellenbogen et al., 1990). These findings cement the notion of the antagonistic nature of sympathetic and vagal nerve stimulation at the ventricular level.

As detailed in Chapter 4, accentuated antagonism with a dominant vagal effect was present in heart rate response at the atrial level validating historical studies (Levy, 1971, Levy and Zieske, 1969). Assessment of ventricular ERP during sympatho-vagal interaction suggested an absence of sympatho-vagal interaction in this electrophysiologic property. Whilst Morady et al suggested a degree of sympathetic tone is required for accentuated antagonism to exist in the ventricles (Morady et al., 1988a), studies in both canine model and humans demonstrated otherwise (Amlie et al., 1982, Prystowsky et al., 1981). In these studies, ventricular ERP was shortened by atropine after pre-treatment with propranolol or vice versa. This would suggest vagal effect in ERP prolongation is not reliant on the presence of sympathetic activity.

This study demonstrated that vagus nerve stimulation led to ERP prolongation at baseline, whilst sympathetic nerve stimulation shortened ERP from baseline ERP. In the controls, concurrent vagal stimulation during background sympathetic stimulation produced similar degree of ERP prolongation compared to that at baseline, reaffirming the findings in Chapter 4. The presence of metoprolol during sympatho-vagal interaction appears to simply nullify the effect of sympathetic-induced ERP shortening such that concurrent vagal stimulation during sympatho-vagal interaction resulted in ERP prolongation paralleled that at baseline. This implies that sympatho-vagal interaction, if any, is very minimal in ventricular refractoriness. This therefore is in accord with the findings in clinical studies (Prystowsky et al., 1981, Shimizu et al., 1994).

5.5.4 Is Sodium Acetate Responsible for Additional Antiarrhythmic Properties of Metoprolol beyond Adrenergic Blockade?

The findings of additional protective effects of metoprolol against ventricular fibrillation in isolated hearts perfused with acetate-free Tyrode solution raises the question of whether this antiarrhythmic property has been unmasksed by the absence of sodium acetate. Historically,

the role of sodium acetate as an energy substrate in contributing carbon atoms within the acetyl group to the citric acid cycle (Krebs cycle) is well established (Krebs HA, 1987, Lowenstein, 1969), forming the rationale for its inclusion in Tyrode solution used for perfusion of Langendorff heart preparations. It has been shown to increase citric acid cycle turnover by 67% in mammalian heart preparations (Randle et al., 1970). In isolated cell and tissue cultures, sodium acetate exerts variable effect on cardiac contractility. Whilst some studies demonstrated an increase in cardiac contractility (Liang and Lowenstein, 1978, Martin et al., 1998), others showed opposing results (Jacob et al., 1997, Kirkendol et al., 1978, Schooley et al., 2014). Interpretation of these results are not only confounded by poor understanding of its cellular mechanisms, but also by its *in vivo* vasodilatory effects (Liang and Lowenstein, 1978). Pertinently in these studies, acetate did not exert any effect on action potential duration (Williams et al., 1980, Schooley et al., 2014).

The link between sodium acetate and ventricular arrhythmias may lie in its effect of causing rapid mitochondrial Ca^{2+} uptake and osmotic swelling, specifically in both liver and cardiac mitochondria (Harris, 1978, Reed and Bygrave, 1975, Lehninger, 1974). The increased cardiac mitochondrial Ca^{2+} uptake was linked to reduced availability of Ca^{2+} for myofilament shortening, hence accounting for the depressant effect of sodium acetate on cardiac contractility (Schooley et al., 2014). From arrhythmia point of view, mitochondrial Ca^{2+} transport provides a buffering mechanism for cytosolic Ca^{2+} dynamics in cardiac myocytes (Williams et al., 2013, Drago et al., 2012) although its importance in Ca^{2+} handling remains debatable (O'Rourke and Blatter, 2009). With prolonged cytosolic Ca^{2+} elevations however, mitochondrial Ca^{2+} uptake could increase 1000 – 2000 folds (Williams et al., 2013). Notably, impaired mitochondrial Ca^{2+} handling resulted in Ca^{2+} transient alternans in cardiac myocytes, facilitating ventricular arrhythmias (Florea and Blatter, 2010). This concept was supported by the protective effect against ventricular arrhythmias by pharmacological inhibition of mitochondrial Ca^{2+} uptake using Ru360 in an ischaemia-reperfusion rodent heart model (Garcia-Rivas Gde et al., 2006). Furthermore, mitochondrial Ca^{2+} overload has been shown to lead to an increase in nitric oxide and reactive oxygen species (ROS) production in cardiac myocytes, perpetuating a vicious cycle of mitochondrial calcium overload and ROS production (Dedkova and Blatter, 2009). This promotes an environment of electrical instability, contributing to the onset of ventricular arrhythmias (Feissner et al., 2009).

In spite of the postulated pro-arrhythmic effect of sodium acetate through mitochondrial dysfunction, VFT in this study remained elevated in the presence of metoprolol at baseline, as well as during individual and concurrent autonomic nerve stimulations when rabbit hearts were perfused with acetate-containing Tyrode solution. Indeed, VFT changes in the controls and during metoprolol infusion are statistically insignificant between acetate-free and acetate-containing perfusates (Figure 5.11). This implies that the additional antifibrillatory property of metoprolol beyond adrenergic blockade is unlikely to be accountable by the absence of mitochondrial metabolic stress and perturbation of mitochondrial calcium dynamics from the use of acetate-free Tyrode solution.

5.6 Conclusion

This study demonstrated additional antifibrillatory effect and flattening of restitution slope beyond adrenergic blockade in the presence of metoprolol. In addition, metoprolol abolishes the prevailing sympathetic effect in ventricular fibrillation inducibility and restitution slope during sympatho-vagal interaction. The lack of sympatho-vagal interaction in ventricular refractoriness is also confirmed. Future studies on myocardial norepinephrine release as well as potential novel pharmacological properties of metoprolol are merited.

5.7 References

- ALMOTREFI, A. A., ABOUL-ENEIN, H. Y. & PREMKUMAR, L. S. 1989. Evaluation of the antifibrillatory activity of fluorinated derivatives of indenolol and nadolol in isolated rabbit and rat hearts: comparison with propranolol. *Arch Int Pharmacodyn Ther*, 301, 122-30.
- AMLIE, J. P., REFSUM, H. & LANDMARK, K. H. 1982. Prolonged ventricular refractoriness and action potential duration after beta-adrenoreceptor blockade in the dog heart *in situ*. *J Cardiovasc Pharmacol*, 4, 157-62.
- ANDERSON, K. P. 2003. Sympathetic nervous system activity and ventricular tachyarrhythmias: recent advances. *Ann Noninvasive Electrocardiol*, 8, 75-89.
- CAO, J. M., QU, Z., KIM, Y. H., WU, T. J., GARFINKEL, A., WEISS, J. N., KARAGUEUZIAN, H. S. & CHEN, P. S. 1999. Spatiotemporal heterogeneity in the induction of ventricular fibrillation by rapid pacing: importance of cardiac restitution properties. *Circ Res*, 84, 1318-31.
- CHOU, C. C., ZHOU, S., HAYASHI, H., NIHEI, M., LIU, Y. B., WEN, M. S., YEH, S. J., FISHBEIN, M. C., WEISS, J. N., LIN, S. F., WU, D. & CHEN, P. S. 2007. Remodelling of action potential and intracellular calcium cycling dynamics during subacute myocardial infarction promotes ventricular arrhythmias in Langendorff-perfused rabbit hearts. *J Physiol*, 580, 895-906.

- CIBIS-II INVESTIGATORS AND COMMITTEES 1999. The Cardiac Insufficiency Bisoprolol Study II (CIBIS-II): a randomised trial. *Lancet*, 353, 9-13.
- CORAM, W. M., OLSON, R. W., BEIL, M. E., CABOT, C. F. & WEISS, G. B. 1987. Effects of metoprolol, alone and in combination with lidocaine, on ventricular fibrillation threshold: comparison with atenolol, propranolol, and pindolol. *J Cardiovasc Pharmacol*, 9, 611-21.
- DEDKOVA, E. N. & BLATTER, L. A. 2009. Characteristics and function of cardiac mitochondrial nitric oxide synthase. *J Physiol*, 587, 851-72.
- DIXON, J. E., SHI, W., WANG, H. S., MCDONALD, C., YU, H., WYMORE, R. S., COHEN, I. S. & MCKINNON, D. 1996. Role of the Kv4.3 K⁺ channel in ventricular muscle. A molecular correlate for the transient outward current. *Circ Res*, 79, 659-68.
- DORIAN, P. 2005. Antiarrhythmic action of beta-blockers: potential mechanisms. *J Cardiovasc Pharmacol Ther*, 10 Suppl 1, S15-22.
- DRAGO, I., DE STEFANI, D., RIZZUTO, R. & POZZAN, T. 2012. Mitochondrial Ca²⁺ uptake contributes to buffering cytoplasmic Ca²⁺ peaks in cardiomyocytes. *Proc Natl Acad Sci USA*, 109, 12986-91.
- ELLENBOGEN, K. A., SMITH, M. L. & ECKBERG, D. L. 1990. Increased vagal cardiac nerve traffic prolongs ventricular refractoriness in patients undergoing electrophysiology testing. *Am J Cardiol*, 65, 1345-50.
- ENDRESEN, K. & AMLIE, J. P. 1990. Effects of propranolol on ventricular repolarization in man. *Eur J Clin Pharmacol*, 39, 123-5.
- FEISSNER, R. F., SKALSKA, J., GAUM, W. E. & SHEU, S. S. 2009. Crosstalk signaling between mitochondrial Ca²⁺ and ROS. *Front Biosci (Landmark Ed)*, 14, 1197-218.
- FENTON, F. & KARMA, A. 1998. Vortex dynamics in three-dimensional continuous myocardium with fiber rotation: Filament instability and fibrillation. *Chaos*, 8, 20-47.
- FENTON, F. H., CHERRY, E. M., HASTINGS, H. M. & EVANS, S. J. 2002. Multiple mechanisms of spiral wave breakup in a model of cardiac electrical activity. *Chaos*, 12, 852-892.
- FLOREA, S. M. & BLATTER, L. A. 2010. The role of mitochondria for the regulation of cardiac alternans. *Front Physiol*, 1, 141.
- GARCIA-RIVAS GDE, J., CARVAJAL, K., CORREA, F. & ZAZUETA, C. 2006. Ru360, a specific mitochondrial calcium uptake inhibitor, improves cardiac post-ischaemic functional recovery in rats in vivo. *Br J Pharmacol*, 149, 829-37.
- GARFINKEL, A., KIM, Y. H., VOROSHILOVSKY, O., QU, Z., KIL, J. R., LEE, M. H., KARAGUEUZIAN, H. S., WEISS, J. N. & CHEN, P. S. 2000. Preventing ventricular fibrillation by flattening cardiac restitution. *Proc Natl Acad Sci USA*, 97, 6061-6.
- HAO, S. C., CHRISTINI, D. J., STEIN, K. M., JORDAN, P. N., IWAI, S., BRAMWELL, O., MARKOWITZ, S. M., MITTAL, S. & LERMAN, B. B. 2004. Effect of beta-adrenergic blockade on dynamic electrical restitution in vivo. *Am J Physiol Heart Circ Physiol*, 287, H390-4.
- HARRIS, E. J. 1978. Anion/calcium ion ratios and proton production in some mitochondrial calcium ion uptakes. *Biochem J*, 176, 983-91.
- HJALMARSON, A., GOLDSTEIN, S., FAGERBERG, B., WEDEL, H., WAAGSTEIN, F., KJEKSHUS, J., WIKSTRAND, J., EL ALLAF, D., VITOVEC, J., ALDERSHVILE, J., HALINEN, M., DIETZ, R., NEUHAUS, K. L., JANOSI, A., THORGEIRSSON, G., DUNSELMAN, P. H., GULLESTAD, L., KUCH, J., HERLITZ, J., RICKENBACHER, P., BALL, S., GOTTLIEB, S. & DEEDWANIA, P. 2000. Effects of controlled-release metoprolol on total mortality, hospitalizations, and well-being in patients with

- heart failure: the Metoprolol CR/XL Randomized Intervention Trial in congestive heart failure (MERIT-HF). MERIT-HF Study Group. *JAMA*, 283, 1295-302.
- INOUE, H. & ZIPES, D. P. 1987. Changes in atrial and ventricular refractoriness and in atrioventricular nodal conduction produced by combinations of vagal and sympathetic stimulation that result in a constant spontaneous sinus cycle length. *Circ Res*, 60, 942-51.
- JACOB, A. D., ELKINS, N., REISS, O. K., CHAN, L. & SHAPIRO, J. I. 1997. Effects of acetate on energy metabolism and function in the isolated perfused rat heart. *Kidney Int*, 52, 755-60.
- JALIFE, J. 2000. Ventricular fibrillation: mechanisms of initiation and maintenance. *Annu Rev Physiol*, 62, 25-50.
- KALLA, M., BUB, G., BURTON, R., LARSEN, H., PATERSON, D. J. & HERRING, N. The sympathetic co-transmitter Neuropeptide Y is a novel pro-arrhythmic trigger even in the presence of maximal beta-blockade. *Autonomic Neuroscience: Basic and Clinical*, 192, 74.
- KIRKENDOL, R. L., PEARSON, J. E., BOWER, J. D. & HOLBERT, R. D. 1978. Myocardial depressant effects of sodium acetate. *Cardiovasc Res*, 12, 127-36.
- KOCH, W. J., LEFKOWITZ, R. J. & ROCKMAN, H. A. 2000. Functional consequences of altering myocardial adrenergic receptor signaling. *Annu Rev Physiol*, 62, 237-60.
- KREBS HA, W. P. 1987. Krebs' Citric Acid Cycle: Half a Century and Still Turning. In: KAY J, W. P., ed. Biochemical Society Symposia, 1987 London. Research Books, 25.
- LEE, M. H., LIN, S. F., OHARA, T., OMICHI, C., OKUYAMA, Y., CHUDIN, E., GARFINKEL, A., WEISS, J. N., KARAGUEUZIAN, H. S. & CHEN, P. S. 2001. Effects of diacetyl monoxime and cytochalasin D on ventricular fibrillation in swine right ventricles. *Am J Physiol Heart Circ Physiol*, 280, H2689-96.
- LEHNINGER, A. L. 1974. Role of phosphate and other proton-donating anions in respiration-coupled transport of Ca²⁺ by mitochondria. *Proc Natl Acad Sci USA*, 71, 1520-4.
- LEVY, M. N. 1971. Sympathetic-parasympathetic interactions in the heart. *Circ Res*, 29, 437-45.
- LEVY, M. N. & ZIESKE, H. 1969. Autonomic control of cardiac pacemaker activity and atrioventricular transmission. *J Appl Physiol*, 27, 465-70.
- LIANG, C. S. & LOWENSTEIN, J. M. 1978. Metabolic control of the circulation. Effects of acetate and pyruvate. *J Clin Invest*, 62, 1029-38.
- LO, C. F. & NUMANN, R. 1998. Independent and exclusive modulation of cardiac delayed rectifying K⁺ current by protein kinase C and protein kinase A. *Circ Res*, 83, 995-1002.
- LOWENSTEIN, J. M. 1969. *Methods in Enzymology, Volume 13: Citric Acid Cycle*, Academic Press.
- LU, T., LEE, H. C., KABAT, J. A. & SHIBATA, E. F. 1999. Modulation of rat cardiac sodium channel by the stimulatory G protein alpha subunit. *J Physiol*, 518 (Pt 2), 371-84.
- MARTIN, B. J., VALDIVIA, H. H., BUNGER, R., LASLEY, R. D. & MENTZER, R. M., JR. 1998. Pyruvate augments calcium transients and cell shortening in rat ventricular myocytes. *Am J Physiol*, 274, H8-17.
- MARTINS, J. B. & ZIPES, D. P. 1980. Effects of sympathetic and vagal nerves on recovery properties of the endocardium and epicardium of the canine left ventricle. *Circ Res*, 46, 100-10.
- MASUDA, Y. & LEVY, M. N. 1985. Heart rate modulates the disposition of neurally released norepinephrine in cardiac tissues. *Circ Res*, 57, 19-27.

- MEREDITH, I. T., BROUGHTON, A., JENNINGS, G. L. & ESLER, M. D. 1991. Evidence of a selective increase in cardiac sympathetic activity in patients with sustained ventricular arrhythmias. *N Engl J Med*, 325, 618-24.
- MESZAROS, J., RYDER, K. O. & HART, G. 1996. Transient outward current in catecholamine-induced cardiac hypertrophy in the rat. *Am J Physiol*, 271, H2360-7.
- MORADY, F., KOU, W. H., NELSON, S. D., DE BUITLEIR, M., SCHMALTZ, S., KADISH, A. H., TOIVONEN, L. K. & KUSHNER, J. A. 1988a. Accentuated antagonism between beta-adrenergic and vagal effects on ventricular refractoriness in humans. *Circulation*, 77, 289-97.
- MORADY, F., NELSON, S. D., KOU, W. H., PRATLEY, R., SCHMALTZ, S., DE BUITLEIR, M. & HALTER, J. B. 1988b. Electrophysiologic effects of epinephrine in humans. *J Am Coll Cardiol*, 11, 1235-44.
- MURPHY, B. J., ROGERS, J., PERDICHIZZI, A. P., COLVIN, A. A. & CATTERALL, W. A. 1996. cAMP-dependent phosphorylation of two sites in the alpha subunit of the cardiac sodium channel. *J Biol Chem*, 271, 28837-43.
- NAKAYA, H., KIMURA, S., NAKAO, Y. & KANNO, M. 1984. Effects of nifradilol (K-351) on the electrophysiological properties of canine cardiac tissues: comparison with propranolol and sotalol. *Eur J Pharmacol*, 104, 335-44.
- NATTEL, S., EULER, D. E., SPEAR, J. F. & MOORE, E. N. 1981. Autonomic control of ventricular refractoriness. *Am J Physiol*, 241, H878-82.
- NG, G. A., BRACK, K. E., PATEL, V. H. & COOTE, J. H. 2007. Autonomic modulation of electrical restitution, alternans and ventricular fibrillation initiation in the isolated heart. *Cardiovasc Res*, 73, 750-60.
- O'ROURKE, B. & BLATTER, L. A. 2009. Mitochondrial Ca²⁺ uptake: tortoise or hare? *J Mol Cell Cardiol*, 46, 767-74.
- OMICHI, C., ZHOU, S., LEE, M. H., NAIK, A., CHANG, C. M., GARFINKEL, A., WEISS, J. N., LIN, S. F., KARAGUEUZIAN, H. S. & CHEN, P. S. 2002. Effects of amiodarone on wave front dynamics during ventricular fibrillation in isolated swine right ventricle. *Am J Physiol Heart Circ Physiol*, 282, H1063-70.
- OPTHOF, T., DEKKER, L. R., CORONEL, R., VERMEULEN, J. T., VAN CAPELLE, F. J. & JANSE, M. J. 1993. Interaction of sympathetic and parasympathetic nervous system on ventricular refractoriness assessed by local fibrillation intervals in the canine heart. *Cardiovasc Res*, 27, 753-9.
- PACKER, M. 2001. Current role of beta-adrenergic blockers in the management of chronic heart failure. *Am J Med*, 110 Suppl 7A, 81S-94S.
- PATTERSON, E. & LUCCHESI, B. R. 1984. Antifibrillatory properties of the beta-adrenergic receptor antagonists, nadolol, sotalol, atenolol and propranolol, in the anesthetized dog. *Pharmacology*, 28, 121-9.
- PRYSTOWSKY, E. N., JACKMAN, W. M., RINKENBERGER, R. L., HEGER, J. J. & ZIPES, D. P. 1981. Effect of autonomic blockade on ventricular refractoriness and atrioventricular nodal conduction in humans. Evidence supporting a direct cholinergic action on ventricular muscle refractoriness. *Circ Res*, 49, 511-8.
- RANDLE, P. J., ENGLAND, P. J. & DENTON, R. M. 1970. Control of the tricarboxylate cycle and its interactions with glycolysis during acetate utilization in rat heart. *Biochem J*, 117, 677-95.
- REED, K. C. & BYGRAVE, F. L. 1975. A kinetic study of mitochondrial calcium transport. *Eur J Biochem*, 55, 497-504.

- RICCIO, M. L., KOLLER, M. L. & GILMOUR, R. F., JR. 1999. Electrical restitution and spatiotemporal organization during ventricular fibrillation. *Circ Res*, 84, 955-63.
- SAMIE, F. H., MANDAPATI, R., GRAY, R. A., WATANABE, Y., ZUUR, C., BEAUMONT, J. & JALIFE, J. 2000. A mechanism of transition from ventricular fibrillation to tachycardia : effect of calcium channel blockade on the dynamics of rotating waves. *Circ Res*, 86, 684-91.
- SCHOOLEY, J. F., NAMBOODIRI, A. M., COX, R. T., BUNGER, R. & FLAGG, T. P. 2014. Acetate transiently inhibits myocardial contraction by increasing mitochondrial calcium uptake. *BMC Physiol*, 14, 12.
- SCHWARTZ, P. J. 1998. The autonomic nervous system and sudden death. *Eur Heart J*, 19 Suppl F, F72-80.
- SHIMIZU, W., TSUCHIOKA, Y., KARAKAWA, S., NAGATA, K., MUKAI, J., YAMAGATA, T., MATSUURA, H., KAJIYAMA, G. & MATSUURA, Y. 1994. Differential effect of pharmacological autonomic blockade on some electrophysiological properties of the human ventricle and atrium. *Br Heart J*, 71, 34-7.
- TAGGART, P., SUTTON, P., CHALABI, Z., BOYETT, M. R., SIMON, R., ELLIOTT, D. & GILL, J. S. 2003. Effect of adrenergic stimulation on action potential duration restitution in humans. *Circulation*, 107, 285-9.
- THE CAST INVESTIGATORS 1989. Preliminary report: effect of encainide and flecainide on mortality in a randomized trial of arrhythmia suppression after myocardial infarction. The Cardiac Arrhythmia Suppression Trial (CAST) Investigators. *N Engl J Med*, 321, 406-12.
- THOMAS, D., KIEHN, J., KATUS, H. A. & KARLE, C. A. 2004. Adrenergic regulation of the rapid component of the cardiac delayed rectifier potassium current, I(Kr), and the underlying hERG ion channel. *Basic Res Cardiol*, 99, 279-87.
- WEISS, J. N., CHEN, P. S., QU, Z., KARAGUEUZIAN, H. S., LIN, S. F. & GARFINKEL, A. 2002. Electrical restitution and cardiac fibrillation. *J Cardiovasc Electrophysiol*, 13, 292-5.
- WILLIAMS, E. S., MIRRO, M. J. & BAILEY, J. C. 1980. Electrophysiological effects of ethanol, acetaldehyde, and acetate on cardiac tissues from dog and guinea pig. *Circ Res*, 47, 473-8.
- WILLIAMS, G. S., BOYMAN, L., CHIKANDO, A. C., KHAIRALLAH, R. J. & LEDERER, W. J. 2013. Mitochondrial calcium uptake. *Proc Natl Acad Sci U S A*, 110, 10479-86.
- ZHANG, L. M., WANG, Z. & NATTEL, S. 2002. Effects of sustained beta-adrenergic stimulation on ionic currents of cultured adult guinea pig cardiomyocytes. *Am J Physiol Heart Circ Physiol*, 282, H880-9.

Chapter 6

Myocardial Remodelling and Organ Congestion in Infarct-driven Heart Failure Model in Rabbits

Autonomic Modulation in a Rabbit Model of Heart Failure

Chapter 6: Myocardial Remodelling and Organ Congestion in Infarct-driven Heart Failure Model in Rabbits

6.1 Introduction

Myocardial remodelling, organ congestion and fluid retention are cardinal features in the clinical syndrome of heart failure. In particular, myocardial remodelling represents a milestone in heart failure progression, leading to myocardial dysfunction and adverse prognosis (McElmurray et al., 1999, Su et al., 1995, Swynghedauw, 1999, Cohn et al., 2000, Konstam et al., 2011). Myocardial remodelling is characterised by alteration in the cardiac structures involving chamber size, mass and dimension following cardiac insult or haemodynamic load associated with neuro-humoral activation. This phenomenon was first observed in animal studies before the findings were validated in patients with myocardial infarction or dilated cardiomyopathy (Chen et al., 2010, Nam et al., 2010, Nakamura et al., 2002). At the histological level, a plethora of pathological processes involving myocyte hypertrophy, myocyte apoptosis, myofibroblast proliferation and increased interstitial collagen deposition contribute to increased ventricular dimensions and mass as well as perturbation of the normal elliptical geometry (Hill, 2003). In both animals and humans, these processes of myocardial remodelling occur within hours following myocardial infarction (Giannuzzi et al., 2001, Korup et al., 1997, Weisman et al., 1985, Hochman and Bulkley, 1982).

Aside from pathological local structural changes following a cardiac insult, the ensuing left heart failure characterised by raised diastolic pressure led to increased back pressure in the pulmonary vasculature, contributing to pulmonary congestion. Left untreated, the right ventricle comes under strain resulting in overload and failure, ultimately leading to hepatic congestion and fluid retention (Harris, 1983, Parmley, 1989). These were further driven by activation of the renin-angiotensin-aldosterone system responsible for both sodium and water retention, hence perpetuating the vicious cycle of heart failure progression (Parmley, 1989).

6.2 Aim

The study aims to investigate the degree of cardiac remodelling and performance by transthoracic echocardiography on rabbits undergoing both coronary ligation and sham surgeries. The extent of organ congestion was assessed by measuring dry weights of hearts, lungs and livers isolated from both groups of rabbits at the terminal experiments 8 weeks post-operatively. Additionally, ex-vivo cardiac scar quantification was performed with cardiac magnetic resonance imaging on a number of hearts following the terminal experiments.

6.3 Method

6.3.1 Transthoracic Echocardiography

The methodology of transthoracic echocardiography is described in detail in Chapter 3.3. In this study, the rabbits were divided into 2 groups: one which had undergone coronary ligation surgeries (HF group, $n = 13$) and one sham procedures (SHM group, $n = 12$). Transthoracic echocardiography was performed on both groups of rabbits 1 – 2 weeks prior to their corresponding terminal experiments, i.e. at week 6 – 7 following the initial surgeries. This were performed after the rabbits were sedated and anaesthetised to allow for a 40 – 45-minute imaging procedure. Rabbits were imaged at the left lateral position for optimal imaging. The following echocardiographic parameters were measured:-

1. left atrial systolic diameter (LAD)
2. end-diastolic left ventricular diameter (LVEDD)
3. interventricular septal thickness (IVS)
4. left ventricular posterior wall thickness (LVPW)
5. end-diastolic and end-systolic endocardial area

With these measurements, fractional area change (FAC) and ejection fraction (EF) can be calculated.

6.3.2 Measurement of Organ Weights

The rationale and methodology of measuring organ weights are detailed in Chapter 3.5. Following euthanasia of rabbits at the terminal experiments 8 weeks following coronary ligation or sham procedures, the livers and lungs were excised and blotted to remove excess blood before their wet weights were recorded. These were then placed in an oven heated to 70 °C and dry weights were recorded once the weights, measured weekly, plateau off. The wet and dry weights of hearts were measured using the same procedure after they were excised from the ribcage following completion of the terminal experiments.

6.3.3 Ex-vivo Cardiac Magnetic Resonance Imaging

The technical details of magnetic resonance imaging were described in Chapter 3.5.2.2. At the end of terminal experiments, five hearts from the HF group and three from the shams group were excised from the residual ribcage, with its great vessels preserved. These whole hearts were fixed with 4% paraformaldehyde overnight before being placed in test tubes containing proton-free fluid, Fomblin-Y (Silma Aldrich). MRI scans were performed on these hearts using a 9.4T Agilent scanner (Agilent Technologies, Santa Clare, CA, USA). Radiofrequency transmission and reception were achieved with a 40mm millipede transmit/receive RF coil. The rabbit hearts were positioned at the isocenter of the magnet and located with fast gradient echo scan. 3D gradient echo shimming of first and second order shims were performed over the entire heart and shim quality was confirmed using point resolved spectroscopy (PRESS) of the water peak.

T2-weighted images were acquired using a fast spin echo (FSE) sequence with TR/TE = 3000/40ms, 30 x 30mm field of view (256 x 256 matrix), 36 x 1mm coronal slices and 3 signal averages (scan duration = 9mins 42sec). The resultant images were used to generate 2D slice montage representations of each heart (Figure 6.1). For accurate quantification of scar volume, T1-weighted images were acquired using a 3-dimensional magnetization prepared rapid gradient-echo (MP-RAGE) sequence with TR/TE = 6.5/3.3ms, 40 x 30 x 30mm field of view (256 x 192 x 192 matrix) and 2

signal averages (scan duration = 57mins 39sec). Scar volume was calculated using manual region of interest (ROI) analysis in 3D Slicer (<http://www.slicer.org>).

Figure 6.1 Ex-vivo T2-weighted 2D slice montage representations of rabbit hearts eight weeks following coronary ligation (Figure 6.1A) or sham procedures (Figure 6.1B)

Figure 6.1A: HF group

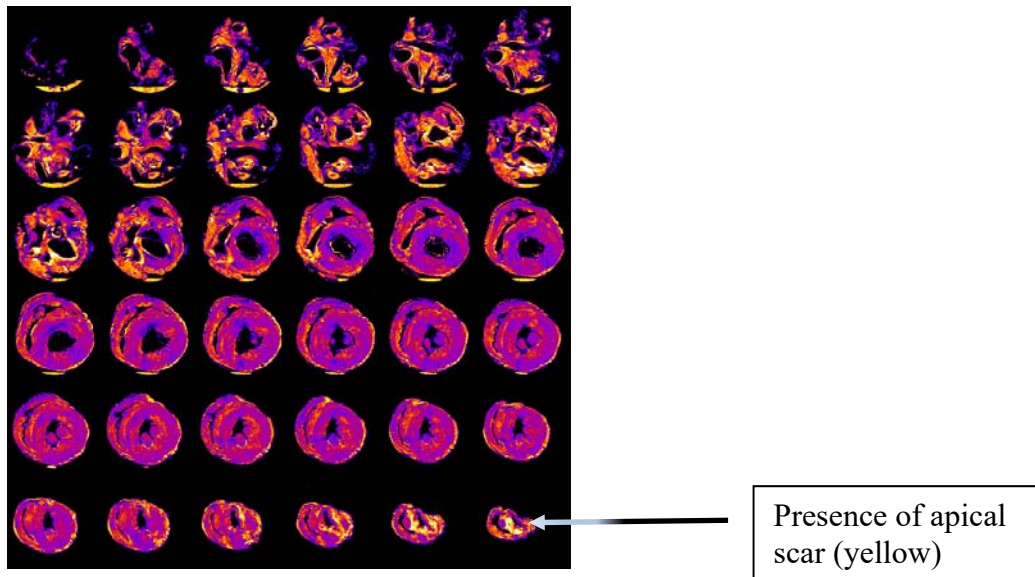
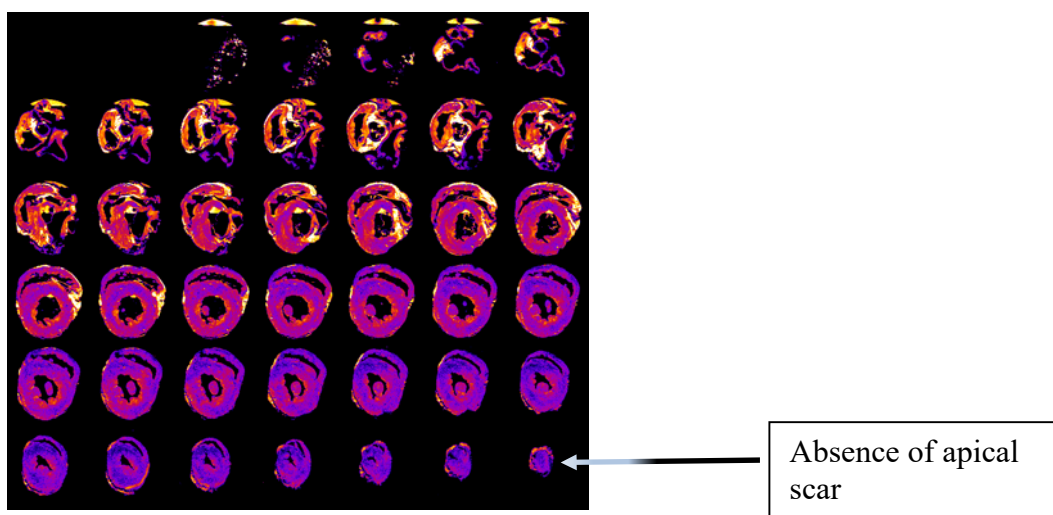


Figure 6.1B: SHM group



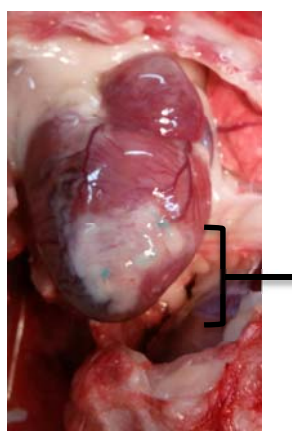
6.4 Results

6.4.1 Cardiac Remodelling

Data in this study suggest that myocardial infarction caused by coronary ligation led to low-output heart failure in the rabbits. Echocardiographic evaluations revealed a significant degree of left ventricular systolic impairment in the HF group as reflected by the lower ejection fraction as well as reduced fractional shortening and fractional area change (Table 6.1). Enlargement of cardiac chambers was evident in the HF group as measured by the left atrial systolic diameter, left ventricular end-diastolic diameter and volume. Relevantly, there was echocardiographic evidence of thinning of the interventricular septum, resulting in an eccentricity in the septum:posterior wall thickness ratio. This suggests that both regional and global structural remodelling occurred in this heart failure model over the 6 weeks following coronary ligation. Indeed, during the terminal experiments when the hearts were procured at 8 weeks, visible apical fibrosis was frequently found on the left ventricular epicardial surface in the HF group (Figure 6.2).

Further analyses demonstrated a significant correlation between structural remodelling and left ventricular performance. In this study, both left ventricular end-diastolic diameter ($r = -0.76$, $p < 0.001$) (Figure 6.3) and left atrial systolic diameter ($r = -0.77$, $p < 0.001$) (Figure 6.4) were found to be correlated with ejection fraction.

Figure 6.2 Gross appearance of rabbit heart eight weeks after coronary ligation



Fibrotic appearance on the apex of left ventricular epicardial surface

Table 6.1 Echocardiographic data of rabbits in heart failure (HF) and sham (SHM) group

Echocardiographic Measurements	HF	SHM
Left ventricular ejection fraction (%) by M-mode	35.19 ± 1.95	$66.62 \pm 2.92^{***}$
Fractional shortening (%) by M-mode	13.57 ± 0.87	$31.26 \pm 2.10^{***}$
Diastolic interventricular septum (IVS) thickness (mm)	2.04 ± 0.12	$2.84 \pm 0.32^*$
Diastolic left ventricular posterior wall (LVPW) thickness (mm)	2.64 ± 0.08	2.63 ± 0.24
Diastolic IVS:LVPW thickness ratio	0.81 ± 0.04	$1.06 \pm 0.04^{***}$
Left ventricular end-diastolic diameter (LVEDD) (mm)	13.37 ± 0.31	$10.68 \pm 0.39^{***}$
Diastolic left ventricular volume (uL)	808.3 ± 88.07	$773.97 \pm 86.58^*$
Left atrial systolic diameter (LAD) (mm)	8.60 ± 0.14	$7.57 \pm 0.24^{**}$
Diastolic endocardial area (mm^2)	136.92 ± 8.81	$111.57 \pm 6.59^*$
Fractional area change (FAC) (%)	27.56 ± 3.47	$55.20 \pm 1.77^{***}$

*P ≤ 0.05; **P ≤ 0.01; ***P ≤ 0.001

Figure 6.3 Correlation between left ventricular end-diastolic diameter (LVEDD) and left ventricular ejection fraction (EF)

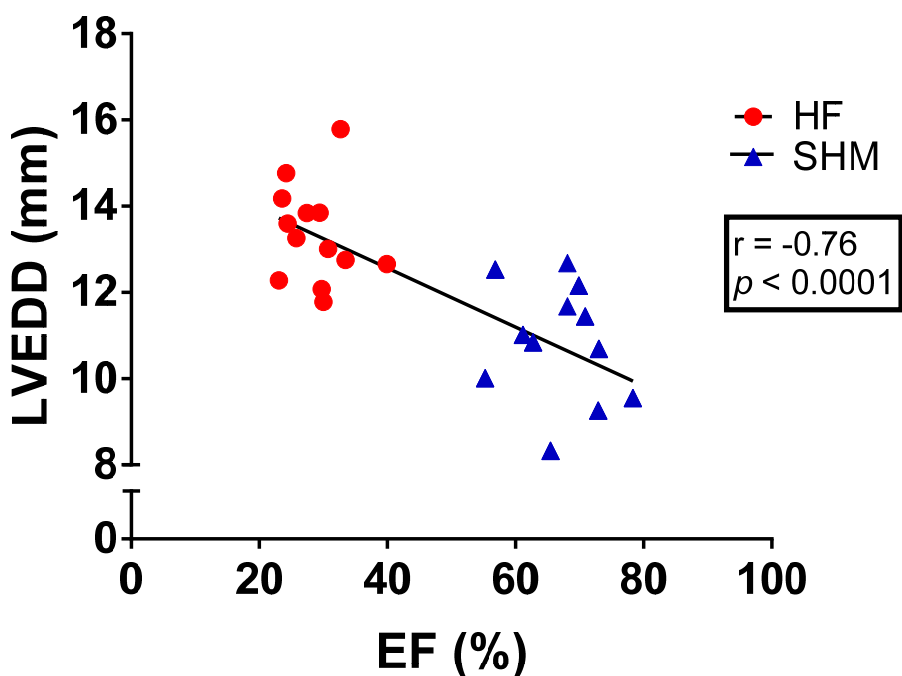
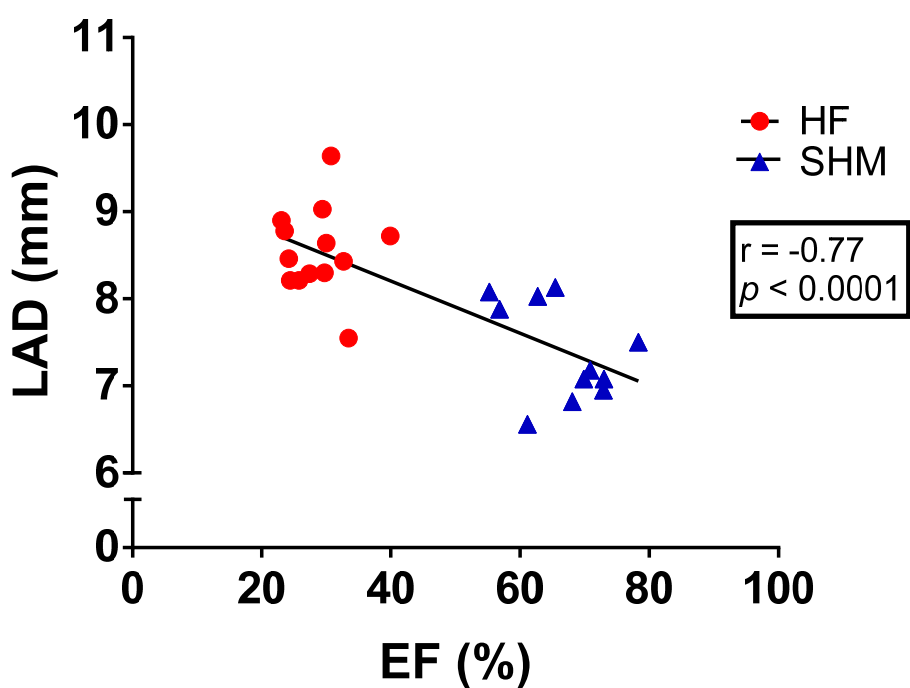


Figure 6.4 Correlation between left atrial systolic diameter (LAD) and left ventricular ejection fraction (EF)



6.4.2 Organ Congestion

Organ weights were in general heavier in the HF group compared to the shams (Table 6.2). Both the wet and dry weight of the hearts in the HF group were significantly higher than those in the shams. When corrected against body weight, the dry weight of the hearts was significantly correlated with the ejection fraction measured by echocardiography ($r = -0.64$; $p < 0.001$) (Figure 6.5), suggesting a strong correlation between cardiac remodelling and left ventricular dysfunction in parallel with the findings of significant correlation shown in relevant echocardiographic parameters (Figure 6.3 and 6.4).

In addition, peripheral organs underwent structural changes in this heart failure model. The wet weights of both lungs and livers were significantly higher in the HF group compared to the shams. In contrast, there was no difference in dry weight for these two organs, implying that the increased liver and lung weights are attributable to fluid congestion prior to the drying process. When the wet weights of the liver and lung are corrected to body weights respectively, there is a demonstrable correlation between these weights and ejection fraction (liver: $r = -0.71$; $p < 0.01$; lung: $r = -0.67$; $p < 0.01$) (Figure 6.5).

Table 6.2 Body weights as well as wet/dry weights of hearts, livers and lungs for rabbits in heart failure (HF) and sham (SHM) groups

Weights		HF	SHM
Body weight (kg)		3.65 ± 0.10	3.73 ± 0.08
Heart weight (g)	Wet	13.19 ± 0.34	$10.61 \pm 0.71^*$
	Dry	2.29 ± 0.11	$1.98 \pm 0.06^*$
Liver weight (g)	Wet	98.63 ± 3.17	$76.48 \pm 3.09^{***}$
	Dry	30.05 ± 0.77	27.11 ± 1.99
Lung weight (g)	Wet	13.52 ± 0.78	$11.61 \pm 0.25^*$
	Dry	2.18 ± 0.77	2.01 ± 0.06

*P ≤ 0.05; **P ≤ 0.01; ***P ≤ 0.001

Figure 6.5 Correlation between left ventricular ejection fraction (EF) with various organ weights corrected by body weight: heart dry weight (Figure 6.5A), liver wet weight (Figure 6.5B) and lung wet weight (Figure 6.5C)

Figure 6.5A

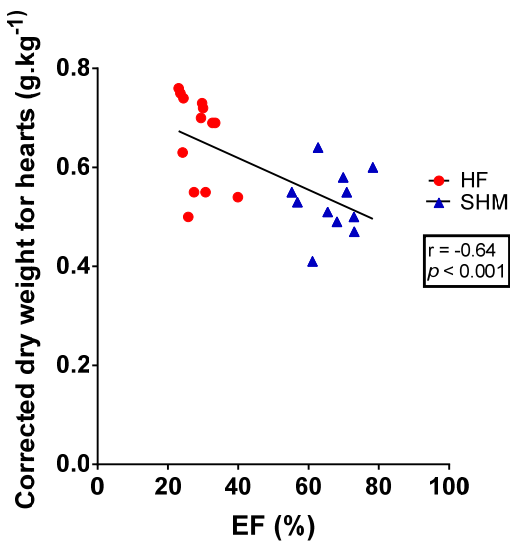


Figure 6.5B

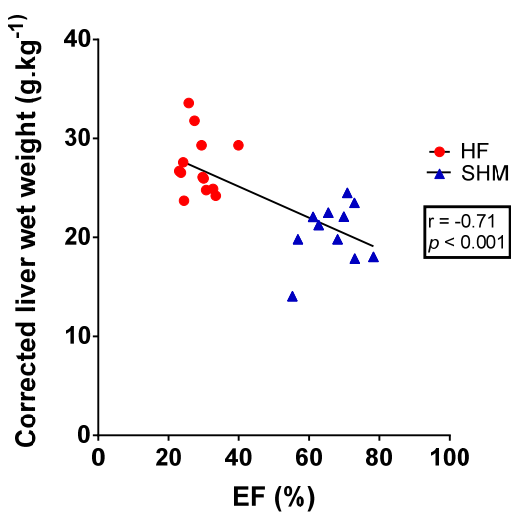
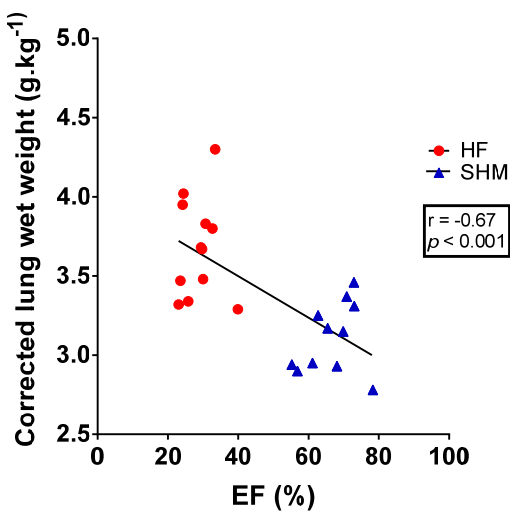


Figure 6.5C



6.4.3 Ex-vivo Left Ventricular Scar Quantification

Ex-vivo cardiac MRI consistently demonstrated the absence of scar in the left ventricles of the sham animals ($n = 3$) (Table 6.3). Out of the five hearts in the HF group, three hearts showed quantifiable left ventricular scar (270.72 ± 33.45 mL). One heart (MI 44) had a negligible scar volume. Scar quantification in the remaining one heart of the HF group was not possible due to unclear images. These MRI data suggest that coronary ligation reliably produced measurable scarring in the left ventricle, with resultant low-output heart failure.

Table 6.3 Scar volume measured by ex-vivo cardiac magnetic resonance imaging

Heart Specimen ID	Visibility of Lesion on MRI	Scar Volume (mL)
MI 42	Yes	302.11
MI 44	Not clear	N/A
MI 46	Yes	18.99
MI 47	Yes	189.49
MI 48	Yes	320.56
Sham 36	No	0
Sham 40	No	0
Sham 41	No	0

6.5 Discussion

Ligation of left circumflex artery in rabbits produces extensive myocardial necrosis and fibrosis, with resultant reduction in both regional and global myocardial contractile performance (Buckberg et al., 2008, Sedmera et al., 1999). Subsequently myocardium undergoes structurally remodelling, leading to increased ventricular stiffness. At the histological level, widespread characteristic cellular processes occur not only at the

infarcted myocardium, but also in the remote non-infarcted myocardium (Beltrami et al., 1994, Anversa et al., 1991, Ng et al., 1998). In particular, myocyte apoptosis is found to occur in a time-sensitive manner not only in the expected infarct area and border zone, but also in the non-infarct area of the heart in both rats (Zhu et al., 2001) and humans (Olivetti et al., 1997). Indeed, increased myocyte apoptosis in the remote non-infarcted area has been correlated with structural remodelling in rabbits (Qin et al., 2005) and mice (Palojoki et al., 2001). Similar correlation has been established in clinical studies with strong association between this cellular phenomenon and left ventricular dilatation as well as left ventricular dysfunction in patients with ischaemic cardiomyopathy (Baldi et al., 2002, Qin et al., 2005) and dilated cardiomyopathy (Akyurek et al., 2001).

Echocardiographic data in this study provides valuable insights in both regional and global ventricular function in the rabbit heart failure model following coronary ligation. The decreased septal thickness in relation to left ventricular posterior wall thickness in the HF group as reflected by the absolute measurements and significantly reduced ratio between the thickness of septal and posterior walls provides imaging evidence of regional wall motion abnormality induced by apical infarct (Table 6.1). The presence of scar tissue visible to the naked eyes (Figure 6.2) and cardiac MRI (Table 6.3) also contributes to limitation of the left ventricular wall motion. Furthermore, the increased end-diastolic volume and endocardial area in the infarcted heart signifies increased left ventricular radius, producing a change in ventricular geometry in which the heart assumes a more spherical shape (Buckberg et al., 2004).

A key evidence of heart failure developing in the HF group is the significantly lower ejection fraction when compared to the shams (Table 6.1). In non-diseased heart, the left ventricle displays forceful contractions during systole, expelling two thirds of the intra-cardiac blood volume present at end-diastole (Milnor, 1989). In the presence of a myocardial infarction, the healthy myocardium is replaced by fibrotic tissue in the apical region (Figure 6.2) with consequent impaired contractility in this region. The heart develops an adaptive response in the form of increased basal contractile force and ventricular mass, the latter being evident from the increased wet and dry weight of hearts in the HF group (Table 6.2). Pertinently, the ability of increasing myocardial

mass to compensate functional load is highly characteristic of mammalian hearts (Hamrell B.B.).

Infarct size and transmurality exert a deterministic influence on both regional and global left ventricular function. In this study, out of the five ex-vivo hearts in the HF group, four demonstrated a quantifiable scar in the apical region when imaged by MRI whereas in the sham group, no myocardial scar was detected (Table 6.3). Ligation of circumflex artery produced a diffuse apical infarct demonstrable by cardiac MRI, an example of which was shown in Figure 6.1A. Visibly the isolated rabbit hearts from the HF group showed a diffuse fibrotic appearance at the apices (Figure 6.2). In contrast, punctate infarcts, which suggest small-vessel disease or collateral circulation, were not observed in the five ex-vivo hearts in the HF group on cardiac MRI, validating the homogeneity of infarcts produced by coronary ligation and affirming the absence of collateral circulation in rabbit hearts. Myocardial scarring, as demonstrated by cardiac MRI in this study, causes impairment of myocardial contractility, thereby leading to reduced stroke volume and ejection fraction, as reflected by the lower ejection fraction on echocardiography in this study. This relationship between myocardial scar on MRI and left ventricular function on transthoracic echocardiography is in parallel with that in humans (Hamrell B.B.).

Structural and hemodynamic maladaptation in heart failure are not confined to the infarct region, but extends to non-infarct regions of the left ventricle as well as the right ventricle (Olivetti et al., 1994). As the ventricular architecture becomes distorted with a more spherical geometry, the left ventricle becomes stiffer. There is increased intraventricular pressure to sustain cardiac contractile force (Goto et al., 1986). In response to a reduced contractile force in the apex, basal contractile force increases with resultant raised back pressure into left atrium, causing mitral regurgitation and increased left atrial pressure (Dal-Bianco et al., 2009) as well as pulmonary congestion, as suggested by the increased left atrial systolic diameter (Table 6.1) and increased lung wet weights (Table 6.2). Mitral regurgitation in this context, is a results of leaflet tethering and displaced papillary muscles in a dilated left ventricle, a mechanism which has been demonstrated in both experimental and clinical studies (Dowell et al., 1979, Buckberg et al., 2004). It is also conceivable that myocardial infarction leads to

papillary ischaemia, providing a more direct contributory role in mitral regurgitation and hence raised left atrial pressure. Ultimately the increased back pressure in left atrium extends to the right heart. This causes right heart failure manifesting as hepatic congestion demonstrable with the significantly higher liver wet weights in the HF group (Table 6.2). The strong correlations between various organ weights with ejection fraction are in support of this postulated mechanism (Figure 6.5) and mirrored clinical phenotypes of heart failure with background ischaemic heart disease in humans (Parmley, 1989).

The use of two imaging modalities in this study provides valuable insights in establishing the structure-function relationship (Figure 6.3 and 6.4) in a myocardial-infarction heart failure model. Future studies using more comprehensive *in vivo* cardiac MRI protocols, such as delayed gadolinium enhancement, myocardial perfusion, and myocardial tagging among others, in this heart failure model will complement echocardiographic functional studies and enhance understanding of cardiac remodelling. Immunohistochemical studies of cardiac tissue as well as autonomic nerves will provide cellular clues to this remodelling process in addition to shedding further lights on the morphology of apical infarcts observed on cardiac MRI.

6.6 Conclusion

Coronary ligation in rabbits causes a heart failure phenotype manifesting as structural remodellings of the heart and such peripheral organs as lungs and livers. These structural remodellings are significantly correlated with impairment of left ventricular function, supporting a structure-function relationship.

6.7 References

- AKYUREK, O., AKYUREK, N., SAYIN, T., DINCER, I., BERKALP, B., AKYOL, G., OZENCI, M. & ORAL, D. 2001. Association between the severity of heart failure and the susceptibility of myocytes to apoptosis in patients with idiopathic dilated cardiomyopathy. *Int J Cardiol*, 80, 29-36.
- ANVERSA, P., OLIVETTI, G. & CAPASSO, J. M. 1991. Cellular basis of ventricular remodeling after myocardial infarction. *Am J Cardiol*, 68, 7d-16d.
- BALDI, A., ABBATE, A., BUSSANI, R., PATTI, G., MELFI, R., ANGELINI, A., DOBRINA, A., ROSSILO, R., SILVESTRI, F., BALDI, F. & DI SCIASCIO, G. 2002.

- Apoptosis and post-infarction left ventricular remodeling. *J Mol Cell Cardiol*, 34, 165-74.
- BELTRAMI, C. A., FINATO, N., ROCCO, M., FERUGLIO, G. A., PURICELLI, C., CIGOLA, E., QUAINI, F., SONNENBLICK, E. H., OLIVETTI, G. & ANVERSA, P. 1994. Structural basis of end-stage failure in ischemic cardiomyopathy in humans. *Circulation*, 89, 151-63.
- BUCKBERG, G., HOFFMAN, J. I., MAHAJAN, A., SALEH, S. & COGHLAN, C. 2008. Cardiac mechanics revisited: the relationship of cardiac architecture to ventricular function. *Circulation*, 118, 2571-87.
- BUCKBERG, G. D., WEISFELDT, M. L., BALLESTER, M., BEYAR, R., BURKHOFF, D., COGHLAN, H. C., DOYLE, M., EPSTEIN, N. D., GHARIB, M., IDEKER, R. E., INGELS, N. B., LEWINTER, M. M., MCCULLOCH, A. D., POHOST, G. M., REINLIB, L. J., SAHN, D. J., SOPKO, G., SPINALE, F. G., SPOTNITZ, H. M., TORRENT-GUASP, F. & SHAPIRO, E. P. 2004. Left ventricular form and function: scientific priorities and strategic planning for development of new views of disease. *Circulation*, 110, e333-6.
- CHEN, X., SALA-MERCADO, J. A., HAMMOND, R. L., ICHINOSE, M., SOLTANI, S., MUUKAMALA, R. & O'LEARY, D. S. 2010. Dynamic control of maximal ventricular elastance via the baroreflex and force-frequency relation in awake dogs before and after pacing-induced heart failure. *Am J Physiol Heart Circ Physiol*, 299, H62-9.
- COHN, J. N., FERRARI, R. & SHARPE, N. 2000. Cardiac remodeling--concepts and clinical implications: a consensus paper from an international forum on cardiac remodeling. Behalf of an International Forum on Cardiac Remodeling. *J Am Coll Cardiol*, 35, 569-82.
- DAL-BIANCO, J. P., AIKAWA, E., BISCHOFF, J., GUERRERO, J. L., HANDSCHUMACHER, M. D., SULLIVAN, S., JOHNSON, B., TITUS, J. S., IWAMOTO, Y., WYLIE-SEARS, J., LEVINE, R. A. & CARPENTIER, A. 2009. Active adaptation of the tethered mitral valve: insights into a compensatory mechanism for functional mitral regurgitation. *Circulation*, 120, 334-42.
- DOWELL, R. T., HAITHCOAT, J. L. & HASSE, E. M. 1979. Pressure-induced cardiac enlargement in neonatal and adult rats. Left ventricular weight and hemodynamic responses during the early adaptive period. *Tex Rep Biol Med*, 39, 139-51.
- GIANNUZZI, P., TEMPORELLI, P. L., BOSIMINI, E., GENTILE, F., LUCCI, D., MAGGIONI, A. P., TAVAZZI, L., BADANO, L., STOIAN, I., PIAZZA, R., HEYMAN, I., LEVANTESI, G., CERVESATO, E., GERACI, E. & NICOLOSI, G. L. 2001. Heterogeneity of left ventricular remodeling after acute myocardial infarction: results of the Gruppo Italiano per lo Studio della Sopravvivenza nell'Infarto Miocardico-3 Echo Substudy. *Am Heart J*, 141, 131-8.
- GOTO, Y., SUGA, H., YAMADA, O., IGARASHI, Y., SAITO, M. & HIRAMORI, K. 1986. Left ventricular regional work from wall tension-area loop in canine heart. *Am J Physiol*, 250, H151-8.
- HAMRELL B.B., A. N. R. Cellular basis of the mechanical properties of hypertrophied myocardium. In: FOZZARD H.A., H. E., JENNINGS R.B., KATZ A.M., MORGAN H.E. (ed.) *The heart and cardiovascular system*. New York (NY): Raven Press.
- HARRIS, P. 1983. Evolution and the cardiac patient. *Cardiovasc Res*, 17, 437-45.

- HILL, J. A. 2003. Electrical remodeling in cardiac hypertrophy. *Trends Cardiovasc Med*, 13, 316-22.
- HOCHMAN, J. S. & BULKLEY, B. H. 1982. Expansion of acute myocardial infarction: an experimental study. *Circulation*, 65, 1446-50.
- KONSTAM, M. A., KRAMER, D. G., PATEL, A. R., MARON, M. S. & UDELSON, J. E. 2011. Left ventricular remodeling in heart failure: current concepts in clinical significance and assessment. *JACC Cardiovasc Imaging*, 4, 98-108.
- KORUP, E., DALSGAARD, D., NYVAD, O., JENSEN, T. M., TOFT, E. & BERNING, J. 1997. Comparison of degrees of left ventricular dilation within three hours and up to six days after onset of first acute myocardial infarction. *Am J Cardiol*, 80, 449-53.
- MCELMURRAY, J. H., 3RD, MUKHERJEE, R., NEW, R. B., SAMPSON, A. C., KING, M. K., HENDRICK, J. W., GOLDBERG, A., PETERSON, T. J., HALLAK, H., ZILE, M. R. & SPINALE, F. G. 1999. Angiotensin-converting enzyme and matrix metalloproteinase inhibition with developing heart failure: comparative effects on left ventricular function and geometry. *J Pharmacol Exp Ther*, 291, 799-811.
- MILNOR, W. R. 1989. *Hemodynamics*, Baltimore (MD), Williams and Wilkins.
- NAKAMURA, R., EGASHIRA, K., MACHIDA, Y., HAYASHIDANI, S., TAKEYA, M., UTSUMI, H., TSUTSUI, H. & TAKESHITA, A. 2002. Probucol attenuates left ventricular dysfunction and remodeling in tachycardia-induced heart failure: roles of oxidative stress and inflammation. *Circulation*, 106, 362-7.
- NAM, M. C., ARAVIND, A., CHAN, K., JAMES, S. & BROWN, N. 2010. Tachycardia-induced cardiomyopathy- a fully reversible phenomenon. *Am Heart Hosp J*, 8, E115-7.
- NG, G. A., COBBE, S. M. & SMITH, G. L. 1998. Non-uniform prolongation of intracellular Ca²⁺ transients recorded from the epicardial surface of isolated hearts from rabbits with heart failure. *Cardiovasc Res*, 37, 489-502.
- OLIVETTI, G., ABBI, R., QUAINI, F., KAJSTURA, J., CHENG, W., NITAHARA, J. A., QUAINI, E., DI LORETO, C., BELTRAMI, C. A., KRAJEWSKI, S., REED, J. C. & ANVERSA, P. 1997. Apoptosis in the failing human heart. *N Engl J Med*, 336, 1131-41.
- OLIVETTI, G., MELISSARI, M., BALBI, T., QUAINI, F., SONNENBLICK, E. H. & ANVERSA, P. 1994. Myocyte nuclear and possible cellular hyperplasia contribute to ventricular remodeling in the hypertrophic senescent heart in humans. *J Am Coll Cardiol*, 24, 140-9.
- PALOJOKI, E., SARASTE, A., ERIKSSON, A., PULKKI, K., KALLAJOKI, M., VOIPIO-PULKKI, L. M. & TIKKANEN, I. 2001. Cardiomyocyte apoptosis and ventricular remodeling after myocardial infarction in rats. *Am J Physiol Heart Circ Physiol*, 280, H2726-31.
- PARMLEY, W. W. 1989. Pathophysiology and current therapy of congestive heart failure. *Journal of the American College of Cardiology*, 13, 771-785.
- QIN, F., LIANG, M. C. & LIANG, C. S. 2005. Progressive left ventricular remodeling, myocyte apoptosis, and protein signaling cascades after myocardial infarction in rabbits. *Biochim Biophys Acta*, 1740, 499-513.
- SEDMERA, D., PEXIEDER, T., RYCHTEROVA, V., HU, N. & CLARK, E. B. 1999. Remodeling of chick embryonic ventricular myoarchitecture under experimentally changed loading conditions. *Anat Rec*, 254, 238-52.

- SU, J. B., BARBE, F., LAPLACE, M., CROZATIER, B. & HITTINGER, L. 1995. Regional alterations of left ventricular contraction and inotropic reserve in conscious dogs with heart failure. *Cardiovasc Res*, 30, 848-56.
- SWYNGHEDAUW, B. 1999. Molecular mechanisms of myocardial remodeling. *Physiol Rev*, 79, 215-62.
- WEISMAN, H. F., BUSH, D. E., MANNISI, J. A. & BULKLEY, B. H. 1985. Global cardiac remodeling after acute myocardial infarction: a study in the rat model. *J Am Coll Cardiol*, 5, 1355-62.
- ZHU, Y. Z., ZHU, Y. C., WANG, Z. J., LU, Q., LEE, H. S. & UNGER, T. 2001. Time-dependent apoptotic development and pro-apoptotic genes expression in rat heart after myocardial infarction. *Jpn J Pharmacol*, 86, 355-8.

Chapter 7

Characterisation of Autonomic Electrocardiology in Isolated Rabbit Heart Failure Model

Under Review for Consideration for Publication

Autonomic Modulation in a Rabbit Model of Heart Failure

Chapter 7: Characterisation of Autonomic Electrocardiology in Isolated Rabbit Heart Failure Model

7.1 Introduction

Heart failure represents a common clinical pathway as a consequence of various cardiac insults, most commonly myocardial infarction but also hypertension, valvular defects, dilated cardiomyopathy, hypertrophic cardiomyopathy, tachycardia-dependent cardiomyopathy, toxic/nutritional cardiomyopathy and so forth. In spite of the diversity of possible pathologic underpinnings, heart failure is universally regarded as a clinical syndrome of a mismatch of cardiac contractility and metabolic demands of peripheral organs (Coronel et al., 2001). In the case of a myocardial infarction, myocardial loss with the resultant impaired contractility are compensated by cardiac hypertrophy before heart failure ensues.

The global incidence of heart failure is reaching epidemic level especially in the industrialised world, with annual mortality approaching 50% in advanced disease (Roger et al., 2012). Although as much as 50% of the heart failure-related mortality can be attributed to pump failure, arrhythmias account for the remainder cause of death in this disease (Tomaselli and Zipes, 2004). This has led to the emergence of implantable device therapy, specifically implantable cardioverter-defibrillator (ICD) as a key strategy to abort malignant arrhythmias. Nonetheless, arrhythmic death remains a major cause of death in heart failure especially in the milder forms of the disease (Hjalmarson and Fagerberg, 2000). This can be accountable by the complex mechanism of arrhythmogenesis in heart failure which represents an interplay between arrhythmogenic triggers and electrophysiological substrates. The overall electrophysiological changes in heart failure is therefore multitude in nature, and highly dependent on the underlying pathological processes driving heart failure. This comprises ion channel remodelling, abnormal calcium handling, extracellular matrix remodelling, the process of fibrosis, over-activation of neuro-hormonal axis as well as structural changes in the form of dilatation, stretch and geometry distortion. The scientific landscape in this arena was further complicated by incongruent results from different animal models of heart failure, including those of infarction and pacing-

induced canine models (Issa et al., 2005), pressure- or volume-overload rabbit models (Vermeulen et al., 1994, Pogwizd, 1995), and gene-mutation murine model (van Oort et al., 2011).

Dysautonomia characterised by sympathetic over-activation and parasympathetic attenuation in heart failure plays a substantial modulatory role in arrhythmogenesis and the aforementioned electrophysiological changes. The autonomic effects on cardiac electrophysiology are well known with sympathetic nerves exerting positive effects on heart rate, atrio-ventricular conduction and contractile function whereas the parasympathetic system having the opposing effects. More importantly, autonomic nervous system plays a central role in initiation of ventricular fibrillation. Preclinical (Schwartz et al., 1988, De Ferrari et al., 1991, Billman et al., 1982, Cerati and Schwartz, 1991) and clinical (Nolan et al., 1998, La Rovere et al., 2009, La Rovere et al., 1998) studies have consistently demonstrated causal link between autonomic tone measured as heart rate variability (HRV) and baroreceptor reflex sensitivity (BRS) with fatal ventricular arrhythmias. As such it is unsurprising that the dysautonomia in heart failure leads to impaired neurocardiological control and ultimately increased susceptibility for lethal ventricular arrhythmias. Indeed, parasympathetic attenuation and sympathetic over-activation were noted to precede development of heart failure phenotype in both preclinical and clinical settings respectively (Grassi et al., 2001, Schwartz, 1998).

The use of in vitro Langendorff perfused rabbit heart with intact dual autonomic nerves has allowed investigation of the effects of direct sympathetic and vagus nerve stimulation in isolation (Ng et al., 2007) and in combination (Chapter 4) on ventricular electrophysiology including ventricular fibrillation threshold (VFT), ventricular effective refractory period (ERP) and electrical restitution (RT). This study is planned to establish a progressive understanding of autonomic neurocardiology control in heart failure by first establishing a rabbit infarction model of heart failure via coronary ligation with subsequent terminal experimental studies using the previously described dual-innervated Langendorff-perfused heart model.

7.2 Aim

The study aims to investigate the effects of direct individual sympathetic nerve (SNS) and vagus nerve stimulations (VNS) on atrial and ventricular electrophysiology in a rabbit heart failure model created surgically by ligation of circumflex artery to induce apical myocardial infarction. Specifically, the autonomic effects on heart rate (HR) and its associated left ventricular pressure (LVP) changes, atrio-ventricular delay (AVD), VFT, ERP and RT are measured.

7.3 Method

7.3.1 Rabbit Myocardial Infarction Heart Failure Model

Weight-matched adult male New Zealand White rabbits with the birth weight of 14 weeks old (3.2 ± 0.1 kg, $n = 25$) were obtained from animal laboratories of Charles River (France). The rabbits were randomly assigned to two groups: a coronary-ligation group (HF, $n = 13$); and a sham group (SHM, $n = 12$). The details of the surgical procedures have been described previously (Chapter 3.1). Briefly, the rabbit was pre-medicated with subcutaneous injections containing a combination of Medetomidine Hydrochloride (Sedator, 0.2 mg/kg), Ketamine (Narketan, 10 mg/kg) and Butorphanol Tartrate (Torbugesic, 0.05 mg/kg). Once adequately sedated, the rabbit was intubated with a size 3 uncuffed endotracheal tube following which its anterior chest wall was shaven. The rabbit was then transferred to the surgical theatre where it was ventilated with a Harvard small animal ventilator (tidal volume 30mL, respiratory rate 55/min) and anaesthetized with 1 – 1.5% isofluorane. A left thoracotomy was performed at the 4th intercostal space under aseptic technique. The heart was exposed following a pericardiotomy, retraction of the 4th and 5th rib as well as the left lung. An apical tie was placed to facilitate manipulation of the heart. In HF group, coronary ligation was performed at the circumflex artery half-way between the atrio-ventricular groove and the apex, thereby creating an immediate apical discolouration consistent with a 30 – 40% left ventricular infarct visually. In SHM group, no coronary ligation was performed. In both groups, the heart was exposed for 20 minutes before chest closure. Once recovered from general anaesthesia, the rabbit was transferred to the post-operative

room for close observation and administration post-operative analgesia. In both groups, the rabbits were left to recover for 8 weeks before being sacrificed for terminal experiments. All procedures were undertaken in strict accordance with the Animals (Scientific Procedures) Act 1986 and the current Guide for the Care and Use of Laboratory Animals published by the National Institute of Health (NIH Publication No. 85-23, revised 2011).

7.3.2 Isolated Langendorff-perfused Rabbit Heart Preparation with Intact Dual Autonomic Nerve Innervation

Adult male New Zealand White rabbits (3.7 ± 0.1 kg, $n = 25$) were sedated with a subcutaneous injection containing a mixture of Medetomidine Hydrochloride (Sedator, 0.2 mg/kg), Ketamine (Narketan, 10 mg/kg) and Butorphanol Tartrate (Torbugesic, 0.05 mg/kg). Once the animal was suitably sedated, surgery was performed to isolate rabbit heart with intact dual autonomic innervation as described in detail in the previous chapter (Chapter 3.4.2.1). The isolated rabbit hearts were then perfused in modified Langendorff mode with Tyrode solution (in mM): 130.0 NaCl, 24.0 NaHCO₃, 1.0 CaCl₂, 1.0 MgCl₂, 4.0 KCl, 1.2 NaH₂PO₄ and 20.0 dextrose (Chapter 3.4.2.2).

7.3.3 Autonomic Nerve Stimulation

As described in Chapter 3.4.2.3 in details, the right and left cervical vagus nerve was supported and stimulated by a pair of custom-made bipolar silver electrodes. Bilateral sympathetic nerve stimulation was achieved by insertion of a quadripolar catheter into the spinal canal to the level of stellate ganglia.

For each of the autonomic nerves, a voltage response curve was constructed by assessing the heart rate response during sympathetic (SNS)/vagus nerve stimulation (VNS) with varying strength from 1 – 10 V. The optimal voltage required by each nerve to induce 80% of maximal heart rate changes was determined and used to assess the frequency response of the corresponding autonomic nerves from 1 to 20 Hz.

SNS was performed at 10 Hz and VNS at 5 Hz during assessment of AVD. The former frequency was chosen to prevent intrinsic sinus rate from overriding atrial pacing rate whereas the latter frequency was chosen to avoid heart block. For the study of ventricular electrophysiology, SNS frequency was defined by the frequency that gave rise to an SNS-induced tachycardia of around 200 – 230 bpm. On the other hand, VNS frequency was determined as the frequency with a resulting bradycardia of around 60 – 70 bpm.

7.3.4 Cardiac Electrical Recording and Pacing

A spring-loaded mini-MAP electrode was placed at the epicardial surface of left ventricular free wall for recording of monophasic action potential (MAP) using a DC-coupled high-input impedance differential amplifier as described in Chapter 3.4.2.2. A bipolar pacing electrode was inserted into the right ventricular apex for ventricular pacing manoeuvres required for measurement of VFT and ERP.

7.3.5 Measurement of Atrio-ventricular and Ventricular Electrophysiology

The effect of direct autonomic nerve stimulation on AVD was examined during constant right atrial pacing at 300 ms. The electrode for measuring monophasic action potentials (MAPs) was applied to the epicardial surface of the basal left ventricular free wall. AVD was defined as the time required from the pacing stimulus to the start of the ventricular MAPs.

VFT and ERP were determined by specific pacing protocols as described in Chapter 3.3.2.4. RT was derived from measurements of MAP duration during S1 – S2 protocol used for ERP measurement. In this study, RT was obtained from both the base and the apex of the 23 hearts. The specifics of RT calculations were explained in Chapter 3.4.2.4. Steady-state HR was determined prior to commencing the pacing protocols in interest.

7.4 Results

7.4.1 Effect of Autonomic Stimulation on Stimulus-Heart Rate Response

To assess the heart rate response, two protocols were designed. The first involved altering stimulus strength at a fixed frequency of 5 Hz, whilst the second consists of changing stimulus frequency at a fixed submaximal voltage that gave rise to 80% of the HR response. Autonomic nerve stimulation characteristically induced an initial change in HR that peaked in its response before plateauing off until the nerve stimulation ceased following which HR returned to its baseline level.

7.4.1.1 Effect of Varying Stimulus Strength

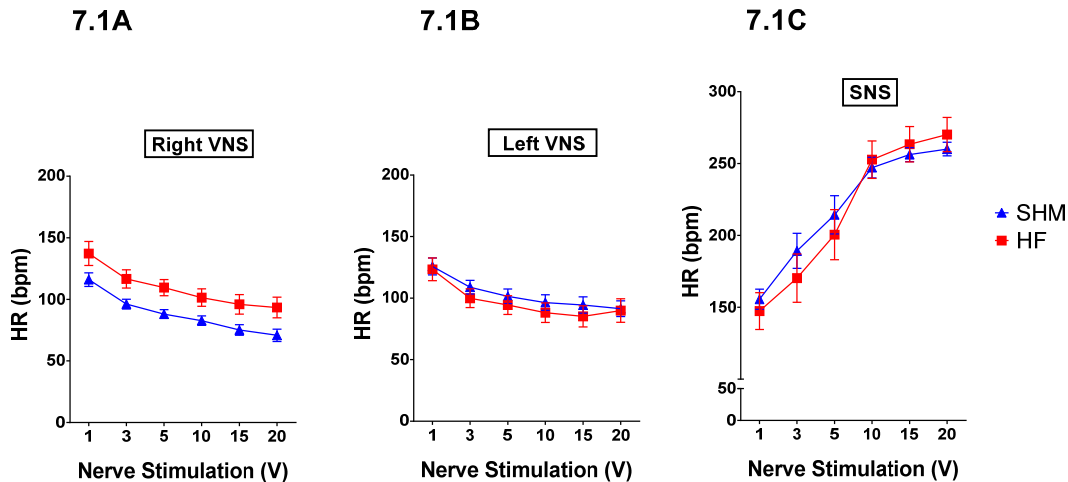
Fixing the frequency of stimulation at 5 Hz, right and left VNS was performed at incremental steps of 1V, 3V, 5V and 10V in HF ($n = 13$) and SHM ($n = 12$) preparations. The minimum steady-state HR was measured at each stimulus strength. Right VNS reduced baseline HR in HF group (red symbols) from 145 ± 7 bpm to 137 ± 10 ($P < 0.005$) at 1 V and 94 ± 8 bpm ($P < 0.005$) at 10 V whereas in SHM group (blue symbols), baseline HR reduced from 145 ± 7 bpm to 116 ± 6 bpm ($P < 0.005$) at 1 V and 71 ± 5 bpm ($P < 0.005$) at 10 V (Figure 7.1A).

In HF group, left VNS decreased baseline HR from 146 ± 7 bpm to 123 ± 9 bpm ($P < 0.005$) at 1 V and 87 ± 9 bpm ($P < 0.005$) at 10 V whilst in SHM group, baseline HR reduced from 145 ± 7 bpm to 126 ± 7 bpm ($P < 0.005$) at 1 V and 91 ± 6 bpm ($P < 0.005$) at 10 V (Figure 7.1B).

On the other hand, SNS increased HR from 144 ± 7 bpm to 154 ± 7 bpm ($P < 0.05$) at 1 V and 270 ± 12 bpm ($P < 0.05$) at 10 V in HF group. In SHM group, SNS increased HR from 143 ± 7 bpm to 156 ± 7 bpm ($P < 0.05$) at 1V and 260 ± 5 bpm ($P < 0.05$) at 10 V (Figure 7.1C).

Overall HR changes in response to varying stimulus strength of autonomic nerve stimulation were not significantly different between the HF and SHM groups.

Figure 7.1 Comparison of heart rate changes with increasing stimulus strength between heart failure (HF) and sham (SHM) groups during vagus nerve stimulation (VNS) and sympathetic stimulation (SNS)



7.4.1.2 Effect of Varying Stimulus Frequency

A fixed submaximal stimulus strength was chosen to assess the effect of varying stimulus frequency on heart rate response. This was defined as the stimulus strength yielding 80% HR response for the corresponding autonomic nerves in section 7.4.1.1. The mean submaximal stimulus strength for SNS as well as right and left VNS, mean baseline HR, peak LVP and end-diastolic LVP were shown in table 7.1.

At fixed stimulus strength, right VNS produced the greater frequency-dependent HR reduction in SHM group as compared to HF group, giving rise to a HR of 15 ± 7 bpm as opposed to 52 ± 14 bpm in HF group at 15 Hz ($P < 0.05$), and a HR of 4 ± 4 bpm as opposed to 46 ± 15 bpm in HF group at 20 Hz ($P < 0.05$) (Figure 7.2A).

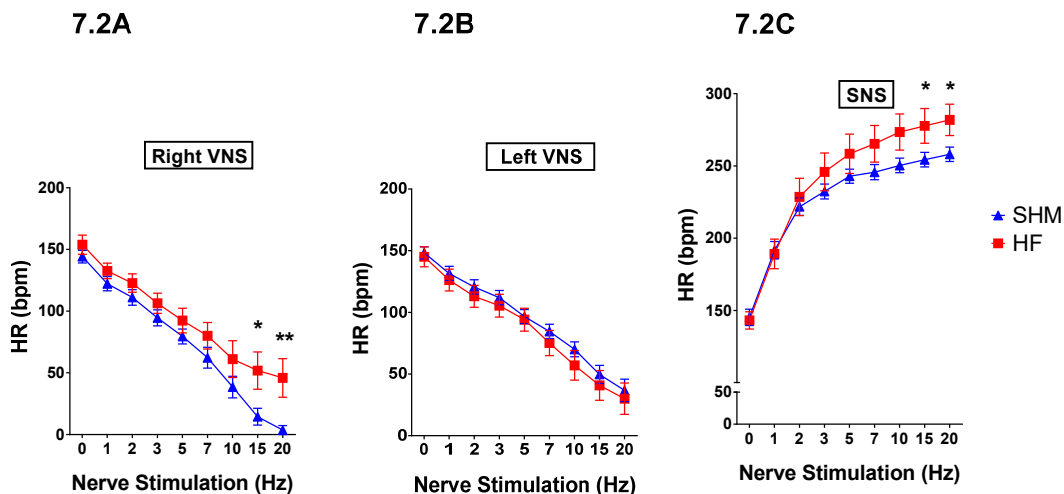
Although left VNS demonstrated similar picture of frequency-dependent HR reduction, there was no significant difference in the magnitude of HR reduction between the HF and SHM groups. Furthermore, the magnitude of HR reduction by left VNS was significantly less than that of right VNS in SHM group. At 20 Hz, left VNS produced a HR reduction of 109 ± 10 bpm as compared to 140 ± 8 bpm by right VNS ($P < 0.05$) (Figure 7.2B).

Conversely, SNS produced an exaggerated HR increment with increasing stimulus frequencies in HF group as compared to SHM group with the greatest tachycardic effect observed at 278 ± 12 bpm at 15 Hz, and 282 ± 11 bpm at 20 Hz in HF group ($P < 0.05$ compared to SHM group) (Figure 7.2C).

Table 7.1 Summary of baseline pre-stimulation values

Group	HF	SHM
Peak LV systolic pressure (mmHg)	72 ± 7	74 ± 5
End-diastolic LV pressure (mmHg)	9 ± 4	5 ± 2
Balloon volume (mL)	5 ± 2	5 ± 2
Perfusion pressure (mmHg)	56 ± 6	58 ± 4
Baseline heart rate (bpm)	150 ± 8	148 ± 5
Stimulus strength for right VNS (V)	8.8 ± 0.8	8.5 ± 0.6
Stimulus strength for left VNS (V)	8.6 ± 0.7	8.5 ± 0.4
Stimulus strength for SNS (V)	7.0 ± 0.7	7.2 ± 0.5

Figure 7.2 Comparison of heart rate changes with increasing stimulus frequency between heart failure (HF) and sham (SHM) groups during vagus nerve stimulation (VNS) and sympathetic stimulation (SNS)



7.4.2 Effect of Low- and High-frequency Autonomic Nerve Stimulation on Atrio-ventricular Delay

In this study, baseline atrio-ventricular delay (AVD) was assessed during fixed right atrial pacing at 300 ms cycle length (Figure 7.3). AVD in SHM group was 104.7 ± 4.2 ms whereas HF group demonstrated a significantly prolonged AV delay of 131 ± 5 ms ($P < 0.05$).

Both right and left VNS exerted a differential effect on AVD prolongation in SHM and HF groups. During right VNS, AVD in SHM group was prolonged from 104.7 ± 4.2 ms to 113.4 ± 4.0 ms at 2 Hz, and 125.0 ± 3.1 ms at 5 Hz whereas in HF group, AVD was prolonged from 131.3 ± 4.7 ms to 137.3 ± 4.3 ms at 2 Hz, and 141.9 ± 4.2 ms at 5 Hz (7.4A). Although both groups demonstrated significant AVD prolongation under right VNS ($P < 0.05$), the effect of AVD prolongation in HF group was significantly diminished at 5Hz when compared to SHM group (Figure 7.4B). At 5 Hz, right VNS prolonged AVD by 20.3 ± 1.3 ms in SHM group, whilst in HF group, AVD was only prolonged by 10.6 ± 0.7 ms.

In general, left VNS produced a greater effect in AVD prolongation when compared to right VNS. In SHM group, AVD was prolonged from 105.2 ± 4.2 ms to 119.9 ± 3.5 ms at 2 Hz, and 139.5 ± 2.6 ms at 5 Hz. In HF group, left VNS prolonged AVD from 133.4 ± 4.3 ms to 142.0 ± 4.2 ms at 2 Hz, and 162.1 ± 3.1 ms at 5 Hz (Figure 7.4C). In spite of the greater AVD prolongation by left VNS, there was no significant difference in the degree of AVD prolongation between the SHM and HF groups at 5Hz (Figure 7.4D).

In contrast, SNS shortened AVD in both SHM and HF groups. In SHM group, AVD was shortened from a baseline of 104.7 ± 4.2 ms to 95.4 ± 4.1 ms at 2 Hz and 89.1 ± 4.1 ms at 10 Hz. In HF group, AVD was shortened from 132.4 ± 4.6 ms to 116.0 ± 4.6 ms at 2 Hz and 105.1 ± 4.3 ms at 10 Hz (Figure 7.5A). Overall, despite a significantly more prolonged AVD in HF group during baseline and SNS, the magnitude of AVD shortening was significantly greater in the HF group at 10 Hz (Figure 7.5B).

Figure 7.3 Atrio-ventricular delay (AVD) measured under constant atrial pacing at 300 ms cycle length with MAP recordings from an unstimulated Langendorff's heart preparation in heart failure (HF) and sham (SHM) groups. Action potential duration was noted to be longer in HF group (data not shown)

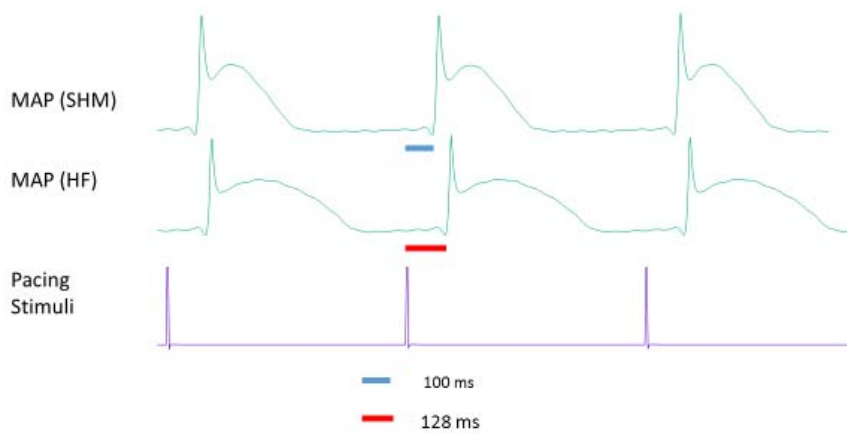


Figure 7.4 Comparison of atrio-ventricular (AV) delay (Figure 7.4A, 7.4C) and changes in AV delay (Figure 7.4B, 7.4D) between heart failure (HF) and sham (SHM) groups at baseline as well as during right and left vagal stimulation

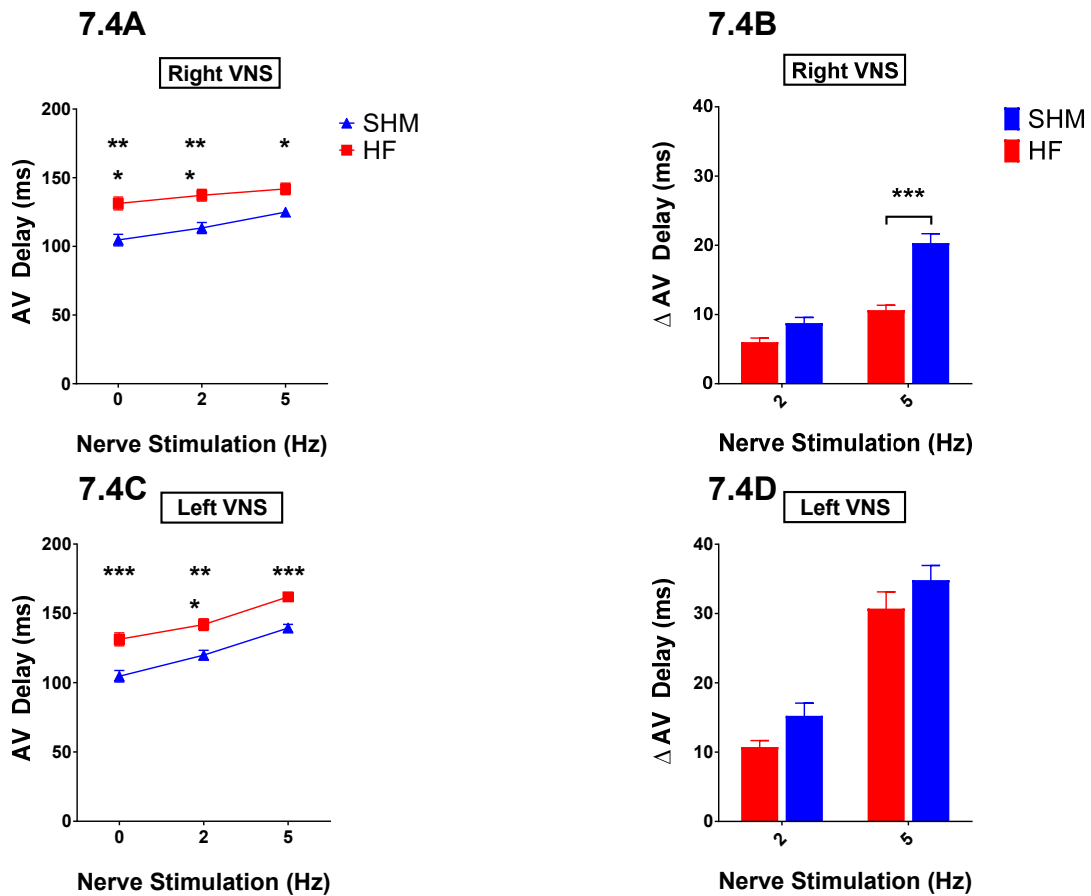
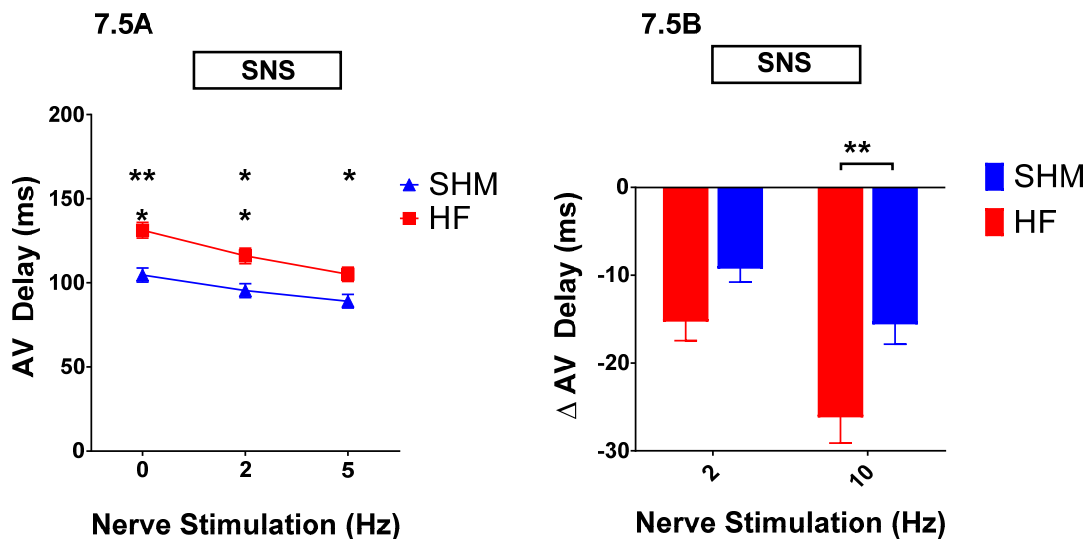


Figure 7.5 Comparison of atrio-ventricular (AV) delay (Figure 7.5A) and changes in AV delay (Figure 7.5B) between heart failure (HF) and sham (SHM) groups at baseline and during sympathetic stimulation



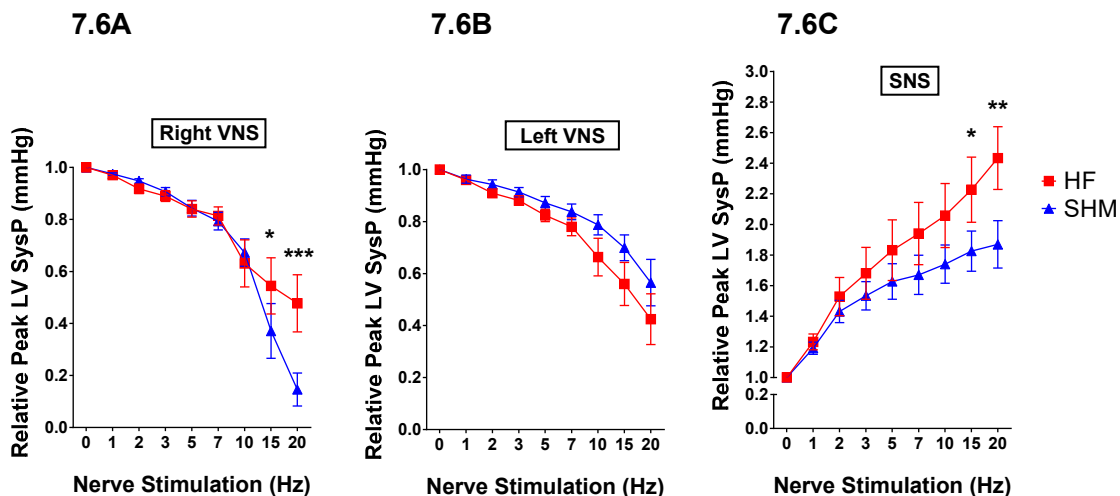
7.4.3 Effect of Autonomic Stimulation on Left Ventricular Pressure at Different Stimulation Frequencies

The left ventricular peak systolic pressure (LVP) was recorded and analysed during incremental stimulation frequencies of SNS and VNS whilst the steady-state heart rate response was studied (Section 7.4.1.2). The maximum peak LVP at each stimulation frequency was expressed relative to the baseline pre-stimulation peak LVP.

The baseline LVP was noted to be similar in both groups: 72 ± 7 mmHg in the HF group and 74 ± 5 mmHg in the SHM group. LVP was noted to decrease with VNS with the effect being more noticeable with increasing stimulation frequency. During right VNS, there was a significant reduction in LVP for the SHM group at 15 Hz and 20 Hz stimulation frequencies ($P < 0.05$) (Figure 7.6A). During left VNS, both HF and SHM group demonstrated a reduction in LVP with increasing stimulation frequencies but there was no discernible difference in LVP reduction between the two groups (Figure 7.6B).

SNS, on the other hand, resulted in an increase in LVP in both HF and SHM groups. In HF group, there was a greater degree of LVP increase under SNS at different stimulation frequencies, culminating in a significantly greater LVP increments at 15Hz and 20 Hz (Figure 7.6C).

Figure 7.6 Comparison of changes in left ventricular peak pressure with increasing stimulus frequency between heart failure (HF) and sham (SHM) groups during vagus nerve stimulation (VNS) (Figure 7.6A and 7.6B) and sympathetic stimulation (SNS) (Figure 7.6C)



7.4.4 Effect of Autonomic Stimulation on Ventricular Electrophysiology

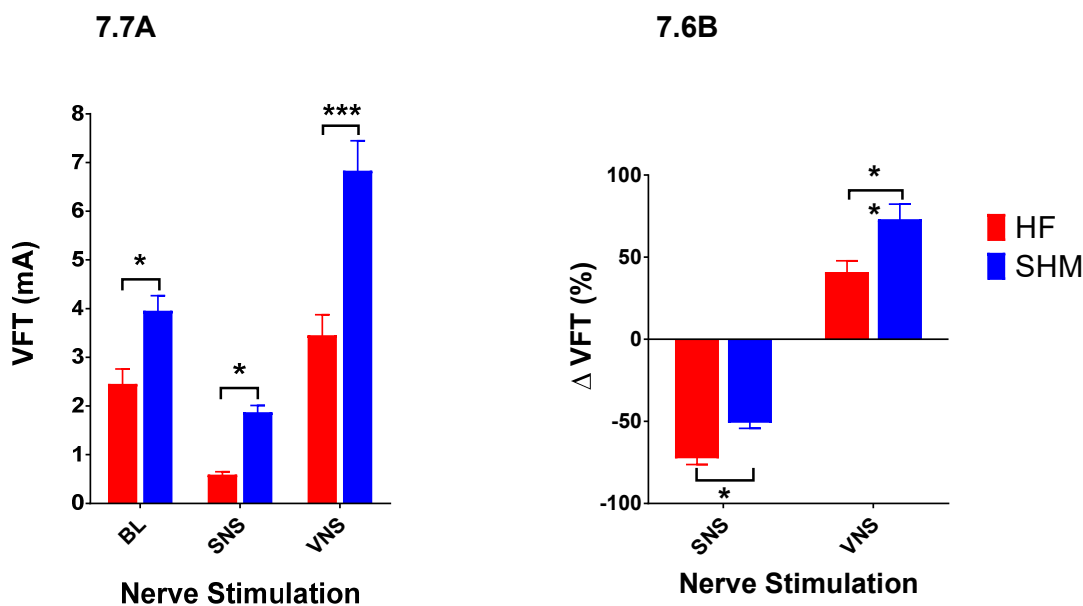
7.4.4.1 Effect of Autonomic Stimulation on Ventricular Fibrillation Thresholds

Baseline VFT was obtained prior to autonomic nerve stimulations. In HF group, the baseline VFT was recorded as 2.5 ± 0.3 mA whereas the baseline VFT in SHM group was significantly higher at 4.0 ± 0.3 mA, demonstrating the propensity of HF group for VF. Under SNS which increased HR of each group to around 230 bpm, VFT was lower in both HF (0.6 ± 0.1 mA) and SHM (1.9 ± 0.1 mA) with the effect of SNS on VFT significantly more profound in the HF group. In contrast, VNS led to higher VFT in both HF (3.5 ± 0.4 mA) and SHM (6.8 ± 0.6 mA) with the effect of VNS on VFT attenuated in the HF group (Figure 7.7A).

Figure 7.7B illustrates relative change from the corresponding baseline VFTs in both HF and SHM groups. This demonstrated that SNS-induced VFT-lowering effect was greater in the HF group ($-72.5 \pm 3.7\%$) compared to the SHM group ($-50.8 \pm 3.4\%$). The effect of VNS in raising VFT, on the other hand, was diminished in HF group ($41.1 \pm 6.8\%$) when compared to the SHM group ($73.2 \pm 9.1\%$).

The stimulation frequency of both SNS and VNS in the HF and SHM groups were similar in these experiments. To attain a HR of around 250 bpm, the required frequencies of SNS were 8.7 ± 0.1 Hz (HF group) and 7.8 ± 1.3 V (SHM group) respectively. The frequencies of VNS required to achieve a HR of around 60 – 70 bpm were 10.5 ± 1.4 Hz (HF group) and 7.8 ± 0.7 Hz (SHM group) respectively.

Figure 7.7 Comparison of ventricular fibrillation threshold (Figure 7.7A) and relative changes from baseline (Figure 7.7B) between heart failure (HF) and sham (SHM) groups at baseline (BL), during sympathetic (SNS) and vagal (VNS) stimulations



7.4.4.2 Effect of Autonomic Stimulation on Action Potential Duration-Restitution and Restitution Dispersion

7.4.4.2.1 Effect of Sympathetic and Vagus Nerve Stimulation on Action Potential Duration Restitution

Action potential duration restitution (APD-RT) was assessed by relationship between MAP duration with its corresponding diastolic interval as previously mentioned. At baseline, the basal APD-RT was calculated as 2.18 ± 0.07 in HF group. The basal APD-RT curve was flatter in the SHM group at 1.32 ± 0.06 (Figure 7.8A). In comparison to basal APD-RT, APD-RT at the non-scarring apex of the hearts (referred from here onwards as apical APD-RT) was steeper in both groups at 2.61 ± 0.08 (HF group)($p = 0.0766$) and 1.51 ± 0.06 (SHM group)($p = 0.037$) correspondingly (Figure 7.8B).

SNS characteristically steepened both basal and apical APD-RT curves. In HF group, basal and apical APD-RT were higher at 3.90 ± 0.10 and 5.12 ± 0.09 respectively. In SHM group, the increase in basal and apical APD-RT was 2.10 ± 0.09 and 2.58 ± 0.08 correspondingly (Figure 7.8).

In contrast, VNS flattened both basal and apical APD-RT curves. Under VNS, basal and apical APD-RT in HF groups were 1.48 ± 0.07 and 1.70 ± 0.11 . In SHM group, the VNS effect on both basal and apical APD-RT was significantly more prominent, resulting in lower APD-RT values (base: 0.61 ± 0.05 ; apex: 0.65 ± 0.06) than those of HF group (Figure 7.8).

Figure 7.9 illustrated relative changes in APD-RT by SNS and VNS from the baseline APD-RTs. This demonstrated SNS effect in steepening APD-RT was significantly greater in the HF group compared to the SHM group whereas VNS effect in flattening APD-RT was attenuated in the HF group.

Figure 7.8 Comparison of basal (Figure 7.8A) and apical (Figure 7.8B) action potential duration-restitution (APD-RT) between heart failure (HF) and sham (SHM) groups at baseline (BL), during sympathetic (SNS) and vagal (VNS) stimulations

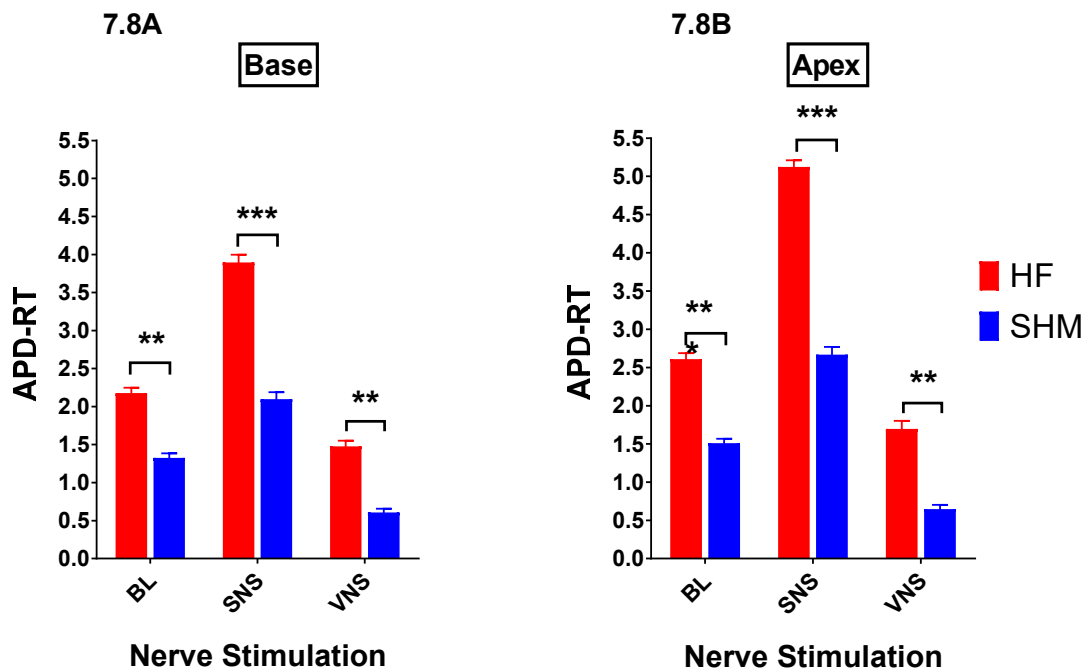
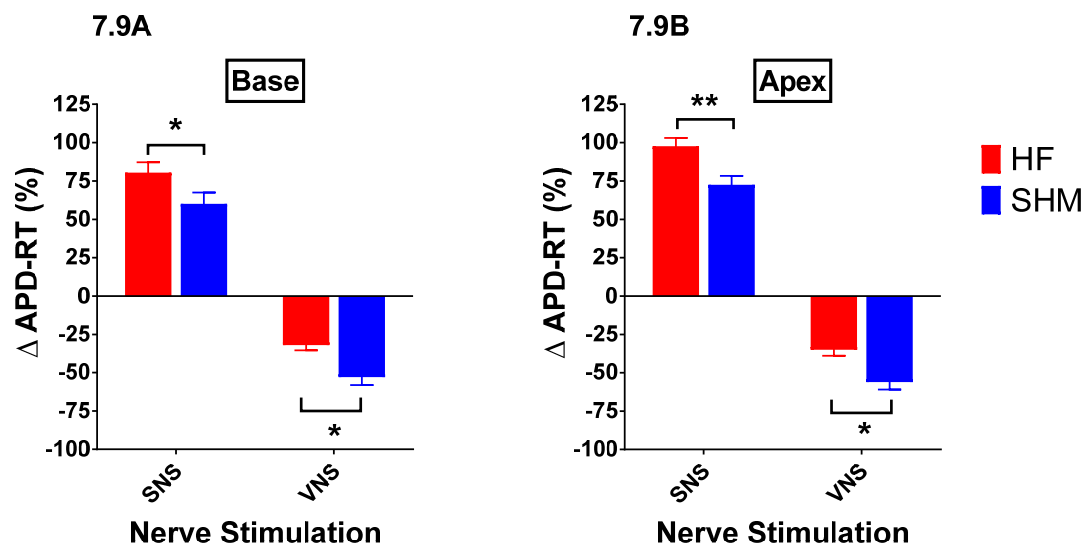


Figure 7.9 Comparison of relative changes from baseline values in basal (Figure 7.9A) and apical (Figure 7.9B) action potential duration-restitution (APD-RT) between heart failure (HF) and sham (SHM) groups during sympathetic (SNS) and vagal (VNS) stimulations



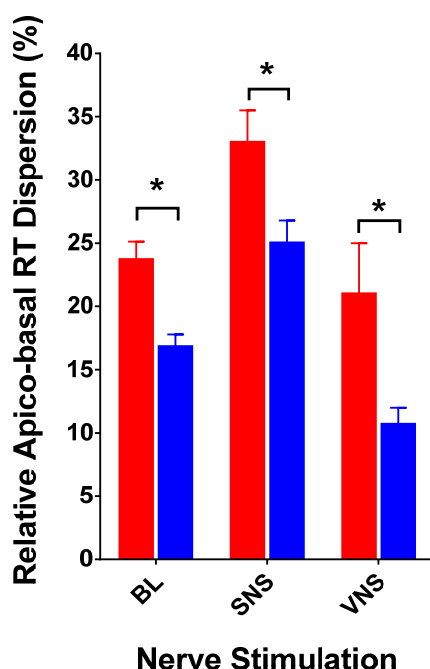
7.4.4.2.2 Effect of Sympathetic and Vagus Nerve Stimulation on Apico-basal Restitution Dispersion

In this study, apical APD-RT slopes were steeper than basal APD-RT in both HF and SHM groups. In order to assess the degree of apico-basal APD-RT restitution dispersion, basal APD-RT was subtracted from apical APD-RT and expressed as a function of change from basal APD-RT:-

$$\text{Apico-basal RT Dispersion} = [(\text{Apical RT} - \text{Basal RT}) / \text{Basal RT}] \times 100\%$$

In the absence of autonomic nerve stimulation, apico-basal RT dispersion was greater in HF group ($23.7 \pm 1.4\%$) than that in SHM group ($16.8 \pm 1.0\%$). SNS resulted in an increase in RT dispersion with its effect augmented in the HF group ($33.0 \pm 2.5\%$) compared to SHM group ($25.0 \pm 1.8\%$). Conversely under the influence of VNS, the apico-basal RT dispersion was not significantly different from that at baseline in general. Nonetheless, dispersion of apico-basal restitution remains greater in the HF group ($21.0 \pm 2.4\%$) as compared to the SHN group ($12.4 \pm 2.6\%$) (Figure 7.10).

Figure 7.10 Comparison of relative apico-basal restitution (RT) dispersion between heart failure (HF) and sham (SHM) groups

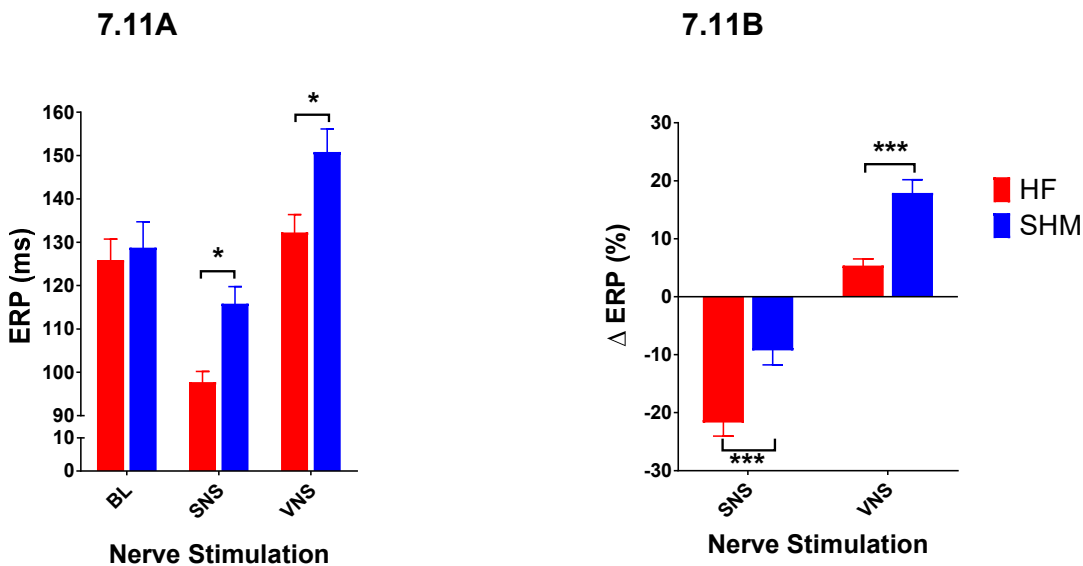


7.4.4.3 Effect of Autonomic Stimulation on Ventricular Refractoriness

At baseline, mean ventricular ERP was similar in both HF and SHM groups at 125.9 ± 4.8 ms and 128.8 ± 5.9 ms respectively. During SNS, ERP was shortened to 97.7 ± 2.5 ms in the HF group and 115.8 ± 3.9 ms in the SHM group. Conversely, VNS produced ERP prolongation, increasing the ventricular ERP to 132.3 ± 4.1 ms in HF group and 150.8 ± 5.3 ms in SHM group (Figure 7.11A).

In spite of the similar ERP at baseline in both groups, SNS exerted a greater effect in shortening ERP in the HF group ($-21.7 \pm 2.3\%$) compared to SHM group ($-9.3 \pm 2.5\%$). Meanwhile, VNS resulted in ERP prolongation although this effect was attenuated in the HF group ($5.4 \pm 1.1\%$) compared to SHM group ($17.9 \pm 2.3\%$) (Figure 7.11B).

Figure 7.11 Comparison of ventricular effective refractory period (Figure 7.11A) and relative changes from baseline (Figure 7.11B) between heart failure (HF) and sham (SHM) groups at baseline (BL), during sympathetic (SNS) and vagal (VNS) stimulations



7.5 Discussion

Heart failure is a clinical syndrome of which dysautonomia characterised by sympathetic overdrive and parasympathetic attenuation are hallmarks. Central to its pathology is activation of the neuro-humoral axis preceding subsequent electrical and structural remodellings. The isolated Langendorff-perfused rabbit hearts with dual autonomic innervation therefore presents a unique and convenient model to study whole-heart electrophysiology under controlled autonomic stimulation, free from the confounding effects of circulating humoral factors. In this study, the effect of sympathetic, right and left vagus nerve stimulations on heart rate and AV conduction were examined at the atrial and atrio-ventricular level. Whereas at the ventricular level, sympathetic and vagal (mostly right) stimulations were performed to demonstrate their effects on ventricular fibrillation inducibility, electrical restitution and ventricular refractoriness, all of which exert important implications on the genesis of malignant ventricular arrhythmias in heart failure.

7.5.1 Effect of Autonomic Nerve Stimulation on Intrinsic Heart Rate

The sino-atrial (SA) node is a compact region at the base of the superior vena cava in the right atrium (Boyett et al., 2000, Bleeker et al., 1980). It is the default pacemaker of the heart, naturally generating action potentials at a rate of approximately 100 times/min. Several ionic currents are responsible for the spontaneous firing activity of the SA node (Irisawa, 1987), the activities of which can be modulated by autonomic nerves thereby altering pacemaker automaticity and intrinsic heart rate.

In the SA node, a pacemaker current (I_f) are responsible for spontaneous diastolic depolarization and subsequent pacemaker firing (DiFrancesco, 1991, Noma et al., 1983). Other major depolarising currents comprise the L-type Ca^{2+} current, I_{CaL} , and sodium current, I_{Na} which account for phase 0 of the action potential although I_{CaL} is also responsible for late phase 3 depolarization (Dokos et al., 1996). Furthermore, I_{CaL} has been shown to contribute partly to local subsarcolemmal calcium release, the latter a determinant of spontaneous SA node cycle length. This periodic local calcium release is responsible for the Ca^{2+} clock in the SA node (Maltsev et al., 2011, Vinogradova et

al., 2010). Whilst I_{CaL} is the major depolarising current in the central cells of SA node, I_{Na} exerts its depolarising influence in the periphery cells (Boyett et al., 2000). Additionally, in mammalian SA node, there is another Ca^{2+} current known as the transient Ca^{2+} current (T-type Ca^{2+} current). Abolishing T-type Ca^{2+} current with Ni^{2+} results in a prolongation of SA node cycle length (Hagiwara et al., 1988) whilst the effect of I_{Na} on the cycle length is insignificant (Dokos et al., 1996).

Sympathetic stimulation through the spinal cord in this study leads to release of norepinephrine which binds to β -adrenoreceptors in the heart, activating a phosphorylation cascade which culminates in increased density of the I_f as well as L- and T-type Ca^{2+} currents. Consequently, this produces an increased rate of diastolic depolarisation and intrinsic heart rate (Hartzell, 1988, Shemarova et al., 2009). In this study, sympathetic stimulation produced graded increment in heart rate in response to increasing strength and frequency of stimulation. Conversely, right and left vagus nerve stimulation led to a reduction in heart rate in response to increasing strength and frequency of vagal stimulation. At the cellular level, this is driven by acetylcholine released from the vagus nerve endings to activate the M_2 muscarinic receptors in the heart, inhibiting cAMP/PKA-dependent phosphorylation cascade (Levy, 1971, Behar et al., 2016).

Whilst the increased strength of stimulation implicates recruitment of increased number of actively-firing nerve fibres (i.e. *spatial* summation), increasing frequency of stimulation resulted in an increased in the firing rate of each nerve fibre (i.e. *temporal* summation) (Eccles, 1957). Upon varying strength of stimulation, there is no difference in sympathetic-induced heart rate increment or vagal-induced heart rate reduction between SHM and HF groups (Figure 7.1). This implies that the density of vagus and sympathetic nerve distribution is similar between the two groups at the atrial level. There is however a significant difference in heart rate response during high-frequency sympathetic and right vagus nerve stimulation. At 15 and 20Hz stimulation, HF group demonstrated exaggerated heart rate increase during sympathetic stimulation (Figure 7.2C). In contrast, at these high frequencies of right vagus nerve stimulation, HF group demonstrated less bradycardic effect when the SHM group were almost asystolic in their heart rate (Figure 7.2A). As *frequency* of stimulation implies *temporal*

summation of the corresponding nerves, this finding suggest heightened sympathetic response and attenuated right vagal response in heart rate changes. Interestingly, the attenuation of vagal response in HF group is limited to the right vagus nerve only. There is no difference in decremental response in heart rate with left vagus nerve stimulation between the HF and SHM groups (Figure 7.2B). The differential effect in negatively chronotropic response between the right and left vagus nerve have been previously demonstrated in both *in vivo* (Cohn, 1912) and *in vitro* (Ng et al., 2001) studies of normal animal hearts, and was accountable by the predominance of right vagus nerve at the SA node (Ardell and Randall, 1986). The findings of this study proved that in heart failure, the right vagus nerve remains the dominant contributing force to the attenuated chronotropic response and may prove to be a useful therapeutic target for clinical studies following an improvement in ventricular function of a canine pacing-induced HF model with right vagus nerve stimulation (Sun et al., 2015).

7.5.2 Effect of Autonomic Nerve Stimulation on Atrio-ventricular Delay

The atrio-ventricular (AV) node acts as an electrical relay station, transmitting atrial electrical impulses to the ventricles. It possesses its own pacemaker activity running at a slower rate than the SA node, and can operate as an independent pacemaker when SA node activity is compromised. There are three distinct cell types in the AV node and the perinodal region, the atrio-nodal (AN), the nodal (N) and the nodal-His (NH) cells. Depolarisation occurs via I_{Na} in AN and NH cells. Whereas in the N cells, the inward calcium I_{CaL} is responsible for the slow depolarisation (Meijler and Janse, 1988). This accounts for the differential conduction velocity with faster conduction through the AH and NH cells, accounting for the rate-dependent property of AV node conduction (Billette et al., 1976). Indeed the fast AV node conduction occurs by bypassing most N cells whilst the slow pathway involved conduction through the compact AV node (Mazgalev et al., 2001).

Similar to SA node, AV node conduction were shown to be modulated by autonomic input in *in vivo* studies (Chen et al., 1999, Loeb and deTarnowsky, 1988). Sympathetic stimulation exerts direct electrophysiological changes on AV node by shortening AV

conduction time (West and Toda, 1967). Indirectly, sympathetic-induced acceleration of sinus rate can slow down AV conduction due to decremental conduction property of the AV node. Conversely, vagal stimulation prolongs AV conduction time directly but can also indirectly shorten AV conduction time by slowing the sinus rate (Mazgalev et al., 1986). As such, the ultimate outcome on AV conduction by sympathetic and vagal branches of the autonomic nerves depend on the balance between their corresponding direct and indirect electrophysiological effects.

In this study, AV delay in general was more prolonged in the HF group compared to SHM group. During vagal stimulation, negative dromotropic effect was observed in both HF and SHM groups. There was an attenuated effect in AV delay prolongation by right vagus nerve stimulation in the HF group, especially during high-frequency right vagus nerve stimulation (Figure 7.4A and 7.4B). On the other hand, there is no significant difference in the dromotropic effect by left vagus nerve stimulation between the two groups (Figure 7.4C and 7.4D). Both groups demonstrated positive dromotropy during sympathetic stimulation with HF group exhibiting exaggerated AV shortening effect during high-frequency sympathetic stimulation (Figure 7.5). At first glance, the exaggerated sympathetic and attenuated right-vagal dromotropic effects mimic the effects seen in chronotropic response (Chapter 7.5.1), these findings could not be ascribed solely to the indirect electrophysiological effect of the corresponding autonomic nerves on AV delay through changes in sinus rate since the heart rate was fixed by atrial pacing. The more pronounced negative dromotropic effect by left vagus nerve stimulation in this study is otherwise in accord with findings in normal heart demonstrating a preferential distribution of post-ganglionic left vagal fibres to the AV node (Ardell and Randall, 1986).

Prolonged AV delay, manifesting as prolonged PR interval on ECG, is a well-known electrophysiological signature in heart failure and is associated with lethal arrhythmias and sudden cardiac death (Olshansky et al., 2012, Luu et al., 1989, Gervais et al., 2009). Indeed, this feature is linked to worse survival even in the absence of heart failure (Cheng et al., 2009). Prolonged AV delay was attributed to a combination of anatomical and ion-channel remodellings (Nikolaïdou et al., 2015, Baruscotti et al., 2011, Zhang et al., 2011). In a volume- and pressure-overload rabbit heart failure

model, imaging of the AV bundle by micro-computer topography revealed enlargement of this structure by 87.5%. In the same study, connexion 40, Cav1.3 (an isoform of I_{CaL}) and HCN currents were found to be downregulated. Given the characteristic changes in AV node remodelling, autonomic nerve staining in AV node region of rabbit heart failure model will provide invaluable insight to the underlying structural cause of deranged dromotropic responses observed in the current study.

7.5.3 Effect of Autonomic Nerve Stimulation on Left Ventricular Contractility

This study demonstrated that peak LVP increased during sympathetic stimulation and decreased during vagal stimulation in a frequency-dependent manner in conjunction with HR changes. This discrepancy in response is particularly appreciable at high frequency sympathetic and right vagal stimulation during which HF group demonstrated an exaggerated sympathetic effect and an attenuated vagal effect. There is otherwise no change between HF and SHM group in frequency-dependent attenuation of peak LVP during left vagus nerve stimulation. The similar changes between peak LVP and HR by the corresponding autonomic nerve stimulation could reflect a positive force frequency relationship between these two parameters, previously demonstrated in a rabbit model (Lewartowski and Pytkowski, 1987). Arguably, this relationship could be distorted in the setting of heart failure (Mulieri et al., 1992). Autonomic modulation of left ventricular inotropy should be assessed with fixed HR by atrial pacing in future studies.

7.5.4 Effect of Autonomic Nerve Stimulation on Ventricular Electrophysiology

This study represents a novel attempt of profiling the effect of autonomic modulation on various ventricular electrophysiologic properties in a rabbit heart failure model. Compared to the shams, rabbits with heart failure demonstrated an increased susceptibility to ventricular fibrillation at baseline as evident from the lower VFT and the associated steeper restitution slope. This is in contrast with the findings of another study in rabbit heart failure model investigating the link between transmural repolarization alternans and VF by optical mapping (Myles et al., 2011). Myles et al concluded that alternans in optical action potential amplitude, but not APD alternans, is associated with VF inducibility by rapid pacing. A number of factors may account for

the different findings between the current study and the aforementioned study. First, MAP was examined in this study as opposed to optical APD. Second, the current study examined epicardial APD changes on whole-heart preparations as opposed to the wedge preparations used in the other study. Third, the use of mechanical uncoupler in optical mapping studies may have an effect on electrophysiologic properties (Brack et al., 2013). In this study, sympathetic stimulation increased propensity of both sham and heart failure groups to VF by lowering VFT and ERP in addition to steepening restitution slopes. These pro-arrhythmic effects are more pronounced in the heart failure rabbits. In contrast, vagal stimulation protects against ventricular arrhythmias by increasing VFT and prolonging ERP with the accompanied flattening of the restitution slopes. In heart failure, these vagal-induced anti-arrhythmic responses were attenuated.

7.5.4.1 Electrical Restitution, Spatial Restitution Dispersion and Ventricular Fibrillation Inducibility in Normal Hearts and Heart Failure

The restitution hypothesis proposed by Weiss et al postulates that a steep slope of an APD restitution curve with a gradient of >1 promotes oscillations and wave breaks, ultimately facilitating the initiation of ventricular fibrillation in the myocardium (Weiss et al., 2002). A steep slope entails a small change in diastolic interval leading to large changes in APD, manifesting as electrical instability. This hypothesis was validated in both mathematical (Karma, 1994, Nolasco and Dahlen, 1968) and biological models (Cao et al., 1999, Gilmour and Chialvo, 1999). Further evidence was provided by pharmacological studies in which anti-arrhythmics possess the effect of flattening APD restitution slope (Garfinkel et al., 2000, Riccio et al., 1999, Lee et al., 2001, Omichi et al., 2002, Hao et al., 2004) as opposed to drugs with pro-arrhythmic effect exerting a steepening effect on APD restitution slope (Taggart et al., 2003).

Baseline restitution slopes are likely to be species- and protocol-dependent. Whilst dynamic restitution obtained from rapid pacing protocol in canine model produced restitution slopes of >1 , standing restitution obtained from S1-S2 extrastimulus pacing protocol in canine model demonstrated restitution slope of <1 (Koller et al., 1998). In contrast, standard restitution slopes in smaller mammals (Choi and Salama, 2000, Pruvot et al., 2004, Banville and Gray, 2002, Goldhaber et al., 2005) were steeper than

dynamic restitution slopes, being in parallel with the trend in humans (Taggart et al., 2003). In this study, baseline standard restitution slopes measured at the left ventricular (LV) base were >1 (i.e. 1.32 ± 0.06 in SHM vs. 2.18 ± 0.07 in HF). This is in agreement with restitution slope values in a normal unstimulated *in vitro* model of rabbit hearts (Ng et al., 2007). More importantly, in unstimulated hearts at baseline, HF group demonstrated a steeper restitution slope than SHM group.

Furthermore, this study demonstrated regional heterogeneity in restitution slopes between the basal and apical regions of the LV epicardium in rabbits. In general, apical restitution slopes are steeper than the restitution slopes at base in both HF and SHM groups. This is likely to be accountable by the right ventricular apical pacing site in close proximity to the left ventricular apex. Further evidence came from previous study in rabbit hearts demonstrating a significant relationship between standard restitution slopes and epicardial left ventricular pacing sites (Pitruzzello et al., 2007). Whilst apico-basal restitution dispersion exists presumably by virtue of apical pacing site, the degree of dispersion is greater in HF group, suggesting greater spatial electrical heterogeneity in HF (Figure 7.10).

Accordingly, the steeper individual restitution slopes and greater apico-basal restitution dispersion in the HF group were reflected as an increased susceptibility to ventricular fibrillation, as evident by the lower VFT in the absence of autonomic stimulation.

7.5.4.2 Autonomic Modulation of Electrical Restitution and Ventricular Refractoriness in Normal Hearts and Heart Failure

The effect of autonomic modulation on electrical restitution and ventricular refractoriness in normal hearts is well known. Adrenergic stimulation by either direct sympathetic nerve stimulation or adrenergic agonists, causes a downward shift in APD restitution curve in addition to steepening the restitution slope in both *in vivo* (Taggart et al., 1990) and *in vitro* (Ng et al., 2007) animal studies as well as clinical studies (Taggart et al., 2003). In addition, the shorter APD during sympathetic stimulation is associated with ERP shortening in both *in vivo* (Martins and Zipes, 1980) and *in vitro* studies (Ng et al., 2007). All these studies validated the sympathetic effects

demonstrated in this study. In both SHM and HF groups, sympathetic stimulation resulted in steepening of both basal and apical restitution slopes in addition to shortening ventricular ERP. Notably, these sympathetic-driven effects on ventricular electrophysiology are more palpable in the HF group (Figure 7.8, 7.9 and 7.11). Furthermore, during sympathetic stimulation, there was an increased apico-basal restitution dispersion (Figure 7.10) with greater dispersion seen in the HF group. This is in accordance to previous study demonstrating increased dispersion of repolarization in rabbit hearts during sympathetic stimulation (Mantravadi et al., 2007).

On the other hand, vagus nerve stimulation produced an upward shift of the APD restitution curve with associated flattening of the restitution slope. Additionally, ventricular ERP was prolonged by vagal stimulation in congruent with its effect on APD prolongation in *in vivo* (Martins and Zipes, 1980) and *in vitro* studies (Ng et al., 2007). In this study, similar vagal effects were observed but in the HF group, the ERP was shorter and restitution slopes were steeper when compared to the shams, suggesting an attenuated vagal effect in heart failure. Spatial heterogeneity in apico-basal restitution kinetics was unaltered during vagal stimulation compared to baseline in both shams and HF groups. The effect of vagal stimulation on dispersion of repolarization has been debatable. Although other study demonstrated greater spatial dispersion of repolarization in the context of vagal bradycardia and APD prolongation (Yamakawa et al., 2014), the findings in this study is in agreement with another study demonstrating unaltered magnitude of dispersion of repolarisation in rabbit hearts (Mantravadi et al., 2007). It should also be noted that in HF group, the apical-basal restitution dispersion remains more pronounced compared to the shams during vagal stimulation.

Accordingly, the exaggerated sympathetic response in restitution slopes and ERP shortening was supported by the finding of greater VFT lowering effect by sympathetic stimulation in the HF group (Figure 7.6B). Conversely, the attenuated vagal response in HF group, as evident by steeper restitution slope and shorter ERP during vagal stimulation in comparison to those in the shams, validated the findings of reduced protective vagal effect against ventricular fibrillation, as demonstrated by the reduction in VFT increment (Figure 7.6B). The effects of sympathetic exaggeration and vagal attenuation on these ventricular electrophysiologic properties can be further validated in

future studies using dynamic restitution protocol to assess the propensity of APD alternans under sympathetic and vagal influences respectively in both the HF and SHM groups. In addition, the mechanism of vagal attenuation can be dissected by using selective muscarinic agents or nitric oxide donor (sodium nitroprusside) to assess for receptor or second-messenger downregulation in the HF animals. Finally, nitric-oxide activity can be assessed using a nitric-oxide-dependent fluorescence dye, i.e. 4,5-diaminofluorescein (DAF-2) in the heart failure model of Langendorff-perfused rabbit hearts to illustrate abnormal downstream intracellular activity of attenuated vagal response since vagal protection against VF via APD restitution flattening has been previously shown to be mediated via a nitric-oxide pathway in healthy rabbit hearts (Brack et al., 2007, Patel et al., 2008).

7.5.4.3 Mechanisms of Neuro-cardiac Remodelling in the Failing Ventricle

Sudden cardiac death due to fatal arrhythmias is a well-recognised catastrophic outcome in heart failure. The mechanisms underpinning these arrhythmias are complex, involving extensive electrical remodelling in response to a structural insult, such as myocardial infarction in the coronary-ligation model used in this study. Repolarization abnormalities as typified by APD prolongation is a hallmark in heart failure. Altered balance in current densities between the inward currents of sodium (I_{Na}) and calcium (I_{Ca}), and the outward potassium currents (I_{Kr} , I_{Ks} , I_{to}). Additionally, spatial distribution of these currents are altered in heart failure, thereby creating a spatial and temporal heterogeneity conducive for the initiation of ventricular arrhythmias (Akar and Rosenbaum, 2003).

Central to the changes of the ionic currents is abnormal calcium homeostasis. Whilst the I_{Ca} is increased in early stages of cardiac hypertrophy (Hill, 2003), this current is paradoxically unchanged or decreased in severe heart failure, complicating the mechanisms underpinning APD prolongation. The commonest pathology observed in I_{Ca} in heart failure is delayed calcium-dependent L-type I_{Ca} inactivation, a process modulated by calcium-calmodulin-dependent kinase (CAMKII) (Wang et al., 2008). Other studies postulated that over-expression of T-type calcium current found in animal models may contribute to increased automaticity in heart failure (Nuss and Houser,

1993, Martinez et al., 1999). Increasing evidence has also linked increased ryanodine receptor calcium leak, otherwise known as diastolic calcium sparks, with propensity for ventricular arrhythmias (Venetucci et al., 2008, Fozzard, 1992).

Disruption in outward currents in heart failure plays a vital part in repolarization abnormalities. Downregulation of I_{to} results in slowing of early repolarization, altering the overall shape of the cardiac action potentials (Tomaselli and Marban, 1999). The changes in potassium currents, i.e. IK_1 , IK_r and IK_s are variable, depending on the underlying aetiology of the heart failure (Akar and Tomaselli, 2005). Recently microRNAs have been implicated in changes in the outward potassium currents. Specifically, in a myocardial infarction model, miR-1 was found to inhibit Kir2.1 (a subunit of IK_1) (Yang et al., 2007). In an animal model of diabetic cardiomyopathy, miR-133 exhibited an inhibitory action on translation of hERG (a subunit of IK_r) (Xiao et al., 2007). Indeed, overexpression of these two micro-RNAs were associated with a protective effect against ventricular arrhythmias (Xiao et al., 2007, Yang et al., 2007).

In addition to changes of ionic currents at the cellular level accounting for the unique electrical remodelling in heart failure, there is a contemporaneous neural remodelling at the tissue level which manifests as perturbed autonomic balance, facilitating the occurrence of ventricular arrhythmias in both animal models (Schwartz and Stone, 1980, Lown and Verrier, 1976, Randall et al., 1976) and humans (La Rovere et al., 1998). Neural remodelling in the form of sympathetic nerve sprouting, denervation and sympathetic hypersensitivity has been demonstrated in an experimental model of myocardial infarction (Chen et al., 2001). The link between nerve sprouting and ventricular arrhythmias were established by the occurrence of ventricular arrhythmias following infusion of nerve growth factor in animal models (Chen et al., 2001, Cao et al., 2000a). In humans, sympathetic nerve sprouting was found only in patients with previous history of ventricular arrhythmias compared to patients free from ventricular arrhythmias but with similar structural heart disease (Cao et al., 2000b). These phenomena strengthen the notion of a synergistic interplay between electrical, neural and structural remodelling in precipitation of ventricular arrhythmias in heart failure.

7.6 Conclusion

This study demonstrated the effects of direct sympathetic and vagus nerve stimulation on a myocardial infarction heart failure model in rabbits, establishing the autonomic phenotype of sympathetic overdrive and vagal attenuation in chronotropy, dromotropy and ventricular electrophysiology. Adverse electrical remodelling in heart failure with underlying autonomic disturbance contributes to susceptibility in ventricular fibrillation in this heart failure model. Future immunohistochemistry on distribution of autonomic nerves and ion channels will provide invaluable insights.

7.7 References

- AKAR, F. G. & ROSENBAUM, D. S. 2003. Transmural electrophysiological heterogeneities underlying arrhythmogenesis in heart failure. *Circ Res*, 93, 638-45.
- AKAR, F. G. & TOMASELLI, G. F. 2005. Ion channels as novel therapeutic targets in heart failure. *Ann Med*, 37, 44-54.
- ARDELL, J. L. & RANDALL, W. C. 1986. Selective vagal innervation of sinoatrial and atrioventricular nodes in canine heart. *Am J Physiol*, 251, H764-73.
- BANVILLE, I. & GRAY, R. A. 2002. Effect of action potential duration and conduction velocity restitution and their spatial dispersion on alternans and the stability of arrhythmias. *J Cardiovasc Electrophysiol*, 13, 1141-9.
- BARUSCOTTI, M., BUCCHI, A., VISCOMI, C., MANDELLI, G., CONSALEZ, G., GNECCHI-RUSCONI, T., MONTANO, N., CASALI, K. R., MICHELONI, S., BARBUTI, A. & DIFRANCESCO, D. 2011. Deep bradycardia and heart block caused by inducible cardiac-specific knockout of the pacemaker channel gene Hcn4. *Proc Natl Acad Sci U S A*, 108, 1705-10.
- BEHAR, J., GANESAN, A., ZHANG, J. & YANIV, Y. 2016. The Autonomic Nervous System Regulates the Heart Rate through cAMP-PKA Dependent and Independent Coupled-Clock Pacemaker Cell Mechanisms. *Front Physiol*, 7, 419.
- BILLETTTE, J., JANSE, M. J., VAN CAPELLE, F. J., ANDERSON, R. H., TOUBOUL, P. & DURRER, D. 1976. Cycle-length-dependent properties of AV nodal activation in rabbit hearts. *Am J Physiol*, 231, 1129-39.
- BILLMAN, G. E., SCHWARTZ, P. J. & STONE, H. L. 1982. Baroreceptor reflex control of heart rate: a predictor of sudden cardiac death. *Circulation*, 66, 874-80.
- BLEEKER, W. K., MACKAAY, A. J., MASSON-PEVET, M., BOUMAN, L. N. & BECKER, A. E. 1980. Functional and morphological organization of the rabbit sinus node. *Circ Res*, 46, 11-22.
- BOYETT, M. R., HONJO, H. & KODAMA, I. 2000. The sinoatrial node, a heterogeneous pacemaker structure. *Cardiovasc Res*, 47, 658-87.
- BRACK, K. E., NARANG, R., WINTER, J. & NG, G. A. 2013. The mechanical uncoupler blebbistatin is associated with significant electrophysiological effects in the isolated rabbit heart. *Exp Physiol*, 98, 1009-27.

- BRACK, K. E., PATEL, V. H., COOTE, J. H. & NG, G. A. 2007. Nitric oxide mediates the vagal protective effect on ventricular fibrillation via effects on action potential duration restitution in the rabbit heart. *J Physiol*, 583, 695-704.
- CAO, J. M., CHEN, L. S., KENKNIGHT, B. H., OHARA, T., LEE, M. H., TSAI, J., LAI, W. W., KARAGUEUZIAN, H. S., WOLF, P. L., FISHBEIN, M. C. & CHEN, P. S. 2000a. Nerve sprouting and sudden cardiac death. *Circ Res*, 86, 816-21.
- CAO, J. M., FISHBEIN, M. C., HAN, J. B., LAI, W. W., LAI, A. C., WU, T. J., CZER, L., WOLF, P. L., DENTON, T. A., SHINTAKU, I. P., CHEN, P. S. & CHEN, L. S. 2000b. Relationship between regional cardiac hyperinnervation and ventricular arrhythmia. *Circulation*, 101, 1960-9.
- CAO, J. M., QU, Z., KIM, Y. H., WU, T. J., GARFINKEL, A., WEISS, J. N., KARAGUEUZIAN, H. S. & CHEN, P. S. 1999. Spatiotemporal heterogeneity in the induction of ventricular fibrillation by rapid pacing: importance of cardiac restitution properties. *Circ Res*, 84, 1318-31.
- CERATI, D. & SCHWARTZ, P. J. 1991. Single cardiac vagal fiber activity, acute myocardial ischemia, and risk for sudden death. *Circ Res*, 69, 1389-401.
- CHEN, P. S., CHEN, L. S., CAO, J. M., SHARIFI, B., KARAGUEUZIAN, H. S. & FISHBEIN, M. C. 2001. Sympathetic nerve sprouting, electrical remodeling and the mechanisms of sudden cardiac death. *Cardiovasc Res*, 50, 409-16.
- CHEN, S. L., KAWADA, T., INAGAKI, M., SHISHIDO, T., MIYANO, H., SATO, T., SUGIMACHI, M., TAKAKI, H. & SUNAGAWA, K. 1999. Dynamic counterbalance between direct and indirect vagal controls of atrioventricular conduction in cats. *Am J Physiol*, 277, H2129-35.
- CHENG, S., KEYES, M. J., LARSON, M. G., MCCABE, E. L., NEWTON-CHEH, C., LEVY, D., BENJAMIN, E. J., VASAN, R. S. & WANG, T. J. 2009. Long-term outcomes in individuals with prolonged PR interval or first-degree atrioventricular block. *Jama*, 301, 2571-7.
- CHOI, B. R. & SALAMA, G. 2000. Simultaneous maps of optical action potentials and calcium transients in guinea-pig hearts: mechanisms underlying concordant alternans. *J Physiol*, 529 Pt 1, 171-88.
- COHN, A. E. 1912. ON THE DIFFERENCES IN THE EFFECTS OF STIMULATION OF THE TWO VAGUS NERVES ON RATE AND CONDUCTION OF THE DOG'S HEART. *J Exp Med*, 16, 732-57.
- CORONEL, R., DE GROOT, J. R. & VAN LIESHOUT, J. J. 2001. Defining heart failure. *Cardiovasc Res*, 50, 419-22.
- DE FERRARI, G. M., VANOLI, E., STRAMBA-BADIALE, M., HULL, S. S., JR., FOREMAN, R. D. & SCHWARTZ, P. J. 1991. Vagal reflexes and survival during acute myocardial ischemia in conscious dogs with healed myocardial infarction. *Am J Physiol*, 261, H63-9.
- DIFRANCESCO, D. 1991. The contribution of the 'pacemaker' current (if) to generation of spontaneous activity in rabbit sino-atrial node myocytes. *J Physiol*, 434, 23-40.
- DOKOS, S., CELLER, B. & LOVELL, N. 1996. Ion currents underlying sinoatrial node pacemaker activity: a new single cell mathematical model. *J Theor Biol*, 181, 245-72.
- ECCLES, J. C. 1957. The excitatory reactions of nerve cells. *The Physiology of Nerve Cells*. Baltimore, USA: The Johns Hopkins Press.
- FOZZARD, H. A. 1992. Afterdepolarizations and triggered activity. *Basic Res Cardiol*, 87 Suppl 2, 105-13.

- GARFINKEL, A., KIM, Y. H., VOROSHILOVSKY, O., QU, Z., KIL, J. R., LEE, M. H., KARAGUEUZIAN, H. S., WEISS, J. N. & CHEN, P. S. 2000. Preventing ventricular fibrillation by flattening cardiac restitution. *Proc Natl Acad Sci U S A*, 97, 6061-6.
- GERVAIS, R., LECLERCQ, C., SHANKAR, A., JACOBS, S., EISKJAER, H., JOHANNESSEN, A., FREEMANTLE, N., CLELAND, J. G., TAVAZZI, L. & DAUBERT, C. 2009. Surface electrocardiogram to predict outcome in candidates for cardiac resynchronization therapy: a sub-analysis of the CARE-HF trial. *Eur J Heart Fail*, 11, 699-705.
- GILMOUR, R. F., JR. & CHIALVO, D. R. 1999. Electrical restitution, critical mass, and the riddle of fibrillation. *J Cardiovasc Electrophysiol*, 10, 1087-9.
- GOLDHABER, J. I., XIE, L. H., DUONG, T., MOTTER, C., KHUU, K. & WEISS, J. N. 2005. Action potential duration restitution and alternans in rabbit ventricular myocytes: the key role of intracellular calcium cycling. *Circ Res*, 96, 459-66.
- GRASSI, G., SERAVALLE, G., BERTINIERI, G., TURRI, C., STELLA, M. L., SCOPPELLITI, F. & MANCIA, G. 2001. Sympathetic and reflex abnormalities in heart failure secondary to ischaemic or idiopathic dilated cardiomyopathy. *Clin Sci (Lond)*, 101, 141-6.
- HAGIWARA, N., IRISAWA, H. & KAMEYAMA, M. 1988. Contribution of two types of calcium currents to the pacemaker potentials of rabbit sino-atrial node cells. *J Physiol*, 395, 233-53.
- HAO, S. C., CHRISTINI, D. J., STEIN, K. M., JORDAN, P. N., IWAI, S., BRAMWELL, O., MARKOWITZ, S. M., MITTAL, S. & LERMAN, B. B. 2004. Effect of beta-adrenergic blockade on dynamic electrical restitution in vivo. *Am J Physiol Heart Circ Physiol*, 287, H390-4.
- HARTZELL, H. C. 1988. Regulation of cardiac ion channels by catecholamines, acetylcholine and second messenger systems. *Prog Biophys Mol Biol*, 52, 165-247.
- HILL, J. A. 2003. Electrical remodeling in cardiac hypertrophy. *Trends Cardiovasc Med*, 13, 316-22.
- HJALMARSON, A. & FAGERBERG, B. 2000. MERIT-HF mortality and morbidity data. *Basic Res Cardiol*, 95 Suppl 1, I98-103.
- IRISAWA, H. 1987. Membrane currents in cardiac pacemaker tissue. *Experientia*, 43, 1131-5.
- ISSA, Z. F., ROSENBERGER, J., GROH, W. J., MILLER, J. M. & ZIPES, D. P. 2005. Ischemic ventricular arrhythmias during heart failure: a canine model to replicate clinical events. *Heart Rhythm*, 2, 979-83.
- KARMA, A. 1994. Electrical alternans and spiral wave breakup in cardiac tissue. *Chaos*, 4, 461-472.
- KOLLER, M. L., RICCIO, M. L. & GILMOUR, R. F., JR. 1998. Dynamic restitution of action potential duration during electrical alternans and ventricular fibrillation. *Am J Physiol*, 275, H1635-42.
- LA ROVERE, M. T., BIGGER, J. T., JR., MARCUS, F. I., MORTARA, A. & SCHWARTZ, P. J. 1998. Baroreflex sensitivity and heart-rate variability in prediction of total cardiac mortality after myocardial infarction. ATRAMI (Autonomic Tone and Reflexes After Myocardial Infarction) Investigators. *Lancet*, 351, 478-84.
- LA ROVERE, M. T., PINNA, G. D., MAESTRI, R., ROBBI, E., CAPOROTONDI, A., GUAZZOTTI, G., SLEIGHT, P. & FEBO, O. 2009. Prognostic implications of

- baroreflex sensitivity in heart failure patients in the beta-blocking era. *J Am Coll Cardiol*, 53, 193-9.
- LEE, M. H., LIN, S. F., OHARA, T., OMICHI, C., OKUYAMA, Y., CHUDIN, E., GARFINKEL, A., WEISS, J. N., KARAGUEUZIAN, H. S. & CHEN, P. S. 2001. Effects of diacetyl monoxime and cytochalasin D on ventricular fibrillation in swine right ventricles. *Am J Physiol Heart Circ Physiol*, 280, H2689-96.
- LEVY, M. N. 1971. Sympathetic-parasympathetic interactions in the heart. *Circ Res*, 29, 437-45.
- LEWARTOWSKI, B. & PYTKOWSKI, B. 1987. Cellular mechanism of the relationship between myocardial force and frequency of contractions. *Prog Biophys Mol Biol*, 50, 97-120.
- LOEB, J. M. & DETARNOWSKY, J. M. 1988. Integration of heart rate and sympathetic neural effects on AV conduction. *Am J Physiol*, 254, H651-7.
- LOWN, B. & VERRIER, R. L. 1976. Neural activity and ventricular fibrillation. *N Engl J Med*, 294, 1165-70.
- LUU, M., STEVENSON, W. G., STEVENSON, L. W., BARON, K. & WALDEN, J. 1989. Diverse mechanisms of unexpected cardiac arrest in advanced heart failure. *Circulation*, 80, 1675-80.
- MALTSEV, A. V., MALTSEV, V. A., MIKHEEV, M., MALTSEVA, L. A., SIRENKO, S. G., LAKATTA, E. G. & STERN, M. D. 2011. Synchronization of stochastic Ca(2)(+) release units creates a rhythmic Ca(2)(+) clock in cardiac pacemaker cells. *Biophys J*, 100, 271-83.
- MANTRAVADI, R., GABRIS, B., LIU, T., CHOI, B. R., DE GROAT, W. C., NG, G. A. & SALAMA, G. 2007. Autonomic nerve stimulation reverses ventricular repolarization sequence in rabbit hearts. *Circ Res*, 100, e72-80.
- MARTINEZ, M. L., HEREDIA, M. P. & DELGADO, C. 1999. Expression of T-type Ca(2+) channels in ventricular cells from hypertrophied rat hearts. *J Mol Cell Cardiol*, 31, 1617-25.
- MARTINS, J. B. & ZIPES, D. P. 1980. Effects of sympathetic and vagal nerves on recovery properties of the endocardium and epicardium of the canine left ventricle. *Circ Res*, 46, 100-10.
- MAZGALEV, T., DREIFUS, L. S., MICHELSON, E. L. & PELLEG, A. 1986. Vagally induced hyperpolarization in atrioventricular node. *Am J Physiol*, 251, H631-43.
- MAZGALEV, T. N., HO, S. Y. & ANDERSON, R. H. 2001. Anatomic-electrophysiological correlations concerning the pathways for atrioventricular conduction. *Circulation*, 103, 2660-7.
- MEIJLER, F. L. & JANSE, M. J. 1988. Morphology and electrophysiology of the mammalian atrioventricular node. *Physiol Rev*, 68, 608-47.
- MULIERI, L. A., HASENFUSS, G., LEAVITT, B., ALLEN, P. D. & ALPERT, N. R. 1992. Altered myocardial force-frequency relation in human heart failure. *Circulation*, 85, 1743-50.
- MYLES, R. C., BURTON, F. L., COBBE, S. M. & SMITH, G. L. 2011. Alternans of action potential duration and amplitude in rabbits with left ventricular dysfunction following myocardial infarction. *J Mol Cell Cardiol*, 50, 510-21.
- NG, G. A., BRACK, K. E. & COOTE, J. H. 2001. Effects of direct sympathetic and vagus nerve stimulation on the physiology of the whole heart--a novel model of isolated Langendorff perfused rabbit heart with intact dual autonomic innervation. *Exp Physiol*, 86, 319-29.

- NG, G. A., BRACK, K. E., PATEL, V. H. & COOTE, J. H. 2007. Autonomic modulation of electrical restitution, alternans and ventricular fibrillation initiation in the isolated heart. *Cardiovasc Res*, 73, 750-60.
- NIKOLAIDOU, T., CAI, X. J., STEPHENSON, R. S., YANNI, J., LOWE, T., ATKINSON, A. J., JONES, C. B., SARDAR, R., CORNO, A. F., DOBRZYNISKI, H., WITHERS, P. J., JARVIS, J. C., HART, G. & BOYETT, M. R. 2015. Congestive Heart Failure Leads to Prolongation of the PR Interval and Atrioventricular Junction Enlargement and Ion Channel Remodelling in the Rabbit. *PLoS One*, 10, e0141452.
- NOLAN, J., BATIN, P. D., ANDREWS, R., LINDSAY, S. J., BROOKSBY, P., MULLEN, M., BAIG, W., FLAPAN, A. D., COWLEY, A., PRESCOTT, R. J., NEILSON, J. M. & FOX, K. A. 1998. Prospective study of heart rate variability and mortality in chronic heart failure: results of the United Kingdom heart failure evaluation and assessment of risk trial (UK-heart). *Circulation*, 98, 1510-6.
- NOLASCO, J. B. & DAHLEN, R. W. 1968. A graphic method for the study of alternation in cardiac action potentials. *J Appl Physiol*, 25, 191-6.
- NOMA, A., MORAD, M. & IRISAWA, H. 1983. Does the "pacemaker current" generate the diastolic depolarization in the rabbit SA node cells? *Pflugers Arch*, 397, 190-4.
- NUSS, H. B. & HOUSER, S. R. 1993. T-type Ca²⁺ current is expressed in hypertrophied adult feline left ventricular myocytes. *Circ Res*, 73, 777-82.
- OLSHANSKY, B., DAY, J. D., SULLIVAN, R. M., YONG, P., GALLE, E. & STEINBERG, J. S. 2012. Does cardiac resynchronization therapy provide unrecognized benefit in patients with prolonged PR intervals? The impact of restoring atrioventricular synchrony: an analysis from the COMPANION Trial. *Heart Rhythm*, 9, 34-9.
- OMICHI, C., ZHOU, S., LEE, M. H., NAIK, A., CHANG, C. M., GARFINKEL, A., WEISS, J. N., LIN, S. F., KARAGUEUZIAN, H. S. & CHEN, P. S. 2002. Effects of amiodarone on wave front dynamics during ventricular fibrillation in isolated swine right ventricle. *Am J Physiol Heart Circ Physiol*, 282, H1063-70.
- PATEL, V. H., BRACK, K. E., COOTE, J. H. & NG, G. A. 2008. A novel method of measuring nitric-oxide-dependent fluorescence using 4,5-diaminofluorescein (DAF-2) in the isolated Langendorff-perfused rabbit heart. *Pflugers Arch*, 456, 635-45.
- PITRUZZELLO, A. M., KRASSOWSKA, W. & IDRIS, S. F. 2007. Spatial heterogeneity of the restitution portrait in rabbit epicardium. *Am J Physiol Heart Circ Physiol*, 292, H1568-78.
- POGWIZD, S. M. 1995. Nonreentrant mechanisms underlying spontaneous ventricular arrhythmias in a model of nonischemic heart failure in rabbits. *Circulation*, 92, 1034-48.
- PRUVOT, E. J., KATRA, R. P., ROSENBAUM, D. S. & LAURITA, K. R. 2004. Role of calcium cycling versus restitution in the mechanism of repolarization alternans. *Circ Res*, 94, 1083-90.
- RANDALL, W. C., EULER, D. E., JACOBS, H. K., WEHRMACHER, W., KAYE, M. P. & HAGEMAN, G. R. 1976. Autonomic neural control of cardiac rhythm: the role of autonomic imbalance in the genesis of cardiac dysrhythmia. *Cardiology*, 61, 20-36.

- RICCIO, M. L., KOLLER, M. L. & GILMOUR, R. F., JR. 1999. Electrical restitution and spatiotemporal organization during ventricular fibrillation. *Circ Res*, 84, 955-63.
- ROGER, V. L., GO, A. S., LLOYD-JONES, D. M., BENJAMIN, E. J., BERRY, J. D., BORDEN, W. B., BRAVATA, D. M., DAI, S., FORD, E. S., FOX, C. S., FULLERTON, H. J., GILLESPIE, C., HAILPERN, S. M., HEIT, J. A., HOWARD, V. J., KISSELA, B. M., KITTNER, S. J., LACKLAND, D. T., LICHTMAN, J. H., LISABETH, L. D., MAKUC, D. M., MARCUS, G. M., MARELLI, A., MATCHAR, D. B., MOY, C. S., MOZAFFARIAN, D., MUSSOLINO, M. E., NICHOL, G., PAYNTER, N. P., SOLIMAN, E. Z., SORLIE, P. D., SOTOODEHNIA, N., TURAN, T. N., VIRANI, S. S., WONG, N. D., WOO, D. & TURNER, M. B. 2012. Heart disease and stroke statistics--2012 update: a report from the American Heart Association. *Circulation*, 125, e2-e220.
- SCHWARTZ, P. J. 1998. The autonomic nervous system and sudden death. *Eur Heart J*, 19 Suppl F, F72-80.
- SCHWARTZ, P. J. & STONE, H. L. 1980. Left stellectomy in the prevention of ventricular fibrillation caused by acute myocardial ischemia in conscious dogs with anterior myocardial infarction. *Circulation*, 62, 1256-65.
- SCHWARTZ, P. J., VANOLI, E., STRAMBA-BADIALE, M., DE FERRARI, G. M., BILLMAN, G. E. & FOREMAN, R. D. 1988. Autonomic mechanisms and sudden death. New insights from analysis of baroreceptor reflexes in conscious dogs with and without a myocardial infarction. *Circulation*, 78, 969-79.
- SHEMAROVA, I. V., KUZNETSOV, S. V., DEMINA, I. N. & NESTEROV, V. P. 2009. [T-channels and Na⁺,Ca²⁺-exchangers as components of the Ca²⁺-system of the myocardial activity regulation of the frog *Rana temporaria*]. *Zh Evol Biokhim Fiziol*, 45, 319-28.
- SUN, J., LU, Y., HUANG, Y. & WUGETI, N. 2015. Unilateral vagus nerve stimulation improves ventricular autonomic nerve distribution and functional imbalance in a canine heart failure model. *Int J Clin Exp Med*, 8, 9334-40.
- TAGGART, P., SUTTON, P., CHALABI, Z., BOYETT, M. R., SIMON, R., ELLIOTT, D. & GILL, J. S. 2003. Effect of adrenergic stimulation on action potential duration restitution in humans. *Circulation*, 107, 285-9.
- TAGGART, P., SUTTON, P., LAB, M., DEAN, J. & HARRISON, F. 1990. Interplay between adrenaline and interbeat interval on ventricular repolarisation in intact heart in vivo. *Cardiovasc Res*, 24, 884-95.
- TOMASELLI, G. F. & MARBAN, E. 1999. Electrophysiological remodeling in hypertrophy and heart failure. *Cardiovasc Res*, 42, 270-83.
- TOMASELLI, G. F. & ZIPES, D. P. 2004. What causes sudden death in heart failure? *Circ Res*, 95, 754-63.
- VAN OORT, R. J., GARBINO, A., WANG, W., DIXIT, S. S., LANDSTROM, A. P., GAUR, N., DE ALMEIDA, A. C., SKAPURA, D. G., RUDY, Y., BURNS, A. R., ACKERMAN, M. J. & WEHRENS, X. H. 2011. Disrupted junctional membrane complexes and hyperactive ryanodine receptors after acute junctophilin knockdown in mice. *Circulation*, 123, 979-88.
- VENETUCCI, L. A., TRAFFORD, A. W., O'NEILL, S. C. & EISNER, D. A. 2008. The sarcoplasmic reticulum and arrhythmogenic calcium release. *Cardiovasc Res*, 77, 285-92.

- VERMEULEN, J. T., MCGUIRE, M. A., OPTHOF, T., CORONEL, R., DE BAKKER, J. M., KLOPPING, C. & JANSE, M. J. 1994. Triggered activity and automaticity in ventricular trabeculae of failing human and rabbit hearts. *Cardiovasc Res*, 28, 1547-54.
- VINOGRADOVA, T. M., BROCHET, D. X., SIRENKO, S., LI, Y., SPURGEON, H. & LAKATTA, E. G. 2010. Sarcoplasmic reticulum Ca²⁺ pumping kinetics regulates timing of local Ca²⁺ releases and spontaneous beating rate of rabbit sinoatrial node pacemaker cells. *Circ Res*, 107, 767-75.
- WANG, Y., TANDAN, S., CHENG, J., YANG, C., NGUYEN, L., SUGIANTO, J., JOHNSTONE, J. L., SUN, Y. & HILL, J. A. 2008. Ca²⁺/calmodulin-dependent protein kinase II-dependent remodeling of Ca²⁺ current in pressure overload heart failure. *J Biol Chem*, 283, 25524-32.
- WEISS, J. N., CHEN, P. S., QU, Z., KARAGUEUZIAN, H. S., LIN, S. F. & GARFINKEL, A. 2002. Electrical restitution and cardiac fibrillation. *J Cardiovasc Electrophysiol*, 13, 292-5.
- WEST, T. C. & TODA, N. 1967. Response of the A-V node of the rabbit to stimulation of intracardiac cholinergic nerves. *Circ Res*, 20, 18-31.
- XIAO, J., LUO, X., LIN, H., ZHANG, Y., LU, Y., WANG, N., ZHANG, Y., YANG, B. & WANG, Z. 2007. MicroRNA miR-133 represses HERG K⁺ channel expression contributing to QT prolongation in diabetic hearts. *J Biol Chem*, 282, 12363-7.
- YAMAKAWA, K., SO, E. L., RAJENDRAN, P. S., HOANG, J. D., MAKKAR, N., MAHAJAN, A., SHIVKUMAR, K. & VASEGHI, M. 2014. Electrophysiological effects of right and left vagal nerve stimulation on the ventricular myocardium. *Am J Physiol Heart Circ Physiol*, 307, H722-31.
- YANG, B., LIN, H., XIAO, J., LU, Y., LUO, X., LI, B., ZHANG, Y., XU, C., BAI, Y., WANG, H., CHEN, G. & WANG, Z. 2007. The muscle-specific microRNA miR-1 regulates cardiac arrhythmogenic potential by targeting GJA1 and KCNJ2. *Nat Med*, 13, 486-91.
- ZHANG, Q., TIMOFEYEV, V., QIU, H., LU, L., LI, N., SINGAPURI, A., TORADO, C. L., SHIN, H. S. & CHIAMVIMONVAT, N. 2011. Expression and roles of Cav1.3 (alpha1D) L-type Ca(2)+ channel in atrioventricular node automaticity. *J Mol Cell Cardiol*, 50, 194-202.

Chapter 8

Synopsis

Autonomic Modulation in a Rabbit Model of Heart Failure

Chapter 8: Synopsis

8.1 Introduction

This thesis represents a journey of characterising autonomic electrocardiology in an *in vitro* model of Langendorff-perfused, dual-innervated rabbit hearts, transitioning from normal hearts to diseased hearts with heart failure following coronary ligation. In normal heart studies, the effect of sympatho-vagal interaction on both atrial and ventricular electrophysiology was investigated, following which the effect of beta-blockade on ventricular electrophysiologic properties during sympatho-vagal interaction was studied. A surgical heart failure model was developed through coronary ligation surgery during which various refinements were employed to resolve the challenges of peri-operative mortality. The maturation of this model allows assessment of structural remodelling with *in vivo* and *ex vivo* imaging techniques. Last but not least, electrical remodelling was studied in detail at the atrial, atrio-ventricular and ventricular level under autonomic stimulation.

8.2 Sympatho-vagal Interaction in Isolated Dual-innervated Langendorff-perfused Rabbit Hearts

Sympatho-vagal interaction studies were performed in an *in vitro* Langendorff-perfused rabbit heart model with intact dual-autonomic nerves (Chapter 4). The studies were carried out in two protocols depending on the sequence of autonomic nerve stimulation. Protocol 1 involved background high-frequency sympathetic stimulation with concurrent low- and high-frequency vagal stimulation. Whereas in protocol 2, background high-frequency vagal stimulation was introduced with concurrent low- and high-frequency sympathetic stimulation. In both protocols, heart rate response exhibited *accentuated antagonism*, with a dominant vagal response in heart rate changes. In contrast, no evidence of *accentuated antagonism* was observed at the ventricular level. Vagal stimulation confers antiarrhythmic properties by increasing ventricular fibrillation threshold (VFT) and flattening action potential duration restitution (APD-RT) (Ng et al., 2007). However, in the presence of concurrent sympathetic stimulation, the pro-arrhythmic sympathetic effects prevail over those of

vagal stimulation, with lower VFT and steepened APD-RT. This phenomenon is irrespective of the sequence of autonomic stimulations, being evident in both Protocol 1 (low- and high-frequency sympathetic stimulation with concurrent high-frequency vagal stimulation) and 2 (low- and high-frequency vagal stimulation with concurrent high-frequency sympathetic stimulation).

The absence of a dominant protective vagal effect against ventricular fibrillation during sympatho-vagal interaction is in contrast with previous studies which concluded that vagal or cholinergic stimulation mediates its protective effect in the presence of adrenergic activity in canine models (Rabinowitz et al., 1976, Kolman et al., 1976, Huang et al., 2015). The prevailing sympathetic effect in steepening action potential duration in the presence of vagal stimulation support the changes seen in the ventricular fibrillation threshold, and in contrast with the findings in an *in vivo* canine model (Huang et al., 2015).

In this study, no sympatho-vagal interaction was found in ventricular refractoriness. The ultimate effective refractory period (ERP) appears to be determined by the sequence of the autonomic nerve stimulation. This contradicts previous studies which demonstrated vagal effect of ERP prolongation following hypersympathetic activity in both *in vivo* experimental and clinical models (Huang et al., 2015, Ophof et al., 1993, Schwartz et al., 1977, Morady et al., 1988).

This study concluded that *accentuated antagonism*, although present at the atrial level for heart rate changes, is absent at the ventricular level VFT, ERP and APD-RT, suggesting a neurocardiac mechanistic interaction distinctive from the known presynaptic mechanism at the atrial level.

8.3 Effect of Beta-Blockade on Heart Rate and Ventricular Electrophysiology during Sympatho-vagal Interaction

Following the findings of prevailing sympathetic effect in ventricular electrophysiology during sympatho-vagal interaction, metoprolol was used to achieve adrenergic blockade to reassess both heart rate response and various aspects of ventricular electrophysiology

(Chapter 5). In this study, low- and high-frequency vagal stimulation was performed on dual-innervated, Langendorff-perfused rabbit hearts with and without background high-frequency sympathetic stimulation. This was used as controls before metoprolol was infused. Metoprolol abolishes sympathetic-induced heart rate increment. Hence no *accentuated antagonism* was observed in heart rate response during sympatho-vagal interaction. When VFT was assessed in the presence of metoprolol, global VFTs were higher even in the absence of autonomic nerve stimulation. Metoprolol did not affect vagal-induced VFT increment but suppressed the lowering of VFT during sympathetic stimulation. In contrast, historical studies were of the opinion of the necessity of adrenergic tone to mediate vagal protective effect against ventricular fibrillation (Kolman et al., 1976, Rabinowitz et al., 1976). Relevantly, the metoprolol effect on VFT in this study was reversible following a washout period.

Accordingly, APD-RT changes mirrored those observed for VFT. In the controls, vagal stimulation flattened APD-RT slopes whilst sympathetic stimulation steepened the slopes. In the presence of metoprolol, overall APD-RT slopes were much flatter whilst vagal effect of further flattening APD-RT slopes were retained in the presence of background sympathetic stimulation. The overall increase in VFT and flattening of APD-RT by metoprolol led to speculations of possible ion-channel modifying effects previously described with other beta-blockers (Patterson and Lucchesi, 1984, Almotrefi et al., 1989). Additionally, it is also conceivable that the use of acetate-free Tyrode solution may act synergistically with metoprolol to provide additional antifibrillatory properties since sodium acetate may contribute to ventricular arrhythmia through perturbed mitochondrial calcium transport (Harris, 1978, Reed and Bygrave, 1975, Lehninger, 1974, Florea and Blatter, 2010). However, when the study was repeated using acetate-containing Tyrode solution, similar results emerged with infusion of metoprolol.

This study revealed that metoprolol abolishes *accentuated antagonism* in heart rate response in addition to suppressing the prevailing pro-arrhythmic sympathetic effect in ventricular electrophysiology during sympatho-vagal interaction. Importantly, additional anti-fibrillatory phenomenon was observed in the presence of metoprolol

beyond that accountable by adrenergic blockade. Future studies to measure local norepinephrine release will shed further light.

8.4 Development of a Surgical Heart Failure Model in Rabbits by Coronary Ligation

This study set out to build a surgical heart failure model in rabbits by coronary ligation (Chapter 3), providing an important platform for subsequent studies of structural and electrical remodelling in the infarct heart failure model. Male New Zealand white rabbits underwent open-chest surgeries under general anaesthesia and invasive ventilatory support. The heart was assessed through lateral thoracotomy. In heart failure (HF) group, circumflex artery was identified and ligated to induce a reproducible and consistent myocardial infarction at the apical region. In the sham (SHM) group, the heart was exposed but no coronary ligation was performed. Both groups of rabbits were then allowed to recover post-operatively for eight weeks before they were sacrificed and their hearts procured for terminal experiments.

There is a learning curve in building a sustainable surgical heart failure model in rabbits. Initial post-operative mortality was high with most deaths occurring within 2 weeks. Animals lighter than 2.7 kg all succumbed to death post-operatively. This led to the decision of opting for a suitable pre-operative weight of 3 kg with the allowance of 10 % variation. Intubation in rabbits can be challenging due to their inherent airway anatomy, and is reflected by the finding of tracheitis on histological examination at post-mortem of rabbits with premature mortality. This led to a modification of intubation and ventilatory techniques, including adopting a prone intubation position, using a water-based lubricant, selecting appropriate sized cuffed endotracheal tube, setting low tidal volume and respiratory rate on ventilator amongst others. During surgery, ventricular fibrillation occurred following coronary ligation in 3 rabbits, accounting for 43% of intra-operative mortality. Another major cause of intra-operative mortality is incorrect endotracheal tube placement, highlighting the technically challenging nature of intubation. In terms of post-operative mortality, tracheitis is by far the most common cause, accounting for 54% of the cases.

This study presents a unique learning experience, during which various refinements have been trialled, following advice from the named veterinary surgeon to curtail animal mortality. A temporal pattern demonstrating declining post-operative mortality is suggestive of a learning curve, ultimately with a satisfying outcome of 100 % survival towards the end of the study period (Figure 3.10).

8.5 Structural Remodelling in Heart Failure

In this study, distinctive structural remodelling occurred in rabbits with heart failure following coronary ligation-induced myocardial infarction (Chapter 6). Evidence of cardiac remodelling were obtained from *in vivo* transthoracic echocardiography and *ex vivo* cardiac magnetic resonance imaging (MRI). Ligation of circumflex artery in rabbits produced region-specific myocardial infarction, manifesting as thinning of the septum on transthoracic echocardiography. In addition to the visible fibrotic scar tissue at the apices upon procurement of the hearts, the transmurality and location-specific myocardial scarring was validated by *ex vivo* cardiac MRI. Furthermore, cardiac architectural disruption in heart failure manifested as increased end-diastolic left ventricular diameter and volume, as well as increased end-diastolic endocardial area. Phenotypically this resulted in not only a dilated left ventricle but also a more spherical left ventricular geometry.

Overall, rabbits with heart failure exhibited impairment in left ventricular contractile performance, demonstrable by significantly lower ejection fraction when compared to the shams. A structure-function relationship was validated by a significant correlation between left ventricular end-diastolic diameter and ejection fraction. Similar correlation also existed between left atrial systolic diameter and ejection fraction. Enlarged left atrium in heart failure rabbits could be due to a number of factors. Increased left ventricular stiffness produced an increased left ventricular end-diastolic pressure which back-pressures into left atrium, resulting in a raised left atrial pressure and a dilated left atrium. Mitral regurgitation, either as a sequelae of annular dilatation or a direct ischaemic insult to the papillary muscles, plays a key role in left atrial dilatation, a mechanism which has been observed in both pre-clinical and clinical studies (Buckberg et al., 2004, Dowell et al., 1979).

Further back-pressure from left atrium to right ventricle results in right heart failure. Indirect evidence was derived from the significantly higher wet weights of both lungs and livers, connoting pulmonary and hepatic congestion in the heart failure group. The link between extra-cardiac congestion and left ventricular systolic impairment was supported by significant correlations between lung/liver wet weights and left ventricular ejection fraction. Importantly cardiac and systemic remodellings observed in this study parallel pathophysiological changes in humans with heart failure as a result of previous myocardial infarction (Parmley, 1989).

8.6 Characterisation of Electrophysiologic Response under Autonomic Stimulation in Heart Failure

Autonomic imbalance is a well-known hallmark in heart failure, with sympathetic overdrive and parasympathetic attenuation preceding development of clinical phenotypes in heart failure. These autonomic disturbances have been observed in both experimental and clinical studies (Ishise et al., 1998, Grassi et al., 2001), and have been implicated in the occurrence of lethal ventricular arrhythmias and sudden death in both canine models and humans (Grassi et al., 2001, Vanoli et al., 1991, Schwartz et al., 1988). This study sought to investigate chronotropy, dromotropy, ventricular fibrillation inducibility, ventricular refractoriness and electrical restitution in the rabbit heart failure model, characterising atrial, atrio-ventricular and ventricular levels of electrophysiologic responses under direct sympathetic and vagus nerve stimulation. The use of *in vitro* Langendorff-perfused rabbit heart preparations allows the study of whole-heart electrophysiology under autonomic influence without the confounding circulating humoral factors.

In both HF and SHM animals, sympathetic nerve stimulation induced similar degree of voltage-dependent heart rate increment between the two groups, suggesting that there was no difference in recruitment of sympathetic nerve fibres (i.e. *spatial* summation). Similar degree of heart rate reduction was observed with right and left vagus nerve stimulation between heart failure and sham animals. However, rabbits with heart failure exhibited heightened sympathetic response in heart rate increment at high-frequency

stimulation (i.e. at 15 and 20 Hz). Additionally, they also demonstrated a much attenuated vagal-induced heart rate reduction during high-frequency stimulations of *right* vagus nerve. This suggests an exaggerated *temporal* summation of sympathetic nerve fibres and a diminished *temporal* summation of parasympathetic nerves. No frequency-dependent difference was observed in chronotropic response during left vagus nerve stimulation between the heart failure animals and the shams. This is in congruent with the notion of right vagus nerve being the main contributor of negative chronotropic response as compared to the left vagus nerve (Cohn, 1912, Ardell and Randall, 1986, Ng et al., 2001).

The positive dromotropy effect by sympathetic stimulation (West and Toda, 1967) and the negative dromotropy effect by vagal stimulation (Mazgalev et al., 1986) were well reported. In the heart failure group, AV delay was in general prolonged, in parallel with the prolonged PR interval observed on surface ECG in patients with heart failure (Olshansky et al., 2012, Gervais et al., 2009). Sympathetic induced AV shortening were observed in both groups but there was exaggerated positive dromotropic effect in the heart failure group. Although vagal-induced negative dromotropy was observed in both groups, there was an attenuated effect in AV prolongation in the heart failure group during *right* vagus nerve stimulation. Similar to what was observed for chronotropic response, there was no difference in dromotropic response during left vagus nerve stimulation between heart failure group and the shams. The mechanism behind differential effect between right and left vagal stimulation in AV conduction could not be ascribed to changes in sinus rate as the heart rate was fixed by atrial pacing, suggesting possible structural and ion-channel remodellings in AV node of rabbits with heart failure (Nikolaïdou et al., 2015).

At the ventricular level, VFT were globally lower in the heart failure group, implying an increased susceptibility for ventricular fibrillation as a result of heart failure. The pro-arrhythmic effect of sympathetic stimulation is reflected by the lowering of VFT whilst vagal stimulation confers protection against ventricular arrhythmia by raising VFT (Ng et al., 2007). In this study, HF rabbits demonstrated a greater reduction in VFT during sympathetic stimulation as compared to shams. Conversely, the vagal effect in increasing VFT was much attenuated in the HF rabbits. Pertinently, action-potential-

duration restitution (APD-RT) slopes were on the whole steeper in the HF group. APD-RT describes the relationship between APD and its preceding diastolic intervals. The restitution hypothesis postulates that if the APD-RT were steep with a gradient of > 1 , the tendency of oscillations and wave breaks increases, promoting the initiation of ventricular fibrillation (Weiss et al., 2000). Sympathetic stimulation was shown to steepen APD-RT slopes with vagal stimulation flattening the slopes (Ng et al., 2007). In this study, sympathetic stimulation led to a greater degree of APD-RT slope steepening in the HF group, whereas during vagal stimulation, the flattening effect of APD-RT slope was diminished. The synchronicity between VFT and APD-RT changes in the HF group portrays a picture of hypersympathetic effect and attenuated vagal effect, accounting for increased propensity in ventricular arrhythmias.

Greater regional differences in APD-RT were evident in the HF group. In both HF and sham groups, APD-RT slopes at apex were steeper than those at the base, likely to be a reflection of right ventricular apical pacing (Pitruzzello et al., 2007). Nonetheless, apico-basal APD-RT dispersion were overall greater in the HF group irrespective of the presence of autonomic stimulation. Sympathetic stimulation increased apico-basal APD-RT dispersion, the effect of which was more observable in the HF group. During vagal stimulation, there was no difference seen in apico-basal RT dispersion when compared to baseline. Increased spatial heterogeneity in restitution kinetics at baseline and during sympathetic stimulation in the HF rabbits may therefore act synergistically with the already steepened overall APD-RT, providing an electrical substrate for increased ventricular fibrillation.

Ventricular effective refractory period (ERP) in the HF group was similar to that of shams at baseline. However, the sympathetic effect in shortening ERP, previously demonstrated in an *in vitro* study of normal rabbit hearts (Ng et al., 2007), was potentiated in the HF group. In contrast, the effect of vagal-induced ERP prolongation was diminished in the HF group.

This study therefore demonstrated various electrophysiologic changes at the atrial, atrio-ventricular and ventricular levels driven by autonomic imbalance characterised by augmented sympathetic effect and attenuated vagal response, contributing to electrical

remodelling, dysfunctional neuro-cardiac axis and increased susceptibility for ventricular fibrillation in a post-infarct rabbit failure model.

8.7 Future Direction

The rabbit surgical heart failure model created by coronary ligation prove to be an invaluable tool in future detailed studies of electrical remodelling in hear failure. In this study, the effects of individual autonomic nerve stimulation on various electrophysiologic properties were investigated. A natural progression of this study involve future sympatho-vagal interaction studies using this HF model. The novel finding of prevailing sympathetic effect in ventricular electrophysiology of normal rabbit hearts will require further mechanistic studies, for instance the measurement of norepinephrine spillover during sympatho-vagal interaction not only in normal hearts and but also in the HF hearts. Measurement of nitric oxide in unstimulated and vagal-stimulated HF hearts would provide an insight into attenuated vagal response in HF rabbits as nitric oxide has been shown to mediate the antifibrillatory effect of vagal stimulation (Brack et al., 2007). Additionally, optical mapping of HF hearts will help to validate restitution kinetics, including spatial characterisation in both apico-basal and endo-epicardial axes, in this HF model. Last but not least, immuno-histochemical studies of HF cardiac tissue will aid in understanding of autonomic nerve distribution and ion-channel remodelling at the ventricular level.

8.8 References

- ALMOTREFI, A. A., ABOUL-ENEIN, H. Y. & PREMKUMAR, L. S. 1989. Evaluation of the antifibrillatory activity of fluorinated derivatives of indenolol and nadolol in isolated rabbit and rat hearts: comparison with propranolol. *Arch Int Pharmacodyn Ther*, 301, 122-30.
- ARDELL, J. L. & RANDALL, W. C. 1986. Selective vagal innervation of sinoatrial and atrioventricular nodes in canine heart. *Am J Physiol*, 251, H764-73.
- BRACK, K. E., PATEL, V. H., COOTE, J. H. & NG, G. A. 2007. Nitric oxide mediates the vagal protective effect on ventricular fibrillation via effects on action potential duration restitution in the rabbit heart. *J Physiol*, 583, 695-704.
- BUCKBERG, G. D., WEISFELDT, M. L., BALLESTER, M., BEYAR, R., BURKHOFF, D., COGHLAN, H. C., DOYLE, M., EPSTEIN, N. D., GHARIB, M., IDEKER, R. E., INGELS, N. B., LEWINTER, M. M., MCCULLOCH, A. D., POHOST, G. M., REINLIB, L. J., SAHN, D. J., SOPKO, G., SPINALE, F. G., SPOTNITZ, H. M., TORRENT-GUASP, F. & SHAPIRO, E. P. 2004. Left ventricular form and

- function: scientific priorities and strategic planning for development of new views of disease. *Circulation*, 110, e333-6.
- COHN, A. E. 1912. ON THE DIFFERENCES IN THE EFFECTS OF STIMULATION OF THE TWO VAGUS NERVES ON RATE AND CONDUCTION OF THE DOG'S HEART. *J Exp Med*, 16, 732-57.
- DOWELL, R. T., HAITHCOAT, J. L. & HASSER, E. M. 1979. Pressure-induced cardiac enlargement in neonatal and adult rats. Left ventricular weight and hemodynamic responses during the early adaptive period. *Tex Rep Biol Med*, 39, 139-51.
- FLOREA, S. M. & BLATTER, L. A. 2010. The role of mitochondria for the regulation of cardiac alternans. *Front Physiol*, 1, 141.
- GERVAIS, R., LECLERCQ, C., SHANKAR, A., JACOBS, S., EISKJAER, H., JOHANNESSEN, A., FREEMANTLE, N., CLELAND, J. G., TAVAZZI, L. & DAUBERT, C. 2009. Surface electrocardiogram to predict outcome in candidates for cardiac resynchronization therapy: a sub-analysis of the CARE-HF trial. *Eur J Heart Fail*, 11, 699-705.
- GRASSI, G., SERAVALLE, G., BERTINIERI, G., TURRI, C., STELLA, M. L., SCOPPELLITI, F. & MANCIA, G. 2001. Sympathetic and reflex abnormalities in heart failure secondary to ischaemic or idiopathic dilated cardiomyopathy. *Clin Sci (Lond)*, 101, 141-6.
- HARRIS, E. J. 1978. Anion/calcium ion ratios and proton production in some mitochondrial calcium ion uptakes. *Biochem J*, 176, 983-91.
- HUANG, J., QIAN, J., YAO, W., WANG, N., ZHANG, Z., CAO, C., SONG, B. & ZHANG, Z. 2015. Vagus nerve stimulation reverses ventricular electrophysiological changes induced by hypersympathetic nerve activity. *Exp Physiol*, 100, 239-48.
- ISHISE, H., ASANOI, H., ISHIZAKA, S., JOHO, S., KAMEYAMA, T., UMENO, K. & INOUE, H. 1998. Time course of sympathovagal imbalance and left ventricular dysfunction in conscious dogs with heart failure. *J Appl Physiol (1985)*, 84, 1234-41.
- KOLMAN, B. S., VERRIER, R. L. & LOWN, B. 1976. Effect of vagus nerve stimulation upon excitability of the canine ventricle. Role of sympathetic-parasympathetic interactions. *Am J Cardiol*, 37, 1041-5.
- LEHNINGER, A. L. 1974. Role of phosphate and other proton-donating anions in respiration-coupled transport of Ca^{2+} by mitochondria. *Proc Natl Acad Sci USA*, 71, 1520-4.
- MAZGALEV, T., DREIFUS, L. S., MICHELSON, E. L. & PELLEG, A. 1986. Vagally induced hyperpolarization in atrioventricular node. *Am J Physiol*, 251, H631-43.
- MORADY, F., KOU, W. H., NELSON, S. D., DE BUITLEIR, M., SCHMALTZ, S., KADISH, A. H., TOIVONEN, L. K. & KUSHNER, J. A. 1988. Accentuated antagonism between beta-adrenergic and vagal effects on ventricular refractoriness in humans. *Circulation*, 77, 289-97.
- NG, G. A., BRACK, K. E. & COOTE, J. H. 2001. Effects of direct sympathetic and vagus nerve stimulation on the physiology of the whole heart--a novel model of isolated Langendorff perfused rabbit heart with intact dual autonomic innervation. *Exp Physiol*, 86, 319-29.

- NG, G. A., BRACK, K. E., PATEL, V. H. & COOTE, J. H. 2007. Autonomic modulation of electrical restitution, alternans and ventricular fibrillation initiation in the isolated heart. *Cardiovasc Res*, 73, 750-60.
- NIKOLAIDOU, T., CAI, X. J., STEPHENSON, R. S., YANNI, J., LOWE, T., ATKINSON, A. J., JONES, C. B., SARDAR, R., CORNO, A. F., DOBRZYNISKI, H., WITHERS, P. J., JARVIS, J. C., HART, G. & BOYETT, M. R. 2015. Congestive Heart Failure Leads to Prolongation of the PR Interval and Atrioventricular Junction Enlargement and Ion Channel Remodelling in the Rabbit. *PLoS One*, 10, e0141452.
- OLSHANSKY, B., DAY, J. D., SULLIVAN, R. M., YONG, P., GALLE, E. & STEINBERG, J. S. 2012. Does cardiac resynchronization therapy provide unrecognized benefit in patients with prolonged PR intervals? The impact of restoring atrioventricular synchrony: an analysis from the COMPANION Trial. *Heart Rhythm*, 9, 34-9.
- OPTHOF, T., DEKKER, L. R., CORONEL, R., VERMEULEN, J. T., VAN CAPELLE, F. J. & JANSE, M. J. 1993. Interaction of sympathetic and parasympathetic nervous system on ventricular refractoriness assessed by local fibrillation intervals in the canine heart. *Cardiovasc Res*, 27, 753-9.
- PARMLEY, W. W. 1989. Pathophysiology and current therapy of congestive heart failure. *Journal of the American College of Cardiology*, 13, 771-785.
- PATTERSON, E. & LUCCHESI, B. R. 1984. Antifibrillatory properties of the beta-adrenergic receptor antagonists, nadolol, sotalol, atenolol and propranolol, in the anesthetized dog. *Pharmacology*, 28, 121-9.
- PITRUZZELLO, A. M., KRASSOWSKA, W. & IDRIS, S. F. 2007. Spatial heterogeneity of the restitution portrait in rabbit epicardium. *Am J Physiol Heart Circ Physiol*, 292, H1568-78.
- RABINOWITZ, S. H., VERRIER, R. L. & LOWN, B. 1976. Muscarinic effects of vagosympathetic trunk stimulation on the repetitive extrasystole (RE) threshold. *Circulation*, 53, 622-7.
- REED, K. C. & BYGRAVE, F. L. 1975. A kinetic study of mitochondrial calcium transport. *Eur J Biochem*, 55, 497-504.
- SCHWARTZ, P. J., VANOLI, E., STRAMBA-BADIALE, M., DE FERRARI, G. M., BILLMAN, G. E. & FOREMAN, R. D. 1988. Autonomic mechanisms and sudden death. New insights from analysis of baroreceptor reflexes in conscious dogs with and without a myocardial infarction. *Circulation*, 78, 969-79.
- SCHWARTZ, P. J., VERRIER, R. L. & LOWN, B. 1977. Effect of stellectomy and vagotomy on ventricular refractoriness in dogs. *Circ Res*, 40, 536-40.
- VANOLI, E., DE FERRARI, G. M., STRAMBA-BADIALE, M., HULL, S. S., JR., FOREMAN, R. D. & SCHWARTZ, P. J. 1991. Vagal stimulation and prevention of sudden death in conscious dogs with a healed myocardial infarction. *Circ Res*, 68, 1471-81.
- WEISS, J. N., CHEN, P. S., QU, Z., KARAGUEUZIAN, H. S. & GARFINKEL, A. 2000. Ventricular fibrillation: how do we stop the waves from breaking? *Circ Res*, 87, 1103-7.
- WEST, T. C. & TODA, N. 1967. Response of the A-V node of the rabbit to stimulation of intracardiac cholinergic nerves. *Circ Res*, 20, 18-31.